Adsorption Kinetics of Polymer/Surfactant Mixtures at an Expanding Air/Water Interface

ANGUS-SMYTH, ANNA

Adsorption Kinetics of Polymer/Surfactant Mixtures at an Expanding Air/Water Interface

A thesis submitted for the degree of Doctor of Philosophy at Durham University

by

Anna Patricia Angus-Smyth

Department of Chemistry and College of St Hild and St Bede

University of Durham

Summer 2012

Abstract

The dynamic adsorption mechanisms of a range of polymer/surfactant mixtures have been studied at the expanding air/water interface created by an overflowing cylinder. The composition of the adsorption layer from mixed systems is obtained using a new approach, co-modelling ellipsometry data and NR data recorded on only one isotopic contrast, without deuterated polymer. The precision and accuracy of the interfacial compositions using this novel approach match those obtained by NR measurements using multiple isotopic contrasts and deuterated polymer, and exceeds those in the absence of deuterated polymer.

For weakly interacting PEO/surfactant mixtures adsorption is competitive, the interfacial composition can be rationalised in terms of competitive adsorption. At high surfactant concentrations polymer adsorption is inhibited by the increasing surfactant coverage, although in PEO/SDS mixtures positive interactions between the two components allow PEO to adsorb until an SDS monolayer is present.

For oppositely charged mixtures of PSS and C_nTAB surfactants, synergistic adsorption occurs at low surfactant concentrations, and the formation of polymer/surfactant complexes has a marked effect on interfacial adsorption, although polymer adsorption is controlled by free polymer molecules. Aggregation occurs around charge neutrality, the material in these aggregates cannot reach the interface due to their size, and at higher surfactant concentrations polymer can no longer adsorb.

Mixtures of PEI/SDS at high pH behave similarly to the PSS/C_nTAB systems, with progressive aggregation depleting the system of surface active material and limiting adsorption. However at low pH the aggregates can reach the interface by convection where they spread material across the surface in the form of a thin layer of nanometer thickness by Marangoni flows.

This work proves that examination of the dynamic adsorption behaviour of polymer/surfactant systems is invaluable to understanding their adsorption mechanisms. Furthermore there is a clear and incontrovertible link between the dynamic interfacial adsorption and bulk phase behaviour.

Table of Contents

Acknowledgements

This work presented in this thesis would not have been possible without the advice and patience of my two supervisors Richard Campbell and Colin Bain, and I offer them both my heartfelt thanks for all of their support.

I also wish to thank Imre Varga, for some truly valuable discussions and his expert answers to all of my questions about bulk phase behaviour and polymer/surfactant mixtures.

I would like to acknowledge and thank all of the members of the Bain group who helped Richard and I with the neutron experiments: John Churchwell, David Woods, Alex Dudgeon and Andy McKeague. Special thanks go to Andy for his help with the endless favours I have asked of him during my project.

Friends and colleagues past and present at the ILL have also played an important role in keeping me sane, special thanks go to Marianna Yanez, Shona Gillespie, Marcus Trapp and Rob Barker. Finally this thesis could not have been written without the patience and support of Stu, who kept me from going slightly mad.

List of Publications

A combination of part of Chapter 4 and the results in Chapter 5 has been published as:

Angus-Smyth, A., Campbell, R.A., Bain, C.D., Dynamic Adsorption of Weakly Interacting Polymer/Surfactant Mixtures at the Air/Water Interface, *Langmuir*, **2012,** 28, 12479-12492

The results in Chapters 6 and 8 are in the following manuscripts in preparation respectively:

Angus-Smyth, A., Campbell, R.A., Bain, C.D., Adsorption kinetics of the oppositely charged polymer/surfactant system PSS/C_{12}TAB at the Air/Water Interface, *In preparation*

Angus-Smyth, A., Bain, C.D., Varga, I., Campbell, R.A., Effects of Aggregates on PEI/SDS Monolayers at the Dynamic Air/Liquid Interface:Depletion by Bulk Flocculation versus Enrichment by a Convection/Spreading Mechanism, *In preparation*

Several other papers have also arisen from work carried out at the same time as that presented in this thesis:

Campbell, R. A.; Angus-Smyth, A.; Arteta, M. Y.; Tonigold, K.; Nylander, T.; Varga, I., New Perspective on the Cliff Edge Peak in the Surface Tension of Oppositely Charged Polyelectrolyte/Surfactant Mixtures. *J. Phys. Chem. Letts.* **2010,** 1, (20), 3021-3026.

Campbell, R. A.; Yanez Arteta, M.; Angus-Smyth, A.; Nylander, T.; Varga, I., Effects of Bulk Colloidal Stability on Adsorption Layers of Poly(diallyldimethylammonium Chloride)/Sodium Dodecyl Sulfate at the Air/Water Interface Studied by Neutron Reflectometry. *J. Phys. Chem. B* **2011,** 115, (51), 15202-15213.

Campbell, R. A.; Yanez Arteta, M.; Angus-Smyth, A.; Nylander, T.; Varga, I., Multilayers at Interfaces of an Oppositely Charged Polyelectrolyte/Surfactant System Resulting from the Transport of Bulk Aggregates under Gravity. *J. Phys.Chem.B* **2012**, 116, (27), 7981-7990.

Yan, C., Angus-Smyth, A., Colgate, D.M., Péron, N., Bain, C.D., Adsorption kinetics of nonionic surfactants in micellar solutions: Effect of added charge, *Submitted to Faraday Discussions*

These four papers are given as appendices to this thesis.

List of Abbreviations and Important Symbols

OFC	Overflowing cylinder
NR	Neutron reflectometry
ILL	Institut Laue Langevin
FIGARO	Fluid Interfaces Grazing Angles ReflectOmeter (at the ILL)
LDV	laser Doppler velocimetry
SDS	Sodium Dodecyl Sulfate
C_nTAB	Alkyl trimethylammonium bromide surfactants with chain length n = 12, 14 or 16.
PEO	Poly(ethylene oxide)
PSS	Poly(styrene sulfonate)
PEI	Poly(ethylene imine)
cmc	critical micelle concentration
cac	critical aggregation concentration (in a polymer/surfactant mixture)
d-surfactant	deuterated surfactant
h-surfactant	hydrogenated surfactant
Γ	Surface excess (in μmol m^{-2}) (where subscript denotes species)
$\bar{\rho}$	Ellipticity
θ	Surface expansion rate
D	Diffusion coefficient (where subscript denotes species)
c_{surf}	Bulk surfactant concentration
$\sigma \times \tau$	Product of the scattering length density (σ) and thickness (τ) of an adsorbed layer
$\sum_i \sigma_i \tau_i$	Sum of the products of σ and τ over several layers
c_s	Subsurface concentration

Chapter 1. Introduction

1.1. Introduction to the Project

The main objective of the research presented in this thesis is to examine the kinetics of adsorption of polymer/surfactant mixtures at an expanding air/water interface, and hence to try to determine the mechanism of adsorption from such mixtures. Mixtures of oppositely charged polymers and surfactants are widely used in industrial applications as detergents, foam stabilisers, wetting agents, emulsifiers, and rheology modifiers. The extent to which polymers and surfactants interact in solution can determine both the bulk and interfacial properties of the system. Previous studies on polymer/surfactant systems can be divided up into those which examine the bulk properties of such systems, and those which examine the interfacial adsorption behaviour, either at the air/liquid or solid/liquid interfaces, and a few which have related the two. Many formulations which employ polymer/surfactant mixtures are routinely used under conditions far from equilibrium, whilst few previous studies have looked at the behaviour of such mixtures under non-equilibrium conditions. This research is aimed at examining the kinetics of adsorption of a range of polymer/surfactant mixtures under the non-equilibrium conditions, and determining the effect of the presence of polymer in solution on the adsorption of surfactant and vice-versa. Understanding of the kinetics of adsorption from these systems will allow us to elaborate on the link between their bulk and interfacial behaviour, and hence to elucidate the mechanism of adsorption to the air/water interface.

The sample environment which we use to study adsorption under non-equilibrium conditions is the overflowing cylinder (OFC) which creates a large, flat, continuously expanding interface with a surface age typically in the range 0.1–1 s. The flowing nature of the OFC enables it to be used to distinguish between the adsorption of different species on the basis of their size, as only small species can diffuse to the interface on the timescale of surface expansion in order to adsorb. Hence the OFC allows to begin to determine the link between the bulk and interfacial behaviours of solutions.

The large steady-state surface of the OFC can be studied using a wide range of experimental techniques. In this project, a combination of ellipsometry and neutron reflectometry [NR] has been employed to study adsorption from polymer/surfactant mixtures at the interface of the OFC. The primary experimental objective of the measurements was to determine the composition of the material adsorbing at the air/water interface, which is commonly obtained using neutron reflectometry

measurements in multiple isotopic contrasts. However, this approach can be limited by the availability of both deuterated chemicals and neutron beamtime. Therefore a further key objective of this project has been to validate a new quantitative approach to determining the adsorbed composition of an adsorbed layer from mixed solutions using a combination of ellipsometry and NR measurements in only one isotopic contrast. This project has been based at the Institut Laue Langevin (ILL) in France, where I have commissioned an OFC for use on the new neutron reflectometer FIGARO [Fluid Interfaces Grazing Angles ReflectOmeter].

The remainder of this chapter provides an introduction to both the bulk and interfacial behaviours of surfactants, polymers and polymer/surfactant mixtures. In section 1.2, I discuss previous studies of the behaviour of polymers in aqueous solution, and their adsorption at interfaces. In section 1.3, I examine the behaviour of pure surfactants, their bulk phase micellisation and interfacial adsorption. In Section 1.4, I introduce the question of polymer/surfactant mixtures and discuss the large number of previous studies which examine their bulk and interfacial adsorption behaviour.

Chapters 2 and 3 present a detailed description of the experimental methodologies used in this research, the OFC, neutron reflectometry, ellipsometry and LDV, and theories on which they are based. Extra detail in Chapter 3 is devoted to the specific considerations necessary for use of the OFC on FIGARO.

Our unique approach to obtaining interfacial compositions using data from ellipsometry and neutron reflectometry is explained and validated in Chapter 4. This co-modelling approach is based on the solution of simultaneous equations which relate the measured quantities from each experimental methodology to the adsorbed amounts of the two components at the interface. Our co-modelling approach is then employed to determine the interfacial compositions on the OFC of several different polymer/surfactant mixtures. In Chapter 5 adsorption from mixtures of the non-ionic polymer PEO and the ionic surfactants SDS and C_{14}TAB is examined. Chapters 6 and 7 discuss adsorption from oppositely charged polymer/surfactant systems containing the polymer PSS and the C_nTAB surfactants. Chapter 8 discusses the link between the bulk and interfacial behaviour of PEI/SDS mixtures at both low and high solution pHs. Finally, Chapter 9 presents the conclusions of this project and some future perspectives of this work in terms of several polymer/surfactant mixtures on which initial studies have been performed.

1.2. Polymers

A polymer is a macromolecule made up of repeating structural units. The number of repeat units, N_p, can vary from small up to several hundreds of thousands, depending on the polymer. Polymers which contain charged groups are commonly known as polyelectrolytes, and they can carry either positive or negative charges. In the simplest case, polymers are *homopolymers*, all of the repeat units are the same, however co-polymers can also be made, which have different repeat units. All of the polymers used in this thesis are simple homopolymers, and are restricted to poly(ethylene oxide) [PEO], poly(styrene sulfonate) [PSS] and poly(ethylene imine) [PEI]. The structures of all three polymers are shown below in Figure 1.1. The notable features of the three polymers show in Figure 1.1 are that PEO is non-ionic, PSS is anionic, but contains hydrophobic styrene groups, and the charge density of PEI depends on the pH of the solution, varying from around 6% charged at pH 10 to around 67% charged at pH 4.[1,2]

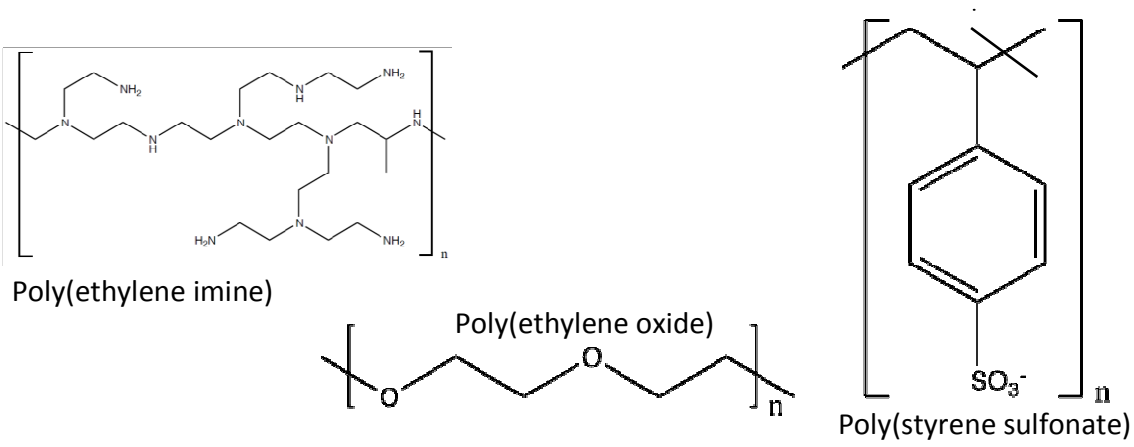

Figure 1.1. Molecular structures of the three polymers used in this thesis

Pure polymer solutions can be defined into three categories: firstly dilute, where excess solvent is present and inter-molecule interactions can be neglected, secondly semi-dilute where monomers in separate chains are in contact with each other forming a network, and finally concentrated solutions in which polymer chains are strongly intertwined. In this study, all of the polymer solutions can be thought of as dilute, with no interactions between the polymer molecules in the absence of added surfactant. In the bulk solution the size and shape of a polymer molecule can be characterised using techniques including small angle neutron scattering (SANS), small angle x-ray scattering (SAXS) and static or dynamic light scattering (SLS and DLS)[3], to determine whether the polymer has a compact sphere, random coil or stiff rod conformation.

The adsorption of polymers onto solid surfaces has been widely studied due to its relevance to industrial processes such as oil recovery, food processing, coating, and drug manufacture, and the recent review of Nylander *et al*.[4] with the references therein gives a good overview of recent work in this area. Unlike at solid interfaces, few polymers adsorb at the air/water interface as they are not surface active due to the low hydrophobic driving force for their adsorption at the interface and the electrostatic repulsion between charged polymer molecules. The only relevant exception to this is PEO, which is neutral and surface active alone,[5] and for which NR measurements have been used to characterise the adsorbed amount and structure of the layer.[6, 7] The other two polymers used in this thesis do not adsorb at the interface in the absence of surfactant under the conditions we have used.

1.3. Surfactants

Surfactants (a contraction of *surf*ace *act*ive age*nts*) are amphiphilic molecules composed of a hydrophilic head group and a hydrophobic tail group. Surfactants are generally categorized by the nature of their headgroups, which can be cationic, anionic, nonionic or zwitterionic. Surfactant tails usually consist of one or more alkyl chains. Surfactant molecules self assemble in aqueous solutions and adsorb to the air/water interface in order to limit the contact of the hydrophobic tail group with water. In the former case aggregates called micelles form, with the surfactant head groups positioned on the outside in order to screen the non-polar tails from the surrounding water. At the interface, surfactants adsorb with their polar headgroups in the aqueous solution and their tail groups in the air. Both adsorption and micellisation are discussed further below.

The surfactants used in this study are sodium dodecyl sulfate (SDS), and the alkyl trimethylammonium bromide surfactants (C_nTABs) where n = 12,14, or 16. Structures of these surfactants are shown in Figure 1.2

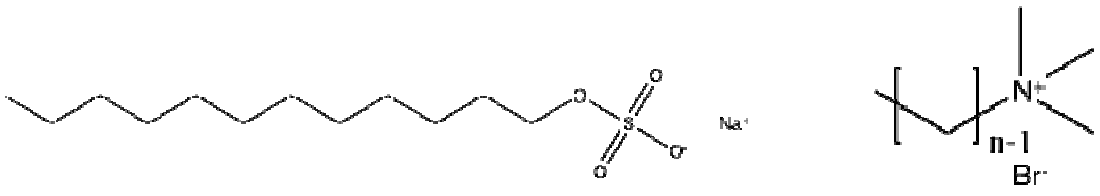

Figure 1.2. Structures of the main surfactants used in this thesis, sodium dodecyl sulphate, SDS (left), and alkyltrimethylammonium bromide surfactants, C_nTAB_s, (right).

1.3.1. Surfactants in Solution

In bulk surfactant solutions micellar aggregates form above a critical concentration due to the unfavourable entropy of water molecules 'caging' the hydrophobic part of the surfactant molecule, the hydrocarbon chain. Micelle formation maximises the entropy of the water molecules. A typical micelle has the hydrophilic head groups in contact with the solvent, with the hydrocarbon chains inside the micelle in a fluid environment due to their constant thermal motion. Micelles are generally spherical, cylindrical or ellipsoid in shape, shown by the schematics in Figure 1.3, however they can also form into larger vesicles and lamellar sheets. Micelles of SDS, C_{12}TAB and C_{14}TAB used in this study are spherical in shape, whereas those of C_{16}TAB are rod-shaped in the presence of added salt.[8, 9] Micelles consist of several tens, hundreds or thousands of surfactant molecules, although the majority contain between 50 and 100 monomers. The average number of surfactants per micelle is known as the 'aggregation number'. For the surfactants used in this study the micellar aggregation number increases with the length of the hydrocarbon chain.[10, 11]

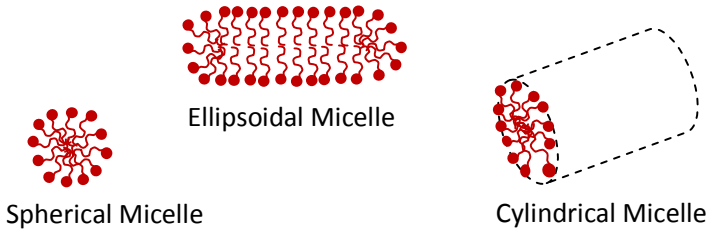

Figure 1.3. Schematic diagram showing surfactant molecules aggregated into different kinds of micelle

The critical bulk concentration above which micelles form in the bulk solution is known as the critical micelle concentration (cmc). At bulk surfactant concentrations above the cmc, the concentration of surfactant monomers in solution remains constant, and excess surfactant added to the solution forms into micelles. The surfactant concentration corresponding to the cmc varies widely between surfactants, and is controlled by factors including the chain length and the nature of the head group. Longer hydrocarbon chains are more hydrophobic, favouring the formation of micelles, whilst increased charge on the headgroup will increase repulsive interactions between the surfactant molecules, disfavouring aggregation. Consequently non-ionic surfactants tend to have much lower cmc values and higher aggregation numbers than their ionic counterparts with similar hydrocarbon chain lengths. For ionic surfactants, addition of electrolyte decreases the cmc and increases micellar size, as it decreases the repulsive interactions between the charged headgroups at the micelle surface. In order for micelles to form in a given surfactant solution, the solution temperature must be above the Krafft temperature, the minimum temperature for the solubility of the monomer to be high enough for micelle

formation at the cmc.[12] The cmc of a surfactant can be determined using a range of experimental techniques, as it corresponds to characteristic changes in the bulk properties of both the bulk solution and the interface. Measurements techniques which can be used to determine the cmc include surface tension, molar conductivity, osmotic pressure, and turbidity measurements.

1.3.2. Surfactants at the Air/Water interface

Surfactants adsorb at the air/water interface for the same reason that they aggregate at high concentrations, the entropic gain from the water molecules no longer being oriented around the hydrophobic part of the surfactant. The ordering of surfactant molecules at the interface lowers the free energy of the surface, but thermal motion makes the ordering imperfect. Surfactant adsorption increases with increasing bulk surfactant concentration up to the cmc, where a limiting surface coverage is reached which cannot be exceeded by further increases in the bulk surfactant concentration. This limiting coverage is less than the theoretical maximum value which cannot usually be reached due to constraints of concentration, such as solubility or micellization. The amount of surfactant which can adsorb at the interface is known as the surface excess, Γ, with units of moles m^{-2}. Neutron reflectometry and surface tension have been used in previous studies to determine the variation in surface excess with concentration of the surfactants used in this study; SDS,[13] C_{12}TAB,[14] C_{14}TAB[15, 16] and C_{16}TAB.[17, 18]

The cohesive forces between liquid molecules at the interface are responsible for the phenomenon of surface tension. As interfacial molecules do not have molecules on all sides of them, they consequently cohere more strongly to those directly associated with them on the surface, resulting in a tendency for the surface to contract. The surface tension, σ, with units of J m^{-2} or N m^{-1}, is defined as the reversible work required to increase the area of a surface by 1 m^2. When surfactant molecules adsorb at the interface they reduce the surface tension as they have replaced some of the water molecules at the interface. As the resulting surfactant-water interaction is weaker than the water-water molecule interaction, and the force for contraction decreases. At bulk surfactant concentrations below the cmc, the surface tension decreases with increasing bulk concentration, as the interfacial surfactant coverage increases. At low surfactant concentrations a gradual decrease in surface tension is observed corresponding to the increase in the surface excess (Γ). At concentrations close to the cmc, Γ tends to a limiting value, and the surface tension appears almost linear. Once the surface coverage reaches its limiting value, increases in the bulk surfactant concentration have no further effect on the surface

tension. Figure 1.4 shows a schematic representation of the relationship between surface tension data for a surfactant and the surface coverage.

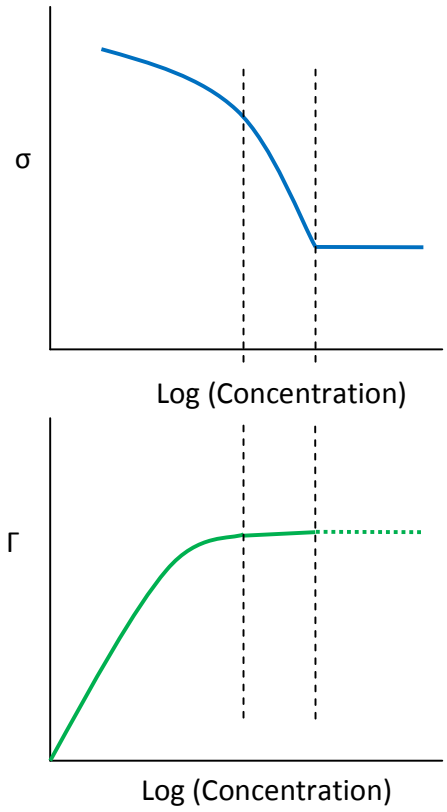

Figure 1.4. Schematic of the relationship between the surface tension, σ, and surface excess, Γ, of a surfactant, which explains how the interfacial adsorption isotherm can be obtained from the surface tension measurement and the Gibbs equation.

The Gibbs equation is used to quantify the adsorption at the interface using the relationships between the surface excess of surfactant and the surface tension, as shown in Figure 1.4. At constant temperature and pressure it is given by

$$d\sigma = -\sum_i \Gamma_i . d\mu_i \qquad (1.1)$$

where dσ is the change in surface tension, Γ_i is the surface excess of component i, and dμ_i is the change in the chemical potential of the adsorbed component i. The change in chemical potential of component i on mixing it with the other component is given by

$$d\mu_i = RT . d \ln a_i \qquad (1.2)$$

Where R is the gas constant (8.314 J $mol^{-1}K^{-1}$), T is the temperature, and a_i the activity of component i. The surface tension of a system of i components is then given by

$$d\sigma = -RT \sum_i \Gamma_i d \ln a_i \quad (1.3)$$

Which for a solution of only water (1) and a surfactant (2) is

$$d\sigma = -RT.(\Gamma_1 . d \ln a_1 + \Gamma_2 . d \ln a_2) \quad (1.4)$$

The surface excess is dependent on the location for the plane dividing the liquid and gas phase. If the plane such that $\Gamma_1 = 0$ is chosen[19] then

$$\Gamma_2 = -\frac{1}{RT}\left(\frac{d\sigma}{d \ln a_2}\right)_{T,P} \quad (1.5)$$

For ideal, dilute solutions the Gibbs equation can be re-written as:

$$\Gamma_2 = -\frac{1}{n_M RT}\left(\frac{d\sigma}{d \ln c}\right) \quad (1.6)$$

Where activity is replaced by the bulk surfactant concentration, c. n_M is a constant which depends on the number of species adsorbing at the surface. For a non-ionic surfactant $n_M = 1$, however for an ionic surfactant n_M depends on the valency of the counterion, where $n_M = 2$ for a 1:1 electrolyte, whilst in excess added electrolyte $n_M = 1$.

Surface tension measurements examine the reduction in the free energy of the interface with respect to the bulk activity, hence although surface tension measurements can be used to determine Γ using Equation 1.5, it is not purely a surface technique, and changes in the bulk solution can affect the surface tension. $\Gamma_2 = -\frac{1}{n_M RT}\left(\frac{d\sigma}{d \ln c}\right)$ A more versatile and direct approach to determining Γ is NR, discussed in Chapter 3.

1.3.3. Dynamic Adsorption of Surfactants on the OFC

Surfactants in both commercial and biological applications are rarely used under equilibrium conditions, with their dynamic interfacial properties important in foaming processes, detergency, coatings, solubilisation and for lung surfactants.[20] As a consequence it is essential to investigate the kinetics of surfactant adsorption at the air/water interface in order to be able to relate lab-based experiments to real applications of surfactants. Dynamic surfactant adsorption is most commonly studied using experimental methodologies which create a fresh air/water interface, as discussed below.

Creation of a fresh interface for a surfactant solution leads to dynamic adsorption of surfactant to the interface. This adsorption of surfactant is driven by a concentration gradient from the bulk solution to the clean interface which exists in the near-surface region known as the 'diffusion layer'. Models of adsorption have to include terms accounting for this diffusion of surfactant to the interface, its adsorption, and back diffusion of surfactant which does not adsorb at the interface. This is described by the Ward-Tordai equation[21]

$$\Gamma(t) = 2c\sqrt{\frac{Dt}{\pi}} - 2\sqrt{\frac{D}{\pi}}\int_0^{\sqrt{t}} c_s d\sqrt{(t-\tau)} \qquad (1.7)$$

where c is the bulk concentration of surfactant, D is the monomer diffusion coefficient, c_s is the sub-surface concentration, and τ is a dummy variable of integration. The first term on the right hand side, which is positive accounts for the situation where a monomer reaching the interface by diffusion adsorbs at a vacant site. The second term, which is negative, accounts for back diffusion of surfactant molecules from the sub-surface to the bulk solution when there is not a free site for surfactant adsorption. Back diffusion occurs to a greater extent with increasing subsurface concentration.

The situation described by the Ward-Tordai Equation assumes that adsorption and desorption to and from the interface are fast compared to diffusion of surfactant to the sub-surface layer. Mass transport of surfactant to the sub surface layer is the rate-limiting step in adsorption. However in some systems, adsorption rather than mass transport may be the rate-limiting step due to barriers to adsorption of surfactant at the interface. Such adsorption barriers can arise from electrostatic repulsions between adsorbing surfactants, steric considerations for large surfactant molecules, micellar breakdown, or rearrangements at the interface.

In order to study the adsorption kinetics, a system which creates an expanding or contracting air/liquid interface is required. The simplest way to examine expanding and contracting air/water interfaces is by use of a Langmuir trough, a piece of equipment which allows the compression and expansion of

monolayers at an air/water interface by the use of moving barriers.[22] A common approach to examining expanding and contracting interfaces is the oscillating bubble method, which is based on the formation of a spherical bubble at the tip of a needle immersed in a surfactant solution by injecting and withdrawing gas causing period surface expansion and contraction.[23] The changes in the bubble size and shape can be used to monitor the adsorption and desorption of surfactant. The maximum bubble pressure (MBP) method also blows bubbles in a liquid by blowing bubbles of inert gas through a defined capillary. The gas pressure is increased until a bubble appears, and is then kept constant with the surface age given by the time between consecutive bubbles. This enables determination of the dynamic surface tension of the solution, although interpretation can be complicated as expansion rates vary during bubble growth.[20] The MBP method has been extensively used to study surfactant adsorption by several groups, with the references[24-26] being a few examples. MBP method is one of the principal techniques to examine surfactant adsorption on millisecond timescales along with the oscillating jet. The oscillating jet ejects surfactant solution from an elliptical nozzle under pressure. The non-uniform nozzle shape makes the jet cross section unstable, and it oscillates sinusoidally around its equilibrium cross sectional shape, at a frequency determined by the surface tension and flow. Surface tension acts to restore the liquid to the equilibrium cross sectional shape, hence the jet can be used to determine the dynamic surface tension of the surfactant solution.

The overflowing cylinder (OFC), the device used in this project to examine adsorption dynamics at the air/water interface, creates a continuously expanding air/water interface on a 0.1-1 s timescale. The interface of the OFC is large, flat and stable, making it possible to study it using a variety of spectroscopic, reflectometry and scattering based techniques. Bain and co-workers have used the OFC extensively in the last two decades to study dynamic adsorption from a range of surfactant solutions using a range of non-invasive experimental techniques.[27-36] The OFC, and its characteristics and operation will be discussed in more detail in Chapter 2. More recently, Bain *et al*. have developed a liquid jet for the study of adsorption dynamics of surfactants using ellipsometry and laser Doppler velocimetry.[37, 38] The liquid jet is a complementary methodology to the overflowing cylinder, as it enables the study of adsorption on a faster timescale (1-100 ms) than on the OFC.

1.4. Polymer/Surfactant Mixtures

Formulations containing mixtures of polymers and surfactants are extensively used in industrial and commercial formulations as detergents, foam stabilizers, wetting agents, emulsifiers and rheology modifiers. As a consequence, their behavior both in the bulk and at interfaces is widely studied, although bulk phase studies are predominant. The bulk and interfacial behaviour of a polymer/surfactant system is determined by the strength of the electrostatic and hydrophobic interactions between the two components. Electrostatic interactions occur between oppositely charged groups on the polymer chain and surfactant headgroups, favouring interactions, as do hydrophobic interactions between the surfactant chains, although repulsive interactions between the surfactant headgroups can limit interactions. Many factors influence the interactions between the polymer and surfactant, including the polymer molecular weight, degree of branching, charge density and backbone rigidity, along with the nature of the surfactant headgroup, the chain length of the surfactant, the concentrations of both components, and the presence or absence of added electrolyte.

Interactions between polymers and surfactants lead to the formation of complexes in the bulk solution and to changes in the adsorption at interfaces. Bulk polymer/surfactant complexes generally consist of a single polymer chain to which surfactant monomers[39, 40] or micelles[41-43] are bound, although multi-chain complexes can also occur. The amount of surfactant bound to polymer molecules increases with increasing bulk surfactant concentration, until, at close to the charge match point, aggregation and precipitation of the complexes occurs in many oppositely charged polymer/surfactant systems.[44, 45] Interactions between polymer and surfactant at an air/water or solid/water interface can significantly alter the composition and structure of the adsorbed layer in comparison to that which would adsorb from a solution of either component alone. The two main effects are synergistic adsorption, which increases the adsorbed amount of both components at the interface, and competitive adsorption, where both components adsorb at the interface independently, but they compete for free space. Furthermore, it is important to remember that bulk and interfacial behaviours of polymer/surfactant mixtures are not always independent, especially when precipitation occurs, depleting the solution of surface active species. It is therefore important to consider both the bulk and interfacial behaviour of a given polymer/surfactant systems in order to understand what controls its adsorption at an interface. Several comprehensive reviews of the bulk[43, 46] and interfacial behaviour[47-49] of such systems have been published in recent years.

In the following pages I discuss the previous studies made of the bulk and interfacial behaviour of a range of polymer/surfactant systems in order to put the work presented in this thesis into the wider

context. Many groups have studied polymer/surfactant mixtures, and an exhaustive review of this work would be lengthy. As a consequence I restrict myself here to a general introduction to the bulk and behaviour of polymer/surfactant systems, whilst reviews of the previous work conducted on the polymer/surfactant systems discussed in this thesis are given at the start of the relevant chapters.

1.4.1. Bulk Phase Behaviour of Polymer/Surfactant Mixtures

Co-operative binding of surfactant to polymer molecules occurs above a critical aggregation concentration (cac) which is much lower than the cmc of the pure surfactant solution. At surfactant concentrations below the cac, no complexation occurs in the bulk solution. As the surfactant concentration is increased above the cac, the amount of surfactant bound to polymer molecules increases, whilst the free surfactant concentration stays constant. Eventually a point is reached where the polymer molecules are saturated with surfactant, and further increases in the bulk surfactant solution increase the concentration of free surfactant molecules until the cmc of the mixture is reached and free micelles form.

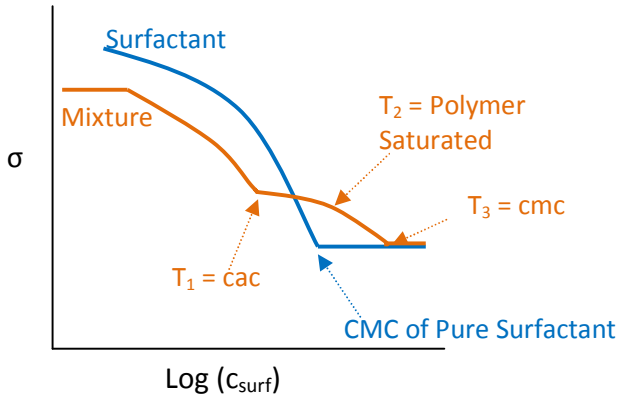

Figure 1.5. Schematic representation of the change in surface tension, σ, with bulk surfactant concentration, c_{surf}, of a mixture of a nonionic polymer and surfactant where the polymer concentration is constant (orange line) as compared with that of a pure surfactant (blue line).

The classical picture of of Jones[50] and Lange[51] is of polymer/surfactant complexes which consist of polymer-wrapped surfactant micelles, where several micelles associate with single polymer molecule, and the complex looks like 'beads on a chain'.[41, 50-54] This model was derived to explain surface tension measurements made on mixtures of neutral polymers with ionic surfactants, with a form similar to the schematic shown in Figure 1.5.[50, 51] For such weakly interacting polymer/surfactant systems, surface tension measurements yield information about both the interfacial and bulk behaviour of the mixture.

In the model of Jones, the breakpoints T_1, T_2 and T_3 in the surface tension data correspond to bulk complexation, with T_1 being the onset of complexation, i.e. the cac, T_2 being the point where polymer is saturated with micelles, and T_3 the onset of micelle formation in the bulk. In the decades since the original studies of Jones, this model of the bulk phase behaviour of non-ionic polymer/ionic surfactant mixtures has been supported by numerous studies, using a wide range of experimental techniques, of which the references 3, 54-61 are only a small selection.

In the decades since the work of Jones *et al*., many groups have studied the bulk interactions between charged or uncharged polymers and surfactants in order to determine the extent to which hydrophobic and electrostatic interactions between polymer and surfactant favour complexation for a given system. If a polymer is charged, it can be considered as having a number of charged binding 'sites' to which individual surfactant molecules are electrostatically attracted and can bind.[43, 62] From this electrostatic argument alone we might expect individual surfactant molecules to be bound to a polymer molecule. Although this may be a viable binding model for some systems,[39, 63-67] in this configuration the hydrophobic part of the bound surfactant continues to be surrounded by water molecules, which is an energetically unfavourable state. Unless the electrostatic interaction between the charged groups can considerably outweigh this negative hydrophobic driving force, it is likely that polymer-monomer complexes only exist as a pre-cursor to polymer-micelle complexes. The binding of one surfactant to a polymer molecule effectively acts as a nucleation point, promoting clustering of surfactant molecules and the formation of micelles.[62, 68]

The presence of polymer in a solution with surfactant significantly increases the favourability of surfactant micelle formation as the polymer can wrap around a surfactant micelle, shielding exposed hydrophobic regions from water, and in the case of polyelectrolytes insulating the repulsive interactions between the charged surfactant headgroups.[69, 70] Furthermore, the interaction of a polymer molecule with a micelle is significantly more entropically favourable than the interactions of a large number of small counterions with the micelle. These effects stabilize micelles, causing the point at which micelles form in the mixture, the cac, to be considerably lower than the cmc of the pure surfactant. As a consequence of the stabilization of micelles by polymer molecules, 'beads on a chain' type complexes form for a large range of polymer/surfactant mixtures. The surfactant micelles which form in these complexes usually have a smaller aggregation number than that of the free surfactant micelles[71] due to the enthalpic cost of aggregation on the polymer and the stabilization of the micelles by the polymer due to reduced water-hydrocarbon contact[43] and decreased headgroup repulsion.[55] The smallest possible polymer-micelle complex that can form is a single polymer-wrapped micelle, and for this to form the number of polymer monomers needs to equal or exceed the aggregation number of a surfactant micelle,[56, 72-75] which defines the minimum polymer molecular weight for complexation.

The stronger the driving force for complexation of polymer and surfactant, the lower the cac of the mixture compared to the cmc of the pure surfactant. Breuer and Robb[76] were the first to try to classify polymer/surfactant mixtures by their tendency to interact, and many studies since have tried to determine the factors controlling complexation in a given polymer/surfactant system. Increasing the alkyl chain length of a surfactant increases its hydrophobicity, which increases the driving force for both interfacial adsorption and micellisation in a pure surfactant solution, lowering the cmc and increasing the micellar aggregation number.[69, 77] The greater the charge density of the polymer the larger the amount of surfactant that can associate with it before the cmc of the system is reached.[78] Polymer flexibility also significantly affects the binding process,[79] as polymer molecules need to be able to orient their charged groups for interaction and to wrap around surfactant micelles in order to complex. Furthermore, addition of simple electrolyte to a polymer/surfactant mixture decreases the electrostatic driving force for interactions, increasing the cac.[80]

In a wide range of polymer/surfactant mixtures, bulk complexes aggregate once their net charge is low as they have lost their colloidal stability, and phase separation occurs, with the aggregates precipitating out of the solution.[44, 45, 81-85] In the model of Hansson, phase separation occurs when the repulsive interaction between surfactant micelles due to the electric double layer are removed as polymer replaces the small counter-ions around the micelle, the attractive interaction between micelles then dominates and phase separation occurs.[84] The group of Meszaros has studied the bulk phase behaviour of a number of precipitating polymer/surfactant systems in recent years, describing them in terms of characteristic surfactant concentration ranges.[40, 86-88] At low bulk surfactant concentration a kinetically stable colloidal dispersion of complexes forms, and the solutions are optically transparent. Above a critical surfactant concentration these complexes collapse, and precipitation can occur when their charge density is low. These solutions are turbid. The region where complexes aggregate and precipitation occurs is commonly defined as the 'phase separation region'. As the surfactant concentration is increased further, excess surfactant attaches to the outside of the aggregates and charge reversal occurs, leading to resolubilisation, and the solutions become clear again. Associative phase separation is driven by the entropy gained when counterions are released from the polyelectrolyte and ionic surfactant.[52]

Stronger polymer/surfactant interactions can increase the bulk surfactant concentration range over which phase separation occurs. For example, for the PSS/C_nTAB systems, phase separation increases with surfactant hydrophobicity.[80, 89] The addition of simple electrolyte to a polymer/surfactant system leads to a reduction in the two-phase region,[81] as it decreases the electrostatic interactions between the polymer and surfactant.[89] However, for some systems, the addition of electrolyte can cause broadening of the precipitation concentration range.[87, 88] For PSS/CTAB, small to moderate amounts of added

electrolyte increase the width of the phase separation region, whilst larger concentrations prevent surfactant binding to the polyelectrolyte.[90]

Several recent studies have shown that the formation of bulk aggregates in strongly interacting polymer/surfactant systems is a non-equilibrium process which is dependent on the mixing procedure. Work from the groups of Claesson[91, 92] and Meszárós[93, 94] has demonstrated that the mixing protocol affects the formation of kinetically trapped non-equilibrium aggregates. The effect of mixing can be understood in terms of the local rate of coagulation of the polymer/surfactant particles, which is largely dependent on concentration gradients present during mixing.[94] These studies showed that in order to have reproducible bulk phase behaviour for a given strongly interacting polymer/surfactant system for which phase separation occurs, strict control of the mixing methodology and sample preparation is necessary.

1.4.2. Adsorption from Polymer/Surfactant Mixtures at Interfaces

Just as polymers and surfactants associate in the bulk solution, they can also associate at interfaces due to both the strong associative interactions between them and the high driving force for surfactant to adsorb at interfaces rather than being in solution. Many applications of formulations containing mixtures of polymers and surfactants are designed for their surface properties. Consequently, studies of adsorption from polymer/surfactant mixtures at the air/water and solid/water interfaces have become increasingly common in recent decades, with several reviews discussing the behaviour of mixtures at both types of interface.[4, 46-49, 95, 96]

At the air/water interface, adsorption of both polymer and surfactant can occur below the bulk cac of the system. For non-ionic polymers, which may interact weakly with surfactant, this is usually due to the inherent surface activity of both components. However for non-surface active polyelectrolytes interfacial adsorption below the bulk cac can be attributed to interactions between the two components at the interface, which cause synergistic adsorption. For such polyelectrolyte/surfactant mixtures the adsorbed material at low bulk surfactant concentrations usually has the form of a surfactant monolayer to which polymer is associated. At higher bulk surfactant concentrations, in regions where bulk phase separation is seen (as discussed above), thicker adsorbed layers are sometimes observed. Adsorption and interaction of polymer and surfactant can be examined using a large range of techniques including surface tensiometry, ellipsometry, neutron and X-ray reflectivity, atomic force microscopy, and interfacial rheology.

Adsorption of polymer/surfactant mixtures at the solid/water interface is also widely studied owing to the wide range of applications which utilise such adsorption. Whilst at the air/water interface adsorption is determined by interactions between the polymer and surfactant in solution, at the solid/water interface interactions between the solid surface and the polymer, surfactant, polymer/surfactant complexes, and solution all affect the adsorption behaviour. The interfacial behaviour of polymer/surfactant mixtures therefore depends strongly on the nature of the surface, i.e. whether the surface exhibits hydrophobicity or hydrophilicity, and whether it is charged or not. Adsorption at hydrophobic interfaces is similar to that at the air/water interface except that the system is confined; adsorption occurs well below the cac. At a hydrophilic surface adsorption of both components does not occur until a polymer/surfactant mixture reaches its cac.

Studies of adsorption at the solid/water interface from polymer/surfactant mixtures are generally conducted in one of two ways, addition of surfactant to pre-adsorbed polymer layers,[97]or adsorption from pre-mixed polymer/surfactant solutions. In both cases the presence of surfactant has a significant effect on polymer adsorption. Sequential additions of surfactant to adsorbed polymer cause the polymer to adopt a more extended conformation away from the surface as surfactant interacts with the polymer.[98] The polymer layer can even be desorbed due to interactions with the surfactant unless the interaction between the polymer and surface is very strong. Adsorption from pre-mixed polymer/surfactant solutions will depend on the bulk phase behaviour, whether there are polymer/surfactant complexes and aggregates present in the bulk solution. The presence of surfactant only enhances adsorption at surfactant concentrations above the cac but below the bulk phase separation region, where the adsorbed amount usually decreases.[99 100] Many studies of adsorption at the solid-water interface also examine the effect of rinsing the surface, as this is relevant to many applications. In different systems this can lead to complete removal or increased deposition of material.[99] As this thesis is concerned with adsorption at the air/water interface, I will not discuss studies at the solid/water interface in the following section. More information on such studies can be found in the reviews[4, 48, 96].

In the following section, I present a survey of the main studies of adsorption from polymer/surfactant mixtures at the air/water interface; further details of the previous work performed on systems studied as part of this thesis are given in the relevant chapters.

1.4.2.1. Adsorption from Polymer/Surfactant Mixtures at the Air/Water Interface

The first systematic investigations of adsorption at the air/water interface from polymer/surfactant systems were those of Jones and Lange, who examined mixtures of non-ionic polymers with ionic surfactants using surface tensiometry.[50, 51] For such weakly interacting polymer/surfactant systems, surface tension measurements yield information about both the interfacial and bulk behaviour of the mixture, as discussed in section 1.4.1. Thomas and Penfold used neutron reflectometry (NR) to determine directly the composition of the material adsorbed at the air/water interface from mixtures of non-ionic polymers and surfactants including PEO/SDS and poly(vinyl pyrrolidone) [PVP]/SDS and to relate the composition to the surface tension behaviour of these systems.[101-103] Their data suggest that competitive adsorption occurs in these systems, with both surface-active polymer and surfactant adsorbing at low surfactant concentrations, but polymer progressively displaced from the interface with increasing surfactant coverage until it is no longer adsorbed at surfactant concentrations above the cac. Cooke *et al*. attributed this displacement of polymer to a combination of the increasing surface pressure on surfactant adsorption and bulk complex formation.[102] However, more recent studies have shown that PEO can continue to adsorb at the interface even at high surfactant coverages,[104] attributing this to the fact that only a small proportion of the monomers of a non-ionic polymer need to be adsorbed for it to remain at the interface.[105, 106]

Goddard and co-workers were the first to examine adsorption at the air/water interface from oppositely charged polymer/surfactant mixtures. [62, 107] They demonstrated that the strong electrostatic interactions between the polymer and surfactant resulted in very different adsorption behaviour to that of uncharged polymers, with surface tension data which could not be described by Jones' models. Goddard *et al*. developed a model for interfacial adsorption from strongly interacting systems which explains the observed lowering of the surface tension below the cac of the system in terms of synergistic adsorption of polymer and surfactant molecules at the interface. In this model, a monolayer of surfactant ions adsorbs at the interface and electrostatically attracts the charged polymer, which acts as counter-ions to the head-groups of the adsorbed surfactant, displacing the surfactant counter-ions from the interface. Furthermore, bulk aggregation effectively strips polymer from the interface in the phase separation region, with only surfactant adsorbing at high bulk concentrations. Interfacial adsorption of complexes which have formed in the bulk solution is not allowed for in this model.

Since the work of Goddard, several groups have examined adsorption from oppositely charged polymer/surfactant systems at the air/water interface, including a substantial body of work by the group of Thomas and Penfold using neutron reflectometry.[1, 108-118] These studies have shown that the

adsorption behaviour of such systems can be more varied than the above model suggests, depending on the nature of the two components. The work of Taylor *et al*. led to the classification of polymer/surfactant mixtures into two broad types depending on their interfacial adsorption behaviour.[49, 109, 110, 116, 117] 'Type 1' systems such as PSS/C_{12}TAB exhibit adsorption of thick layers consisting of more than a surfactant monolayer, even exhibiting multilayers in some cases. In contrast, 'Type 2' systems such as poly(dimethyldiallylammonium chloride) [PDMDAAC]/SDS adsorb with a compact layer at the interface, more characteristic of weakly interacting systems, but also exhibit a characteristic 'cliff edge peak' in the surface tension isotherm, as shown in Figure 1.6.

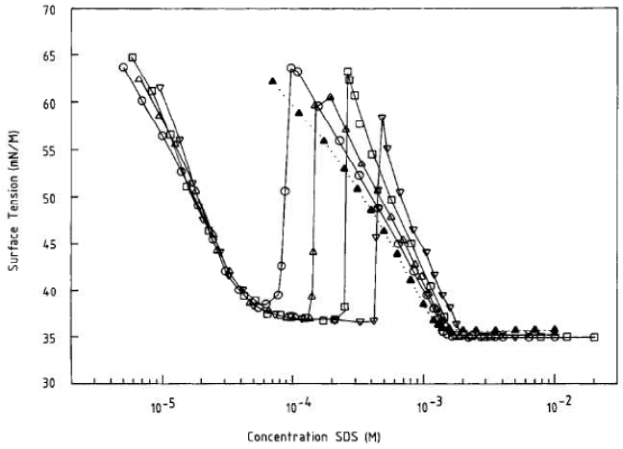

Figure 1.6. Surface tension of PDMAAC/SDS mixtures as a function of surfactant concentration reproduced from the work of Staples *et al*.[110]

The two different types of surface tension and adsorption behaviour in the work of Taylor et al were rationalized by the authors in terms of the competition between the formation of two basic types of polymer/surfactant complex, one at the interface, denoted PS_s and a polymer/micelle complex in the bulk solution, PS_M.[49, 116, 117] In order to explain multilayer adsorption they also proposed the formation of a second sub-surface complex, PS_s', which could bind to the underside of a layer of surface complexes, PS_s. The formation of PS_s' rather than bulk complexes, PS_M, was suggested to depend on the gap in stability between PS_s and PS_M being large. If the gap in stability is too small, PS_M forms at lower surfactant concentrations, and PS_s' does not form. This results not only in the formation of no interfacial multilayers but also in the depletion of polymer and/or surfactant from the interface into solution, which is associated with a peak in the surface tension. This description of adsorption has been used by Bell *et al*. as the basis of their thermodynamic model for adsorption from polymer/surfactant systems for a two-phase (air/liquid) system at equilibrium[119, 120].

Other studies performed on the systems classified as 'Type 1' and 'Type 2' by Taylor *et al*., have suggested alternative explanations for the trends in interfacial adsorbed amount and surface tension,

linking the interfacial behaviour to changes in the bulk phase behaviour including bulk aggregation, which is not included in the model discussed above. In their studies of PSS/C_nTAB mixtures, Monteux *et al*.,[121-123] and Kristen *et al*.[124] demonstrated that surface gels and foams are only stable in concentration regions where bulk precipitation does not occur. Near charge equivalence, aggregates form and films at the air/water interface collapse. Monteux *et al*. attributed this behaviour to the decrease in favourability of interfacial adsorption with increasing phase separation.[123] Following from this work, the dynamic studies of Noskov *et al*. on the same systems demonstrated a significant decrease in surface elasticity of some polymer/surfactant mixtures near the charge equivalence point of the systems, and attributed this to the formation of a heterogeneous film containing microgel particles.[125-127]

In the examination of other polymer/surfactant mixtures such as that of PEI and SDS, different interpretations of the interfacial behaviour are reached if the bulk phase behaviour is also considered. The work of Penfold *et al*. showed using NR measurements that multilayer adsorption can occur in PEI/SDS at high pH, but not at low pH.[1, 112, 113] The work of Tonigold *et al*. on the same system (albeit using a higher molecular weight polymer) showed that bulk polymer/surfactant aggregates could be incorporated into the interfacial layer. [128] At pH 4, where Penfold *et al*. observed monolayer adsorption, these aggregates were only at the interface due to the sample preparation methods and could be removed. However at pH 10, where Penfold *et al*. observed multilayer adsorption, Tonigold *et al*. demonstrated that bulk aggregates could adsorb spontaneously at the interface.[128] It is clear from the work of such as Monteux and co-workers, Noskov and co-workers, and Tonigold *et al*., that interfacial adsorption from interacting polymer/surfactant mixtures cannot, as previously discussed, be considered in isolation from their bulk phase behaviour.

The recent work of Campbell *et al*. on PDADMAC/SDS has examined the link between the bulk phase behaviour and the production of the 'cliff edge peak' in the surface tension.[129, 130] These studies demonstrated that the peak is produced by slow changes in the bulk phase behavior resulting in comprehensive precipitation of virtually all of the polymer from the liquid phase after three days. Furthermore it was also demonstrated that changes in the sample preparation or handling could result in vastly different surface tension and adsorption behaviour. In their most recent study, the authors have demonstrated that interfacial multilayers observed for this system originate from the transport of structured bulk aggregates under gravity rather than a self-assembly process initiated by the presence of the interface itself.[131] The non-equilibrium nature of this system has therefore been comprehensively and systematically demonstrated. The same authors have recently shown that a surface tension peak can form in the PSS/C_{12}TAB system in the region where bulk phase separation occurs, despite the fact

that it was classified as 'Type 1' by Taylor *et al*. (compared to the 'Type 2' classification of PDADMAC/SDS).[132] It is clear from these studies that conclusions about the interfacial adsorption mechanism cannot be reached for interacting polymer/surfactant mixtures unless the effect of the bulk phase behaviour is fully understood and controlled.

1.4.2.2. Adsorption Isotherms

The adsorption of surface active species at the air/water interface is often described by an adsorption isotherm. In order to give some context to the discussions of adsorption mechanisms of polymer/surfactant mixtures which follow in this thesis, I will briefly discuss here the basis of adsorption isotherms of pure surfactants, binary surfactant mixtures, and the possible extension to polymer/surfactant mixtures. The following discussion follows the formalism of Kralchevsky,[133] within which subscript 1 refers to surfactant ions (eg DS^-), subscript 2 to surfactant counter ions (eg Na^+), subscript 3 to added counterions (eg Cl^- from added NaCl) and subscript 4 denotes non-ionic polymer or surfactant molecules.

The simplest example of adsorption is that of a pure non-ionic surfactant, as only one species adsorbs at the interface, and its adsorption can be accounted for by the van der Waals isotherm:

$$K_4 c_4 = \frac{\alpha_{44}\Gamma_4}{1-\alpha_{44}\Gamma_4} exp\left[\frac{\alpha_{44}\Gamma_4}{1-\alpha_{44}\Gamma_4} - \frac{2\beta_{44}\Gamma_4}{k_B T}\right] \quad (1.8)$$

where K_4 is the adsorption constant, c_4 is the concentration of species, α_{44} is the excluded area per mole at the interface, Γ_4 is the surface excess of surfactant, and β_{44} is the Van der Waals interaction parameter between the non-ionic surfactant molecules. Such an isotherm has been shown in previous studies to provide a good fit to adsorption data recorded on the OFC for non-ionic surfactants.[36]

For an ionic surfactant in the absence of added salt, the binding of the counter-ion to the surfactant at the interface also needs to be accounted for in the adsorption isotherm. For this purpose, the van der Waals isotherm can be coupled to the Stern isotherm for counter-ion binding to give

$$1 + K_{St} c_{2,z=0} = \frac{\alpha_{11}(\Gamma_1-\Gamma_2)}{1-\alpha_{11}\Gamma_1} exp\left[\frac{\alpha_{11}\Gamma_{11}}{1-\alpha_{11}\Gamma_1} - \frac{2\beta_{11}\Gamma_1}{k_B T}\right] \quad (1.9)$$

$$\frac{\Gamma_1}{\Gamma_2} = \frac{K_{St} c_{2,z=0}}{1+K_{St} c_{2,z=0}} \quad (1.10)$$

Where K_{St} is the Stern constant that describes the strength of binding of the counter-ion to the surfactant monolayer, and $c_{i,Z=0}$ is not the same as c_s in the mass transport equations.

The version of the van der Waals isotherm which accounts for counter-ion binding (Equation 1.9) can then be extended to describe adsorption from a binary mixture of an ionic surfactant with a neutral surfactant or surface active polymer (such as C_{14}TAB and PEO in Chapter 5). In this model we need to add terms to account for the interactions between the two species at the interface, and the space taken up by the combination of the two species.

$$\left(1 + K_{St}c_{2,z=0}\right)K_1c_{1,z=0} = \frac{\alpha_{11}(\Gamma_1-\Gamma_2)}{1-\alpha_{11}(\Gamma_1+\Gamma_4)} exp\left[\frac{(2\alpha_{11}-\alpha)\Gamma_1+(2\alpha_{14}-\alpha)\Gamma_4}{1-\alpha(\Gamma_1+\Gamma_4)} - 2k_BT(\beta_{11}\Gamma_1 + \beta_{14}\Gamma_4)\right] \quad (1.11)$$

where β_{14} is the interaction parameter between the surfactant ions and the polymer molecules in the monolayer. α_{14} is given by

$$\alpha_{14} = \left(\frac{\alpha_{11}^{1/2}+\alpha_{44}^{1/2}}{2}\right)^2 \quad (1.12)$$

and α is the excluded area per mole, given by

$$\alpha = \alpha_{11}x_1^2 + 2\alpha_{14}x_1x_4 + \alpha_{44}x_4^2 \quad (1.13)$$

Where x_i is the mole fraction of component i in the monolayer. This approach (Equation 1.11) has been shown previously to be appropriate for a binary mixture of an ionic and a non-ionic surfactant.[36]

In order to use the approach above to account for the adsorption from a mixture of an ionic surfactant and a charged polyelectrolyte (such as PSS and C_{12}TAB in Chapter 6) in the presence of added electrolyte, we will need to account for the adsorption and interactions between five species which would significantly complicate the adsorption isotherm compared to Equation 1.11. Furthermore, the model used would depend on the assumptions or evidence for the structure of the adsorbed layer. For example, if we assume that the polymer acts only as a sub-layer to an adsorbed surfactant layer, it would take up no space at the interface. The main role of the polymer would then be to displace small ions from the surfactant layer, whilst the counter-ions would also be displaced from the polymer, and this would have to be accounted for in any calculation of the various α and β values. Conversely, if we assumed that polymer and surfactant co-adsorbed at the interface they would both take up space, and the isotherm would be dominated by firstly α for both the polymer and the surfactant, and secondly the relative sizes of the interaction parameters between the polymer and surfactant or between the surfactant or polymer molecules. In this situation the composition of the interfacial material would have to be used to determine the contribution of the small ions to the adsorption isotherm. Between the

two possibilities outlined above there are many other possible structures of the polymer/surfactant layer at the interface, which will affect the validity of any proposed adsorption isotherm for the mixture. If both the structure and composition of the material at the interface can be determined with complete certainty, it may be possible to extend the formalism of Kralchevsky to include interacting polymer/surfactant mixtures. However, as it will be seen in this thesis, it is difficult to fully determine the structure of the material which adsorbs at the interface of the OFC from interacting polymer/surfactant mixtures. As a consequence, the determination of adsorption isotherms for such mixtures is beyond the scope of the work presented in this thesis. Therefore, where it is relevant, the discussion will principally be based around assessing how the interactions between the two components affect the adsorption isotherm of each component alone.

1.4.2.3. Adsorption from Polymer/Surfactant Systems on the OFC

The research presented in this thesis examines the kinetics of adsorption of several polymer/surfactant mixtures using the overflowing cylinder. Although the majority of previous studies using the OFC have examined the adsorption dynamics of pure surfactants and surfactant mixtures,[28, 30, 32-34, 36, 134] we can use a similar approach to examine adsorption from polymer/surfactant mixtures. The main aim for each polymer/surfactant system is to determine how the presence of polymer in the system affects the adsorption of surfactant and vice-versa. Pure surfactants generally adsorb under diffusion control;[33, 134] there is no barrier to adsorption at the interface and mass transport is the rate limiting step in the adsorption process, except at close to saturation coverage where adsorption commonly deviates from diffusion control. The presence of polymer in solution with surfactant is likely to affect the kinetics of surfactant adsorption in one of two ways, enhancing adsorption due to synergistic effects at the interface, or hindering surfactant adsorption due to the formation of large polymer/surfactant complexes which diffuse more slowly to the interface than surfactant molecules. The formation of large bulk species such as aggregates in polymer/surfactant mixtures will also affect the adsorption kinetics of the system, as large species cannot reach the OFC on the timescale of surface expansion and hence any species in a bulk aggregate are unlikely to contribute to the interfacial adsorption behaviour of the system.

Noskov's group has examined dynamic adsorption from polymer/surfactant mixtures using the oscillating barrier and oscillating drop methods.[126, 127] These studies have shown that the formation of bulk aggregates causes an abrupt drop in the dynamic surface elasticity of these systems, implying that less material is adsorbed at the expanding interface. Studies using these methods are somewhat limited

to states of the interface near its static condition, unlike the OFC, which can examine polymer/surfactant adsorption under dynamic conditions closer to those under which formulations are used.

One study of the adsorption of a polymer/surfactant system on the OFC precedes this thesis, that of the strongly interacting polymer/surfactant system PDMDAAC/SDS of Campbell *et al*.[135] This study found that neither the amount nor the composition of the material at the expanding surface of the OFC bore any simple relationship to the composition of the bulk solution or that at the static air/water interface, and that no polymer adsorbed at the interface above the charge equivalence point of the system.

In this thesis, the adsorption kinetics of a range of polymer/surfactant systems are examined using the OFC in order to try to determine the mechanism of interfacial adsorption for each mixture. The hope is that in developing an understanding of the factors which control dynamic adsorption in several different systems, we will be able to begin to predict both the static and dynamic adsorption behaviour of other polymer/surfactant mixtures in the future.

1.5. References for Chapter 1

1. Penfold, J.; Tucker, I.; Thomas, R. K.; Zhang, J., Adsorption of polyelectrolyte/surfactant mixtures at the air-solution interface: Poly(ethyleneimine)/sodium dodecyl sulfate. *Langmuir* **2005,** 21, (22), 10061-10073.
2. Wang, H.; Wang, Y. L.; Yan, H.; Zhang, J.; Thomas, R. K., Binding of sodium dodecyl sulfate with linear and branched polyethyleneimines nn aqueous solution at different pH values. *Langmuir* **2006,** 22, (4), 1526-1533.
3. Venohr, H.; Fraaije, V.; Strunk, H.; Borchard, W., Static and dynamic light scattering from aqueous poly(ethylene oxide) solutions. *European Polymer Journal* **1998,** 34, (5-6), 723-732.
4. Nylander, T.; Samoshina, Y.; Lindman, B., Formation of polyelectrolyte-surfactant complexes on surfaces. *Advances in Colloid and Interface Science* **2006,** 123, 105-123.
5. Mahn Won, K., Surface activity and property of polyethyleneoxide (PEO) in water. *Colloid. Surf. A* **1997,** 128, (1-3), 145-154.
6. Rennie, A. R.; Crawford, R. J.; Lee, E. M.; Thomas, R. K.; Crowley, T. L.; Roberts, S.; Qureshi, M. S.; Richards, R. W., Adsorption of poly(ethylene oxide) at the air-solution interface studied by neutron reflection. *Macromolecules* **1989,** 22, (8), 3466-3475.
7. Henderson, J. A.; Richards, R. W.; Penfold, J.; Thomas, R. K.; Lu, J. R., Organization of poly(ethylene oxide) monolayers at the air-water interface. *Macromolecules* **1993,** 26, (17), 4591-4600.
8. Imae, T.; Ikeda, S., Sphere-rod transition of micelles of tetradecyltrimethylammonium halides in aqueous sodium halide solutions and flexibility and entanglement of long rodlike micelles. *The Journal of Physical Chemistry* **1986,** 90, (21), 5216-5223.
9. Roelants, E., De Schryver, F.C. , Parameters Affecting Aqueous Micelles of CTAC, TTAC, and DTAC probed by fluorescence quenching. *Langmuir* **1986,** 3, 209-214.
10. Mandal, A. B., Self-diffusion studies on various micelles using ferrocene as electrochemical probe. *Langmuir* **1993,** 9, (7), 1932-1933.
11. Mandal, A. B.; Nair, B. U., Cyclic voltammetric technique for the determination of the critical micelle concentration of surfactants, self-diffusion coefficient of micelles, and partition coefficient of an electrochemical probe. *The Journal of Physical Chemistry* **1991,** 95, (22), 9008-9013.
12. Atkins, P. W., *Physical Chemistry*. OUP: Oxford, 1998; Vol. 6th ed.
13. Lu, J. R.; Purcell, I. P.; Lee, E. M.; Simister, E. A.; Thomas, R. K.; Rennie, A. R.; Penfold, J., The Composition and Structure of Sodium Dodecyl-Sulfate Dodecanol Mixtures Adsorbed at the Air-Water-Interface - a Neutron Reflection Study. *J. Colloid Interface Sci.* **1995,** 174, (2), 441-455.
14. Lyttle, D. J.; Lu, J. R.; Su, T. J.; Thomas, R. K.; Penfold, J., Structure of a Dodecyltrimethylammonium Bromide Layer at the Air-Water-Interface Determined by Neutron Reflection - Comparison of the Monolayer Structure of Cationic Surfactants with Different Chain Lengths. *Langmuir* **1995,** 11, (3), 1001-1008.
15. Simister, E. A.; Thomas, R. K.; Penfold, J.; Aveyard, R.; Binks, B. P.; Cooper, P.; Fletcher, P. D. I.; Lu, J. R.; Sokolowski, A., Comparison of Neutron Reflection and Surface-Tension Measurements of the Surface Excess of Tetradecyltrimethylammonium Bromide Layers at the Air-Water-Interface. *J. Phys. Chem.* **1992,** 96, (3), 1383-1388.
16. Simister, E. A.; Lee, E. M.; Thomas, R. K.; Penfold, J., Structure of a Tetradecyltrimethylammonium Bromide Layer at the Air-Water-Interface Determined by Neutron Reflection. *Journal of Physical Chemistry* **1992,** 96, (3), 1373-1382.
17. Lu, J. R.; Hromadova, M.; Simister, E. A.; Thomas, R. K.; Penfold, J., Neutron Reflection from Hexadecyltrimethylammonium Bromide Adsorbed at the Air/Liquid Interface - the Variation of the

Hydrocarbon Chain Distribution with Surface Concentration. *Journal of Physical Chemistry* **1994,** 98, (44), 11519-11526.
18. Gilanyi, T.; Varga, I.; Stubenrauch, C.; Mészáros, R., Adsorption of alkyl trimethylammonium bromides at the air/water interface. *Journal of Colloid and Interface Science* **2008,** 317, (2), 395-401.
19. Adamson, A. W., *Physical Chemistry of Surfaces*. 5 ed.; Wiley: New York, 1990.
20. Dukhin, S. S., Kretzschmar, G., Miller., R., Eds, *Dynamics of adsorption at liquid interfaces*. Elsevier: Amsterdam, 1995.
21. Ward, A. F. H., Tordai, L.J., *J. Chem. Phys.* **1946,** 14, 453.
22. Vanvoorstvader, F.; Erkens, T. F.; Vandente.M, Measurement of Dilatational Surface Properties. *Transactions of the Faraday Society* **1964,** 60, (4986), 1170-&.
23. Johnson, D. O.; Stebe, K. J., Experimental Confirmation of the Oscillating Bubble Technique with Comparison to the Pendant Bubble Method: The Adsorption Dynamics of 1-Decanol. *Journal of Colloid and Interface Science* **1996,** 182, (2), 526-538.
24. Frese, C.; Ruppert, S.; Schmidt-LewerkÃ¼hne, H.; Wittern, K. P.; Eggers, R.; Fainerman, V. B.; Miller, R., Adsorption dynamics of micellar solutions of a mixed anionicâ€“cationic surfactant system. *Colloids and Surfaces A: Physicochemical and Engineering Aspects* **2004,** 239, (1â€“3), 33-40.
25. Danov, K. D.; Vlahovska, P. M.; Horozov, T.; Dushkin, C. D.; Kralchevsky, P. A.; Mehreteab, A.; Broze, G., Adsorption from Micellar Surfactant Solutions: Nonlinear Theory and Experiment. *Journal of Colloid and Interface Science* **1996,** 183, (1), 223-235.
26. Zhmud, B. V.; Tiberg, F.; Kizling, J., Dynamic surface tension in concentrated solutions of CnEm surfactants: A comparison between the theory and experiment. *Langmuir* **2000,** 16, (6), 2557-2565.
27. Manning-Benson, S.; Bain, C. D.; Darton, R. C., Measurement of dynamic interfacial properties in an overflowing cylinder by ellipsometry. *J. Colloid Interface Sci.* **1997,** 189, (1), 109-116.
28. Manning-Benson, S.; Parker, S. R. W.; Bain, C. D.; Penfold, J., Measurement of the dynamic surface excess in an overflowing cylinder by neutron reflection. *Langmuir* **1998,** 14, (5), 990-996.
29. Bell, G. R.; Manning-Benson, S.; Bain, C. D., Effect of chain length on the structure of monolayers of alkyltrimethylammonium bromides (C(n)TABs) at the air-water interface. *J. Phys. Chem. B* **1998,** 102, (1), 218-222.
30. Bain, C. D.; Manning-Benson, S.; Darton, R. C., Rates of mass transfer and adsorption of hexadecyltrimethylammonium bromide at an expanding air-water interface. *J. Colloid Interface Sci.* **2000,** 229, (1), 247-256.
31. Goates, S. R.; Schofield, D. A.; Bain, C. D., A study of nonionic surfactants at the air-water interface by sum-frequency spectroscopy and ellipsometry. *Langmuir* **1999,** 15, (4), 1400-1409.
32. Valkovska, D.; Wilkinson, K. M.; Campbell, R. A.; Bain, C. D.; Wat, R.; Eastoe, J., Measurement of the dynamic surface excess of the nonionic surfactant C8E4OMe by neutron reflection and ellipsometry. *Langmuir* **2003,** 19, (14), 5960-5962.
33. Battal, T.; Shearman, G. C.; Valkovska, D.; Bain, C. D.; Darton, R. C.; Eastoe, J., Determination of the dynamic surface excess of a homologous series of cationic surfactants by ellipsometry. *Langmuir* **2003,** 19, (4), 1244-1248.
34. Sekine, M.; Campbell, R. A.; Valkovska, D. S.; Day, J. P. R.; Curwen, T. D.; Martin, L. J.; Holt, S. A.; Eastoe, J.; Bain, C. D., Adsorption kinetics of ammonium perfluorononanoate at the air-water interface. *Phys. Chem. Chem. Phys.* **2004,** 6, (21), 5061-5065.
35. Campbell, R. A.; Parker, S. R. W.; Day, J. P. R.; Bain, C. D., External Reflection FTIR Spectroscopy of the Cationic Surfactant Hexadecyltrimethylammonium Bromide (CTAB) on an Overflowing Cylinder. *Langmuir* **2004,** 20, (20), 8740-8753.
36. Day, J. P. R.; Campbell, R. A.; Russell, O. P.; Bain, C. D., Adsorption kinetics in binary surfactant mixtures studied with external reflection FTIR spectroscopy. *J. Phys. Chem. C* **2007,** 111, (25), 8757-8774.

37. Battal, T.; Bain, C. D.; Weiss, M.; Darton, R. C., Surfactant adsorption and Marangoni flow in liquid jets - I. Experiments. *Journal of Colloid and Interface Science* **2003,** 263, (1), 250-260.
38. Weiss, M.; Darton, R. C.; Battal, T.; Bain, C. D., Surfactant adsorption and Marangoni flow in liquid jets. 2. Modeling. *Industrial & Engineering Chemistry Research* **2004,** 43, (17), 5203-5220.
39. Winnik, M. A.; Bystryak, S. M.; Chassenieux, C.; Strashko, V.; Macdonald, P. M.; Siddiqui, J., Study of interaction of poly(ethylene imine) with sodium dodecyl sulfate in aqueous solution by light scattering, conductometry, NMR, and microcalorimetry. *Langmuir* **2000,** 16, (10), 4495-4510.
40. Mészáros, R.; Thompson, L.; Bos, M.; Varga, I.; Gilányi, T., Interaction of sodium dodecyl sulfate with polyethyleneimine: Surfactant-induced polymer solution colloid dispersion transition. *Langmuir* **2003,** 19, (3), 609-615.
41. Cabane, B., Structure of Some Polymer Detergent Aggregates in Water. *J. Phys. Chem.* **1977,** 81, (17), 1639-1645.
42. Kuhn, P. S.; Levin, Y.; Barbosa, M. C., Complex formation between polyelectrolytes and ionic surfactants. *Chem. Phys. Lett.* **1998,** 298, (1-3), 51-56.
43. Goddard, E. D., Ananthapadmanabhan K.P. Eds. , *Interactions of Surfactants with polymers and protein*. Bocan Rotan: CRC Press: 1993.
44. Kogej, K., Skerjanz, J. , *In Surfactant Science Series, Radeva, T., Ed.* Marcell Dekker Inc.: New York, 2001; Vol. 99, p 793.
45. Holmberg, K., Jönsson, B., Kronberg, B., Lindman, B., , *Surfactants and Polymers in Aqueous Solution, 2nd ed.* John Wiley & Sons, Ltd., New York. : 2007.
46. Langevin, D., Complexation of oppositely charged polyelectrolytes and surfactants in aqueous solutions. A review. *Adv. Coll. Int. Sci.* **2009,** 147-148, 170-177.
47. Goddard, E. D., Polymer/surfactant interaction: Interfacial aspects. *J. Colloid Interface Sci.* **2002,** 256, (1), 228-235.
48. Bain, C. D.; Claesson, P. M.; Langevin, D.; Mészáros, R.; Nylander, T.; Stubenrauch, C.; Titmuss, S.; von Klitzing, R., Complexes of surfactants with oppositely charged polymers at surfaces and in bulk. *Adv. Coll. Int. Sci.* **2010,** 155, (1-2), 32-49.
49. Taylor, D. J. F.; Thomas, R. K.; Penfold, J., Polymer/surfactant interactions at the air/water interface. *Adv. Coll. Int. Sci.* **2007,** 132, (2), 69-110.
50. Jones, M. N., Interaction of Sodium Dodecyl Sulfate with Polyethylene Oxide. *J. Colloid Interface Sci.* **1967,** 23, (1), 36-42.
51. Lange, H., Interaction between Sodium Alkylsulfates and Polyvinylpyrrolidone in Aqueous Solutions. *Kolloid-Zeitschrift and Zeitschrift Fur Polymere* **1971,** 243, (2), 101-&.
52. Kwak, J. C. T. E., *Polymer-Surfactant Systems;*. Marcel Dekker, New York: 1998; Vol. 77.
53. Shiraham.K; Tsujii, K.; Takagi, T., Free-Boundary Electrophoresis of Sodium Dodecyl Sulfate-Protein Polypeptide Complexes with Special Reference to Sds-Polyacrylamide Gel-Electrophoresis. *Journal of Biochemistry* **1974,** 75, (2), 309-319.
54. Nagarajan, R., *Polym. Prepr. Am. Chem. Soc. Polym. Chem.* **1982,** 23, 41.
55. Nagarajan, R., Thermodynamics of nonionic polymerâ€"micelle association. *Colloids and Surfaces* **1985,** 13, (0), 1-17.
56. Mészáros, R.; Varga, I.; Gilányi, T., Effect of polymer molecular weight on the polymer/surfactant interaction. *J. Phys. Chem. B* **2005,** 109, (28), 13538-13544.
57. Wang, Y. L.; Han, B. X.; Yan, H.; Cooke, D. J.; Lu, J. R.; Thomas, R. K., Interaction between poly(ethylene oxide) and dodecyl sulfates with different monovalent metal counterions studied by microcalorimetry. *Langmuir* **1998,** 14, (21), 6054-6058.
58. Vanstam, J.; Almgren, M.; Lindblad, C., Sodium Dodecyl-Sulfate-Poly(Ethyleneoxide) Interactions Studied by Time-Resolved Fluorescence Quenching. In *Trends in Colloid and Interface Science V*, Dr Dietrich Steinkopff Verlag: Berlin, 1991; Vol. 84, pp 13-20.

59. Pettersson, E.; Topgaard, D.; Stilbs, P.; Soderman, O., Surfactant/nonionic polymer interaction. a NMR diffusometry and NMR electrophoretic investigation. *Langmuir* **2004,** 20, (4), 1138-1143.
60. Bernazzani, L.; Borsacchi, S.; Catalano, D.; Gianni, P.; Mollica, V.; Vitelli, M.; Asaro, F.; Feruglio, L., On the interaction of sodium dodecyl sulfate with oligomers of poly(ethylene glycol) in aqueous solution. *J. Phys. Chem. B* **2004,** 108, (26), 8960-8969.
61. Varga, I.; Gilányi, T.; Mészáros, R., Characterisation of ionic surfactant aggregates by means of activity measurements of a trace probe electrolyte. In *Adsorption and Nanostructure*, Springer Berlin / Heidelberg: 2002; Vol. 117, pp 136-140.
62. Goddard, E. D., Polymer Surfactant Interaction .2. Polymer and Surfactant of Opposite Charge. *Colloid. Surf.* **1986,** 19, (2-3), 301-329.
63. Saito, S., *Kolloid Z* **1957**, 154.
64. Von Ferber, C., Lowe, H.,, *Journal of Chemical Physics* **2003,** 118, 23.
65. Nishio, T.; Shimizu, T., Model analysis of surfactant-polymer interaction as cooperative ligand binding to linear lattice. *Biophysical Chemistry* **2005,** 117, (1), 19-25.
66. Li, Y.; Xu, R.; Couderc, S.; Bloor, D. M.; Warr, J.; Penfold, J.; Holzwarth, J. F.; Wyn-Jones, E., Structure of the complexes formed between sodium dodecyl sulfate and a charged and uncharged ethoxylated polyethyleneimine: Small-angle neutron scattering, electromotive force, and isothermal titration calorimetry measurements. *Langmuir* **2001,** 17, (18), 5657-5665.
67. Li, Y.; Ghoreishi, S. M.; Warr, J.; Bloor, D. M.; Holzwarth, J. F.; Wyn-Jones, E., Binding of sodium dodecyl sulfate to some polyethyleneimines and their ethoxylated derivatives at different pH values. Electromotive force and microcalorimetry studies. *Langmuir* **2000,** 16, (7), 3093-3100.
68. Goddard, E. D., Polymer/Surfactant Interaction - Its Relevance to Detergent Systems. *Journal of the American Oil Chemists Society* **1994,** 71, (1), 1-16.
69. Almgren, M.; Hansson, P.; Mukhtar, E.; Van Stam, J., Aggregation of alkyltrimethylammonium surfactants in aqueous poly(styrenesulfonate) solutions. *Langmuir* **1992,** 8, (10), 2405-2412.
70. Goddard, E. D., Polymer Surfactant Interaction .1. Uncharged Water-Soluble Polymers and Charged Surfactants. *Colloid Surf.* **1986,** 19, (2-3), 255-300.
71. Varga, I., Gilanyi, T., , *Prog Colloid Polym Sci.,* **2001,** 117, 136.
72. Meszaros, R.; Varga, I.; Gilanyi, T., Effect of Polymer Molecular Weight on the Polymer/Surfactant Interaction. In 2005; Vol. 109, pp 13538-13544.
73. Francois, J.; Dayantis, J.; Sabbadin, J., Hydrodynamical Behavior of the Poly(Ethylene Oxide) Sodium Dodecylsulfate Complex. *European Polymer Journal* **1985,** 21, (2), 165-174.
74. Schwuger, M. J., Mechanism of Interaction between Ionic Surfactants and Polyglycol Ethers in Water. *Journal of Colloid and Interface Science* **1973,** 43, (2), 491-498.
75. Dai, S.; Tam, K. C., Isothermal titration calorimetry studies of binding interactions between polyethylene glycol and ionic surfactants. *Journal of Physical Chemistry B* **2001,** 105, (44), 10759-10763.
76. Breuer, M. M.; Robb, I. D., Interactions between Macromolecules and Detergents. *Chemistry & Industry* **1972**, (13), 530-&.
77. Zana, R., Ionization of Cationic Micelles - Effect of the Detergent Structure. *J. Colloid Interface Sci.* **1980,** 78, (2), 330-337.
78. Fundin, J.; Brown, W., Polymer/Surfactant Interactions - Sodium Poly(Styrenesulfonate) and Ctab Complex-Formation - Light-Scattering Measurements in Dilute Aqueous-Solution. *Macromolecules* **1994,** 27, (18), 5024-5031.
79. Diamant, H.; Andelman, D., Self-assembly in mixtures of polymers and small associating molecules. *Macromolecules* **2000,** 33, (21), 8050-8061.

80. Hansson, P.; Almgren, M., Interaction of Alkyltrimethylammonium Surfactants with Polyacrylate and Poly(Styrenesulfonate) in Aqueous-Solution - Phase-Behavior and Surfactant Aggregation Numbers. *Langmuir* **1994,** 10, (7), 2115-2124.
81. Thalberg, K.; Lindman, B.; Karlstrom, G., Phase-Diagram of a System of Cationic Surfactant and Anionic Polyelectrolyte - Tetradecyltrimethylammonium Bromide Hyaluronan Water. *Journal of Physical Chemistry* **1990,** 94, (10), 4289-4295.
82. Piculell, L.; Lindman, B., Association and Segregation in Aqueous Polymer/Polymer, Polymer Surfactant, and Surfactant Surfactant Mixtures - Similarities and Differences. *Advances in Colloid and Interface Science* **1992,** 41, 149-178.
83. Bergfeldt, K.; Piculell, L.; Linse, P., Segregation and association in mixed polymer solutions from Flory-Huggins model calculations. *Journal of Physical Chemistry* **1996,** 100, (9), 3680-3687.
84. Hansson, P., Self-assembly of ionic surfactants in polyelectrolyte solutions: A model for mixtures of opposite charge. *Langmuir* **2001,** 17, (14), 4167-4180.
85. Hansson, P.; Almgren, M., Interaction of CnTAB with Sodium (Carboxymethyl)cellulose:â€‰ Effect of Polyion Linear Charge Density on Binding Isotherms and Surfactant Aggregation Number. *The Journal of Physical Chemistry* **1996,** 100, (21), 9038-9046.
86. Mészáros, R., The thermodynamic stability of the mixtures of hyperbranched poly(ethyleneimine) and sodium dodecyl sulfate at low surfactant-to-polyelectrolyte ratios. *J. Colloid Interface Sci.* **2009,** 338, (2), 444-449.
87. Mezei, A.; Abraham, A.; Pojjak, K.; Mészáros, R., The Impact of Electrolyte on the Aggregation of the Complexes of Hyperbranched Poly(ethyleneimine) and Sodium Dodecyl Sulfate. *Langmuir* **2009,** 25, (13), 7304-7312.
88. Abraham, A.; Mezei, A.; Mészáros, R., The effect of salt on the association between linear cationic polyelectrolytes and sodium dodecyl sulfate. *Soft Matter* **2009,** 5, (19), 3718-3726.
89. Thalberg, K.; Lindman, B.; Karlstrom, G., Phase-Behavior of Systems of Cationic Surfactant and Anionic Polyelectrolyte - Influence of Surfactant Chain-Length and Polyelectrolyte Molecular-Weight. *J. Phys. Chem.* **1991,** 95, (8), 3370-3376.
90. Pojjak, K.; Bertalanits, E.; Mészáros, R., Effect of Salt on the Equilibrium and Nonequilibrium Features of Polyelectrolyte/Surfactant Association. *Langmuir* **2011,** 27, (15), 9139-9147.
91. Naderi, A.; Claesson, P. M.; Bergstrom, M.; Dedinaite, A., Trapped non-equilibrium states in aqueous solutions of oppositely charged polyelectrolytes and surfactants: effects of mixing protocol and salt concentration. *Colloids and Surfaces A: Physicochemical and Engineering Aspects* **2005,** 253, 83-93.
92. Naderi, A.; Claesson, P. M., Association between Poly(vinylamine) and Sodium Dodecyl Sulfate: Effects of Mixing Protocol, Blending Procedure, and Salt Concentration. *Journal of Dispersion Science and Technology* **2005,** 26, (3), 329-340.
93. Mezei, A.; Mészáros, R.; Varga, I.; Gilanyi, T., Effect of mixing on the formation of complexes of hyperbranched cationic polyelectrolytes and anionic surfactants. *Langmuir* **2007,** 23, (8), 4237-4247.
94. Mezei, A. l.; PojjaÌk, K.; Mészáros, R., Nonequilibrium Features of the Association between Poly(vinylamine) and Sodium Dodecyl Sulfate: The Validity of the Colloid Dispersion Concept. *The Journal of Physical Chemistry B* **2008,** 112, (32), 9693-9699.
95. Penfold, J.; Thomas, R. K.; Taylor, D. J. F., Polyelectrolyte/surfactant mixtures at the air-solution interface. *Current Opinion in Colloid & Interface Science* **2006,** 11, (6), 337-344.
96. Langevin, D., Polyelectrolyte and surfactant mixed solutions. Behavior at surfaces and in thin films. *Adv. Coll. Int. Sci.* **2001,** 89, 467-484.
97. Claesson, P. M.; Fielden, M. L.; Dedinaite, A.; Brown, W.; Fundin, J., Interactions between a 30 Charged Polyelectrolyte and an Anionic Surfactant in Bulk and at a Solidâˆ'Liquid Interface. *The Journal of Physical Chemistry B* **1998,** 102, (7), 1270-1278.

98. Kjellin, U. R. M.; Claesson, P. M.; Audebert, R., Interactions between Adsorbed Layers of a Low Charge Density Cationic Polyelectrolyte on Mica in the Absence and Presence of Anionic Surfactant. *Journal of Colloid and Interface Science* **1997,** 190, (2), 476-484.
99. Terada, E.; Samoshina, Y.; Nylander, T.; Lindman, B., Adsorption of cationic cellulose derivative/anionic surfactant complexes onto solid surfaces. II. Hydrophobized silica surfaces. *Langmuir* **2004,** 20, (16), 6692-6701.
100. Terada, E.; Samoshina, Y.; Nylander, T.; Lindman, B., Adsorption of cationic cellulose derivatives/anionic surfactant complexes onto solid surfaces. I. Silica surfaces. *Langmuir* **2004,** 20, (5), 1753-1762.
101. Cooke, D. J.; Blondel, J. A. K.; Lu, J.; Thomas, R. K.; Wang, Y.; Han, B.; Yan, H.; Penfold, J., Interaction between Poly(ethylene oxide) and Monovalent Dodecyl Sulfates Studied by Neutron Reflection. *Langmuir* **1998,** 14, (8), 1990-1995.
102. Cooke, D. J.; Dong, C. C.; Lu, J. R.; Thomas, R. K.; Simister, E. A.; Penfold, J., Interaction between poly(ethylene oxide) and sodium dodecyl sulfate studied by neutron reflection. *J. Phys. Chem. B* **1998,** 102, (25), 4912-4917.
103. Purcell, I. P.; Lu, J. R.; Thomas, R. K.; Howe, A. M.; Penfold, J., Adsorption of sodium dodecyl sulfate at the surface of aqueous solutions of poly(vinylpyrrolidone) studied by neutron reflection. *Langmuir* **1998,** 14, (7), 1637-1645.
104. Darvas, M.; Gilányi, T.; Jedlovszky, P., Competitive Adsorption of Surfactants and Polymers at the Free Water Surface. A Computer Simulation Study of the Sodium Dodecyl Sulfate Poly(ethylene oxide) System. *J. Phys. Chem. B* **2011,** 115, (5), 933-944.
105. Darvas, M.; Gilányi, T.; Jedlovszky, P., Adsorption of Poly(ethylene oxide) at the Free Water Surface. A Computer Simulation Study. *J. Phys. Chem. B* **2010,** 114, (34), 10995-11001.
106. Lu, J. R.; Su, T. J.; Thomas, R. K.; Penfold, J.; Richards, R. W., The determination of segment density profiles of polyethylene oxide layers adsorbed at the air-water interface. *Polymer* **1996,** 37, (1), 109-114.
107. Goddard, E. D.; Hannan, R. B., Cationic polymer/anionic surfactant interactions. *Journal of Colloid and Interface Science* **1976,** 55, (1), 73-79.
108. Staples, E.; Tucker, I.; Penfold, J.; Warren, N.; Thomas, R. K., The structure and composition of surfactant-polymer mixtures of sodium dodecyl sulphate, hexaethylene glycol monododecyl ether and poly-(dimethyldialyl ammonium chloride) adsorbed at the air-water interface. *Journal of Physics-Condensed Matter* **2000,** 12, (28), 6023-6038.
109. Taylor, D. J. F.; Thomas, R. K.; Hines, J. D.; Humphreys, K.; Penfold, J., The adsorption of oppositely charged polyelectrolyte/surfactant mixtures at the air/water interface: Neutron reflection from dodecyl trimethylammonium bromide/sodium poly(styrene sulfonate) and sodium dodecyl sulfate/poly(vinyl pyridinium chloride). *Langmuir* **2002,** 18, (25), 9783-9791.
110. Staples, E.; Tucker, I.; Penfold, J.; Warren, N.; Thomas, R. K.; Taylor, D. J. F., Organization of polymer-surfactant mixtures at the air-water interface: Sodium dodecyl sulfate and poly(dimethyldiallylammonium chloride). *Langmuir* **2002,** 18, (13), 5147-5153.
111. Penfold, J.; Taylor, D. J. F.; Thomas, R. K.; Tucker, I.; Thompson, L. J. In *Adsorption of polymer/surfactant mixtures at the air-water interface: Ethoxylated poly(ethyleneimine) and sodium dodecyl sulfate*, Conference on Advances in the Study of Interfaes with Neutron Reflection, Grenoble, France, Oct 24-26, 2002; Amer Chemical Soc: Grenoble, France, 2002; pp 7740-7745.
112. Penfold, J.; Tucker, I.; Thomas, R. K.; Taylor, D. J. F.; Zhang, J.; Bell, C., Influence of the polyelectrolyte poly(ethyleneimine) on the adsorption of surfactant mixtures of sodium dodecyl sulfate and monododecyl hexaethylene glycol at the air-solution interface. *Langmuir* **2006,** 22, (21), 8840-8849.

113. Penfold, J.; Tucker, I.; Thomas, R. K.; Taylor, D. J. F.; Zhang, J.; Zhang, X. L., The impact of electrolyte on the adsorption of sodium dodecyl sulfate/polyethyleneimine complexes at the air-solution interface. *Langmuir* **2007,** 23, (7), 3690-3698.
114. Penfold, J.; Thomas, R. K.; Zhang, X. L.; Taylor, D. J. F., Nature of Amine-Surfactant Interactions at the Air-Solution Interface. *Langmuir* **2009,** 25, (7), 3972-3980.
115. Zhang, X. L.; Taylor, D. J. F.; Thomas, R. K.; Penfold, J., Adsorption of Polyelectrolyte/Surfactant Mixtures at the Air-Water Interface: Modified Poly(ethyleneimine) and Sodium Dodecyl Sulfate. *Langmuir* 27, (6), 2601-2612.
116. Taylor, D. J. F.; Thomas, R. K., The adsorption of oppositely charged polyelectrolyte/surfactant mixtures: Neutron reflection from dodecyl trimethylammonium bromide and sodium poly(styrene sulfonate) at the air/water interface. *Langmuir* **2002,** 18, (12), 4748-4757.
117. Taylor, D. J. F.; Thomas, R. K.; Li, P. X., Adsorption of oppositely charged polyelectrolyte/surfactant mixtures. Neutron reflection from alkyl trimethylammonium bromides and sodium poly(styrenesulfonate) at the air/water interface: The effect of surfactant chain length. *Langmuir* **2003,** 19, (9), 3712-3719.
118. Penfold, J.; Taylor, D. J. F.; Thomas, R. K.; Tucker, I.; Thompson, L. J., Adsorption of polymer/surfactant mixtures at the air-water interface: Ethoxylated poly(ethyleneimine) and sodium dodecyl sulfate. *Langmuir* **2003,** 19, (19), 7740-7745.
119. Bell, C. G.; Breward, C. J. W.; Howell, P. D.; Penfold, J.; Thomas, R. K., Macroscopic modeling of the surface tension of polymer-surfactant systems. *Langmuir* **2007,** 23, (11), 6042-6052.
120. Bell, C. G.; Breward, C. J. W.; Howell, P. D.; Penfold, J.; Thomas, R. K., A theoretical analysis of the surface tension profiles of strongly interacting polymer-surfactant systems. *J. Colloid Interface Sci.* **2010,** 350, (2), 486-493.
121. Monteux, C.; Williams, C. E.; Meunier, J.; Anthony, O.; Bergeron, V., Adsorption of oppositely charged polyelectrolyte/surfactant complexes at the air/water interface: Formation of interfacial gels. *Langmuir* **2004,** 20, (1), 57-63.
122. Monteux, C.; Llauro, M. F.; Baigl, D.; Williams, C. E.; Anthony, O.; Bergeron, V., Interfacial microgels formed by oppositely charged polyelectrolytes and surfactants. 1. Influence of polyelectrolyte molecular weight. *Langmuir* **2004,** 20, (13), 5358-5366.
123. Monteux, C.; Williams, C. E.; Bergeron, V., Interfacial microgels formed by oppositely charged polyelectrolytes and surfactants. Part 2. Influence of surfactant chain length and surfactant/polymer ratio. *Langmuir* **2004,** 20, (13), 5367-5374.
124. Kristen, N.; Vullings, A.; Laschewsky, A.; Miller, R.; von Klitzing, R., Foam Films from Oppositely Charged Polyelectolyte/Surfactant Mixtures: Effect of Polyelectrolyte and Surfactant Hydrophobicity on Film Stability. *Langmuir* 26, (12), 9321-9327.
125. Noskov, B. A.; Loglio, G.; Miller, R., Dilational surface visco-elasticity of polyelectrolyte/surfactant solutions: Formation of heterogeneous adsorption layers. *Adv. Coll. Int. Sci.* **2011,** 168, (1â€“2), 179-197.
126. Noskov, B. A.; Grigoriev, D. O.; Lin, S. Y.; Loglio, G.; Miller, R., Dynamic surface properties of polyelectrolyte/surfactant adsorption films at the Air/Water interface: Poly(dially1dimethylammonium chloride) and sodium dodecylsulfate. *Langmuir* **2007,** 23, (19), 9641-9651.
127. Noskov, B. A.; Loglio, G.; Miller, R., Dilational viscoelasticity of polyelectolyte/surfactant adsorption films at the air/water interface: Dodecyltrimethylammonium bromide and sodium poly(styrenesulfonate). *J. Phys. Chem. B* **2004,** 108, (48), 18615-18622.
128. Tonigold, K.; Varga, I.; Nylander, T.; Campbell, R. A., Effects of Aggregates on Mixed Adsorption Layers of Poly(ethylene imine) and Sodium Dodecyl Sulfate at the Air/Liquid Interface. *Langmuir* **2009,** 25, (7), 4036-4046.

129. Campbell, R. A.; Angus-Smyth, A.; Arteta, M. Y.; Tonigold, K.; Nylander, T.; Varga, I., New Perspective on the Cliff Edge Peak in the Surface Tension of Oppositely Charged Polyelectrolyte/Surfactant Mixtures. *J. Phys. Chem. Letts.* **2010,** 1, (20), 3021-3026.
130. Campbell, R. A.; Yanez Arteta, M.; Angus-Smyth, A.; Nylander, T.; Varga, I., Effects of Bulk Colloidal Stability on Adsorption Layers of Poly(diallyldimethylammonium Chloride)/Sodium Dodecyl Sulfate at the Air/ater Interface Studied by Neutron Reflectometry. *J. Phys. Chem. B* **2011,** 115, (51), 15202-15213.
131. Campbell, R. A.; Yanez Arteta, M.; Angus-Smyth, A.; Nylander, T.; Varga, I., Multilayers at Interfaces of an Oppositely Charged Polyelectrolyte/Surfactant System Resulting from the Transport of Bulk Aggregates under Gravity. *The Journal of Physical Chemistry B* **2012,** 116, (27), 7981-7990.
132. Campbell, R. A., Personal Correspondance. In August 2012.
133. Kralchevsky, P. A.; Danov, K. D.; Kolev, V. L.; Broze, G.; Mehreteab, A., Effect of Nonionic Admixtures on the Adsorption of Ionic Surfactants at Fluid Interfaces. 1. Sodium Dodecyl Sulfate and Dodecanol. *Langmuir* **2003,** 19, (12), 5004-5018.
134. Valkovska, D. S.; Shearman, G. C.; Bain, C. D.; Darton, R. C.; Eastoe, J., Adsorption of ionic surfactants at an expanding air-water interface. *Langmuir* **2004,** 20, (11), 4436-4445.
135. Campbell, R. A.; Ash, P. A.; Bain, C. D., Dynamics of adsorption of an oppositely charged polymer-surfactant mixture at the air-water interface: Poly(dimethyldiallylammonium chloride) and sodium dodecyl sulfate. *Langmuir* **2007,** 23, (6), 3242-3253.

Chapter 2 . Experimental Techniques & Theory

2.1. Overflowing Cylinder

The overflowing cylinder (OFC) is a sample environment which creates a continuously expanding air/liquid interface. In an OFC, liquid flows up an inner cylinder and overflows its rim to be collected in an outer cylinder from where it is recycled by a pumping system. The interface expands radially from a central stagnation point towards the rim of the inner cylinder. Surface-active material which reaches the interface of the OFC can adsorb at the interface, however surface expansion causes adsorbed material to be continuously lost and replaced by other material, so that the adsorbed amount remains constant. The continuous adsorption and loss of material at the interface means that the OFC can be used as a platform for the study of adsorption kinetics of systems containing surface-active species. Examination of the adsorbed amount of material at the expanding interface enables us to obtain information about the mass transport and species in the bulk solution.

Figure 2.1. Photograph of the overflowing cylinder used in this work in situ on the neutron beamline FIGARO.

The steady-state nature of the interface of the OFC, along with the size of the interface created (80 mm in diameter) enables adsorption kinetics to be studied on the OFC using a wide range of experimental techniques. These include laser Doppler velocimetry[1], ellipsometry[2, 3], surface light scattering[3], external reflection Fourier transform Infra-red spectroscopy, (ER-FTIRS)[4], and neutron reflectometry[5, 6]. The OFC has been extensively employed in the Bain group to study the dynamic adsorption of many different systems using different combinations of these techniques. The systems

examined include the cationic alkyltrimethyl ammonium bromide surfactants (C_nTABs),[1, 7] ammonium perfluorononanoate (APFN),[6] non-ionic alkyl poly(ethylene glycol) ethers (C_nE_ms),[8] mixtures of surfactants[4] and polymer/surfactant mixtures.[9]

The original OFC was designed at the Kodak laboratories by Padday[10], and by Ferroni and Piccardi[11], as a method of studying dynamic liquid systems, using a Wilhelmy plate to measure the dynamic surface tension. More recently, Manning-Benson et al[12] altered the original OFC designs in order to use it in the study of adsorption kinetics of surfactants. The OFC used in the experiments presented in this thesis is very similar to the one designed by Manning-Benson, with only a few minor modifications. This OFC was commissioned for use at the Institut Laue-Langevin (ILL) both in the lab and on the NR beamline FIGARO, and is currently offered to users as a sample environment for their studies. A photograph of the OFC used in this study in situ on FIGARO is shown in Figure 2.1, and a schematic representation of the OFC is given in Figure 2.2.

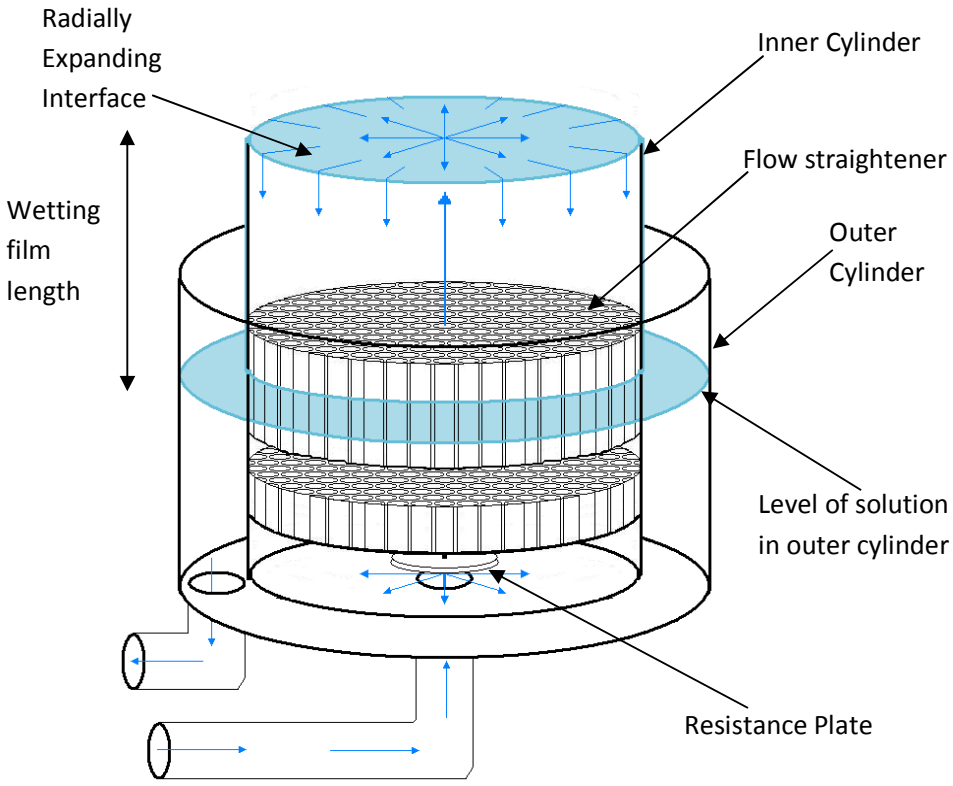

Figure 2.2. Schematic of the overflowing cylinder showing specific design features. The arrows blue arrows within the diagram indicate the direction of liquid flow.

The OFC consists of two concentric cylinders of stainless steel. Within the inner cylinder, the combination of a Teflon flow straightener punched with evenly spaced, 3-mm holes and a small

circular resistance plate ensures an even flow profile through the cylinder. The cylinder is carefully leveled so that it overflows uniformly in all directions. The OFC is connected by Teflon tubing to a magnetic drive pump and two glass reservoirs. Reservoirs facilitate both the decoupling of pump vibrations from the cylinder, and control of the flow rate in the system. The flow rate was kept constant for all experiments, above the threshold value of around 15 cm^3s^{-1} at which the surface properties become independent of the flow rate[13, 14] (this decoupling of the surface and bulk flows in the presence of surfactants is a remarkable feature of the OFC that remains unexplained). The wetting length on the outside of the inner cylinder, l_h, (as marked in Figure 2.2) was chosen to be large enough that the water in the moat around the inner cylinder does not influence the flow at the surface of the OFC (l_h> 40 mm[13]).

The whole system has been designed to be able to run on around 1.25 l, the minimum amount possible whilst still maintaining the same cylinder dimensions. Use of a minimum system volume is very important for NR experiments which involve the use of expensive deuterated materials. Smaller OFCs have been used previously[9], and the interfacial properties have been shown to be independent of the cylinder dimensions[13], however use of a smaller OFC gives rise to compromises in available flat area of the interface for study and this compromises the performance of NR measurements. On the OFC used in this study, the interface is flat over the central 30 mm for pure water, the most domed solution, as shown by data in Figure 3.12 in Chapter 3. Furthermore, the surface coverage, Γ, is a quadratic function of the radial position (r),[5, 15] hence the variation in properties with r near the centre of the cylinder is small. For the surfactant C_{16}TAB, Γ has been shown to change by less than 5% of a monolayer over the central 40 mm of the cylinder.[13] The combination of the flatness of the central area of the interface with the minimal variation in surface coverage in the same region makes the OFC ideal for study using techniques requiring a large surface area such as NR as well as other techniques. In this work, adsorption at the interface of the OFC is studied using a combination of ellipsometry, neutron reflectometry and laser Doppler velocimetry (LDV).

The OFC expands radially from the central stagnation point, with a rate of surface expansion $\theta = \mathrm{d} \ln A / \mathrm{d}t$, where A is the area of an element of the surface. For 2-D radial flow the surface expansion rate can be expressed in terms of the change in radial velocity, v_r, with radial position,

$$\theta = r^{-1} \frac{\mathrm{d}(r v_r)}{\mathrm{d}r} \tag{2.1}$$

For pure water θ depends on the flow rate, but is around 0.6 s^{-1} for the flow rates used in this study. The presence of surfactant in the solution induces surface tension gradients, $\mathrm{d}\sigma/\mathrm{d}r$, which induce radial

flows at the interface due to the Marangoni effect. This causes a tenfold increase in v_r with the radial position. This causes higher surface expansion rates (θ), typically 1 – 7 s^{-1}. The radial velocity v_r was measured as a function of r using laser Doppler velocimetry (LDV) as described in Section 2.2, and these values were used in Equation 2.1 to calculate θ. Further details of the fluid dynamics of the OFC are described elsewhere,[14, 16] and will not be replicated at length in this thesis.

The adsorption of material at the interface of the OFC is controlled by convection and mass transport to the region near to the interface and by the likelihood of adsorption from the sub-surface region. The quantitative model of the convection and mass transport of material to the interface of the OFC of Bain et al is similar to that of van Voorst Vader et al.[16, 17], and is based on the principle that the adsorbed material lost from the interface through surface expansion is balanced by transport of molecules to the sub-surface by convection and diffusion.

Mass transport of material in an OFC obeys the standard convection-diffusion equation, which for a non-ionic surfactant below the cmc can be written as

$$\frac{\partial c}{\partial t} = D\nabla^2 \mathrm{c} - \mathrm{v} \,.\, \nabla \mathrm{c}, \qquad (2.2)$$

where c and D are the concentration and diffusion coefficient of the surfactant and **v** is the fluid velocity. For an ionic surfactant this equation would also need to contain terms for the counterions and co-ions, and in a polymer/surfactant mixture, a further term for the polymer would also be necessary. However here, to explain the principle, I am only considering the most simple situation, adsorption from a solution containing only one species: a non-ionic surfactant.

In the OFC the concentration gradients are much smaller in the radial than in the axial (z) direction, hence transport in the radial direction can be neglected. At steady state $\partial c/\partial t = 0$. With use of the continuity equation, $\nabla . \mathrm{v} = 0$, and the boundary condition $\mathrm{v_z} = 0$ at z = 0 (where z is the normal to the surface) which eliminates the convective term, gives

$$v_r = \theta r/2 \qquad \text{and} \qquad v_z = -\theta z \quad . \qquad (2.3.)$$

Substituting into Equation 2.2 gives

$$D\frac{d^2c}{dz^2} + \theta z \frac{dc}{dz} = 0. \qquad (2.4.)$$

Expansion of the interface causes a decrease in the dynamic surface excess of the surfactant, Γ_{dyn}, which is replenished by diffusion to the interface. At steady-state these two fluxes are equal:

$$\Gamma\theta = -D\left(\frac{\delta c}{\delta z}\right)_{z=0}. \quad (2.2)$$

Solving equation 2.4 subject to the boundary condition 2.5[16-18] gives

$$\Gamma_{dyn} = \sqrt{\frac{2D}{\pi\theta}}\,(c - c_s) \quad (2.3)$$

where c_s is the subsurface concentration. All of the quantities in Equation 2.6 can be measured experimentally except c_s, which is calculated using the experimental values of the other variables and used to analyse the adsorption kinetics of the system.

For an ionic surfactant in the absence of salt, the self-diffusion coefficient in Equation 2.6 is replaced by the mutual diffusion coefficient. With excess salt (as in the experiments here) D reverts to the self-diffusion coefficient since the electrolyte eliminates the migration fields. For a mixture of non-interacting monomeric components, Equation 2.6 applies to each of the components in the mixture.[19] For a surfactant solution above the cmc, the adsorption model must also account for the diffusion of micelles and monomers and their interconversion.[20, 21] Valkovska et al developed a quantitative methodology for the calculation of the effective diffusion coefficient of surfactants in a solution in which the bulk concentration is above the cmc, assuming fast interconversion of micelles and monomers In this work we will develop an adsorption model to account for the adsorption from mixtures of polymers and surfactants, which form complexes in solution above the critical aggregation concentration as an extension of the approach of Valkovska et al to the modeling of adsorption from micellar surfactant systems. This approach will be discussed at length in Chapter 6.

Adsorption is described as being under diffusion, kinetic, or mixed kinetic/diffusion control depending on whether the overall rate of adsorption is dictated by mass transport, i.e. diffusion, convection, and migration in the bulk phase, or by the free energy barrier for adsorption to the interface. Under diffusion control, adsorbed surfactant is locally in equilibrium with surfactant in the sub-surface region, and the relationship between the dynamic surface excess, Γ_{dyn}, and the sub-surface concentration, c_s, is equivalent to that between the equilibrium surface excess, Γ_{dyn}, and the bulk surfactant concentration, c_b, $\Gamma_{dyn}(c_s) = \Gamma_{eq}(c_b)$. For a pure surfactant adsorbing under diffusion control, saturation coverage of the interface of the OFC ($\Gamma_{max,dyn} = \Gamma_{max,eq}$) is not reached until the sub-surface concentration of surfactant, c_s, reaches the cmc, which does not occur until the bulk surfactant concentration, c_b, is significantly above the cmc on the OFC. We can determine whether adsorption of a surfactant on the OFC is under diffusion control by comparing $\Gamma_{dyn}(c_s)$ determined on the OFC using Equation 2.6 with an equilibrium isotherm, $\Gamma_{eq}(c_b)$, determined for the same system. This approach is used in Chapter 5 of this thesis for simple polymer/surfactant systems. An alternative approach in the

absence of an appropriate adsorption isotherm is comparison of the Γ_{dyn} data to the calculated amount of material which would adsorb under diffusion control, which can be approximated using Equation 2.6 and setting $c_s = 0$. This assumption can only be made when the surface is far from equilibrium, and there is no barrier to adsorption of material from the diffusion layer, as this results in $\Gamma_{dyn} << \Gamma_{eq}$ and therefore in Equation 2.6 $c_s << c_b$, and hence we can replace c_b-c_s with c_b (i.e. $c_s = 0$).

Two further possibilities exist for adsorption from a pure surfactant solution, if the barrier to adsorption from the subsurface layer to the interface is rate-determining, then $c_s = c_b$ and diffusion plays no part in the adsorption kinetics. If the system is under mixed kinetic/diffusion control, c_s is greater than it would be for a given Γ when the system is under diffusion control, but less than c_b. A barrier to adsorption may arise from (i) a lack of empty sites at the interface, (ii) re-orientation of the surfactant for adsorption, (iii) electrostatic or steric repulsions, or (iv) slow break-up of micelles.

Although the above discussion is appropriate for the examination of surfactant adsorption, adsorption from mixtures of polymers and surfactants is more complicated due to interactions between the two components. We can consider the factors which affect adsorption from mixtures by analogy to the study of Day et al of adsorption from mixed surfactant systems on the OFC.[19] This study showed that even in a non-interacting system, the surface composition does not generally reflect the bulk composition for a combination of thermodynamic reasons (one component is more surface active than the other) and kinetic reasons (one surfactant diffuses faster than the other). In Chapter 5, I will examine the kinetics of adsorption of non- and weakly-interacting polymer/surfactant systems. If there are interactions between the components in the system, one additionally needs to know the interaction parameters at the surface and, if applicable, in micelles (or polymer/surfactant complexes): the resulting adsorption kinetics can become very complicated. [22, 23] In Chapters 6 and 7, I will examine the kinetics of adsorption of interacting polymer/surfactant mixtures by extension from the principles of Day et al[19] and Valkovska et al[20] as discussed above.

2.2. Laser Doppler Velocimetry (LDV)

Laser Doppler velocimetry (LDV) is used to determine the radial velocity profile and thus the surface expansion rate (θ) of a solution on the OFC.[16] The surface expansion rate is related to the surface velocity, v_r, and radial position, r, by [14]

$$\theta = \frac{\mathrm{d}\ln A}{\mathrm{d}t} = \frac{v_r}{r} + \frac{dv_r}{dr}. \quad (2.4)$$

In LDV a laser beam is split into two equal parts which are then re-focussed on the same point at the surface of the OFC. An interference pattern is set up where the two beams cross. The spacing of the fringes in this pattern is given by

$$d = \frac{\lambda}{2\sin\phi/2} \quad (2.5)$$

where ϕ is the half angle between the laser beams. For the measurements made in this thesis the half angle of crossing is 26.6°, and the plane of crossing was tilted 15 degrees from the horizontal. For LDV measurements at the interface of the OFC the fringes are set up perpendicular to the radial vector, so that material at the expanding interface passes through them. The solution is seeded with microscopic particles which pass through the fringes and scatter light with an intensity modulated at a frequency (f) determined by the spacing of the fringes and the speed of the particles perpendicular to the fringes (v_r):

$$f = \frac{2v_r\sin\phi}{\lambda} \quad (2.6)$$

Light scattered from particles passing through the interference pattern is recorded using a photomultiplier tube and these signals are Fourier transformed into a plot of intensity against frequency.

In the LDV measurements made as part of this thesis, a HeNe laser was used, and TiO_2 particles (2μm, 99%+ rutile, from Alfa) were used to seed the solution, as they do not interact with the polymer or surfactant, and are not surface active. The measured Fourier transformed signals were averaged over 100 scans and the frequency corresponding to the highest peak was converted into a surface velocity using Equation 2.9.

Previous studies have shown that v_r changes significantly with the depth of the focus below the interface[16] To confirm that measurements are made at the interface, the focus is lowered from above the surface until the first peaks in the Fourier transformed signal are observed.

To obtain θ from v_r, the frequency (and hence the surface velocity) is recorded as a function of radial position over a distance of up to 20 mm either side of the central stagnation point. Figure 2.3 shows the interference signal which results from a particle passing through the interference fringes at the interface of the OFC. This signal is Fourier transformed to obtain the frequency of the particle, and an average is taken over 100 sweeps.

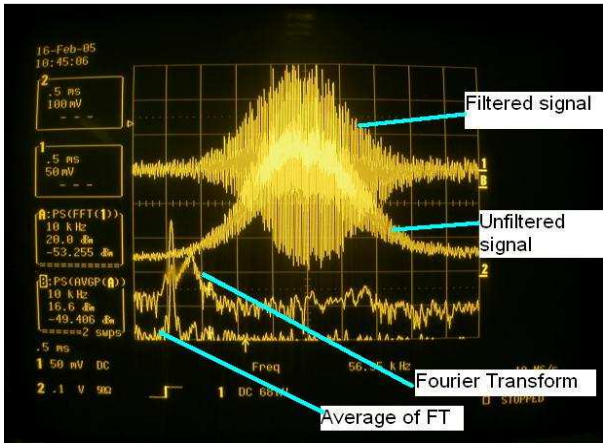

Figure 2.3. Photograph of the screen of the oscilloscope during LDV measurements, showing the signal which arises from a particle passing through the interference fringes along with the Fourier transform of this signal, and the average of these Fourier transforms over multiple signals.

The measured frequency is converted into the surface velocity, v_r, using Equation 2.9, and v_r is then plotted as a function of the radial position, as shown in Figure 2.4.

The surface expansion rate is obtained from the data in Figure 2.4 from a fit to the v_r v r data, using a cubic function, $v_r = a_1 + a_3 r^3$. This can be combined with Equation 2.7 to give a function for θ in terms of r:

$$\theta = 2a_1 + 3a_3 r^2 \qquad (2.10)$$

From the data in Figure 2.4 we can see that the cubic function can be neglected over the central region, as the relationship between v_r and r is linear. This is the region over which NR measurements are made (as discussed in Chapter 3). At the centre of the cylinder the surface expansion rate is therefore given by $\theta = 2a_1$.

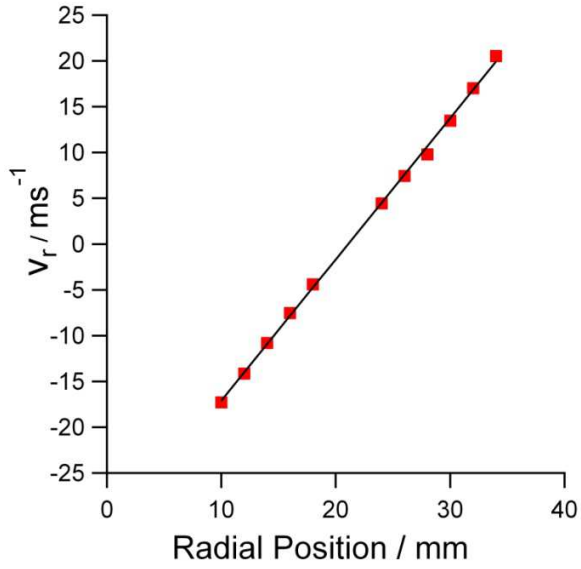

Figure 2.4. Radial velocity as a function of radial position as recorded on 0.9 mM C_{12}TAB with 0.1 M NaBr. The v_r values one one side of the cylinder are plotted as negative (although negative velocities are not measured) in order to allow a line to be fitted through all of the data, and to allow for an offset in the position of the cylinder centre from 20 mm.

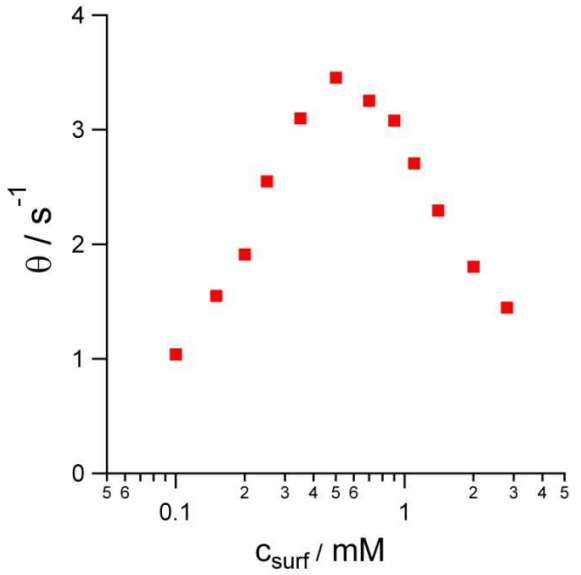

Figure 2.5. Surface expansion rate (θ) against bulk surfactant concentration of C_{12}TAB in the presence of 0.1 M NaBr. These data were measured as part of the work in this thesis, and are used in discussions in Chapters 6 and 7.

For a given system, the surface expansion rate is usually measured as a function of surfactant concentration, and for pure surfactant solutions the shape of θ v c_{surf} is typically a 'volcano plot',[20] as shown in Figure 2.5. The shape of the volcano can be qualitatively explained in terms of the ability of the surface to sustain surface tension gradients. At low bulk surfactant concentrations the surfactant

coverage is too low to cause significant deviations in the surface tension from that of pure water, hence no surface tension gradients accelerate the surface. At high surfactant concentrations the surface coverage is high and mass transport to the interface becomes fast compared to θ, hence the surface is unable to sustain surface tension gradients due to the rapid transport of surfactant from the bulk to the interface. Consequently as the surface reaches saturation ($\Gamma_{dyn} \rightarrow \Gamma_{max}$), the sub-surface concentration c_s in Equation 2.7 approaches the bulk surfactant concentration. The largest Marangoni effects (resulting in the highest expansion rates) occur at bulk compositions where small changes in the coverage lead to big changes in the surface tension. Deviations from the classical volcano plot shape for pure surfactants or polymer/surfactant mixtures as studied here, may arise from kinetic barriers to adsorption which prevent the surface from reaching local equilibrium, or from changes in the adsorption mechanism.

2.3. Ellipsometry

2.3.1. Principles of Reflection of Light

Before discussing the theory behind the technique of ellipsometry I will first discuss the principles of the reflection of light from an interface. This explanation serves a dual purpose, as due to wave-particle duality, neutron reflectometry can be explained using similar principles, as I will discuss in Chapter 3.

The propagation of light through a medium is given by the refractive index of the medium, n. Fundamentally, n is defined as the factor by which the wavelength, λ, and velocity, v, of light are reduced in a medium with respect to their values in a vacuum. The speed of light in a medium is given by $v = c/n$, where c is the speed of light in a vacuum. This implies that a vacuum has a refractive index of one. The refractive index of materials varies with the wavelength of the incident light. In absorbing media, the refractive index is a complex number where the real part described refraction and the imaginary part accounts for adsorption. However, none of the materials examined as part of this project adsorb either visible or neutron wavelengths to a significant extent, and hence only real refractive indices (or neutron scattering length densities) will be considered here.

When light travels between two different media, it changes direction, i.e. it is refracted. The relationship between the angle of incidence, θ_i, the angle of refraction θ_j, and the refractive indices of the incident and transmitting media (n_i and n_j respectively) is given by Snell's law

$$n_i \sin\theta_i = n_j \sin\theta_j \qquad (2.11)$$

When light is incident at an ideal (by which I mean laterally homogeneous, isotropic, planar and with zero roughness) interface between two media, not all of it is transmitted into the second medium, some of it is reflected, as shown schematically in Figure 2.6. As light is specularly reflected from the interface, the incident and reflected angles are equal, $\theta_i = \theta_r$. If $n_i > n_j$ the reflection at the interface is termed 'internal reflection' and if $n_i < n_j$ 'external reflection' occurs.

The extent to which light is reflected from the interface or transmitted into the second medium can be calculated using Fresnel's equations. However, the calculations of Fresnel's coefficients depend on the polarisation of light, hence we will first discuss the polarisation of light.

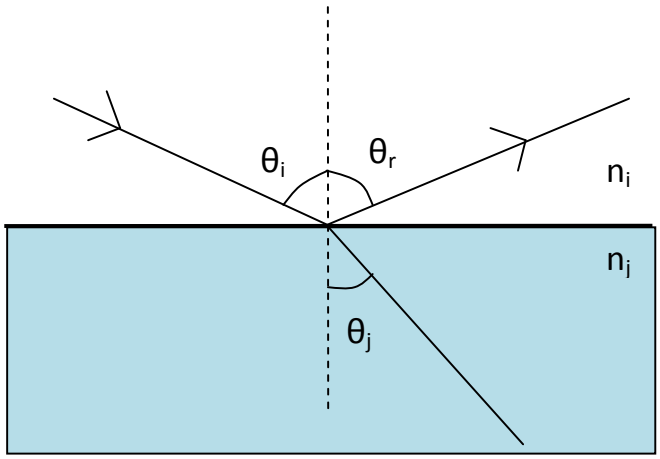

Figure 2.6. Schematic showing the geometry of reflection of light from an interface following Snell's law, $n_i \sin\theta_i = n_j \sin\theta_j$, where $\theta_i = \theta_r$ and $n_j > n_i$

Unpolarised light has an equal distribution of electric field orientations in all directions. Light can be linearly polarised so that its electric vector is confined to one plane, perpendicular to the direction of travel. When light strikes a surface at a non-perpendicular angle, the reflection and transmission characteristics depend upon the direction of its planar polarisation. In order to discuss this it is simplest to define a co-ordinate system by the plane of the interface, and a plane perpendicular to the interface which contains the incident and reflected beams, the plane of incidence. Plane polarised light with its electric field vector in the plane of incidence is defined as p-polarised light, whilst plane polarised light with its electric field vector perpendicular to the plane of incidence (into and out of the page in Figure 2.7) is defined as s-polarised light.

The (complex) amplitude of the reflected beam relative to the incident beam (denoted r_p and r_s for p and s polarised light, respectively) is given by Fresnel's equation

$$r_{ij,p} = \frac{n_j \cos\theta_i - n_i \cos\theta_j}{n_i \cos\theta_j + n_j \cos\theta_i} \quad \text{and} \quad r_{ij,s} = \frac{n_i \cos\theta_i - n_j \cos\theta_j}{n_i \cos\theta_i + n_j \cos\theta_j} \tag{2.12}$$

The reflectivity, R, is the square of the amplitude of the Fresnel co-efficient, $R = |r|^2$.

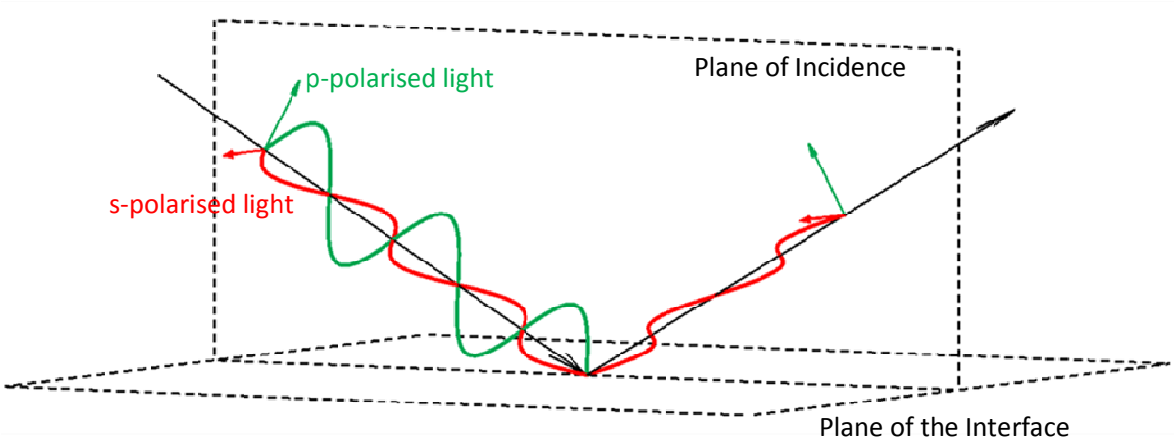

Figure 2.7. Schematic diagram to show the directions of s and p-polarised light in the incident beam, as well as the reflected beam at the Brewster angle, as discussed below.

The principles of reflection described above apply to a single ideal interface between two media with no adsorbed layer. For a single thin film at the air/water interface, such as a surfactant monolayer, reflection can be approximated as occurring from two interfaces, above and below the film. A three-layer model can then be used to describe such a layer, where layer 1 is the air, layer 2 is the monolayer, and layer 3 is the solution, the reflectivity R_{123} is then given by

$$R_{123} = |r_{123}|^2 = \frac{{r_{12}}^2 + {r_{23}}^2 + 2r_{12}r_{23}cos2\beta}{1 + {r_{12}}^2{r_{23}}^2 + 2r_{12}r_{23}cos2\beta} \tag{2.13}$$

where β is the change in phase of a wave which has travelled twice obliquely through the layer

$$\beta = \left(\frac{2\pi}{\lambda_1} n_2 h cos\theta_2\right) \tag{2.14}$$

where h is the layer thickness, and λ is the wavelength of the incoming light. For the purposes of these discussions we will assume that the layers are optically isotropic, and hence that they have a unique refractive index (as in Equations 2.12-2.14). This assumption is appropriate within the thin film limit, where the film thickness is much smaller than the wavelength of incident light, and not greater than a few tens of nm, as discussed below. If we were not in the thin film limit an optical matrix model[24] is

commonly used to model stratified media consisting of more than three layers. This approach is unnecessary to account for our ellipsometry measurements, although it will be discussed further in the context of NR measurements in Chapter 3.

2.3.2. Principles of Ellipsometry

Ellipsometry can be used to characterise layers and films, both at the air/water interface and on solid substrates. Ellipsometry involves the reflection of a beam of light of known polarisation from an interface. Interaction of light with the interface causes a change in polarisation on reflection. The polarisation of the reflected light is then measured, and the change can be used to deduce the optical properties of the layer, the thickness and refractive index, the latter of which can give us an indication of the amount of material of known refractive index adsorbed at the interface. For thin films only one optical property of the layer can be determined from ellipsometry measurements (as discussed below), and this relates to the total surface excess of a single component. An incoming beam which is polarised at 45° to the plane of incidence has equal amplitudes of incoming s and p waves, the polarisation of each of which is changed to different extents upon reflection, depending on the refractive index and thickness of an isotropic layer. Ellipsometry measures the reflectivity ratio, $r = r_p/r_s$.

Ellipsometry measurements commonly record the amplitude (Ψ) and the phase shift (Δ) of r: [25]

$$r = \frac{\widehat{r_p}}{\widehat{r_s}} = tan\Psi expi\Delta = tan\Psi(cos\Delta + isin\Delta) \quad (2.15)$$

Many studies use ellipsometry to determine the film thickness, d, the refractive index, n, and the extinction co-efficient, k, of thick films and adsorbed layers by measurement of r as a function of either θ or λ, and fitting d, n, and k to Equation 2.13. From these parameters, an estimation of the surface excess, Γ, can be made from the de Feijter's formula for films adsorbed from the bulk solution (not spin coated films etc) from

$$\Gamma = \frac{(n_{layer} - n_{soln})}{dn/dc} d \quad (2.16)$$

where dn/dc is the refractive index increment as a function of the bulk concentration.

If an interface is ideal and n_i and n_j are real, then there is an incident angle at which p polarised light is totally transmitted and the reflection coefficient for p-polarised light, r_p, vanishes. This angle is known as the Brewster angle, θ_B. For a real interface there is no angle where r_p vanishes and the Brewster

angle is defined as the angle where the real part of r vanishes: $\mathrm{Re}(r_p/r_s) = 0$, The imaginary part of r at the Brewster angle is known as the co-efficient of ellipticity, $\bar{\rho}$

$$Im\left(\frac{\hat{r}_p}{\hat{r}_s}\right) = tan\Psi sin\Delta = \bar{\rho} \qquad (2.17)$$

The coefficient of ellipticity can be considered to be a measurement of the deviation from ideality of the interface.

At the air/liquid interface Ψ is very insensitive to the optical properties of the thin film, therefore many studies of layers at the air/water interface simply present measurements of Δ at a given incident angle. In this work we perform our measurements at the Brewster angle of water, 53.1° at the wavelength of a HeNe laser 632.8 nm, and therefore instead present our data in terms of the co-efficient of ellipticity, $\overline{\rho}$. The measured quantity, $\overline{\rho}$, the coefficient of ellipticity, can be related to the amount of material at the interface, although the relationship between the two is not necessarily simple.[26] For a single component system such as a surfactant monolayer, approximate values of Γ can be obtained from $\overline{\rho}$ using a simple calibration function, as discussed later.

Ellipsometry is a very convenient and accurate tool for the examination of material adsorbed at the interface of the OFC, as it is quick, local and extremely precise, with precision to < 0.2 % of a monolayer for pure surfactant adsorption, and a spatial resolution of < 1 mm.[13] For measurements of polymer/surfactant mixtures, measurement of $\overline{\rho}$ can tell us about the total amount of material adsorbed at the air/water interface, however information which can be obtained from this single parameter is limited, and we cannot obtain compositional information about mixed layers. NR measurements (discussed in chapter 3) do allow us to obtain compositional information about mixed layers, and in the work presented in this thesis I have co-modelled data from one isotropic contrast of NR data and ellipsometry data in order to obtain compositional information (see Chapter 4).

2.3.3. Information obtained from Ellipsometry Measurements

Ellipsometric measurements of a thin layer adsorbed at the air/water interface can give us an idea of the amount of material adsorbed at the interface. For a bare air/water interface, the ellipticity, $\overline{\rho}$, can be split up into contributions from the thickness and the roughness of the interface. Once a layer of surfactant or polymer is adsorbed, the ellipticity can give us information about the thickness and nature of the adsorbed layer.

Drude derived equations for the reflectivity of an optically isotropic layer in terms of the ellipsometric thickness, η, an integral function of the relative permittivities of the different media across the interface,[27]

$$\eta = \int \frac{(\varepsilon-\varepsilon_1)(\varepsilon-\varepsilon_2)}{\varepsilon} dz \qquad (2.18)$$

where ε, ε_1, ε_2 are the relative permittivities of the surface, the incident media (in this case air) and the substrate (in this case water), where $\varepsilon_1 = 1$ and $\varepsilon_2 = 1.78$ at the wavelength λ of the He-Ne laser. Equation 2.18 is only useful in the thin film limit, when the thickness of the layer is much less than the wavelength of the incident light.

If the layer is assumed to be uniform (i.e. the properties of the film are invariant with depth) with a constant density, the relative permittivities can be taken out of the integral in Equation 2.16 and η becomes a linear function of the thickness of the monolayer, d.

$$\eta = \frac{(\varepsilon-\varepsilon_1)(\varepsilon-\varepsilon_2)}{\varepsilon} d \qquad (2.19)$$

Furthermore, the layer thickness, d, is proportional to the surface excess of the component, Γ, as determined by NR measurements (Chapter 3).

The ellipsometric thickness, η, is related to the coefficient of ellipticity $\overline{\rho}$ (the imaginary part of the reflectivity at the Brewster angle) by

$$\bar{\rho} = \frac{\pi}{\lambda} \frac{\sqrt{\varepsilon_1+\varepsilon_2}}{\varepsilon_1-\varepsilon_2} \eta \qquad (2.20)$$

As the relative permittivity of an adsorbed layer of a hydrocarbon surfactant (ε) is greater than that of air (ε_1) or water (ε_2) Equations 2.18 and 2.19 lead to negative values of $\bar{\rho}$, which will be increasingly negative as η increases. In other words, as long as we remain in the thin film limit at the air/water interface, $\bar{\rho}$ becomes increasingly negative as Γ increases. However, although $\bar{\rho}$ is related to the

surface excess of the component at the interface, it is impossible to tell using ellipsometry measurements alone whether a change in $\overline{\rho}$ for a thin film is associated with a change in thickness or density at the interface, as the three properties are interlinked.

A simple and surprisingly effective model for surfactant monolayers treats the hydrocarbon chain as an oil film of constant density and uses an effective medium approximation to model the polar head groups in water. If we consider equations 2.19 and 2.20 together it is clear that for 'oil-like' behaviour of a surfactant layer at the air/water interface, where n is constant and only d changes, the ellipticity $\overline{\rho}$ is proportional to the film thickness, d, and is therefore linearly related to the surface excess of surfactant, Γ. If instead we had particle-like behaviour, d is constant and n for the inhomogeneous film is calculated from an effective medium approximation in which the particles are immersed in air or water or both. Provided the interface remains in the thin film limit, with an adsorbed layer thicknesses not greater than a few tens of nm, and n is constant, $\overline{\rho}$ is virtually independent of the film thickness at constant Γ; this allows us to model ellipsometry data without reproducing the multi-layer model obtained from fitting of NR data (as discussed in Chapter 3).

Previous studies have shown that for many common hydrocarbon surfactants the relationship between Γ (determined by NR measurements) and $\overline{\rho}$ is approximately linear, consistent with an oil-like adsorbed layer of constant density and changing thickness.[7, 28, 29] For the parts of the surfactant immersed in water, the linearity between Γ and $\overline{\rho}$ is always good as long as the volume fraction is unity. However, for the hydrocarbon chain groups of the surfactant the linear relationship between Γ and $\overline{\rho}$ breaks down at low coverages of surfactant as the molecules 'lie down', with a minimum layer thickness given by the chain diameter, and the layer becomes particle-like instead of oil-like. Previous studies have alternatively accounted for this behaviour at low coverages by the need to mix the sparse hydrocarbon chains with either air or water.[19, 29] Consequently, previous studies used a calibration plot of Γ v $\overline{\rho}$ to convert $\overline{\rho}$ measurements to values of Γ for a pure surfactant. This behaviour will not affect the relationship between Γ and $\overline{\rho}$ for the polymer, only for the surfactant. Data which demonstrate the extent of this effect for the surfactants used in this project are shown and discussed in Chapter 4.

For a pure surfactant adsorbing at the interface, each of the constituent parts of the surfactant at the interface: the hydrocarbon chain, the surfactant headgroup, the surfactant counterion as well as the interfacial roughness, contribute to the measured ellipticity signal. These contributions can be considered as additive, and can be given by

$$\bar{\rho}_{\mathrm{expt}} = \bar{\rho}_{\mathrm{chains}} + \bar{\rho}_{\mathrm{hgp}} + \bar{\rho}_{\mathrm{rough}} + \bar{\rho}_{\mathrm{ion}} \qquad (2.21)$$

I will now discuss how we can model the contributions to $\overline{\rho}$ of an adsorbed surfactant layer, in this case C_{14}TAB with NaBr, using methodologies which have previously be used elsewhere.[29,30]

To find the contribution of the headgroup to the ellipticity, $\bar{\rho}_{\mathrm{hgp}}$, we first need to estimate the relative permittivity of the headgroups using the Clausius-Mossotti equation:

$$\frac{\varepsilon-1}{\varepsilon+2}=\frac{R_m}{V_m} \tag{2.22}$$

where R_{m} is the molar refractivity, and V_{m} is the molar volume, which are given for C_{14}TAB in Table 2.1.

Species	Vm/A^3	Rm/cm^{3}mol^{-1}
Headgroup: N(CH_3)+	108[30,31]	20.05[30]
Counter Ion: Br^-	32[30]	12
Hydrocarbon Chain: $C_{13}H_{26}CH_3$	425[29]	63.45

Table 2.1. Literature values of molecular volumes and refractivities for use in the modelling of C_{14}TAB/NaBr. The value of R_m for the hydrocarbon chain is calculated from the bond values, and that for Br^- is the value for HBr.[32]

The headgroups are hydrated in their interfacial layer, and hence we need to include the contribution of the water to the relative permittivity of the headgroup layer. The overall relative permittivity of the headgroup layer is obtained using the Lorentz-Lorentz effective medium approximation

$$\frac{\varepsilon_{HL}-1}{\varepsilon_{HL}+2}=\phi_{H_2O}\frac{\varepsilon_{H_2O}-1}{\varepsilon_{H_2O}+2}+\phi_{HGP}\frac{\varepsilon_{HGP}-1}{\varepsilon_{HGP}+2} \tag{2.23}$$

where ϕ is the volume fraction of a species in the layer, which can be calculated from molar volume, the area per molecule at the interface using neutron reflectometry measurements (as discussed in Chapter 3), and the layer thickness, $\phi = {}^{V_m}/_{A}.d$. The layer thickness is approximated to 4 Å due to the value of the headgroup volume, although the work of Knock et al used 8 Å from the work of Lu et al. It makes little difference which we use, as it scales both ϕ and $\bar{\rho}_{\mathrm{hgp}}$, which cancel each other out. The contribution of the headgroups to the ellipsometric thickness can then be found from Equation 2.17, and that to the ellipticity from Equation 2.18.

The contribution of the chain layer can be calculated using a similar approach, but varying the thickness rather than the volume fraction of the layer, as the hydrocarbon chain behaves similarly to oil spread on water. The thickness of the layer is calculated from the ratio of the molecular volume of the hydrocarbon chain to the area per molecule of surfactant at the interface (V_m/A), and the layer permittivity from the Clausius-Mossotti equation as in Equation 2.23. η and $\bar{\rho}_{\mathrm{chains}}$ can then be

calculated from Equation 2.17 and 2.18 as previously. The 'oil film' model ceases to be physically sensible when the thickness of the film becomes less than the width of a hydrocarbon chain (5 Å). To calculate the contribution of the chain layer for low surface excesses, the thickness of the layer is set to 5 Å and the volume fraction of the hydrocarbon chains is calculated from the surface excess. The remaining volume is occupied either by air or water . For fluorocarbon surfactants, Day et al and Tyrode et al showed that the experimental data were best described if the chains were immersed 70% in water and 30% in air.[19, 33] For surfactants with hydrocarbon rather than fluorocarbon chains, Bell et al demonstrated that the volume fraction of a hydrocarbon layer (defined as the density divided by that of a liquid hydrocarbon) has a significant effect on the value of $\bar{\rho}$, changing sign for volume fractions less than 0.8.[29]

The contribution of the bromide counter ion can be calculated in two different ways. Firstly, it can be calculated using an approach similar to that above, using the Lorentz-Lorentz EMA assuming that there is one counterion per headgroup. The ions can then be distributed over a solvent depth equivalent to the Debye length. An alternative approach is to treat the counterions as a layer of NaBr of increased concentration, and then to use tabulated values of the refractive indices of NaBr (from the CRC handbook) in the equation for the ellipticity. The thickness of the layer over which the Br- ions are distributed has a negligible effect on $\bar{\rho}$ for physically reasonable thicknesses.

The roughness of the layer can be considered by capillary wave theory, which regards the interface as sharp but distorted by capillary waves which scatter the light. Accordingly the contribution of roughness to the ellipsometric thickness, η_r, can be obtained from capillary wave theory, as demonstrated by Meunier. [34]

$$\eta_r = -\frac{3(\varepsilon_1-\varepsilon_2)^2}{2(\varepsilon_1+\varepsilon_2)}\sqrt{\frac{\pi k_B T}{6\sigma}} \qquad (2.24)$$

where k_B is the Boltzmann constant, T is the temperature, and σ is the surface tension. As $\varepsilon_2 > \varepsilon_1$, the surface roughness results in a positive value, which for pure water can be calculated from Equation 2.20 as $\bar{\rho} \approx 6 \times 10^{-4}$, whilst measurements give a slightly lower value of $\bar{\rho} = 3.8 \times 10^{-4}$. The roughness contribution for an adsorbed layer has an inverse square root dependence on the surface tension, which varies with surface coverage. This contribution is a highly non-linear function of the surface coverage, but its variation over the range of surface tension is small, 0.15×10^{-3} for the C_nTAB surfactants.[7] For the purpose of this discussion and the following calculation, I will treat it as a constant with a value of 5×10^{-4}.

Figure 2.8 shows the calculated contribution of each of the components of $C_{14}TAB$ to its ellipticity using the approach outlined above. As we can see, all 4 components have a substantial contribution to

the ellipticity of the surfactant, with the contribution from the surfactant headgroups and the counterion proportional to the surface excess of surfactant provided that the volume fraction in the headgroup region is unity (a reasonable assumption).

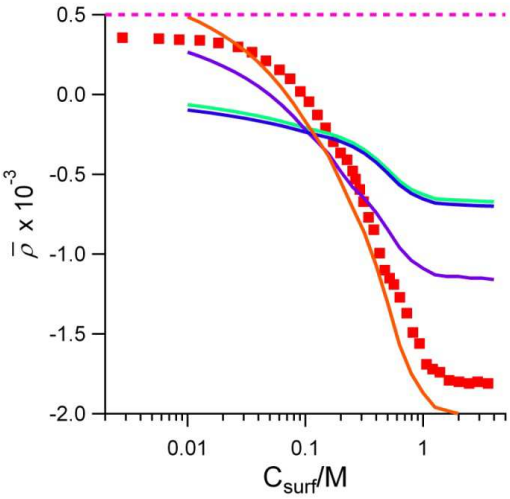

Figure 2.8. Calculated contribution to the ellipticitiy of an adsorbed layer of C_{14}TAB from the hydrocarbon chains (purple line), surfactant headgroups (blue line), counterions (green line, difficult to distinguish from the blue line), using values of the surface excess obtained from NR measurements, and the set value of the roughness at 5×10^{-4} (pink dashed line). The orange line is the sum of these contributions, and is compared to the measured ellipticity of C_{14}TAB in the presence of 0.1 M NaBr (red squares).

In the experiments discussed in this thesis, we are not focusing on the adsorption of pure surfactants at the air/water interface of the OFC, rather on the adsorption from mixtures of polymers and surfactants. As for a surfactant monolayer, a linear relationship between $\overline{\rho}$ and Γ is also expected for pure polymer adsorbed at the interface.[8] The contribution of the polymer to $\overline{\rho}$ for the mixture can be estimated for the adsorption of 1 μmol m^{-2} of polymer using Equations 2.19 and 2.20 with $\varepsilon_{\text{poly}} = \left(\Delta n + \sqrt{\varepsilon_{\text{H2O}}}\right)^2$, where Δn is calculated from the literature value of dn/dc for the polymer and the mass per ml of 1 μmol m^{-2} of polymer. As long as dn/dc is independent of the concentration, the calculated contribution of polymer to $\overline{\rho}$ for the mixture is independent of the layer thickness, and only weakly dependent on the volume fraction of the polymer.

In order to use the above discussed contributions of surfactant and polymer to $\bar{\rho}$ for adsorption from mixtures of the two components we need to know that their contributions are linearly additive. The previous study of Campbell et al showed that an additive function of the contributions of the polymer and surfactant at interface is a good approximation to $\bar{\rho}$ for the mixture.[9] This will be the case as long as the

total volume fraction of polymer, surfactant, and water in the layer is unity. Deviations from linear additivity will occur when the hydrocarbon chains of the surfactant are mixed with both air and water at low surfactant coverages as discussed above. The effect of this on $\bar{\rho}$ for the mixture will be discussed and evaluated further in Chapter 4.

2.3.4. Ellipsometer Set-Up & Ellipsometry Measurements

2.3.4.1 Ellipsometer Set-UP

There are many different ellipsometer types and systems. The one used in all of the measurements presented in this thesis was the Beaglehole Picometer Light Ellipsometer, in the Partnership for Soft Condensed Matter (PSCM) at the ILL, shown in Figure 2.9. Below I will briefly discuss the principles of operation of the ellipsometer, however more detailed information can be found in the literature[26] or the instrument manual.

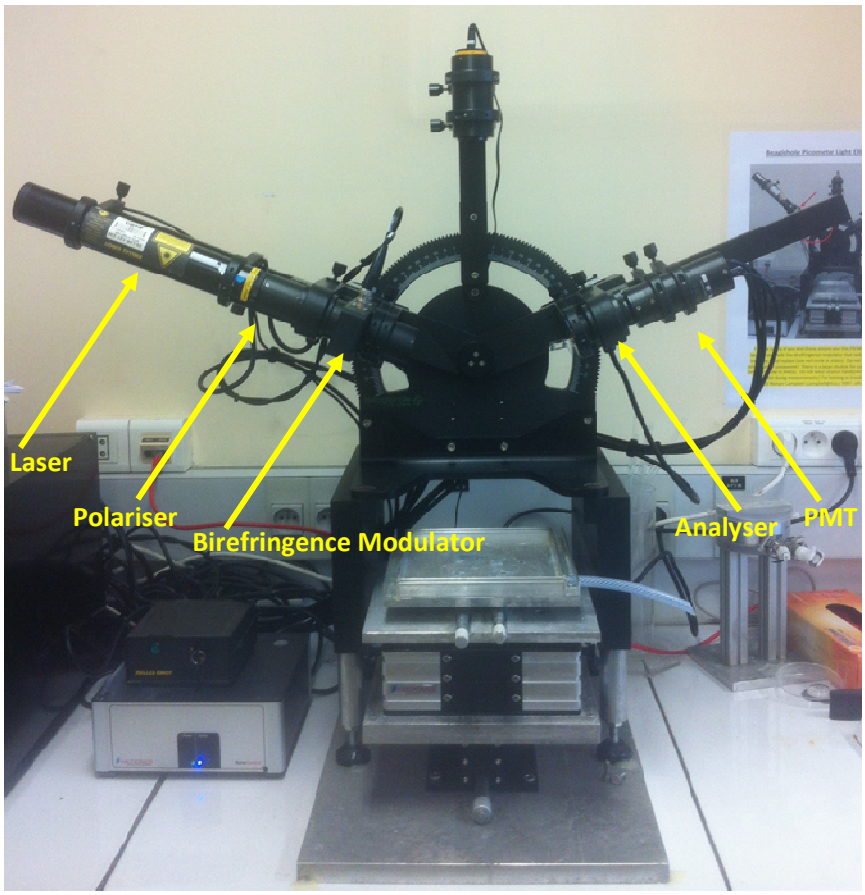

Figure 2.9. Photograph of the Beaglehole Picometer Light Ellipsometer as installed in the PSCM laboratories at the ILL. Arrows on the photograph indicate the optical components discussed in the following text.

A beam of light from a HeNe laser (λ =632.8 nm) is polarised by a polariser oriented at 45° to the optical axis to provide equal s and p components amplitudes which are in phase. The polarized light then passes through a birefringence modulator, which works on similar principles to a quarter-wave plate in that it retards one of the components of light, inducing a phase shift between the two components. A quarter wave plate divides linearly polarized light into two components with different indices of refraction, in this case the light with the larger index of refraction is retarded by 90° compared to the other component, resulting in circularly polarized light. Rather than inducing a single phase shift between the components, a birefringence modulator modulates the phase shift, in other words it continuously varies the phase shift between the two components between a minimum and a maximum shift, over a time period given by the frequency of the phase shift, 50 kHz. This is effected by inducing a periodic change in the refractive index of the optical component of the birefringence modulator by oscillating the quartz crystal which makes up the birefringence modulator. This modulation in the phase shift of the two components of light results in elliptically rather than circularly polarized light being incident on the interface.

The light reflected from the interface passes through an analyser to a photomultiplier. The analyser is oriented parallel or perpendicular to the polariser, and is rotated between the two positions. Lock-in amplifiers measure the modulated signals at 50 kHz and 100 kHz (the first and second harmonics of the modulator's oscillation frequency), resulting in a low level of noise and a high sensitivity. The detected ac signals are proportional to the imaginary and real parts of the complex reflectivity ratio, respectively, allowing us to determine the ellipticity of the sample. All of the measurements in this thesis are made at the Brewster angle of water, which minimizes the real part of the reflectivity.

The set-up of the ellipsometer in the PSCM at the ILL (as shown in Figure 2.9) includes a sample mount consisting of an anti-vibration table, a horizontal leveling plate, and manual vertical translation stages, all of which were commissioned or installed as part of the experimental work contributing to this thesis.

2.3.4.2. Ellipsometry Experiments

All of the ellipsometry data presented in this thesis were recorded using the Beaglehole Picometer Light ellipsometer, and measurements were recorded at the Brewster angle of water (53.1°), in order to obtain the coefficient of ellipticity, $\overline{\rho}$. The majority of measurements were recorded on the overflowing cylinder, and unless stated otherwise measurements were recorded as a function of surfactant concentration, performed by consecutive additions of a concentrated surfactant stock solution to a base salt or polymer and salt solution. For many polymer/surfactant mixtures, the procedure used in mixing the two components has been shown to have an effect on the bulk phase behaviour,[35-38] which might be reflected in the adsorption behaviour on the OFC. To increase the surfactant concentration of a pure surfactant system on the OFC, aquilots of a concentrated stock solution are usually added to the flowing system. This creates localized concentration gradients, and for a polymer/surfactant system the bulk phase behaviour may be affected. In order to minimize the effect of mixing on the bulk phase behaviour, the largest stock volumes possible were added to the solution, whilst limiting the necessity of removing solution from the system. In NR measurements 10 mls of surfactant and 10 mls of compensatory polymer and salt solution were added for each increase in concentration. These solutions were added dropwise to the reservoirs in the OFC system over a period of several minutes, enough time for the solution to flow several times around the system.

Data were recorded principally on mixtures of hydrogenated surfactant, with hydrogenated polymer and salt. However measurements made on protonated and deuterated surfactants were also made to evaluate the errors incurred, and the results obtained were within experimental error. Unless stated otherwise, measurements were made at 5 second time intervals and averaged over a period of at least 300 s per measurement in order to obtain precise values of $\overline{\rho}$. For the majority of measurements, the standard deviation in the value of $\overline{\rho}$ thus measured is within the symbols shown.

2.4. References for Chapter 2

1. Bain, C. D.; Manning-Benson, S.; Darton, R. C., Rates of mass transfer and adsorption of hexadecyltrimethylammonium bromide at an expanding air-water interface. *Journal of Colloid and Interface Science* **2000,** 229, (1), 247-256.
2. Manning-Benson, S.; Bain, C. D.; Darton, R. C., Measurement of Dynamic Interfacial Properties in an Overflowing Cylinder by Ellipsometry. *Journal of Colloid and Interface Science* **1997,** 189, (1), 109-116.
3. Manning-Benson, S.; Bain, C. D.; Darton, R. C.; Sharpe, D.; Eastoe, J.; Reynolds, P., Invasive and Noninvasive Measurements of Dynamic Surface Tensions. In 1997; Vol. 13, pp 5808-5810.
4. Campbell, R. A.; Day, J. P. R.; Bain, C. D., External reflection Fourier transform infrared spectroscopy of surfactants at the air-water interface: Separation of bulk and adsorbed surfactant signals. *Applied Spectroscopy* **2005,** 59, (8), 993-1001.
5. Manning-Benson, S.; Parker, S. R. W.; Bain, C. D.; Penfold, J., Measurement of the Dynamic Surface Excess in an Overflowing Cylinder by Neutron Reflection. In 1998; Vol. 14, pp 990-996.
6. Sekine, M.; Campbell, R. A.; Valkovska, D. S.; Day, J. P. R.; Curwen, T. D.; Martin, L. J.; Holt, S. A.; Eastoe, J.; Bain, C. D., Adsorption kinetics of ammonium perfluorononanoate at the air-water interface. *Physical Chemistry Chemical Physics* **2004,** 6, (21), 5061-5065.
7. Battal, T.; Shearman, G. C.; Valkovska, D.; Bain, C. D.; Darton, R. C.; Eastoe, J., Determination of the dynamic surface excess of a homologous series of cationic surfactants by ellipsometry. *Langmuir* **2003,** 19, (4), 1244-1248.
8. Goates, S. R.; Schofield, D. A.; Bain, C. D., A study of nonionic surfactants at the air-water interface by sum-frequency spectroscopy and ellipsometry. *Langmuir* **1999,** 15, (4), 1400-1409.
9. Campbell, R. A.; Ash, P. A.; Bain, C. D., Dynamics of adsorption of an oppositely charged polymer-surfactant mixture at the air-water interface: Poly(dimethyldiallylammonium chloride) and sodium dodecyl sulfate. *Langmuir* **2007,** 23, (6), 3242-3253.
10. Padday, J. F., *Proc. Int. Congr. Surf. Act* **1957**.
11. Piccardi, G., Ferroni, E. , *Ann Chim, (Rome)* **1951,** 41, 3.
12. Manning-Benson, S. The Dynamics of Surfactant Adsorption'. Oxford, 1998.
13. Manning-Benson, S.; Bain, C. D.; Darton, R. C., Measurement of dynamic interfacial properties in an overflowing cylinder by ellipsometry. *J. Colloid Interface Sci.* **1997,** 189, (1), 109-116.
14. Bergink-Martens, D. J. M.; Bos, H. J.; Prins, A., Surface Dilation and Fluid-Dynamical Behavior of Newtonian Liquids in an Overflowing Cylinder: II. Surfactant Solutions. *Journal of Colloid and Interface Science* **1994,** 165, (1), 221-228.
15. Manning-Benson, S., *PhD Thesis* **1996**.
16. Bain, C. D.; Manning-Benson, S.; Darton, R. C., Rates of mass transfer and adsorption of hexadecyltrimethylammonium bromide at an expanding air-water interface. *J. Colloid Interface Sci.* **2000,** 229, (1), 247-256.
17. Joos, P.; Van Uffelen, M., Adsorption Kinetics with Surface Dilatation: 1. Desorption of Slightly Soluble Monolayers at Constant Surface Pressure. *Journal of Colloid and Interface Science* **1993,** 155, (2), 271-282.
18. Vanvoorstvader, F.; Erkens, T. F.; Vandente.M, Measurement of Dilatational Surface Properties. *Transactions of the Faraday Society* **1964,** 60, (4986), 1170-&.
19. Day, J. P. R.; Campbell, R. A.; Russell, O. P.; Bain, C. D., Adsorption kinetics in binary surfactant mixtures studied with external reflection FTIR spectroscopy. *J. Phys. Chem. C* **2007,** 111, (25), 8757-8774.
20. Valkovska, D. S.; Shearman, G. C.; Bain, C. D.; Darton, R. C.; Eastoe, J., Adsorption of ionic surfactants at an expanding air-water interface. *Langmuir* **2004,** 20, (11), 4436-4445.
21. Breward, C. J. W.; Howell, P. D., Straining flow of a micellar surfactant solution. *Eur. J. Appl. Maths.* **2004,** 15, 511-531.

22. Woods, D. A.; Petkov, J.; Bain, C. D., Surfactant Adsorption Kinetics by Total Internal Reflection Raman Spectroscopy. 2. CTAB and Triton X-100 Mixtures on Silica. *J. Phys. Chem. B* **2011,** 115, (22), 7353-7363.
23. Woods, D. A.; Petkov, J.; Bain, C. D., Surfactant Adsorption Kinetics by Total Internal Reflection Raman Spectroscopy. 2. CTAB and Triton X-100 Mixtures on Silica. *The Journal of Physical Chemistry B* 115, (22), 7353-7363.
24. Born, M., Wolf, E., *Principles of Optics*. Pergamon Press: Oxford, 1997.
25. Azzam, R. M. A., Bashara, N.M. , *Ellipsometry and Polarised Light*. Elsevier: Amsterdam, 2003.
26. Beaglehole, D., Ellipsometric Study of the Surface of Simple Liquids. *Physica B* **1980,** 100, 163-174.
27. Drude, P., *The Theory of Optics*. Dover: New York, 1959.
28. Valkovska, D.; Wilkinson, K. M.; Campbell, R. A.; Bain, C. D.; Wat, R.; Eastoe, J., Measurement of the dynamic surface excess of the nonionic surfactant C8E4OMe by neutron reflection and ellipsometry. *Langmuir* **2003,** 19, (14), 5960-5962.
29. Bell, G. R.; Manning-Benson, S.; Bain, C. D., Effect of chain length on the structure of monolayers of alkyltrimethylammonium bromides (C(n)TABs) at the air-water interface. *J. Phys. Chem. B* **1998,** 102, (1), 218-222.
30. Knock, M. M.; Bain, C. D., Effect of Counterion on Monolayers of Hexadecyltrimethylammonium Halides at the Airâˆ'Water Interface. *Langmuir* **2000,** 16, (6), 2857-2865.
31. Lu, J. R.; Simister, E. A.; Thomas, R. K.; Penfold, J., Structure of an octadecyltrimethylammonium bromide layer at the air/water interface determined by neutron reflection: systematic errors in reflectivity measurements. *The Journal of Physical Chemistry* **1993,** 97, (22), 6024-6033.
32. Atkins, P. W., *Physical Chemistry*. OUP: Oxford, 1998; Vol. 6th ed.
33. Tyrode, E.; Johnson, C. M.; Rutland, M. W.; Day, J. P. R.; Bain, C. D., A Study of the Adsorption of Ammonium Perfluorononanoate at the Air-Liquid Interface by Vibrational Sum-Frequency Spectroscopy. *The Journal of Physical Chemistry C* **2007,** 111, (1), 316-329.
34. Meunier, J., In *Light Scattering by Liquid Surfaces and Complementary Techniques*, Langevin, D., Ed. Dekker: New York, 1992.
35. Mezei, A.; Meszaros, R.; Varga, I.; Gilanyi, T., Effect of mixing on the formation of complexes of hyperbranched cationic polyelectrolytes and anionic surfactants. *Langmuir* **2007,** 23, (8), 4237-4247.
36. Mezei, A. l.; Pojjaì k, K.; Meì szaì ros, R. b., Nonequilibrium Features of the Association between Poly(vinylamine) and Sodium Dodecyl Sulfate: The Validity of the Colloid Dispersion Concept. *The Journal of Physical Chemistry B* **2008,** 112, (32), 9693-9699.
37. Mezei, A.; Abraham, A.; Pojjak, K.; Meszaros, R., The Impact of Electrolyte on the Aggregation of the Complexes of Hyperbranched Poly(ethyleneimine) and Sodium Dodecyl Sulfate. *Langmuir* **2009,** 25, (13), 7304-7312.
38. Pojjak, K.; Bertalanits, E.; Mészáros, R., Effect of Salt on the Equilibrium and Nonequilibrium Features of Polyelectrolyte/Surfactant Association. *Langmuir* **2011,** 27, (15), 9139-9147.

Chapter 3. Neutron Reflectometry

3.1. Introduction

In the past three decades neutron reflectometry (NR) has become an invaluable tool for the study of a variety of surfaces and interfaces. The specular reflection of neutrons at an interface provides information about the concentration and composition profiles normal to the interface. Neutrons interact with atomic nuclei, and are scattered or adsorbed. The scattering power of a nucleus is given by a characteristic known as its scattering length, and that of a material is given by its scattering length density. The reflection of neutrons from an interface is related to the neutron refractive index profile normal to the interface, which is itself related to the scattering length density of the material normal to the interface, and hence the composition of the material at the interface. Furthermore, due to the short wavelengths of neutrons (2-30Å on FIGARO), NR can be used to examine structure on the molecular length scale with a resolution of a fraction of a nanometer.

Neutron reflectometry can be described either using classical thin film optics,[1, 2] or scattering theory.[3] NR is therefore in many ways analogous to other reflection techniques such as X-Ray reflectometry (XRR) and ellipsometry, however it has many advantages over these techniques. The unique ability to manipulate the scattering length density of the material using hydrogen/deuterium substitution enables the examination of different interfacial components, and helps in obtaining a unique interpretation of recorded data. Furthermore, NR is non-destructive to samples in comparison to XRR measurements, and is a penetrating probe, enabling the accessing of buried interfaces such as liquid-liquid, solid-liquid and solid-solid surfaces.

Some of the earliest soft-matter applications of NR examined the adsorption of pure surfactant[4, 5] and polymer[6-8] monolayers at the air/water interface, however more recently NR has been used to examine more complex systems containing combinations of polymers, surfactants, lipids, proteins, and bio-membranes. NR can also be used to examine solid films, do in situ-electochemistry and examine surface magnetism, however as this thesis only examines NR of simple soft matter systems the principles of reflectivity from such systems will not be discussed here. Several good reviews discuss the theory[9-11] and applications[12-15] of NR.

In this chapter I will first discuss the theory behind neutron scattering in general and neutron reflectometry measurements, as well as the use of isotopic contrast variation. I will then discuss the characteristics and components of the horizontal reflectometer FIGARO at the ILL, on which all of the measurements presented in this thesis have been performed. Due to the relatively small and domed nature of the interface of the OFC, specific instrument settings were required for the experiments performed as part of this thesis. The interfacial curvature means that the optimum neutron footprint for measurements on the OFC is different to that used for that for standard samples, and exacerbates the effect of gravity on the data. The determination of both the optimum footprint and the effect of gravity on measurements are discussed in the later part of this chapter, along with further specific details of our measurements on FIGARO.

3.2. Theory of Neutron Reflectometry

3.2.1. Neutrons and Neutron Scattering

Neutrons are particles with a mass m_n and a speed v, which therefore have a momentum, p, given by classical mechanics, $p = m_n v$. However, due to wave particle duality (neutrons are particles but also undergo Bragg scattering) they can also be described by a de Broglie wavelength λ:

$$\lambda = \frac{h}{m_n v} \tag{3.1}$$

where h is Planck's constant, and therefore $p = \frac{h}{\lambda}$.

Consequently the kinetic energy of the neutron E is

$$E = \frac{1}{2} m v^2 = \frac{h^2}{2 m_n \lambda^2} \tag{3.2}$$

In neutron scattering the wave nature of the neutron means that it is commonly referred to in terms of the neutron wavenumber $k = \frac{2\pi}{\lambda}$ or the wavevector $\mathbf{k}$ with length k in the same direction as the velocity

$$\mathbf{k} = \frac{m_n v}{\hbar} \tag{3.3}$$

where the reduced Planck's constant $\hbar = h/2\pi$. Neutron wavelengths are given in Å, and wavenumbers in Å^{-1}, velocity is in ms^{-1}, and kinetic energy is in eV or meV. From equations 3.2 and 3.3 the kinetic energy of a neutron can therefore be given in terms of wavenumbers by

$$E = \frac{\hbar^2 k^2}{2m_n} \tag{3.4}$$

The scattering of a neutron by a sample is characterised by the resultant change in momentum **p** and energy E. A neutron incident with wavevector $\mathbf{k}_i$ and angular frequency ω_i is scattered with wavevector $\mathbf{k}_f$ and angular frequency ω_f.

The momentum transfer can therefore be given by

$$\boldsymbol{p} = \hbar k_i - \hbar k_f = \hbar Q \tag{3.5}$$

and therefore the wavevector transfer $Q = k_i - k_f$.

The energy transfer can be similarly described as $E = \hbar\omega$, where $\omega = \omega_i - \omega_f$. In the case of elastic scattering of neutrons (as in neutron reflectometry) there is no exchange of energy and $\Delta E = 0$, $\Delta\omega = 0$. When there is no energy transfer, only a momentum transfer, the magnitude of the wavevector is unchanged by scattering and

$$|\mathbf{k_i}| = |\mathbf{k_f}| = 2\pi/\lambda \tag{3.6}$$

A vector diagram for an elastic scattering event is shown in Figure 3.1, where an incoming neutron is deflected through an angle of 2θ. From equation 3.2 the triangle is isosceles with each side having a length $k = 2\pi/\lambda$.

Trigonometry then gets us to an equation for the momentum transfer Q which occurs on scattering

$$Q = \frac{4\pi sin\theta_i}{\lambda} \tag{3.7}$$

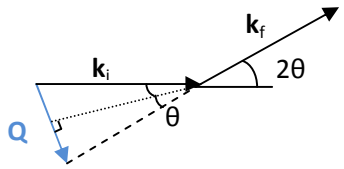

Figure 3.1. The vector diagram for elastic scattering, $|\mathbf{k_i}| = |\mathbf{k_f}|$ through an angle 2θ.

The strength of the interaction of a neutron with a given nucleus, i, is given by the scattering length, b_i. b_i is a known quantity for most nuclei, and has been determined experimentally because b_i varies significantly and non-monotonically across the periodic table. Notably, b_i also varies significantly between different isotopes of the same element. For a given material, the scattering length density, σ, is defined as the scattering length of the material per unit volume. The scattering length density of a molecule is calculated from the sum of the scattering lengths of all of the component atoms, divided by the molar volume of the molecule V_m

$$\sigma = \frac{\sum_i b_i n_i}{V_m} \tag{3.8}$$

where b_i is the scattering length as discussed above, and n_i is the number of atoms of component i, although the contribution of V_m is not always stated as number density, $n_i(z)$, can be substituted for number.

As Q is dependent on both the incident angle and wavelength of an incoming neutron, neutron scattering measurements can be made as a function of either or both parameters. Monochromatic measurements made as a function of incident angle are recorded using a narrow distribution of neutron wavelengths, which is a common approach with a reactor source. The wavelength is selected using either a monochromator or by velocity selection using a mechanical device. The alternative is to make measurements at one or a small number of incident angles using a broad range of incident wavelengths. This is known as a time-of-flight (TOF) measurement, and is used at both spallation and reactor neutron sources and is the approach used in the NR experiments described in this chapter. TOF measurements require a pulsed incoming beam, where the energy (or velocity) of the scattered neutrons is measured according to their relative arrival time at the detector. As the wavelength is inversely proportional to the velocity, short wavelength neutrons travel quickly, reaching the detector first, and long wavelength neutrons have slower speeds, taking longer to reach both the interface and the detector. TOF measurements are best for kinetic experiments due to the broad Q-range that can be accessed simultaneously. Several kinetic NR measurements are presented in this thesis.

3.2.2. Neutron Reflection

Due to wave particle duality, the reflection of neutrons from interfaces can be treated by the principles of classical optics as presented in Lekner[2] and Born & Wolff[1], similarly to the discussion of the reflection of light as discussed in Chapter 2. This approach is called the dynamical theory of neutron reflection, however the interaction of neutrons with matter is more classically described by the kinematic or Born approximation, based on the Fourier transform of the scattering length density function of a material, as described in a variety of texts.[3] For ease of comparison, I will discuss the principles of neutron reflectometry below using the dynamical approach. I will start by re-considering the reflection of a simple wave from a surface, as we did for light in Chapter 2. Despite the fact that neutron reflection is scalar and light reflection is vector, the same approach can be used for both when some approximations for one dimensional waves are applied (discussed further below). Figure 3.2 shows the geometry of the incident, reflected and transmitted waves. Note that the angles are defined relative to the interface rather than relative to the normal as they were in Chapter 2, considerations of reflection for NR theory usually use this representation due to the small angles of incidence in NR measurements. As a consequence the trigonometric relations in equations 3.8 and 3.9 appear different to those given in Chapter 2.

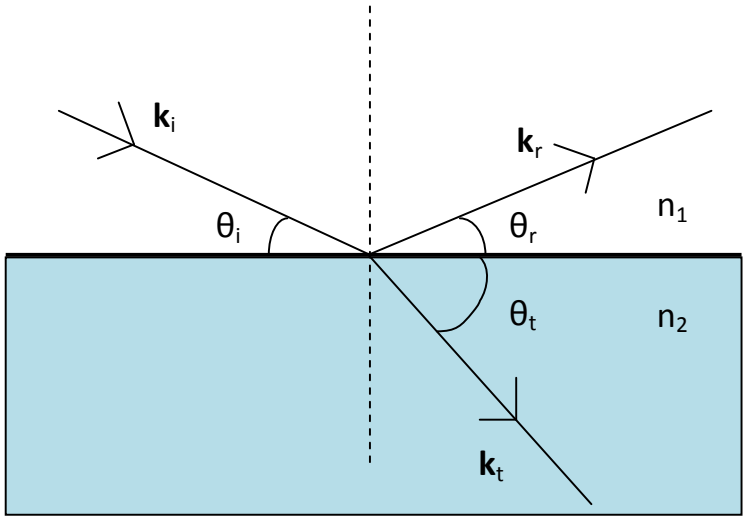

Figure 3.2. Schematic showing the geometry of neutron reflection from a smooth planar interface. θ_i, θ_r, θ_t, are the angles of incidence, reflection, and transmission respectively, whilst $\mathbf{k}_i$ $\mathbf{k}_r$ and $\mathbf{k}_t$ are the relevant wavevectors, and n_1 and n_2 are the refractive indices of the media above and below the interface; note that in experiments grazing angles are used and the large angles shown here are simply for clarity.

I will first consider the reflection of neutrons from a single planer interface (no adsorbed layers) with zero roughness between two homogeneous materials. Neutrons incident on a homogeneous interface between two media can be reflected from the interface at an angle identical to the angle of incidence θ_i, or transmitted through the material with a change in direction at angle θ_t. As discussed in Chapter 2, the ratio of the cosines of these angles is given by the refractive index (n_{12}) according to Snell's law

$$n_{12} = \frac{n_2}{n_1} = \frac{\cos\theta_1}{\cos\theta_2} = \frac{\boldsymbol{k}_t}{\boldsymbol{k}_i} \tag{3.9}$$

Neutrons transmitted into the medium below the interface will change direction, they will be refracted, and the ratio of the incident and transmitted wavevectors $\mathbf{k}_i$ and $\mathbf{k}_t$ is also related by the inverse ratio of the cosines of the angles, as shown in Equation 3.8.

The extent to which the wave is reflected and refracted is given by Fresnel's Equation:

$$R = |r_{12}|^2 = \left|\frac{n_1\sin\theta_i - n_2\sin\theta_t}{n_1\sin\theta_i + n_2\sin\theta_t}\right|^2 \tag{3.10}$$

For neutrons, the reflectivity R is determined from the ratio of the number of reflected neutrons to the number incident on the sample.

The neutron refractive index of a medium depends on the wavelength of a given incident neutron, and the scattering length profile of the medium normal to the interface. This is given by the scattering length density of the material (Equation 3.8) normal to the interface, $\sigma(z) = \sum_i b_i n_i(z)$. Hence the neutron refractive index and the reflection of neutrons from an interface depends on the composition of the media. In the following section I will derive the relationship between the scattering length density of the material and the neutron refractive index.

As the neutron refractive index depends on only the composition of the medium normal to the interface, specular reflection only gives structural information about samples which have layers parallel to the interface but not in the plane of the interface. Structure in the plane of the interface in the direction of the incident beam results in off-specular scattering, which will be discussed briefly later, and structure lateral to the beam can only be resolved using grazing incidence small angle scattering measurements which require a different slit geometry to NR measurements. For a surface with no in-plane structure, a neutron can be assumed to only interact with the structure normal to the interface, hence only the scattering length density profile normal to the interface $\sigma(z)$ affects the wavevector in the medium. As a consequence, it can be useful to express the neutron wavevectors $\mathbf{k}_i$ and $\mathbf{k}_t$ in terms of their two components perpendicular and parallel to the interface ($\mathbf{k}_z$ and $\mathbf{k}_x$ respectively), $\mathbf{k}_i^{\,2} = \mathbf{k}_x^{\,2} + \mathbf{k}_z^{\,2}$, as only $\mathbf{k}_z$ will be affected by interaction with the medium.

The interaction of an incident neutron with a given kinetic energy, E, with a medium depends on the potential of interaction of the neutron with the medium,V. E and V can be related by the Schrödinger equation

$$-\frac{h^2}{8\pi m_n}\nabla^2\psi + V\psi = E\psi \qquad (3.11)$$

where ψ is the neutron wavefunction. Despite the fact that E and V can be related by the Schrödinger equation, the effect of the potential and neutron kinetic energy can be described by classical mechanics, and we will return to the quantum mechanical interpretation of reflectivity later.

The potential of the medium, V, is that which is experienced by the neutron on interacting with the nuclei in the medium, which is dependent on the scattering length density profile of the material perpendicular to the interface σ(z). The potential of the material normal to the interface is given by

$$V = \frac{h^2}{2\pi m_{\mathrm{n}}}\sigma(z) \qquad (3.12)$$

The potential of the medium changes the kinetic energy of an incident neutron, and it changes direction (refracts). The difference between the kinetic energy of the neutron and the potential determines whether or not the neutron is totally reflected from the barrier potential of the material or whether it is transmitted. The normal component of the kinetic energy of a neutron as in Equation 3.4 is

$$E_{\perp} = \frac{(hk_i sin\theta_i)^2}{8\pi^2 m_n} \qquad (3.13)$$

To return to our discussion of reflection as related to classical optics using Figure 2 and Equation 3.9, we can see that as with light, as neutrons pass from a medium of higher refractive index to one of lower refractive index ($n_1 > n_2$) total reflection may occur. As the neutron refractive indices of most materials are only slightly less than that of air (see below), this is total external reflection rather the total internal reflection which occurs for light. There is a critical value of the incident angle, θ_c, below which only reflection (total external reflection) occurs, and above which both reflection and transmission occur. In the situation where the top medium is air and the lower one a liquid or solid, n_1 =1, and the critical angle for total reflection is found from rearranging Equation 3.9 to $\cos\theta_c = n2\cos\theta t$ with $\theta_t = 0$ as there is no transmission. θ_c is given by $\cos\theta_c = n_2$.

When a neutron with wavevector $\mathbf{k}_i$ is incident on an interface at an angle greater than the critical angle, θ_c it is reflected from the interface or transmitted into the material, where it is reflected by nuclei in the material. The wavevector of a neutron transmitted into the medium, $\mathbf{k}_t$, is altered by interactions

between the neutron and the nuclei of atoms in the material, which result in a transfer of momentum, given by equation 3.7, $Q = \frac{4\pi sin\theta_i}{\lambda}$.

On FIGARO, NR measurements are made at a fixed incident angle (or often at two consecutive fixed angles) with a range of incident wavelengths, i.e. a range of incident neutron energies. Therefore rather than there being a critical angle for total reflection there is a critical value of the momentum transfer from the neutron to the medium, Q_c, below which the neutron cannot penetrate the medium and only total reflection occurs. Q_c can be determined from the relative magnitudes of the kinetic energy of the neutron, E, and the potential of the medium, *V*, as given in Equations 3.12 and 3.13. If the energy of the neutron $E_\perp$ is less than the potential *V* ($E_\perp < V$) total reflection occurs. However if $E_\perp > V$ the neutron is either reflected or transmitted into the medium. Q_c is then given by $E_\perp = V$

$$Q_c = \sqrt{16\pi\sigma(z)} \qquad (\text{as } Q = 2sin\theta k_i) \tag{3.14}$$

For the neutron to penetrate into the medium, $E_\perp > V$, and the incident energy of the neutron $E_{\perp,i}$ is modified by the potential to give the transmitted energy of the neutron $E_{\perp,t}$, from $E_{\perp,t} = E_{\perp,i} - V$ (from Equations 3.12 and 3.13), we can determine the change in the wave-vector normal to the interface, k_z, which occurs when the neutron interacts with the medium

$$k_{t,z}^2 = {k_{i,z}}^2 - 4\pi\sigma(z) \tag{3.15}$$

For a homogeneous medium, this allows us to define the neutron refractive index n_{12}, from the ratio of the wavevector in the material to that in the vacuum:

$${n_{12}}^2 = \frac{{k_t}^2}{{k_i}^2} = \frac{{k_{i,x}}^2 + \left({k_{i,z}}^2 - 4\pi\sigma(z)\right)}{{k_i}^2} = 1 - \frac{4\pi\sigma(z)}{{k_i}^2} = 1 - \frac{\lambda^2}{\pi}\sigma(z) \tag{3.16}$$

This gives the dependence of the refractive index on the wavelength of the neutrons and the composition of the material normal to the interface (as given by $\sigma(z)$).

For most materials the scattering length density is small, hence n is close to 1 and a good approximation to n is given by

$$n \approx 1 - \frac{\lambda^2}{2\pi}\sigma(z) \tag{3.17}$$

As discussed earlier, the neutron refractive index of a material depends only on the neutron wavelength and the scattering length density of the interface normal to the interface.

In order to explain reflectivity further, we need to return to the Schrödinger Equation (Equation 3.10), and consider the wavefunction which describes the propagation of a neutron as a one-dimensional particle wave in the z x plane incident on a planar interface (where the dimensions x and y define the plane of the surface, and z defines the dimension into the material), using an approach identical to that used for electromagnetic radiation[2] for reasons explained below. As V is only dependent on z in this geometry, the incident wave can be considered only perpendicular to the planar interface, with the form

$$\psi(z) = \psi(z)e^{ik_i x} \tag{3.18}$$

Subsitution of 3.16 into 3.7 gives the wavefunction describing the probability amplitude near the surface

$$\frac{d^2\psi}{dz^2} + {k_z}^2 = 0 \tag{3.19}$$

Where k_z can be expressed as

$${k_z}^2 = \frac{4\pi m_n}{h}(E - V) - {k_x}^2 \tag{3.20}$$

The incident wave can be either transmitted or reflected at the interface, and the probability amplitudes for reflection and transmission r_{12} and t_{12} are given by the limiting forms of 3.19, when there is some transmission, the solution to 3.19 above the surface is

$$\psi_z = e^{ik_{z,i}z} + r_{12}e^{-ik_{z,i}z} \tag{3.21}$$

And below the surface is

$$\psi_z = t_{12}e^{ik_{z,t}z} \tag{3.22}$$

r_{12} and t_{12} can also be defined as the Fresnel coefficients of $e^{-ik_{z,i}z}$ and $e^{ik_{z,t}z}$. At this point it becomes clear why neutrons can be treated by the same equations as light, as boundary conditions can be imposed which mean that at the interface ($z = 0$) both $\psi(z)$ and $d\psi(z)/dz$ must be continuous. That is to say that

$$\psi_i + \psi_r = \psi_t \quad \text{and} \quad \frac{d}{dz}(\psi_i + \psi_r) = \frac{d\psi_t}{dz} \tag{3.23}$$

hence

$$1 + r_{12} = t_{12} \quad \text{and} \quad k_{z,i}(1 - r_{12}) = t_{12}k_{z,t} \tag{3.24}$$

the second relation only holds when $E > V$, i.e. below the critical angle, where only total reflection occurs. Simultaneous solution of equations 3.21 and 3.22 leads directly to the Fresnel coefficients found in optics:

$$r_{12} = \frac{k_{z,i} - k_{z,t}}{k_{z,i} + k_{z,t}} \tag{3.25}$$

and

$$t_{12} = \frac{2k_{z,i}}{k_{z,i} + k_{z,t}} \tag{3.26}$$

We can therefore relate the measured reflectivity R to Q using the Fresnel Equation as in Equation 3.5, along with the Equations 3.14, 3.15 and 3.25

$$R = {r_{12}}^2 = \frac{{Q_c}^4}{\left[Q + \left(Q^2 - {Q_c}^2\right)^{1/2}\right]^4} \tag{3.27}$$

When $Q >> Q_c$, $R = |r_{12}|^2 < 1$ and this reduces to,

$$R \approx \frac{16\pi^2}{Q^4}\Delta\sigma^2 \tag{3.28}$$

In the kinematic or Born approximation (rather than using the dynamical approach as above) the reflectivity is related to the Fourier transform of $\sigma(z)$ or its gradient such that

$$R(Q) = \frac{16\pi^2}{Q^2}\left|\sigma(z)e^{iQz}dz\right|^2 \tag{3.29}$$

As mentioned earlier, the discussion up to this point aimed to describe the reflectivity of neutrons from a smooth interface between two media, with no adsorbed layers. NR measurements of such an interface yield R as a function of Q, which is known as the specular reflectivity profile. In equation 3.29, R is proportional to $1/Q^4$, hence the reflectivity will decay rapidly with increasing Q. An example reflectivity profile R(Q), recorded at the air water interface of D_2O, is shown in Figure 3.3. At $Q < Q_c$, total reflection occurs, and R = 1. The point where Q increases above Q_c is known as the critical edge, and at higher values of Q the reflectivity decays with $1/Q^4$.

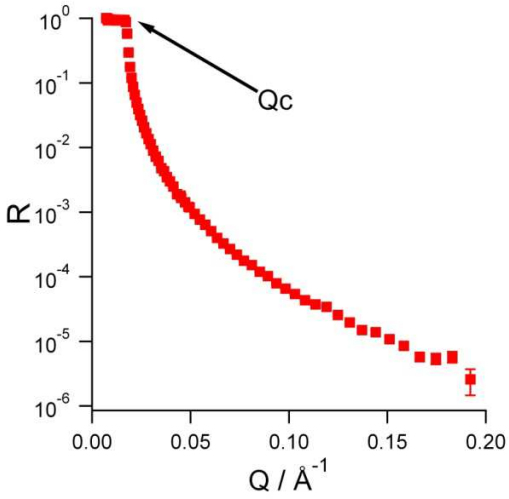

Figure 3.3. Example of a reflectivity profile obtained on pure D_2O. The critical value of the momentum transfer, Q_c, below which total reflection occurs, is marked with an arrow.

We can now extend this explanation in order to consider the situation where neutrons are reflected from a single homogeneous thin film at the smooth interface between two homogeneous media. For a single film, reflection can be considered as occurring from two interfaces, above and below the film. Constructive and destructive interference between the neutrons reflected from the two different interfaces of the film causes an oscillatory pattern of fringes to be superimposed on the Q^4 decay. The period of these oscillations, ΔQ is related to the thickness of the film, d, by $\Delta Q = 2\pi/d$. The amplitude of the fringes is indicative of the sharpness of the interfaces, with large fringes indicative of sharp interfaces and small fringes indicative of diffuse interfaces. In soft matter systems a small number of small interference fringes are usually seen. Fringes are only seen if the film is above a threshold thickness, due to the limited Q range before measurements reach the background.

For a single thin film at the interface an exact expression for the reflectivity can be expressed in terms of thin film optics, as it was in Chapter 2, where 1 is the air, 2 is the layer and 3 is the medium beneath the layer:

$$R = \left|\frac{r_{12}+r_{23}e^{-2i\beta}}{1+r_{12}r_{23}e^{-2i\beta}}\right|^2 \qquad (3.30)$$

where $\beta=(2\pi/\lambda)n_2 d\sin\theta_2$ (optical path length in the film or phase factor) and the Fresnel co-efficient r_{ij} is given by equation 3.10. Commonly for the purpose of this discussion, Equation 3.10 is simplified to

$$r_{ij} = \frac{p_i - p_j}{p_i + p_j} \qquad (3.31)$$

where $p_j = n_j \sin\theta_j$ and $p_i = n_i \sin\theta_i$ In real systems, the boundaries are not entirely smooth, and local roughness will modify the specular reflectivity. The Fresnel coefficient can be modified to include an error function as described by Nevot and Croce[16] to become

$$r_{ij} = \frac{p_i - p_j}{p_i + p_j} \exp\left(-2 p_i p_j \gamma_{ij}{}^2\right) = \frac{n_1 \sin\theta_i - n_2 \sin\theta_t}{n_1 \sin\theta_i + n_2 \sin\theta_t} \exp\left(-2 n_1 \sin\theta_i n_2 \sin\theta_t \gamma_{ij}{}^2\right) \quad (3.32)$$

where γ_{ij} is the roughness at the interface between the layers i and j. The roughness causes R to fall off faster with increasing Q than the $R = 1/Q^4$ relationship described above for a smooth interface.

This approach can be extended to three or four successive layers. However analysis of a more complex structure at an interface, either for a number of discrete multilayers or for a material with a refractive index gradient which can be approximated to a series of layers, R can be found from an extension of thin film optics known as the optical matrix method of Born & Wolff.[1] A more convenient method is that of Abeles.[1] In this method a characteristic matrix per layer is defined from the relationship between the vectors in consecutive layers. Between successive layers i j,

$$r_{ij} = \begin{bmatrix} e^{i\beta_i} & r_j e^{i\beta_{j-i}} \\ r_j e^{-i\beta_i} & e^{-i\beta_i} \end{bmatrix} \quad (3.33)$$

From this, transmission and reflection from one layer to another is described as a matrix multiplication product for each layer. The resultant reflectivity for n layers is then obtained from the product of the characteristic matrices $M_R=[M_1]\ [M_2]....\ [M_n]$.

The usual way to analyse reflectivity data is to compare measured reflectivity profiles to those calculated using the optical matrix method. In this thesis, this was achieved using the program MOTOFIT[17], which enables model profiles to be generated by variation of different properties of a given layer including scattering length density, thickness, solvent penetration and roughness. It is important to ensure that the model is physically representative of the system being studied, as phase information is lost in a reflectivity experiment due to the measurement of the square of the amplitude, and hence multiple different models can be used to fit a given reflectivity curve. Measurement of multiple isotopic contrasts is a common way to reduce this problem, as it is unlikely that the wrong structural model will provide good fits to all of the contrasts measured.

3.2.3 Information Obtained from NR Experiments

The objective of an NR experiment is to measure the reflectivity as a function of Q, hence the output of an experiment is a specular reflectivity profile R(Q), such as that shown in Figure 3.3. This shows the reflected intensity relative to the incident neutron intensity as a function of the scattering vector. For a pure surfactant monolayer, this can be fitted to obtain values of the scattering length density (σ) in $Å^{-2}$ and monolayer thickness (τ) in Å. These can be used to calculate the surface excess of surfactant from

$$\Gamma = \frac{\sigma\tau}{\sum n_i b_i} \tag{3.34}$$

where b_i is the scattering length of atom in Å $molecule^{-1}$ and n_i is the number of times that atom i appears in the molecular formula for the surfactant. In order for Γ to be in moles per m^2 rather than molecules per $Å^2$, the value calculated from equation 3.34 needs to be scaled by both Avogadro's constant N_A and by 1 x 10^{20}.

The area per molecule, A, is then given by

$$A = \frac{N_A}{\Gamma} \tag{3.35}$$

where N_A is Avogadro's constant, and is used to convert from area per mole to area per molecule. In order to obtain reliable values of Γ and A, isotopic contrast variation is usually used in order to ensure that a reasonable structural model is used in fitting the data, as discussed below.

This study has not simply been of the adsorption of surfactant layers at the air/water interface, rather the adsorption from polymer/surfactant systems has been examined. As both polymer and surfactant are adsorbed at the interface, equation 3.34 cannot be used to simply obtain the surface excess of either component. Usually, contrast variation is used to determine the adsorbed amounts of different components by selective deuteration of the surfactant and/or the solvent, as few polymers are available in deuterated forms.

However, one of the aims of this project has been to obtain compositional information using NR data measured on only one isotopic contrast, and ellipsometry data. NR data recorded on the isotopic contrast of hydrogenated polymer and deuterated surfactant in null reflecting water (a mixture of H_2O and D_2O which has the same scattering length density as air and therefore does not significantly contribute to the meausurements), can be fitted to yield the scattering length density, σ, and thickness, τ, of the adsorbed layer. As deuterated surfactant is used, with a scattering length density much greater than the hydrogenated polymer, this NR measurement is primarily sensitive to Γ_{surf}. The quantity

obtained from ellipsometry measurements, $\bar{\rho}$, however has similar sensitivities to Γ_{poly} and Γ_{surf} due to the comparable refractive indices. As a consequence of the different sensitivities of the two approaches, the measured quantities $\sigma \times \tau$ and $\bar{\rho}$ can be co-modelled to obtain values of Γ_{poly} and Γ_{surf}. This co-modelling approach, which will applicable to a wide range of systems, is discussed in much greater detail in Chapter 4.

None of the data measured for polymer/surfactant mixtures on the OFC as part of this project exhibited significant structure normal to the interface (see Chapter 4), which is in part due to the dynamic nature of the interface on the OFC. However, for NR measurements on other soft matter systems, including polymer/surfactant mixtures at the static air/water interface, the interfacial structure can be more complicated, with multilayers present at the interface (where the references[18-21] are only a few examples relevant to the systems studied in this thesis). One or more Bragg diffraction peaks in the specular reflectivity profile indicate the presence of repeating structure such as multilayers perpendicular to the plane of the interface, and the position of the Bragg peak gives us information about the repeat d-spacing of this structure. As no Bragg peaks or other indicators of significant structure of the adsorbed material perpendicular to the interface were observed for any of the measurements in this study I will not discuss the examination of Bragg peaks further in this thesis.

All of the above discussion assumes that the interface under examination is homogeneous in the plane of the interface, i.e. there is only structure that can be resolved by NR in the direction normal to the interface. However, interfaces may have significant repeating structure in the plane of the interface, which leads to off-specular scattering of neutrons.[22] On a 2D TOF detector such as that on FIGARO (see later) off-specular scattering leads to a diagonal line on the detector image. In this study no significant off specular scattering is observed, due to the simple layers adsorbed at the interface and the flowing nature of the OFC, hence I will not discuss this any further.

3.2.4 Isotopic Contrast Variation

As discussed above, it is possible to calculate a neutron reflectivity profile using an optical matrix method, however it is possible that more than one structural model will result in the same reflectivity profile. The most common solution to this problem for soft matter systems is to measured NR data on multiple isotopic contrasts, as it is unlikely that an incorrect model will fit data obtained on multiple contrasts.

Contrast variation exploits the fact that neutrons are scattered very differently by hydrogen and deuterium, which have scattering lengths of -3.7406 x10^{-5}Å and 6.671 x10^{-5}Å, respectively. For species containing multiple hydrogen atoms such as the polymers and surfactants used in this study, replacement of the hydrogens by deuterium will significantly change the scattering length density of the component. Selectively deuterating different species in a system or varying the solution phase from D_2O (with SLD 6.35 x 10^{-6}Å^{-2}) to H_2O (with SLD -0.56 x 10^{-6}Å^{-2}) enables us to obtain information about the thickness and composition of the adsorbed layer of a chemically identical system. A mixture of 91.1% H_2O with 8.9% D_2O by weight yields a liquid subphase with the same scattering length density as air, known as null reflecting water (NRW). As a consequence, if NRW is used as the liquid for an air/liquid experiment, there is no contribution to the specular reflectivity signal from the solvent and the reflectometry profiles obtained are only due to the adsorbed material at the interface, although H_2O does contribute to the incoherent background.

The primary isotopic contrast used in the measurements presented in this thesis is that of deuterated surfactant with hydrogenated polymer and NRW (d-surfactant/h-polymer/NRW), in which the majority of the specular reflectivity signal is from the deuterated surfactant. For polymer/surfactant systems an equivalent measurement using deuterated polymer and hydrogenated surfactant, h-surfactant/d-polymer/NRW, can be used to examine the amount and structure of the adsorbed polymer, however this is typically limited by the availability of deuterated polymer, especially for measurements on the OFC which require large solution volumes. The obvious alternative contrasts are h-surfactant/h-polymer/D_2O which gives us information about the change in the solvent distribution at the interface due to the penetration of polymer and surfactant, and d-surfactant/h-polymer/D_2O which gives us information about the displacement of D_2O by polymer or surfactant headgroups, as the surfactant chains have a similar SLD to D_2O However, as we will show in Chapter 4, measurements on these two contrasts along with d-surfactant/h-polymer/NRW do not always give an accurate measurement of the composition of the adsorbed layer from a mixture. As an alternative to multi-contrast measurements, one of the primary aims of the work in this thesis was to develop an approach to determining the

composition of an adsorbed interface using only one contrast, d-surfactant/h-polymer/NRW, with ellipsometry measurements acting as a second contrast for the determination of the interfacial composition. Use of only one isotopic contrast enables us to obtain the same information whilst making significant savings in the amount of beamtime and deuterated material necessary. Furthermore, Γ_{poly} values obtained from NR measurements in the absence of deuterated polymer are limited in their accuracy, use of our co-modelling approach enables Γ_{poly} to be obtained with greater accuracy.

For information, the scattering length densities (σ) of the species used in this study are given in Table 1 as calculated from their calculated scattering lengths and molar volumes

Species	**σ /10^6 Å^{-2}**
NRW	0
D_2O	6.35
dSDS	6.88 with Cl, 6.86 without
$dC_{12}TAB$	4.93 with Br, 5.12 without
$dC_{14}TAB$	5.11 with Br, 5.29 without
$dC_{16}TAB$	5.26 with Br, 5.43 without
PEO	0.935
PSS	1.85

Table 3.1. Scattering length densities of species used in this study

3.3. Instrumentation: FIGARO

Fluid Interfaces Grazing Angles ReflectOmeter (FIGARO) is the new horizontal reflectometer at the Institut Laue-Langevin (ILL). FIGARO is a reflectometer for horizontal samples, and can therefore be used in the study of liquids at the free air-liquid interface which is not possible with D17, the other reflectometer at the ILL due to its vertical sample plane, although both can be used to look at buried liquid-liquid and solid-liquid interfaces. FIGARO can be used in reflection down or reflection up configurations, with neutrons directed at an interface from above or below the horizontal, depending on the required application. FIGARO is suitable for a wide range of applications due to the ability to balance the flux with respect to the wavelength resolution and Q range, which enables fast kinetic studies to be performed and optimises the data acquisition efficiency according to the needs of a given experiment. FIGARO is equipped with a range of sample environments including free liquid adsorption troughs, a Langmuir trough, a range of solid/liquid sample cells, and of course the OFC. This section will give an over-view of the components and workings of FIGARO, more details are given in the recent paper of Campbell *et al*.[23]

Figure 3.4 shows a schematic representation of FIGARO, highlighting its main components. From right to left, the main components are two frame overlap mirrors and a four disk chopper assembly used to select the wavelength and resolution, two deflector mirrors and a collimation guide, which reflect the beam up or down and focus it on the sample, a sample stage with motorized goniometers, and a 2D detector. More details of the set-up and purposes of each of these components will be given in the following section.

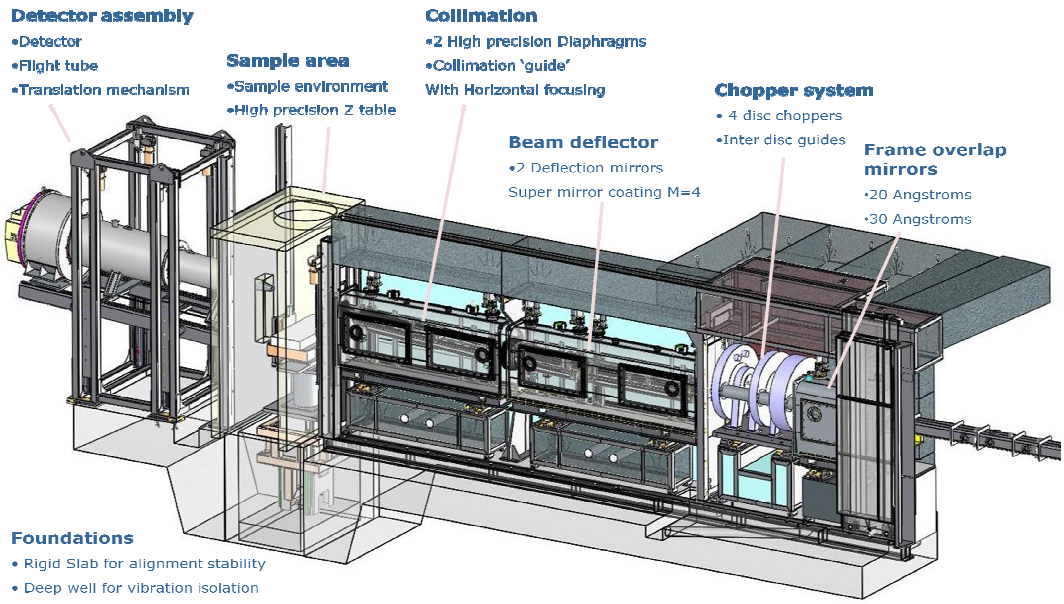

Figure 3.4. Schematic of the layout of FIGARO, highlighting each of its components

3.3.1 Choppers and Frame Overlap Mirrors

Thermal neutrons produced by a reactor such as the one at the ILL are moderated to a wavelength band suitable for measurements by a cold source, and arrive at the instrument with a Maxwellian range of wavelengths. For a time-of-flight instrument, distinct pulses of neutrons with a defined range of wavelengths are required,[24] and at a facility such as the ILL where neutrons come from a continuous source reactor, these are created by the choppers. Choppers are rotating disks which block the passage of neutrons for the majority of the time, but let them through a small window. The greater the distance between a pair of choppers the more neutrons in the selected wavelength band, i.e. the higher the flux but the lower the wavelength resolution ($d\lambda/\lambda$). The wavelength resolution controls the Q resolution of a NR measurement dQ/Q

$$\left(\frac{dQ}{Q}\right)^2 = \left(\frac{d\lambda}{\lambda}\right)^2 + \left(\frac{d\theta}{\theta}\right)^2 \tag{3.36}$$

On a time of flight instrument such as FIGARO, $d\lambda/\lambda$ is replaced by dt/t where dt is given by the pulse width defined by the choppers and t is the time of flight of a neutron. On FIGARO, a four chopper disks assembly is employed, however only two of these choppers define the neutron pulse at any one time. The purpose of having four choppers is that different chopper pairs can be chosen to control the pulse shape, enabling selection of different distances between the choppers, and hence the use of different fluxes or wavelength resolutions. A close pair of choppers (minimum = 10 cm) favours a high resolution, whilst a pair with a greater separation (maximum = 80 cm) favours increased flux at the expense of fine detail in Q. As most FIGARO users look at liquid interfaces, they choose one of the high flux options.

Figure 3.5. Photographs of (a) the frame overlap mirror and (b) the choppers in the FIGARO instrument

Each pulse of neutrons consists of neutrons of a wide range of energies and speeds. Frame overlap mirrors separate two consecutive neutron pulses by removing neutrons above a certain wavelength before they reach the choppers. If the pulses are not separated in time it is impossible to determine which neutrons are the slow neutrons of pulse A and which are the fast neutrons from pulse B.

3.3.2 Deflector Mirrors and Collimation Guide

Once defined neutron pulses are made by the choppers, supermirror guides transport the neutrons to the sample. Supermirrors are widely used in neutron guides as they enable the transport of neutrons over large distances with small losses and result in high flux at the sample. A supermirror has a complex coating of many individual layers, in this case of nickel and titanium, which is designed to enlarge the critical angle of reflection of neutrons to high values, meaning that all neutrons hitting the surface with an angle shallower than the critical angle are transported to the sample, resulting in a significant increase in flux compared to not using supermirrors.

As discussed above, an additional feature of FIGARO is that neutrons can be aimed at the sample from either above or below for 'reflection up' or 'reflection down' configurations, implemented by the use of the deflector mirrors. 'Reflection up' is defined as the standard configuration used for free liquid interfaces where the neutrons approach the studied interface from above, and 'reflection down' is when the neutrons approach the studied interface from below. The supermirrors used allow a deflection of up to 1.7° without a significant loss in intensity, hence for the horizontal samples the maximum angle of incidence for 'reflection up' is 3.8° and for 'reflection down' is -2.7°, whilst for buried interfaces the sample can typically be tilted to further extend the Q-range if necessary.

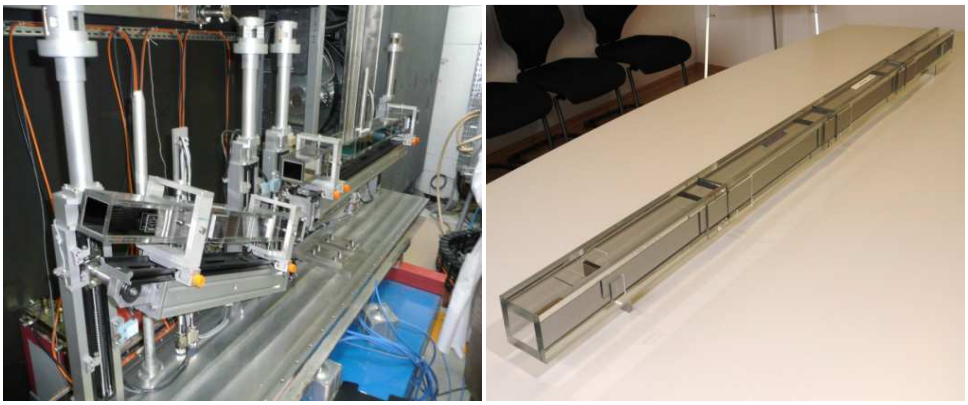

Figure 3.6. Photographs of (a) the deflector mirrors and (b) the collimation guide used on FIGARO

After the reflection direction is selected by the deflector mirrors, the beam is focussed to a defined footprint (from 60 to 40 mm) using a collimation guide. The neutron footprint on the sample is defined by use of very precise collimation slits before and after the collimation guide. The collimation guide is situated downstream of the deflector mirrors so that the collimation slits reduce the background created by off-specular scattering from the supermirrors. The two sets of beam defining collimation slits have four boron carbide blades to define the four sides of the neutron footprint. The size of the collimation slits controls the flux on the sample, with respect to the length of the footprint, opening the slits results in a gain in intensity but at a cost to the resolution (Equation 3.36). The width of the footprint is set to illuminate the optimum sample area for a given experiment.

3.3.3. Sample Area

The sample area of FIGARO is based on a steel frame embedded in concrete in a 2m deep hole to damp the low-frequency vibrations. On top of this frame are two flexible crossed goniometers, two vertical translation stages, a horizontal translation stage, and an active anti-vibration control unit. Damping using a anti-vibration unit is necessary for free liquid measurements, as external vibrations can increase the surface capillary waves, significantly reducing the reflectivity. Furthermore, the whole area is additionally enclosed by a frame of acoustic foam shielding to further reduce the ambient noise.

Figure 3.7. The Sample Environment on FIGARO

3.3.4. Area Detector

The general theory of neutron detection is based on the fact that neutrons can only be detected when they undergo a nuclear reaction with a gas such as ^3He or BF_3. The most commonly used reaction is :

$$n + {}^3He \rightarrow {}^3H + {}^1H + 0.76\ MeV$$

The particles produced from this reaction then ionize the ^3He, CF_4 or BF_3, (8 bar ^3He and 2 bar CF_4 in FIGARO's detector) gas producing an electron. The production of each electron leads to further ionization of gas, and therefore further electron production in a cascade effect. Freed electrons are detected using a low voltage biased wire. In FIGARO's detector the wires are located in hollow channels drilled into a single block of aluminium, each of which is contained within a separate gas containing tube, which limits the charge saturation to individual wires. The collected electrons constitute a current in the wire, which is proportional to the rate at which neutrons strike the detector, and can be measured by an external amplifier. When electrons hit the wire, the charge travels either way along the wire, to the anode and cathode. The proportion of the charge reaching either end enables event position determination. Only events which are correlated in time are selected by the software. The result is a 2D image of the neutrons which strike the detector. It does not matter if a given neutron hits the left or right of the sample as we do not measure horizontal displacement, instead the two dimensions recorded are 2θ and λ (or time).

Use of a 2D detector such as that on FIGARO enables the examination of a wide range of $2\underline{\theta}$, including background and offspecular information. Instruments with a single detector require separate measurements of the background in an off-specular position, and are insensitive to off-specular scattering from samples, an increasingly common feature of experiments on FIGARO.

In order to maximize detection efficiency, it is necessary to minimize the interaction of the scattered neutrons with air. For this reason an evacuated flight tube connects the sample and the detector.

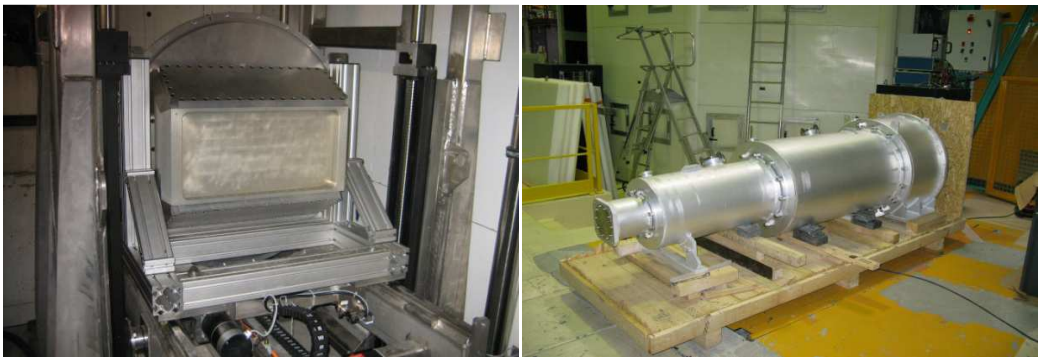

Figure 3.8. (a) Detector and (b) Evacuated flight tube used on FIGARO

At very high neutron intensities the detector efficiency becomes diminished and the maxima in the time of flight spectra become distorted, as neutrons arrive at the detector at a rate faster than the rate of dissipation of the ionized gas molecules. Therefore, for high intensity measurements such as direct beam measurements for which the collimation slits have to be opened at high incident angles to produce the same neutron footprint on the sample as at lower angles, an oscillating beam attenuator is used to limit the intensity. This device consists of a narrow vertical opening which oscillates over the full width of the incident beam at constant speed, and reduces the intensity by a constant attenuation factor.

3.3.5 Instrument Control

FIGARO is run using the ILL instrument control software NOMAD, which allows measurements to be controlled using a graphical user interface. Data obtained from NR measurements on FIGARO are reduced using the data reduction software COSMOS, part of the LAMP suite at the ILL. COSMOS allows us to select only the pixels around the specular reflection in the detector image (such as that in Figure 3.10) and to subtract the pixels a certain distance away from this peak so that the background is subtracted live for every sample measured. Furthermore, COSMOS enables us to group the measured data points to obtain a fittable specular reflectivity profile, which is normalized to the data below the critical edge of D_2O, and furthermore the factor which causes data obtained on the two angles to overlap is calculated in COSMOS. Once a correct neutron reflectivity profile is obtained from COSMOS it can be imported into a fitting package for comparison to a model of the material at the interface. In the work presented in this thesis, that data was then imported into IGOR in order to obtain fits to the specular reflectivity profiles using the MOTOFIT[17] package. For further information on the

set-up and data reduction procedures used for measurements on standard sample environments, see the instrument paper.[23]

3.4. NR Measurements on the OFC

NR measurements on FIGARO on sample environments other than the OFC have standard instrument set-ups, however as the OFC was first used on FIGARO as part of this project, experiments and calculations to determine the optimum experimental set up and data reduction procedures are an important part of this thesis. The key differences between the OFC and other sample environments are that the OFC has a small area, its diameter is only 80 mm, and the flowing nature of the system means that the interface is slightly curved. If neutrons are incident on a curved area of the interface, errors in the measured reflectivity profile will result if data are not corrected for the effect of this curvature. Consequently, the first experiment performed on FIGARO was devoted to the determination of the size of the optimum footprint size which could be used in neutron experiments whilst minimizing the resultant errors. The first part of this section (3.4.1) will discuss the procedure used to determine the optimum footprint.

Even once the optimum footprint is determined, the curvature of the interface will still have an effect on the measured data, as it exacerbates the effects of gravity on the neutron trajectory. For measurements made on planar surfaces in other sample environments, the effects of gravity are accounted for in the data reduction software COSMOS, but the extra contribution to the gravity effect on the OFC is not accounted for, which will incur further errors in the data. Therefore the second part of this section (3.4.2 and 3.4.3) will discuss the effect of gravity on OFC measurements, starting with the standard effect of gravity on the neutron trajectory and then combining it with the effect of interfacial curvature. The final part of this section (3.4.4) will discuss further details of the experimental set-up of the OFC on FIGARO, and the experimental procedures used.

3.4.1. Determination of the Optimum Footprint for OFC Measurements on FIGARO

Due to the small sample area (80 mm diameter) and interfacial curvature of the OFC, different instrument settings are necessary for these measurements than for other free liquid experiments on FIGARO. Samples of different bulk composition will have different interfacial curvatures due to the changing marangoni flows at the interface (discussed in Chapter 2 section 2.2). The effect of bulk composition on curvature is much greater than that of the flow rate of the system, which has a minimal effect on interfacial curvature. Neutrons reflected from a curved part of the interface will have a spread of directions, which will incur uncertainty in the incident angle, a loss of Q-resolution, and a possible shift in Q which will cause systematic errors in Γ. It is therefore necessary to use a footprint or illuminated area of incident neutrons which minimizes the errors introduced into the reflectivity profiles by the curvature of the interface. Due to the diameter and curvature of the OFC, this footprint will be much smaller than used for other free liquid experiments, for which footprints of up to 150 mm in length are used to maximize neutron flux and minimize acquisition times. A balance was sought between limiting the effect of surface curvature and the reduction in the flux and consequent increase in measurement time which results from decreasing the footprint size. Although the optimum neutron footprint for use in NR measurements on the OFC has previously been determined, this was done on the reflectometer SURF (ISIS, United Kingdom)[25], FIGARO has quite different instrument characteristics to SURF, including a 2D detector.[23] Hence the optimum set-up needed to be re-characterised for FIGARO.

Previous studies on the OFC have shown that due to the quadratic variation of the surface excess, Γ, with radial position, Γ changes by less than 5% of a monolayer over the central 40 mm of the cylinder.[25, 26] Furthermore, the data shown later in Figure 3.14 show that even for the most curved interfaces, the central 30 mm of the interface is reasonably flat. We would therefore expect that a footprint of around 30 to 40 mm would be the optimum for use on the OFC, with larger footprints introducing errors in the measurements.

The size of the footprint on the surface of the OFC is determined by the height and width settings of the collimation slits used, and also by the effect of gravity on the neutrons, which will cause them to travel a different horizontal distance before the sample to that defined by the collimation slits, lengthening the footprint. This effect of gravity will be discussed further in sections 3.4.2 and 3.4.3. Note that the footprints used had lengths shorter than their widths in order to allow a tolerance on the micronscale for vertical misalignment. The size of the footprints resulting from the collimation slit settings and the effect of gravity was simulated using Gitwit, a plugin to the ILL data suite LAMP.

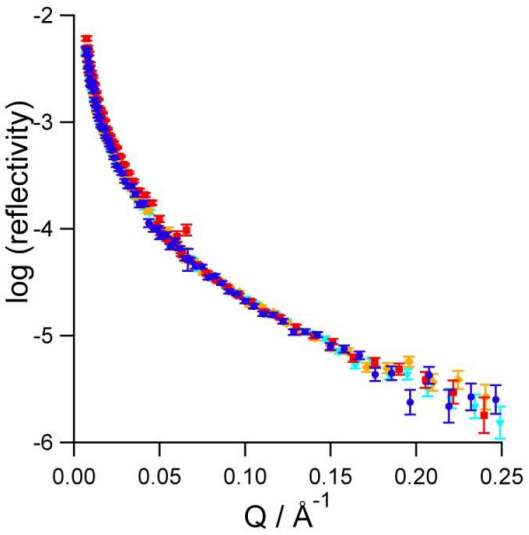

Figure 3.9. Specular reflectivity profiles recorded on 4 mM APFN solutions in NRW on the OFC in order to evaluate the optimal incident neutron footprint to use in experiments. The footprints shown are 30 x 41 mm (blue), 40 x 52 mm (turquoise), 60 x 30 mm (orange) and 80 x 30 mm (red). All footprints are defined in terms of length x width.

To determine the maximum footprint for which the effects of curvature of the free liquid surface on the OFC could be neglected, reflectivity profiles of D_2O and 4 mM ammonium perfluorononanoate (APFN) solution in null reflecting water (NRW) were measured for a range of footprint sizes. These two solutions will result in the most curved and flattest surfaces respectively that are likely to be measured on the OFC, water will result in a domed surface (as discussed above), and 4 mM is above the cmc of APFN[27], resulting in low surface tension gradients across the interface, which is therefore almost flat. APFN is a fluorinated surfactant and was chosen for its high scattering length density (SLD) and its relatively low cost compared with deuterated surfactants.

To test the effect of the footprint size, different openings of collimation slits S2H, S3H, S2W and S3W were chosen which, with umbra and penumbra of divergence taken into account, resulted in the following footprints: 25 x 30, 30 x 41, 40 x 52, 60 x 30 and 80 x 30 mm (length x width). The lengths of the footprints given include calculations of the effect of gravity on the neutron trajectory, which will be explained further in section 3.4.2. Footprints of up to and including 40 x 52 mm yielded satisfactory reflectivity profiles for the APFN solutions, with the parts of the specular reflectivity profiles from the two different incident angles overlapping to within 5% in R in the mid-Q region. However, as we can see in Figure 3.9, larger footprints (60 x 30 and 80 x 30) led to greater deviations from the other reflectivity profiles and were therefore rejected.

Although the data in Figure 3.9 suggest that a 40 x 52 mm footprint is optimal for use on the OFC, the detector images from measurements using this footprint on D_2O (Figure 3.10) show significant off-specular scattering attributable to surface curvature which is not present in the data recorded using the 30 x 41 mm footprint. Consequently, we used 30 x 41 mm as the footprint for all subsequent measurements, despite the cost in flux. The slit settings for this footprint are given in Table 3.2.

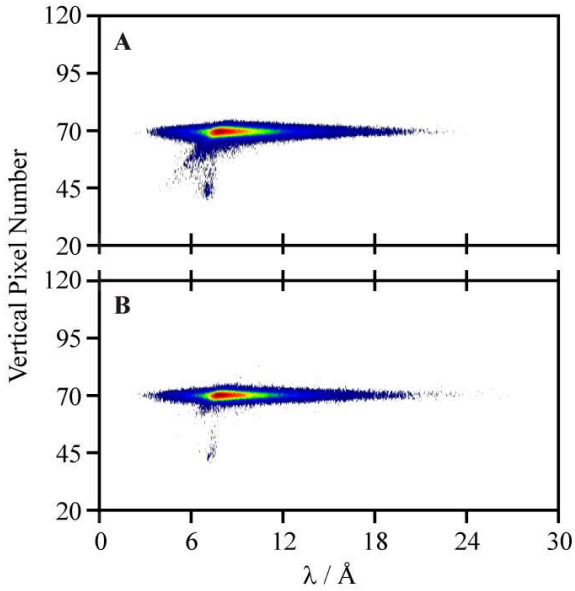

Figure 3.10. Detector images for neutron reflectivity measurements at the air/D_2O interface using incident neutron footprints of 40 x 52 mm (length x width; A) and 30 x 41 mm (B); angle of incidence is 0.624°. The small number of counts at around pixel 45/ 7 Å in B can simply be attributed to the edge of the refracted beam, whereas the much larger signal away from the specular ridge in A cannot.

Slits	Openings for Angle 1 - 0.624° / mm	Openings for Angle 2 - 3.78° / mm
S2H	0.44	3.00
S3H	0.22	1.50
S2W	35	35
S3W	35	35

Table 3.2. Slit openings for the 30 x 41 (length x width) neutron footprint used in our measurements on the OFC on FIGARO, where S2H and S3H are the vertical openings of the first and second collimation slits, respectively, and S2W and S3W are their corresponding horizontal openings. The S2–S3 separation is 2165 mm and S3–sample centre separation, noting that the OFC was positioned closer to slit 3 than in typical experiments, is 195 mm.

3.4.2 Corrections for the Effect of Gravity

Even once the optimum neutron footprint to limit scattering from the most curved parts of the surface has been determined and used, the measured region of the interface will have some curvature, especially at low surfactant concentrations. This curvature will have an effect on the measured reflectivity profiles, as it will exacerbate the effect that gravity has on neutrons trajectories. For flat samples measured on FIGARO, the effect of gravity has been incorporated into the data reduction program COSMOS. For curved surfaces such as that of the OFC, the effect of gravity is more significant, as reflection of neutrons from the curved parts of the cylinder will affect the resultant data. In addition to the loss of Q-resolution from an increased spread of incident angles, if the effect of gravity on the neutron trajectory is not accounted for, a systematic error in the calculation of Q would result. As a consequence we need to evaluate the combined effects on gravity and curvature on OFC measurements to determine the magnitude of the error incurred in the data.

The effect of gravity relates to the fact that cold (long wavelength) neutrons travel more slowly and therefore fall a greater distance vertically (by several millimeters) during their time-of-flight than the fast neutrons. Due to this effect of gravity, all the neutrons follow a parabolic trajectory to the sample, which results in a significant horizontal shift of the slow neutrons at the sample position compared to the position which would result from a straight line path of travel. The neutrons also strike the sample with a higher incident angle, which means the true value of Q is altered, and they have an earlier or later start time through the choppers depending on whether the choppers are spinning up or down. However, this latter effect is accounted for routinely in the chopper settings.

The neutrons follow a parabolic path through the two collimation slits which results in their arrival at the sample at a position horizontally shifted compared to that which would be calculated for a straight line trajectory, by the distance δx, as shown in Figure 3.11.

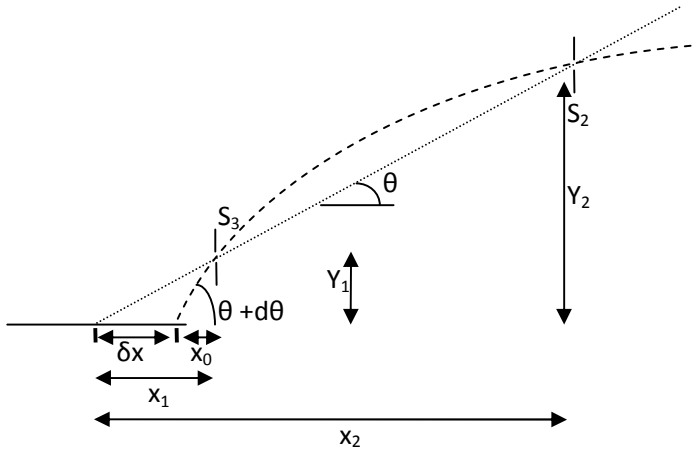

Figure 3.11 . Schematic showing the straight line path through the slits to the samples of neutrons with an angle θ to the horizontal (dotted line) as compared to the path of a neutron affected by gravity (dashed line). The straight line path hits the centre of the sample.

The horizontal shift of the neutrons at the sample due to gravity, δx, is defined in terms of the parabolic trajectory of the neutrons after the final collimation slit, S3, with parabola height, h, and horizontal distance x_0. The equation for the height to the top of a parabola is

$$h = y_1 + k(x_1 - x_0)^2 \tag{3.37}$$

Where k is the characteristic length, $k = g/2v^2$, $g = 9.81$, and the neutron speed $v = 3956/\lambda$. y_1 is the vertical sample to S3 distance, and x_1 is the horizontal sample to S3 distance.

The equation for the horizontal component of the parabola is:

$$x_0 = \frac{y_1 - y_2}{k} - \frac{(x_2^2 - x_1^2)}{2(x_1 - x_2)} \tag{3.38}$$

where x_2 is the horizontal sample to S2 (first collimation slit) distance and y_2 is the vertical sample to S2 distance.

It is important to note that the vertical distances are not simply the heights to the centre of the slits, as the footprint on the sample is defined by the positive and negative halves of the slits, and hence will depend on the vertical slit openings. Hence y_1 and y_2 are given by:

$$y_1 = tan\theta * x_1 \pm dy_1 \text{ and } \quad y_2 = tan\theta * x_2 \pm dy_2 \tag{3.39}$$

where dy is half the vertical slit openings [in mm]. Hence the side of the footprint furthest from the collimation slits is principally defined by negative dy_1 and positive dy_2 (i.e. by the upper half of the first collimation slit and the lower half of the second collimation slit).

The shift in x position on the sample due to the effect of gravity, δx, can be calculated from x_0 and h using trigonometry.

$$\delta x = x_0 - \sqrt{\frac{h}{k}} \tag{3.40}$$

As δx is calculated relative to the centre of the cylinder, the exact position of a neutron of given wavelength to the right hand side of the centre is given by δx + ½ the OFC diameter (40 mm).

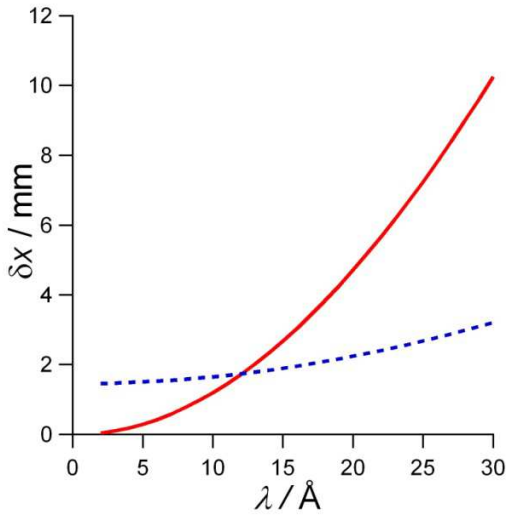

Figure 3.12. The difference in horizontal position at the sample (δx) of neutrons following a parabolic trajectory and those following a theoretical straight line path unaffected by gravity, calculated as a function of the neutron wavelength. The solid red line gives the calculated δx values for measurements made at the first angle, and the blue dashed line for measurements at the second angle. N.B. The slit settings for use in Equation 3.39. are those standardly used in OFC measurements as given in Table 3.2.

Figure 3.12 shows that only the longer wavelength neutrons are significantly shifted at the sample due to gravity, hence the position of the side of the footprint closest to the collimation slits will be almost identical to that calculated for a linear trajectory. From the calculated data it can be seen that for measurements at the first angle the shift in the position of the side of the footprint furthest from the collimation slits is around 10 mm, whilst at A2 it is only around 3 mm as tan (θ) is smaller. If a shift of 10 mm at the sample position and the consequent increase in footprint size is not acceptable, the high wavelength neutrons should be excluded from the data reduction. In our experiments on the OFC, data were only reduced to 22 Å in order to limit the shift in position due to gravity, although they were recorded for wavelengths up to 30 Å to ensure good overlap between the data recorded at the two incident angles in the mid-Q region. If the data in Figure 3.12 are fitted using a quadratic function, an

equation for δx in terms of λ is obtained, which will be used later to calculate the combined effects of gravity and interafacial curvature on measurements on the OFC.

In a time-of-flight neutron reflectometry experiment, each pulse incident on the interface contains neutrons of a range of wavelengths. However, the number of long wavelength neutrons in the pulse is considerable smaller the number of short wavelength neutrons, with the median wavelength being 5.3 Å. From Figure 3.12 we can see that 5.3 Å neutrons are only shifted by 0.33 mm. Therefore, although δx is large for long wavelength neutrons, only a small proportion of the incident neutrons will be shifted to a significant extent, and the shortest wavelength neutrons will be unaffected by gravity. This is demonstrated in Figure 3.13 which shows the calculated effect of the shift due to gravity on the incident TOF spectrum of neutrons at the interface. The red line is the calculated TOF spectrum which would result from the slit settings chosen in section 3.4.1, and the green line that which results from the effect of gravity.

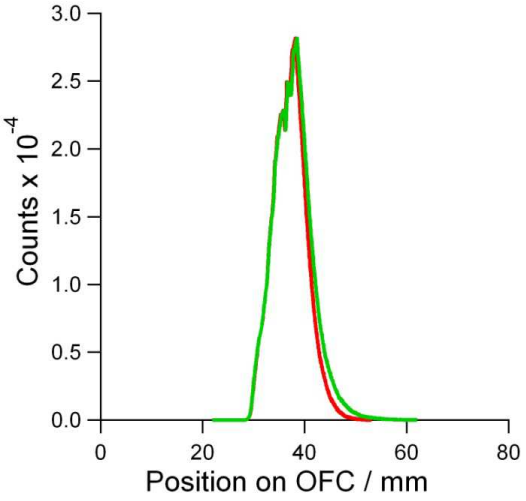

Figure 3.13. Calculated incident position of neutrons at the interface against their intensity as calculated from a recorded time of flight spectrum (counts v λ) and the δx v λ values in Figure 3.12. The red line shows the calculated positions for neutrons following a straight line trajectory, and the green line the positions of neutrons which have followed a parabolic trajectory due to the effect of gravity.

The calculations above give the effect of gravity the neutron trajectory for any sample on FIGARO, and explain the calculation of the footprint dimensions discussed in section 3.4.1. In order to minimize the effect of gravity on OFC measurements, the OFC was moved closer to the final collimation slits, to decrease the distance the neutrons travelled under gravity. In order to determine whether the neutron trajectory under gravity incurs further errors in OFC measurements, I will now combine these calculations with data on the interfacial curvature.

3.4.3. Combined effect of Gravity and Curvature

In order to evaluate the error incurred in our NR measurements due to the curved surface of the OFC, we mapped the height as a function of radial distance across the interface for pure water and two polymer/surfactant systems, PEO/SDS/H_2O and PEO/C_{14}TAB/H_2O using an optical height sensor (Keyence, LKG-152, Japan) which is installed on FIGARO. Figure 3.14 shows the height of the interface as a function of radial distance for pure water and several PEO/C_{14}TAB mixtures of different compositions. The curvature of the interface of water is much greater than that of a solution containing a large amount of surface active species such as 1.25 mM C_{14}TAB/100 ppm PEO, because surface active species at the interface lower the surface tension and radially accelerate the solution, resulting in a flat interface. The radial force that accelerates H_2O arises only from a hydrostatic pressure gradient resulting in a slight doming of the interface. Figure 3.14 shows that even for the most curved surface (pure water) the central 30 mm is flat to within 0.2mm.

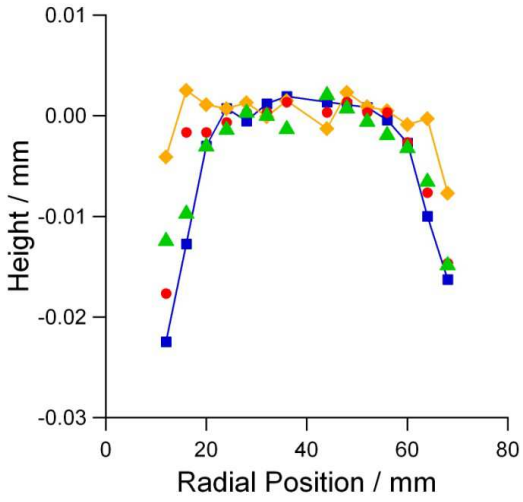

Figure 3.14. Height of the air/solution interface of the OFC as a function of radial position (x) for several different solutions including water (blue squares), 0.027 mM C_{14}TAB/100 ppm PEO (red circles), 0.18 mM C_{14}TAB/100 ppm PEO (green triangles) and 1.25 mM C_{14}TAB/100 ppm PEO (yellow diamonds). The blue and yellow lines are added as guides to the eye only. The height is set to zero at the centre of the interface for water, all other measurements are offsets from this value.

Curvature of the interface on the OFC effectively results in a change of the angle of the interface as seen by incident neutrons as a function of radial distance, and hence a change in the incident angle of the neutrons. As the quantity measured in NR experiments (Q) is dependent on the incident angle, $= \frac{4\pi sin\theta}{\lambda}$, the extent of the curvature of the interface will affect the measured values of Q. We can use a fit to the data in Figure 3.14 along with the functions which account for the shift the horizontal position of the neutrons due to gravity obtained from Figure 3.12 to determine the necessary correction

to Q for the combined effects of gravity and curvature. The following calculations use the interfacial curvature data for the 0.027 mM C_{14}TAB/PEO system (as shown in Figure 3.14), this solution was chosen as it has a high curvature due to the low concentration of surfactant, and will hence give an approximation of the maximum error.

For a given solution in Figure 3.14, a function for the change in height with radial position, d*h*/d*x*, can be fitted to the data. The angle of the interface from the horizontal at a given radial position (θ) can then be approximated by trigonometry from $\tan^{-1}(dh/dx)$. The gradient of these θ v x data gives the change in the angle of the interface with radial position, dθ/d*x*.

The combined effects of gravity and curvature on the values of the momentum transfer, Q, measured in NR experiments on the OFC experiments can be approximated by combining the equations for the shift in x as a function of λ, δx, as obtained from Figure 3.12 with that for the change in interfacial angle as a function of x, dθ/dx. Combining these two equations gives us a function for dθ with respect to λ**,** which is plotted in Figure 3.15. As $Q = \frac{4\pi sin\theta}{\lambda}$, we can use our equation for dθ with respect to λ to calculate the change in Q as a function of λ which results from the combination of gravity and interfacial curvature, $dQ = \frac{4\pi sin(d\theta)}{\lambda}$.

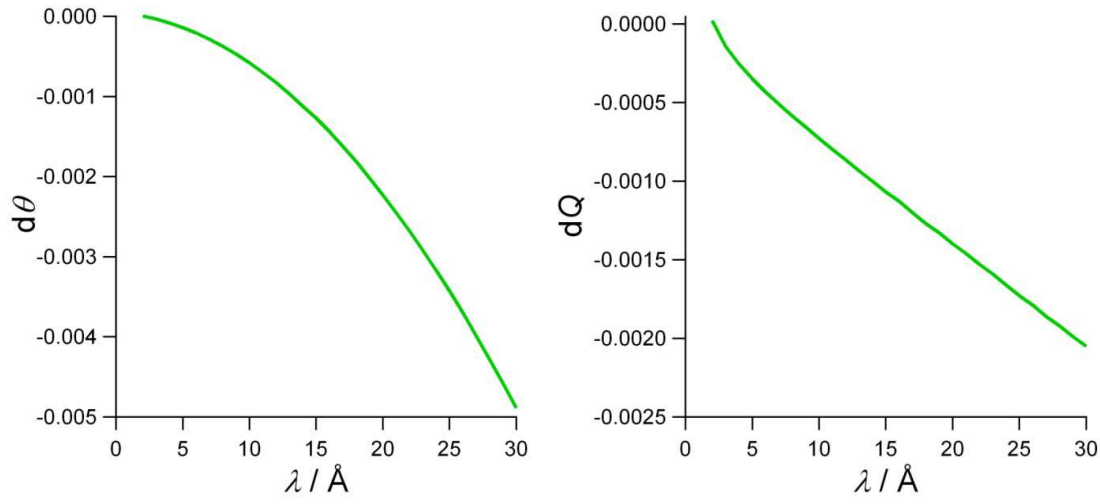

Figure 3.15. (a) Calculated combined effects of gravity and interfacial curvature as shown by the change in interfacial angle, dθ, with neutron wavelength, λ, calculated by combining dθ/dx and δx as a function of λ from Figure 3.12 and (b) Calculated change in momentum transfer, Q, with neutron wavelength, λ, as calculated from the function in Figure 3.15(a) using the equation $Q = 4\pi\text{Sin}(\theta)/\lambda$.

dQ as function of Q can be plotted at both incident angles used in this project (0.624° and 3.78°) , and can be used to work out the alterations which could be made to the measured specular reflectivity

profiles for data at both angles (reflectivity as a function of Q). As Q is inversely proportional to λ, the largest dQ will be at low Q for each angle.

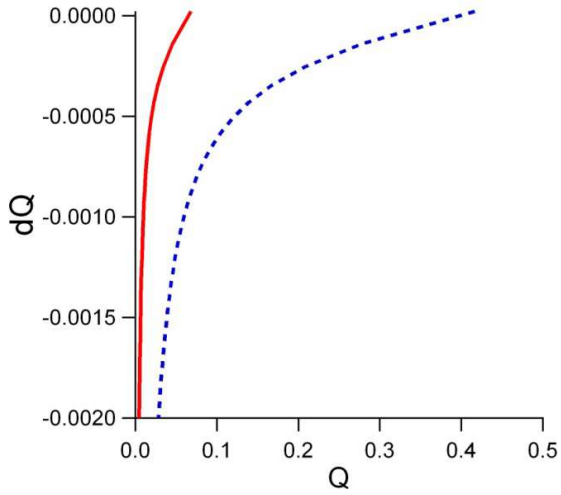

Figure 3.16. Calculated change in the reflectivity, dQ, which would result from the combined effects of gravity and curvature for a system with a curved interface measured using NR on the OFC. The solid red line gives the calculated values for measurements at the first angle, and the dashed blue line for measurements at the second angle (as in Figure 3.12).

If the recorded Q values at both angles are altered by the dQ values given in Figure 3.16, we would expect that the overlap between the data from the two angles would be slightly altered due to the high dQ at low Q for the second angle measurement, and the critical edge may be slightly shifted due to the high dQ at low Q for the first angle.

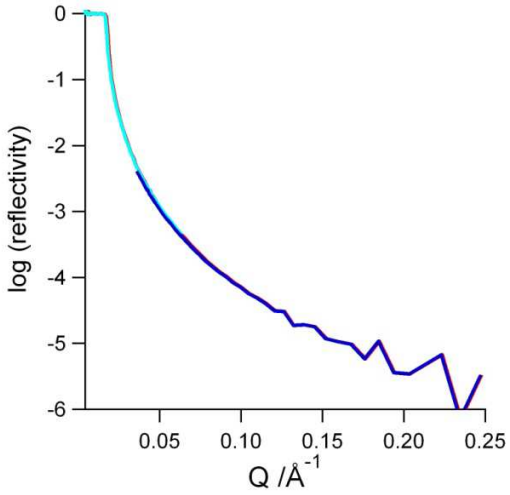

Figure 3.17. Specular reflectivity profile recorded for 0.1 mM h-SDS/100 ppm PEO/D_2O (red line, underneath the other lines), with data corrected by dQ from Figure 3.16 at the first angle (turquoise line) and the second angle (dark blue line).

In order to minimize the effect of gravity and curvature on Q, the data were only reduced up to 22 Å, even though they were measured up to 30 Å. This will significantly decrease the effects of curvature and gravity on the reflectivity profile, as 22 Å are only shifted by around 5 mm compared to the position defined by the collimation slits, whereas 30 Å neutrons are shifted around 10 mm. Figure 3.17 shows the effect of dQ on data recorded at both angles for 0.1 mM h-SDS/100 ppm PEO in D_2O, and reduced up to 22 Å.

An alternative approach to examining the effect of surface curvature on the data reduction is to consider how the factor used in COSMOS to cause the data from the two incident angles to overlap varies with the composition of the sample and therefore the surface curvature. This factor must be used in the data reduction due to the use of the attenuator for direct beam measurements, we do not precisely know the attenuation used hence a function COSMOS is required to stitch the data together. However calculation of the factor relies on the calculation of Q, hence a challenge with this work was to define conditions under which the factor could be derived. For the h-SDS/h-PEO/D_2O measurements discussed above, the factor calculated by COSMOS to cause the data to overlap decreases from 0.4 on the D_2O sample, which has the most curved surface, to 0.34 on the sample with the highest SDS concentration. Figure 3.18 shows the slight error in overlap which is caused if the factor derived from the D_2O sample (most curved) is used in reducing the highest concentration h-SDS/h-PEO/D_2O (least curved) data, compared with the factor calculated for this sample. During all of the experiments in this thesis, the factor used for data reduction has been derived for the flattest sample, one with a high surfactant concentration in order to limit errors from curvature in the sample reduction.

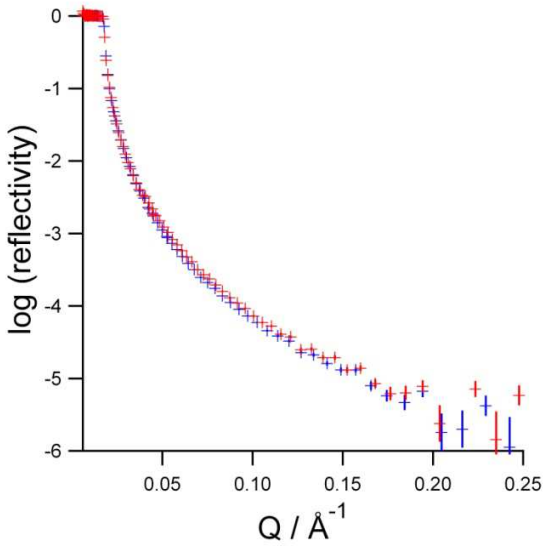

Figure 3.18. Specular reflectivity curves for 1.25 mM hSDS/100ppm 25k PEO/D_2O, obtained by data reduction using the factor obtained for pure D_2O (red crosses) and using the factor obtained for the sample itself (blue crosses). After the overlap region the former data set is slightly higher than the latter due to the use of these different factors.

The overall effect of the error in Q due to the combined effects of gravity and curvature results in a shift in momentum transfer (Q) of around just 2%, and resulting in a propagated error in the scattering length density and thickness of just 3%. As a result of the small magnitude of this effect, this dQ correction has not been undertaken for every data set recorded in this project, and this error has instead simply been included in our error analysis.

3.5. Details of NR experiments using the OFC on FIGARO

In Section 3.4 I have discussed the fact that different instrument settings are required for measurements using the OFC compared with measurements involving other free liquid samples on FIGARO due to the combined effects of gravity and curvature and the small size of the interface. The three main resulting differences for measurements on the OFC as compared to standard FIGARO measurements are the limited neutron footprint of 30 x 41 mm (settings in Table 3.2), the shifted position of the OFC 195 mm closer to the final collimation slits, and the limiting of the maximum wavelength of the reduced data to 22 Å. The shift in position is used because the beam emerges from the slits at different heights for the different incident angles, hence the sample has to move by around 20 cm vertically

between angles. In this section I will further discuss the set-up of OFC experiments on FIGARO and the instrument parameters used, many of which are standard to other measurements on FIGARO. [23]

The set-up of the OFC on FIGARO is slightly more complicated than the set-up of other sample environments, due to the attached flow system which needs to be attached to the sample table in a way which allows the OFC to be able to move vertically with the sample table for measurements at the two incident angles. Furthermore, due to the use of a pump, the flow system causes vibrations which need to be minimised for NR measurements. The main components of the flow system are the two liquid reservoirs and the pump, which are mounted on the steel frame of the sample table, which helps to damp the vibrations which result from them. Vibrations are further reduced by the use of small clamps to anchor parts of the tubing which connects the system together either to the steel frame or the anti-vibration table, and by ensuring that the tubing which supplies liquid to each reservoir is insulated from the reservoirs themselves. This vibration limiting set-up was refined in early experiments, to limit early anomalies in the data caused by vibrations. As the main components of the flow system are attached to the frame around the sample table, the issues surrounding moving the table up and down for two angle measurements are limited. However the glass coil used to regulate the temperature of the solution is placed is in water bath within the sample area, and in order to allow for movement of rest of the system the coil is connected by tubes with sufficient excess length to enable travel between the two angles.

Failures of the OFC flow system sometimes occur, especially during the study of polymer/surfactant systems which phase separate forming aggregates which can block constrictions in the system. In order to limit the impact of such floods on FIGARO, and to try to prevent the loss of deuterated samples, two new refinements to the classic OFC set-up (as described in Chapter 2) were made. Firstly, a Teflon overflow catching dish was fitted to the outside of the outer cylinder. In the event the OFC overflowed, any liquid would be caught in this dish and fed by a tube to a bottle. Secondly, a relay circuit connected to two electrodes was attached to the pump power supply. These electrodes are positioned in the aforementioned overflow bottle within the sample area, which is also fed by an overflow tube from the lower reservoir, which itself is fed by an overflow tube from the upper reservoir. If liquid overflows from either reservoir or the OFC into the bottle, the solution conducts electricity between the two electrodes and the circuit which powers the pump is cut off, significantly limiting the possibility of floods in the experimental zone and the overheating of the pump which should not run dry.

The OFC is positioned on the FIGARO sample table centrally with respect to the direction of the incident neutrons, but close to the final collimation slits (as mentioned above) and secured with double sided sticky tape. The sample table is leveled in both horizontal directions using a spirit level. In order to ensure that the incident neutrons fall at the centre of the interface of the OFC, it needs to be

vertically and horizontally aligned. A horizontal alignment scan is performed by moving the horizontal translation motor, STR, over a range of around 100 mm with a width of around 10 mm to obtain a triangular peak shape of plotted reflected intensities, which can be fitted with a centre of mass to determine the position of the centre of the cylinder. For some experiments later is this project the horizontal alignment scan was skipped as the precise positioning required had been noted from a previous experiment. The height of the interface of the cylinder is determined from two scans of SHT1 (vertical translation), a coarse scan over around 40 mm in 10 steps, and a fine scan 4 mm and 25 steps. It is clear from the data which positions are above and which are below the interface. Once the alignment procedure is complete, a measurement on D_2O is recorded at both angles, both for a reference and to ensure that the alignment procedure has been successful.

Once the height of the interface has been determined using the vertical alignment scan, it is kept constant in experiments despite the changes in interfacial height with solution composition using an optical sensor (LKG-152, Keyence, Japan) which detects the height of the interface using laser reflection, and a feedback loop to the sample height positioning motor SHT2. At the height of the interface of D_2O the height on the Keyence system is set to zero, and all other heights are relative to this. The Keyence has to be specifically positioned for OFC experiments due to the unusual position of the OFC (closer to the collimation slits) compared to other sample environments. This position is set manually to ensure that the laser beam is incident at the centre of the interface during the set up of the OFC.

All of the reflectivity measurements presented in this thesis were recorded at either one (0.624°) or two angles (0.624° and 3.78°). For the majority of NR experiments on free liquid surfaces, data are standardly recorded at both angles, as measurements at both angles are necessary to check the structural model applied to the data fitting, however compositional information can be obtained from first angle measurements alone. For all of the systems studied on the OFC as part of this thesis, the adsorbed layers were only thin films, and the amount of structural information which can be obtained from second angle or measurement in multiple isotopic contrasts was limited. As a consequence, the primary objective of this work has been to obtain compositional information about adsorbed material at the interface using NR measurements at only the first angle and only in null reflecting water (NRW) combined with ellipsometry measurements. Even in the absence of significant structural information, high Q data (at angle 2) can give an indication of the layer thickness to use in fitting the specular reflectivity profile. However in Chapter 4 we show that the structural model used in fitting the data has a minimal effect on the composition obtained from our co-modelling approach, hence NR measurements at only the first angle are sufficient to obtain the information we require. Furthermore, measurements at the first angle are much faster than those at angle two, hence neglecting angle two

measurements results in the ability to measure a much greater number of samples per experiment, enabling us to obtain much more information for a given system. Nevertheless, for the majority of the systems studied several samples were recorded at both angles in order to examine the structural information available and hence to use an optimal structural model in fitting the NR data, whilst optimizing our use of deuterated materials.

Although the majority of the data recorded in this project were measured only at the first angle and only in NRW as compositional information can be obtained using our co-modelling approach, some measurements employing the technique of contrast variation (as discussed in Section 3.2.4.) were performed with the purpose of validating this approach. Data on three polymer/surfactant systems were recorded in multiple isotropic contrasts, d-surfactant/h-polymer/NRW, d-surfactant/h-polymer/D_2O, and h-surfactant/d-polymer/D_2O, at both angles, in order to determine whether the compositions obtained using our co-modelling approach were consistent with the structural information obtained from multiple contrasts. These data and the conclusions reached are discussed in Chapter 4.

Reflectivity measurements were recorded in the range λ = 2–30 Å in order to ensure good overlap between data measured at the two incident angles (0.624° and 3.78°, Q = 0.005–0.4 $Å^{-1}$), but were reduced between 2.8 and 22 Å in order to limit the effect of gravity on the data, as discussed above. Measurements were recorded with a chopper pair giving constant $d\lambda/\lambda$ = 5.6%. Although a high flux setting was also available on FIGARO, using a 20 Å frame overlap mirror and chopper settings producing a constant 9.8% $d\lambda/\lambda$, this setting was not used in initial experiments in order to give a good overlap between the data at the first and second angles. However, as we found that only thin films adsorbed at the interface of the OFC for the systems measured, the higher flux settings would be appropriate for use in future measurements, and in fact were used in an experiment on the OFC with an external user late in this project.

The NR data in this project were recorded for acquisition times of between 15 min–3 hr in NRW and 15 min–1 hr 30 min in D_2O depending on the sample measured. These are longer than the standard acquisition times for measurements on static adsorption troughs due to the smaller neutron footprint required for the OFC. For several of the polymer/surfactant systems kinetic measurements were also taken, using short time slices of between 30 seconds and 5 minutes in order to determine whether changes in adsorbed layer composition were occurring with time. These short measurements can either all be fitted or binned into larger time periods during data reduction in order to reduce errors in the data. Kinetic data measured on the OFC on FIGARO are shown in Chapters 6,7, and 8.

Data were reduced using COSMOS, part of the LAMP suite at the ILL, between 2.8 and 22 Å as mentioned above. Normalization factors were derived from the reflectivity of a surfactant solution above its critical micelle concentration rather than from D_2O measurements as is standard, as this use of D_2O incurs errors in the other measurements due to surface curvature. The factor for the lower incident angle was derived by scaling the data below Q_c (in the range 0.10-0.15 $Å^{-1}$) to unity, and the factor for the higher incident angle was derived by fitting the reflectivity in the intermediate region of q where there is overlap. The normalized reflectivity data were binned in intervals of 0.8 × the resolution in q (dq). The reduced data were fitted to a structural model to obtain compositional information in the form of the product of the scattering length density, σ, and thickness, τ, of the layer ($\sigma \times \tau$) for use in our comodelling methodology using the MOTOFIT program[17] in IGOR. Information about the fitting methodology used for data from each system is given in the relevant chapters of this thesis.

The primary sources of error in NR measurements are from the positioning of the collimation slits (< 1% of the maximum value of $\sigma \times \tau$), fluctuations in the reactor power and chopper phasing (< 2% of the maximum value of $\sigma \times \tau$ for the acquisition times used), and systematic errors from the scaling of the data from an air/D_2O reflectivity measurement below its critical angle and the curved interface of the OFC combined with the effect of gravity (< 3% of the maximum value of $\sigma \times \tau$ in total). Other errors in $\sigma \times \tau$ arising from counting statistics and the choice of model, do not exceed 4% of the maximum value of $\sigma \times \tau$.

With regards to samples, experiments on FIGARO were performed as similarly to ellipsometry experiments as possible. Initially a solution of polymer and salt (or salt for pure surfactant measusrements) was added to the OFC, and measurements were performed as a function of increasing surfactant concentration, with a volume of concentration surfactant stock added for each consecutive measurement. The total volume of surfactant stock added each time was kept constant at 10 ml, which was possible due to the smaller number of samples measured by NR than by ellipsometry. For every addition of surfactant, polymer and salt were also added to the system to keep their concentrations constant.

3.6. References for Chapter 3

1. Born, M., Wolf, E., *Principles of Optics*. Pergamon Press: Oxford, 1997.
2. Lekner, J., *Theory of Reflection*. Martinus Nijhoff Publishers: Dordrecht, 1987.
3. Silva, D. S., *Elementary Scattering Theory*. Oxford University Press: 2011.
4. Simister, E. A.; Thomas, R. K.; Penfold, J.; Aveyard, R.; Binks, B. P.; Cooper, P.; Fletcher, P. D. I.; Lu, J. R.; Sokolowski, A., Comparison of Neutron Reflection and Surface-Tension Measurements of the Surface Excess of Tetradecyltrimethylammonium Bromide Layers at the Air-Water-Interface. *J. Phys. Chem.* **1992,** 96, (3), 1383-1388.
5. Lu, J. R.; Purcell, I. P.; Lee, E. M.; Simister, E. A.; Thomas, R. K.; Rennie, A. R.; Penfold, J., The Composition and Structure of Sodium Dodecyl-Sulfate Dodecanol Mixtures Adsorbed at the Air-Water-Interface - a Neutron Reflection Study. *J. Colloid Interface Sci.* **1995,** 174, (2), 441-455.
6. Rennie, A. R.; Crawford, R. J.; Lee, E. M.; Thomas, R. K.; Crowley, T. L.; Roberts, S.; Qureshi, M. S.; Richards, R. W., Adsorption of poly(ethylene oxide) at the air-solution interface studied by neutron reflection. *Macromolecules* **1989,** 22, (8), 3466-3475.
7. Lu, J. R.; Su, T. J.; Thomas, R. K.; Penfold, J.; Richards, R. W., The determination of segment density profiles of polyethylene oxide layers adsorbed at the air-water interface. *Polymer* **1996,** 37, (1), 109-114.
8. Henderson, J. A.; Richards, R. W.; Penfold, J.; Thomas, R. K.; Lu, J. R., Organization of poly(ethylene oxide) monolayers at the air-water interface. *Macromolecules* **1993,** 26, (17), 4591-4600.
9. Crowley, T. L., Lee, E.M., Simister, E.A., Thomas, R.K., Penfold, J., Rennie, A.R., The application of neutron reflection to the study of layers adsorbed at liquid interfaces. *Colloids and Surfaces* **1990,** 52, 85-106.
10. Zhou, X.-L.; Chen, S.-H., Theoretical foundation of X-ray and neutron reflectometry. *Physics Reports* **1995,** 257, (4â€‘5), 223-348.
11. Cubitt, R., Fragneto, G. , Neutron Reflection: Principles and Examples of Applications. In *Scattering: Scattering and Inverse Scattering in Pure and Applied Science*, Pike, E. R., Sabatier,P, Ed. Academic Press: San Diego, CA, 2002; pp 1198-1207.
12. Penfold, J.; Thomas, R. K., The Application of the Specular Reflection of Neutrons to the Study of Surfaces and Interfaces. *Journal of Physics-Condensed Matter* **1990,** 2, (6), 1369-1412.
13. Penfold, J.; Richardson, R. M.; Zarbakhsh, A.; Webster, J. R. P.; Bucknall, D. G.; Rennie, A. R.; Jones, R. A. L.; Cosgrove, T.; Thomas, R. K.; Higgins, J. S.; Fletcher, P. D. I.; Dickinson, E.; Roser, S. J.; McLure, I. A.; Hillman, A. R.; Richards, R. W.; Staples, E. J.; Burgess, A. N.; Simister, E. A.; White, J. W., Recent advances in the study of chemical surfaces and interfaces by specular neutron reflection. *Journal of the Chemical Society-Faraday Transactions* **1997,** 93, (22), 3899-3917.
14. Penfold, J., Neutron reflectivity and soft condensed matter. *Current Opinion in Colloid & Interface Science* **2002,** 7, (1-2), 139-147.
15. Thomas, R. K., Neutron reflection from liquid interfaces. *Annual Review of Physical Chemistry* **2004,** 55, 391-426.
16. Nevot, L.; Croce, P., Characterization of Surfaces by Grazing X-Ray Reflection - Application to Study of Polishing of Some Silicate-Glasses. *Revue De Physique Appliquee* **1980,** 15, (3), 761-779.
17. Nelson, A., Co-refinement of multiple-contrast neutron/X-ray reflectivity data using MOTOFIT. *Journal of Applied Crystallography* **2006,** 39, 273-276.
18. Campbell, R. A.; Yanez Arteta, M.; Angus-Smyth, A.; Nylander, T.; Varga, I., Multilayers at Interfaces of an Oppositely Charged Polyelectrolyte/Surfactant System Resulting from the Transport of Bulk Aggregates under Gravity. *The Journal of Physical Chemistry B* **2012,** 116, (27), 7981-7990.
19. Penfold, J.; Tucker, I.; Thomas, R. K.; Zhang, J., Adsorption of polyelectrolyte/surfactant mixtures at the air-solution interface: Poly(ethyleneimine)/sodium dodecyl sulfate. *Langmuir* **2005,** 21, (22), 10061-10073.

20. Staples, E.; Tucker, I.; Penfold, J.; Warren, N.; Thomas, R. K.; Taylor, D. J. F., Organization of polymer-surfactant mixtures at the air-water interface: Sodium dodecyl sulfate and poly(dimethyldiallylammonium chloride). *Langmuir* **2002,** 18, (13), 5147-5153.
21. Taylor, D. J. F.; Thomas, R. K.; Li, P. X., Adsorption of oppositely charged polyelectrolyte/surfactant mixtures. Neutron reflection from alkyl trimethylammonium bromides and sodium poly(styrenesulfonate) at the air/water interface: The effect of surfactant chain length. *Langmuir* **2003,** 19, (9), 3712-3719.
22. Dalgleish, R., Application of off-specular scattering of X-rays and neutrons to the strucy of soft matter. *Current Opinion in Colloid and Interface Science* **2002,** 7, 244-248.
23. Campbell, R. A., Wacklin, H. P., Sutton, I., Cubitt, R., Fragneto, G, FIGARO: the new horizontal neutron reflectometer at the ILL. *Eur. Phys. J. Plus* **2011,** 126, 107.
24. Schober, H., *Neutron Scattering Applications and Techniques*. Springer: 2009.
25. Manning-Benson, S.; Parker, S. R. W.; Bain, C. D.; Penfold, J., Measurement of the dynamic surface excess in an overflowing cylinder by neutron reflection. *Langmuir* **1998,** 14, (5), 990-996.
26. Manning-Benson, S., *PhD Thesis* **1996**.
27. Sekine, M.; Campbell, R. A.; Valkovska, D. S.; Day, J. P. R.; Curwen, T. D.; Martin, L. J.; Holt, S. A.; Eastoe, J.; Bain, C. D., Adsorption kinetics of ammonium perfluorononanoate at the air-water interface. *Phys. Chem. Chem. Phys.* **2004,** 6, (21), 5061-5065.

4. Co-modelling of NR and Ellipsometry Data

4.1 Introduction

Adsorption from polymer/surfactant mixtures at the air/water interface can be characterised by a wide range of experimental techniques, with a combination of surface tensiometry and neutron reflectometry (NR) being one of the most common, and with the references[1-7] being by no means exhaustive. However, there are drawbacks to the use of both methods. Quantitative interpretation of tensiometry data in terms of surface composition is complicated by interactions in the bulk solution which make it difficult to determine the chemical potentials of the two components. NR measurements alone are one of the most effective methods for obtaining compositional information about the interface of mixed systems,[8, 9] as measurements in different isotopic contrasts allows the polymer, surfactant, and solution to be distinguished. Furthermore NR provides information on structure, which is inaccessible by many other methods including tensiometry. The weakness of NR is the need for deuterated components in order to record multiple isotopic contrasts, as isotopically substituted polymers are expensive and not widely available. Although hydrogenated polymers can be used for NR measurements, their low scattering length densities (SLDs) limits the sensitivity in the surface excess, for example to 2 μmol m^{-2} of EO units in PEO,[10] a coverage equivalent to half a monolayer of surfactant.

One of the primary aims of this project was to validate a new quantitative approach to the characterisation of an adsorbed layer at the air/water interface from a two-component mixture using a combination of ellipsometry involving entirely protonated species and one isotopic contrast of NR measurements involving deuteration of the surfactant but not the polymer. Ellipsometry can be used alone to obtain useful semi-quantitative information about the amount of material adsorbed at the air/water interface of polymer surfactant mixtures, however it cannot be used independently to obtain the interfacial composition. Consequently, ellipsometry is often used in conjunction with other experimental techniques such as surface tensiometry[11-15], shear viscosity measurements[14], and external reflection Fourier transform infrared spectroscopy (ER-FTIRS)[16], to characterize adsorbed interfacial layers. Ellipsometry and NR are often used as complementary techniques due to their very different sensitivities to the two components in a mixture, with the references 17-22 being only a few examples. However, to the best of our knowledge no study has previously co-modelled data from the two techniques in order to obtain quantitative compositional information about the interfacial layers.

The complementary sensitivities of ellipsometry and NR to the different components in the mixture is the basis of our co-modelling approach to obtaining interfacial compositions for polymer/surfactant mixtures. Whilst NR is primarily sensitive to deuterated components, in our case deuterated surfactants and not hydrogenated polymer, ellipsometry is similarly sensitive to both surfactant and polymer at the interface. The measured quantities for each technique, $\sum_i \sigma_i \tau_i$ (the sum of the product of the scattering length and thickness over i layers) obtained from fitting specular reflectivity profiles from NR measurements, and the ellipticity, $\bar{\rho}$, will both be assumed to be made up of additive contributions from the surface excesses of the two components, although this assumption will be tested later.

We can therefore approximate the relationships between the measured quantities from each technique and the surface excesses of both components using equations containing coefficients to account for the sensitivity of the technique to each component. From two techniques we obtain two equations in terms of surface excess which can be solved simultaneously to obtain the surface excesses of the two components.

The motivations for developing a new co-modelling approach to determining the interfacial compositions of layers adsorbed from mixed solutions are threefold. Firstly, using NR and ellipsometry we can obtain adsorbed amounts of both polymer and surfactant for systems for which only one deuterated component is available. Numerous NR studies of polymer/surfactant mixtures in the literature (refs) have obtained interfacial compositions for systems for which deuterated polymer was unavailiable, and this resulted in poor precision of the polymer surface excess. Our co-modelling approach increases the precision of the polymer surface excess determined using the same chemicals, and without the custom synthesis of deuterated polymers. Secondly, NR beamtime is a valuable commodity. Use of our approach can cut the requirement for beamtime by at least a factor of 3, as measurements on only one isotopic contrast are required. For measurements on the OFC, the cost of deuterated materials is also a concern, as the OFC uses a minimum sample volume of 1.25 litres and therefore the amount of deuterated materials required for multiple contrast measurements is large. Thirdly, this methodology should be equally applicable to mixtures containing species which cannot be deuterated.

This chapter discusses the methodology of, and assumptions behind, our co-modelling approach and its application to the determinination of the composition of interfacial layers adsorbed from polymer/surfactant mixtures. Section 4.2 discusses the methodology used; how the coefficients which represent the sensitivity of the two techniques to each component are calculated. For NR the measured quantity $\sum_i \sigma_i \tau_i$ is approximately linearly related to Γ for both components. For ellipsometry, however,

the relationship between $\bar{\rho}$ and Γ for a pure surfactant is best approximated by either a linear or a cubic function, depending on the surfactant. The choice of function used to approximate the contribution to $\bar{\rho}$ for a polymer/surfactant mixtures can affect the calculated composition. Section 4.3 discusses the effect of the function chosen on the calculated interfacial compositions of the systems examined in this thesis, and the systematic errors thus incurred. Finally, in Section 4.4, I will present multiple isotopic contrast NR data for some of the systems studied, and show that these data are consistent with the compositions obtained using our co-modelling methodology in order to validate the approach.

4.2. Co-Modelling Methodology

The first step in co-modelling data from ellipsometry and NR measurements in order to obtain surface compositions is to establish the relationships between the two measured quantities, the product of the scattering length density and thickness of the layer, $\sum_i \sigma_i \tau_i$, and the ellipticity, $\bar{\rho}$, and the surface excesses of the two components. For NR, there is a simple linear relationship between $\sum_i \sigma_i \tau_i$, and the surface excesses of polymer (Γ_{poly}) and surfactant (Γ_{surf}) as in Equation 4.1.

$$\sum_i \sigma_i \tau_i = \left(b_{surf}\Gamma_{surf} + b_{poly}\Gamma_{poly}\right)N_A \quad (4.1)$$

where b_a is the scattering length of component a, Γ_a is the surface excess of component a, and N_A is Avogadro's constant. For clarity, we will simplify Equation 4.1. by writing $A = b_{surf} \times N_A$ and $B = b_{poly} \times N_A$, with a conversion from $Å^2$ to m^2 implicit in the calculation of the coefficients (corresponding to a division of A and B by 1 x 10^{20}). The values of b_{surf} and b_{poly} for the surfactants and polymers in this study are given in Tables 4.1 and 4.2. Equation 4.1 is therefore simplified to:

$$\sum_i \sigma_i \tau_i = A\Gamma_{surf} + B\Gamma_{poly} \quad (4.2)$$

In order to obtain values for Γ_{surf} and Γ_{poly} from Eq. 4.2 we also need an equivalent equation for the relationship between $\bar{\rho}$ and Γ, however the formulation of this equation is more complicated.

Previous work has shown that there is an approximately linear relationship between $\bar{\rho}$ and Γ for pure surfactants,[17, 23-25] and that for polymer/surfactant mixtures $\bar{\rho}$ can be assumed to a first approximation to be an additive combination of the contributions of the two components.[16] It should therefore be possible to write an analogous linear relationship to Equation. 4.2 between $\bar{\rho}$ and the surface excesses of both components as an extension of Equation. 2.18 in Chapter 2. The rationale for a linear relationship between $\bar{\rho}$ and Γ is that the adsorbed polymer and the surfactant head groups can be

treated by an effective medium approximation (which is quite accurately linear when the relative permittivity of the water and the organic material are not too dissimilar) and the hydrophobic chains form an oil film of constant refractive index and varying thickness.

The effective medium approximation used here is the Lorentz-Lorentz effective medium approximation,

$$\frac{\varepsilon_{layer}-1}{\varepsilon_{layer}+2} = \phi_{H_2O}\frac{\varepsilon_{H_2O}-1}{\varepsilon_{H_2O}+2} + \phi_{PEO}\frac{\varepsilon_{PEO}-1}{\varepsilon_{PEO}+2}, \quad (4.3)$$

where ϕ is the volume fraction and ε is the relative permittivity of a species in the layer. This equation was previously given in Chapter 2, but is repeated here for clarity. For a layer of given surface excess at the interface, we can use the Equation 4.3. to demonstrate that variations in the volume fraction of polymer in the layer have no effect on $\bar{\rho}$. If we use a layer of adsorbed PEO as an example, we can calculate ε_{PEO} from $\varepsilon_{poly} = \left(\Delta n + \sqrt{\varepsilon_{H2O}}\right)^2$ where Δn is calculated from dn/dc = 0.134[26] multiplied by the mass per unit volume of 1 μmol m^{-2} of polymer. Equations 4.4 and 4.5 (previously given in Chapter 2 but repeated here for clarity) are then used to calculate $\bar{\rho}$.

$$\eta = \frac{(\varepsilon_{poly}-\varepsilon_{air})(\varepsilon_{poly}-\varepsilon_{H_2O})}{\varepsilon_{poly}} d \quad (4.4)$$

and

$$\overline{\rho} = \frac{\pi}{\lambda}\frac{\sqrt{\varepsilon_{H_2O}+\varepsilon_{air}}}{\varepsilon_{air}-\varepsilon_{H_2O}}\eta \quad (4.5)$$

where ε_{H2O} and ε_{air} are the permittivities of the solution and the air respectively, λ is the wavelength of the HeNe laser, and the ellipsometric thickness, η, is found from the Drude equation assuming uniform density.

For 6 μmol m^{-2} of PEO at the interface, the calculated values of $\bar{\rho}$ using Equations 4.3 - 4.5 vary by only 2×10^{-7} (0.5% of the value of $\bar{\rho}$) as the volume fraction of PEO in the layer is varied from 0.01 to 0.6. The measured value of $\bar{\rho}$ is independent of the volume fraction of the species in the layer at constant surface excess.

The linear relationship between $\bar{\rho}$ and Γ for a pure surfactant system breaks down at low coverages where the hydrocarbon tails of the surfactant are too sparse to fully cover the interface and must therefore be mixed either with water or air. [27, 28] In the former case, an effective medium approximation still gives a linear relationship between $\bar{\rho}$ and Γ; in the latter case the relationship is

strongly nonlinear and changes sign when the volume fraction of air in the mixed layer is >0.2.[27] In previous work on adsorbed layers of APFN,[29] the chains needed to be immersed 75 % in water and 25 % in air in order to model the $\bar{\rho}$ data, which is consistent with a slight maximum in the $\bar{\rho}$ v Γ data. This deviation from linearity for the $\bar{\rho}$ v Γ data at low coverages means that it may sometimes be more appropriate to use a non linear fit (or other function) to the $\bar{\rho}$ v Γ data for pure surfactants in order to minimise the errors in this region[16].

Figure 4.1 and Figure 4.2 show the pure surfactant $\bar{\rho}$ v Γ data for all of the surfactants used in the experiments presented in this thesis, along with several lines which denote a cubic fit to the data (solid line), a linear fit to the data (dashed line), a linear fit to the data where $\Gamma > 1$ μmol m^{-2} (dash-dot line) and a line between the Γ_{max} and $\Gamma = 0$ values (dotted line). I will first discuss the two fits to the pure surfactant data (solid and dashed lines), whilst the purposes of all four will be discussed below in the context of polymer/surfactant mixtures.

It is clear from the data in Figure 4.1 and Figure 4.2 that the deviation from linearity of the $\bar{\rho}$ *v* Γ data is much more pronounced for some surfactants than others, with the C_{12}TAB and C_{14}TAB data well fitted by either the linear or cubic functions (dashed and solid lines respectively), whilst for SDS and C_{16}TAB data the cubic fit is clearly a better approximation to the recorded data. The gentle maximum observed in the cubic fits for the latter two systems is not just an artifact of the fitting procedure: addition of very small amounts of surfactant to water yields a detectable increase in $\bar{\rho}$ before it starts to decline at higher concentrations. For the SDS data, the deviation of the ellipticity from linearity is in absolute terms very similar to that for the C_{12}TAB and C_{14}TAB systems, but the difference is more notable for SDS as the values of $\bar{\rho}$ are smaller than for C_{14}TAB. In a previous study the cubic fit was used to approximate the contribution of SDS to $\bar{\rho}$, as the linear approximation was calculated to lead to errors of up to 6% in a monolayer of SDS.[16] For the C_{16}TAB data the deviation from linearity is greater than that of the other surfactants. It is not clear whether this can be attributed to a trend with increasing chain length, as Bell et al. concluded that increasing the chain length of the C_nTAB surfactants does not perturb the structure and conformation of the chains at the interface, although increasing the surfactant chain length increased the sensitivity of $\bar{\rho}$ to the volume fraction of the chain length at low coverage.[27] It is probable that the poor linearity may be due to a systematic error in the original experiments, however in order to determine whether this is the case we would need to repeat the NR measurements.

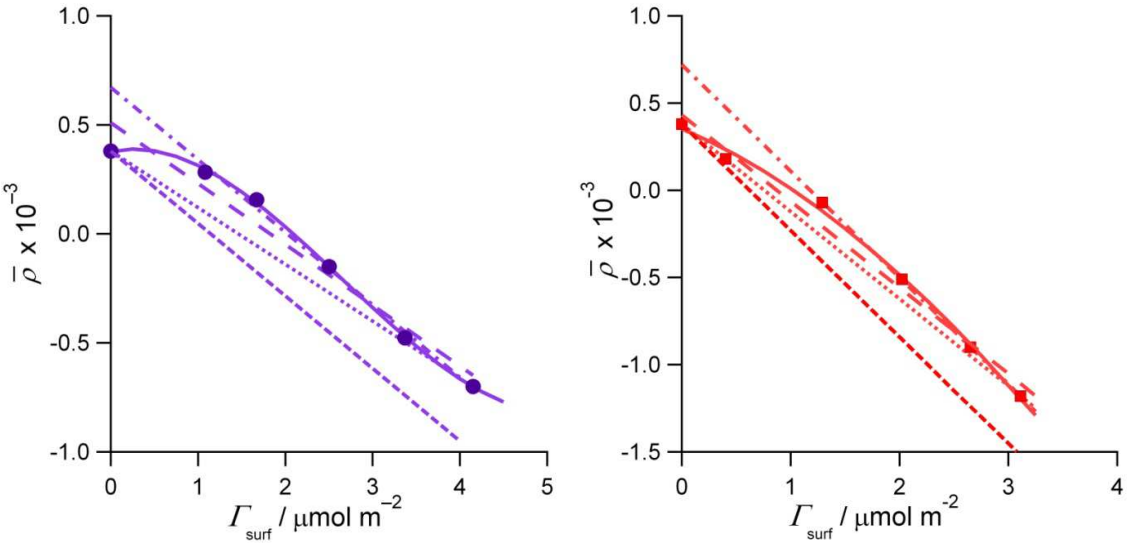

Figure 4.1. Relationship between dynamic ellipticity, $\bar{\rho}$, and dynamic surface excess, Γ_{surf} as recorded using NR, of (a) SDS in the presence of 0.1 M NaCl and (b) C_{12}TAB in the presence of 0.1 M NaBr. Four different functions relating Γ and $\bar{\rho}$ are given on each graph, the solid line is a cubic fit to the data, the wide-dashed line is a linear fit, the dash-dot line is a linear fit through the data where $\Gamma > 1\ \mu molm^{-2}$, the dotted line joins the maximum and minimum values, and the close-dashed line has the gradient of the data at $\Gamma > 1\ \mu molm^{-2}$ but passes through the pure water value. For both data sets the point plotted at $\Gamma = 0$ is the value of $\bar{\rho}$ for pure water, 0.00038.

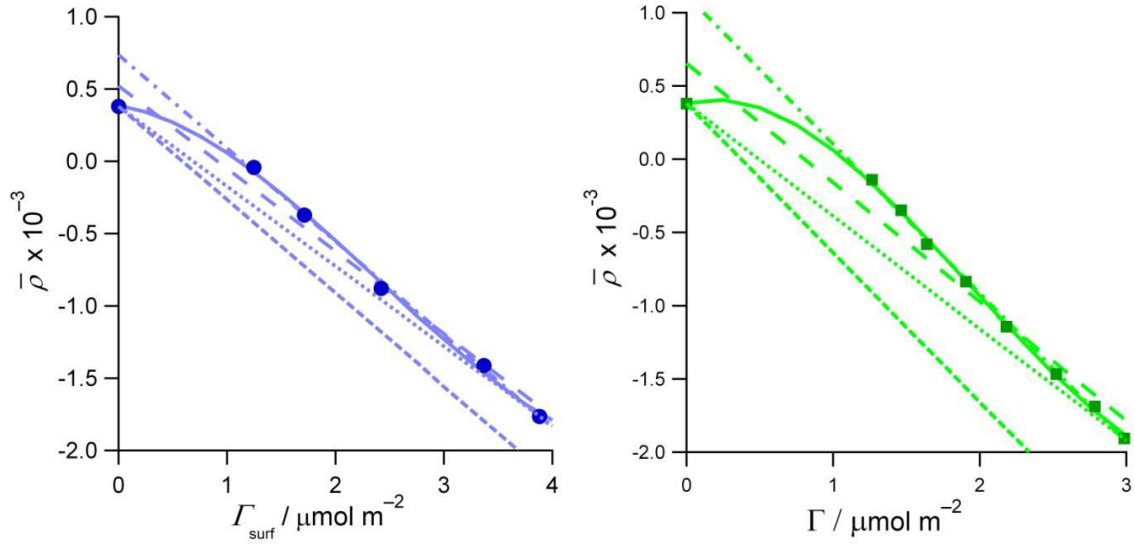

Figure 4.2. Relationship between dynamic ellipticity, $\bar{\rho}$, and dynamic surface excess, Γ_{surf} as recorded using NR, of (a) C_{14}TAB and (b) C_{16}TAB solutions on the OFC. All measurements were made in the presence of 0.1M NaBr. Four different functions relating Γ and $\bar{\rho}$ are given on each graph, the solid line is a cubic fit to the data, the wide-dashed line is a linear fit, the dash-dot line is a linear fit through the data where $\Gamma > 1\ \mu molm^{-2}$, the dotted line joins the maximum and minimum values, and the close-dashed line has the gradient of the data at $\Gamma > 1\ \mu molm^{-2}$ but passes through the pure water value. For both data sets the point plotted at $\Gamma = 0$ is the value of $\bar{\rho}$ for pure water, 0.00038.

Although it is clear from Figure 4.1 and Figure 4.2 that a cubic function gives the best approximation to the relationship between $\bar{\rho}$ and Γ for a pure surfactant at low coverages, this will not necessarily be the case for polymer/surfactant mixtures. Adsorption of polymer at the interface at low surfactant coverages may result in mixing of the polymer and surfactant chains, which would result in a higher volume fraction in the chain region for the mixture than the monolayer, which may eliminate the need for a cubic function to account for the low surfactant volume fraction, and a linear function can be used. However, the most appropriate linear function to relate $\bar{\rho}$ and Γ for the surfactant in the mixture may not be that obtained from a fit through the pure surfactant data. For all of the polymer/surfactant mixtures in this study, the optimum function to use to relate $\bar{\rho}$ and Γ for the surfactant in the mixture will need to be examined to determine the effect of the adsorption of polymer on this relationship, as the function used will affect the calculated surface excesses of both components.

In the presence of polymer at the interface, the most appropriate linear relationship between Γ and $\bar{\rho}$ for the surfactant may not be the linear fit to the pure surfactant data, depending on the effect of polymer on the relationship. For all of the surfactants in Figures 4.1 and 4.2, the linear fit to the pure surfactant data (dashed line) does not go through the pure water value, instead crossing the y axis at higher values of $\bar{\rho}$, which will inevitably incur errors in the calculated compositions at very low surfactant coverages. A possible alternative linear function to relate Γ and $\bar{\rho}$ for the surfactant in the mixture would connect the Γ and $\bar{\rho}$ values for the pure surfactant at monolayer and zero coverages (pure water), shown as a dotted line in Figures 4.1 and 4.2. This function will probably give reasonable interfacial compositions at high and low surfactant coverages, but incur errors at intermediate coverages. One issue with this approach is that it overweights a single data point at high coverages and disregards the others. In order to examine the effect of the use of this single data point, a line through the pure surfactant $\bar{\rho}$ v Γ data for $\Gamma > 1$ μmol m^{-2} is shown in Figures 4.1 and 4.2 as a dash-dot line. The values of $\bar{\rho}$ and Γ at high coverages which would be determined using this line are very close to the measured values, hence we will use the measured $\bar{\rho}$ and Γ values at high coverage in this additional function.

One further linear function which may be appropriate in the presence of significant amounts of polymer at the surface is a line with the gradient of the fit through the pure surfactant $\bar{\rho}$ v Γ data for $\Gamma >$ 1 μmol m^{-2}, but applied over the whole range of coverages, i.e. with a y-axis intercept corresponding to the pure water value (shown as a close-dashed line in Figures 4.1 and 4.2). This function may be correct for mixtures at low coverages, but will clearly result in errors at intermediate and high coverages, as it results in ellipticities which are more negative than the experimental data.

In Section 4.3 I will discuss the effect of using the four functions relating $\bar{\rho}$ and Γ for the surfactant discussed here on the interfacial compositions calculated for each of the polymer/surfactant systems examined in this thesis. Before doing so, however I will outline how an equation relating $\bar{\rho}$ and Γ for the mixtures for use in co-modelling, similar to Equation 4.2 for the NR data, can be formulated.

As it is not clear at this point what will be the most appropriate function to use to relate $\bar{\rho}$ and Γ for the surfactant in the polymer/surfactant mixture, the equation to relate the two quantities for the mixture (Equation 4.6) contains a function f(Γ_{surf}) which can be linear or cubic.

$$\bar{\rho} = f(\Gamma_{surf}) + D\Gamma_{poly} + E \tag{4.6}$$

where D is the sensitivity of ellipsometry measurements to $\bar{\rho}$, the calculation of which will be discussed later, and E accounts for the contribution to $\bar{\rho}$ from the capillary wave roughness of the surface. The roughness is theoretically expected to scale as the inverse root of the surface tension, $\gamma^{-0.5}$, and yields a positive contribution to $\bar{\rho}$ of 4–6 x 10^{-4}.[30] As we have not independently measured the dynamic surface tension for the solutions studied in this work we will use the y intercept of the plot of $\bar{\rho}$ v Γ for the pure surfactant (including the datum for pure water) to approximate E.

In the case where f(Γ_{surf}) is linear, it may be represented by $C\Gamma_{surf}$, where C is obtained from a linear fit to the pure surfactant $\bar{\rho}(\Gamma)$ data. When a cubic relationship between Γ and $\bar{\rho}$ is more appropriate, f(Γ_{surf}) is represented by the co-efficients of the cubic fit to the data, and Eq. 4.6. becomes Eq. 4.7.

$$\bar{\rho} = x{\Gamma_{surf}}^3 + y{\Gamma_{surf}}^2 + z\Gamma_{surf} + D\Gamma_{poly} + E \tag{4.7}$$

where x, y, z and E are the co-efficients of the cubic fit to the data.

The composition of an adsorbed layer from a polymer/surfactant mixture is therefore determined from the measured quantity by solution of the pairs of simultaneous equations Eq. 4.2. and Eq.4.6. or Eq. 4.2. and Eq. 4.7, depending on whether a linear or cubic function is deemed to give the best approximation to the adsorption behaviour of the surfactant at low coverages.

For each surfactant, the co-efficients of the cubic fit, linear fit and line between the minimum and maximum values of Γ and $\bar{\rho}$ in Figure 4.1 and Figure 4.2 are given in Table 4.1.

Function	Coefficient	SDS	C_{12}TAB	C_{14}TAB	C_{16}TAB
Cubic Fit to Data	*x*	2.19 x 10^{-5}	3.30 x 10^{-6}	3.35 x 10^{-5}	1.20 x 10^{-4}
	y	-1.75 x 10^{-4}	-8.70 x 10^{-5}	-2.4 x 10^{-4}	-6.99 x 10^{-4}
	z	8.97 x 10^{-5}	-2.58 x 10^{-4}	-1.21 x 10^{-4}	2.60 x 10^{-4}
	E	3.77 x 10^{-4}	3.52 x 10^{-4}	3.85 x 10^{-4}	3.82 x 10^{-4}
Linear Fit to Data	*C*	-2.79 x 10^{-4}	-4.95 x 10^{-4}	-5.71 x 10^{-4}	-8.13 x 10^{-4}
	E	5.10 × 10^{-4}	4.32 x 10^{-4}	5.22 x 10^{-4}	6.54 x 10^{-4}
Line between Γ_{max} and Γ_0	*C*	-2.60 x 10^{-4}	-5.02 x 10^{-4}	-5.52 x 10^{-4}	-7.66 x 10^{-4}
	E	3.80 x 10^{-4}	3.80 x 10^{-4}	3.80 x 10^{-4}	3.80 x 10^{-4}
Line with high coverage gradient	*C*	-3.33 x 10^{-4}	-6.11 x 10^{-4}	-6.45 x 10^{-4}	-10.2 x 10^{-4}
	E	3.80 x 10^{-4}	3.80 x 10^{-4}	3.80 x 10^{-4}	3.80 x 10^{-4}
	b_{surf} / Å	2.79 × 10^{-3}	2.49 x 10^{-3}	2.89 × 10^{-3}	3.56 x 10^{-3}

Table 4.1. Constants for the contribution of the surfactant to the ellipticity obtained from or used to plot each of the functions relating the surfactant $\bar{\rho}$ v Γ data shown in Figure 4.1 and Figure 4.2. C is the co-efficient of the linear fit, and x, y, z, are the co-efficients of the cubic fit, and E is the roughness contribution which comes from the y intercept of either the linear or cubic fit. These numerical values are consistent with Γ in μmol m^{-2}, Γ_{poly} in terms of monomers, and $\sum_i \sigma_i\tau_i$ in $Å^{-1}$. The scattering length of the surfactant b_{surf} is also given for use in Eq. 4.2.

The co-efficient which accounts for the contribution of the polymer to $\bar{\rho}$ for the mixture, *D* in Eqns. 4.6. and 4.7., can be calculated also assuming an effective medium approximation, where the contribution of the polymer to $\bar{\rho}$ is linearly proportional to Γ and only weakly dependent on the degree of hydration (i.e., the volume fraction of polymer) in the adsorbed film.[31] As we do not have NR data for deuterated polymers under similar conditions to those used in the experiments presented in this thesis, a calibration plot approach to determining the contribution of polymer to $\bar{\rho}$ is not possible. *D* is obtained by calculation of value of $\bar{\rho}$ which would result from a Γ_{poly} of 1 μmol m^{-2}, using Equations 4.4 and 4.5 and the method of calculating ε_{poly} from dn/dc given above.

Values of the co-efficients representing the contribution of the polymer to $\sum_i \sigma_i\tau_i$ (the co-efficient *B*, here given as the scattering length b_{poly} without any conversion factors) and to the ellipticity (*D*) used for co-modelling the data are given in Table 4.2.

	PEO	PSS	PEI
b_{poly} / Å	4.13×10^{-5}	5.08×10^{-4}	3.76×10^{-5} at pH 10 1.41×10^{-5} at pH 4
D	-7.45×10^{-5}	-4.61×10^{-4}	-1.34×10^{-4}
dn/dc /cm^{3}g^{-1}	0.134[26]	0.198[32]	0.25

Table 4.2. Constants to account for the contribution of the polymer to $\sum_i \sigma_i \tau_i$ and $\bar{\rho}$ for the mixture, where b_{poly} is the calculated neutron scattering length of the polymer monomer, calculated from the sum of the scattering lengths of the constituent atoms for use in Eq. 4.2, and D is the contribution to the ellipticity, and is calculated as detailed above from the literature dn/dc value. D is in units consistent with Γ in μmol m^{-2}.

4.3. Effect of Co-Modelling Methodology on the Interfacial Composition

In section 4.2 I introduced the idea that there are several possible functions which can be used in the co-modelling methodology to relate $\bar{\rho}$ and Γ for the surfactant in the mixture, depending on the effect of polymer adsorption. The function chosen can have a significant effect on the calculated interfacial composition. The choice is not arbitrary, since the chosen function has to give physically reasonable results; for example, the polymer surface excess has to be positive (for the dilute solutions studied here) and cannot exceed the maximum diffusion-controlled limit.. In this section I will discuss the variation in the interfacial compositions obtained for each of the polymer/surfactant systems examined in this thesis due to the choice of function used to relate $\bar{\rho}$ and Γ for the surfactant. The four functions evaluated are a cubic fit to the pure surfactant data, a linear fit to the pure surfactant data, a line joining the data points for zero and maximum coverage, and a line with the gradient of the higher coverage data but passing through the pure water value. It will become clear from the data below that one or more of these functions is inappropriate, as physically impossible values of the polymer surface excess will result from the calculations. For each of the systems studied in this thesis a comparison of the interfacial coverages calculated using each approach is presented, and a justified choice of one function to calculate the data for interpretation in the remainder of this thesis is given.

The first systems for which I will examine the effects of the function used to represent the pure surfactant $\bar{\rho}$ v Γ data on the calculated interfacial composition of the mixture are the PEO/surfactant mixtures, PEO/SDS and PEO/C_{14}TAB. Figure 4.3 shows the polymer and surfactant surface excesses (empty and filled symbols respectively) calculated for both systems using the coefficients for a cubic

function (green triangles) a linear function obtained from a fit to the pure surfactant (orange squares), a line between the maximum and minimum values of Γ and $\bar{\rho}$ (blue diamonds), and a line with the gradient of the high coverage data, passing through the pure water value (turquoise inverted triangles). The choice of function has a limited effect on the surfactant surface excess, since it is derived almost exclusively from the NR data, whilst the polymer surface excess varies dramatically with the function used.

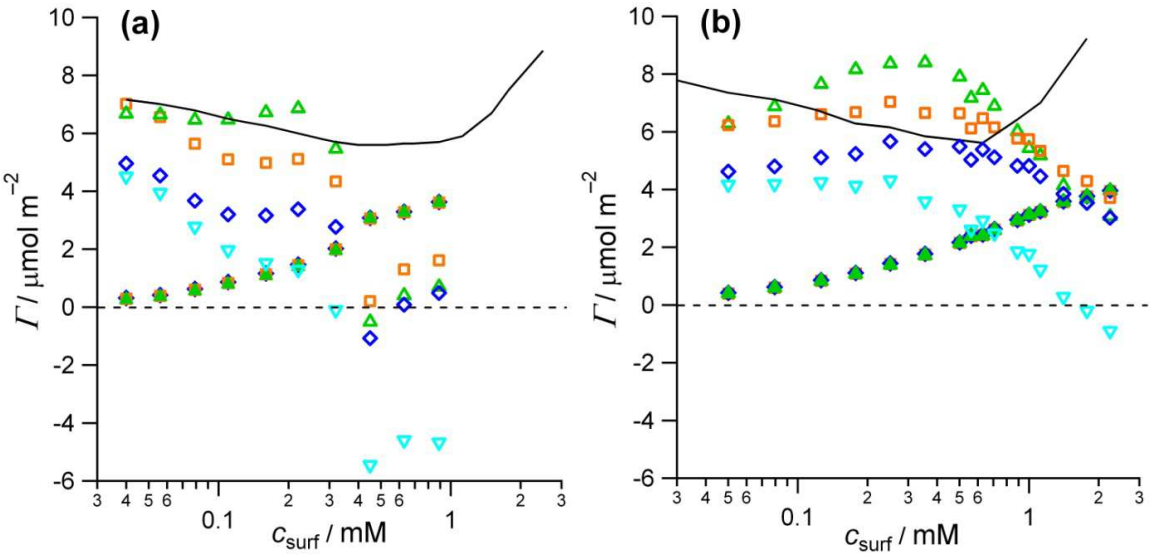

Figure 4.3 - Surface excesses of surfactant (filled symbols) and PEO (empty symbols) adsorbing at the interface of the OFC from a mixed solution containing 100 ppm 25k PEO and (a) C_{14}TAB or (b) SDS. The green triangles are the data calculated using the coefficients of a cubic function in Table 4.1, the orange squares using a linear function, and the blue diamonds using the coefficients of a linear function between maximum and minimum coverage, and the turquoise inverted triangles from a line with the gradient of the high coverage $\bar{\rho}$ *v* Γ surfactant data but passing through the pure water values (all shown in Figures 4.1 and 4.2). The black solid line is an approximation to the diffusion controlled maximum polymer surface excess $\Gamma_{poly,max}$, the calculation of which is discussed in Chapter 5, whilst the black dashed line denotes the zero value of the y-axis.

In order to determine which of the functions used to calculate the surface composition in Figure 4.3 gives the most physically reasonable values of the Γ_{poly}, we can start by asking two questions of the coverages shown in Figure 4.3 for each function; first, how does the maximum calculated value of Γ_{poly} compare to $\Gamma_{poly,max}$ under diffusion control (solid black line), and do we obtain negative Γ_{poly} values in any region? Any approximation which exceeds the diffusion-controlled limit or which gives negative surface excesses must be physically wrong, at least over part of the c_{surf} range.

Using the two criteria given above we can quickly dismiss the use of two of the functions. Firstly, for the PEO/C_{14}TAB system in Figure 4.3 (a) it is clear that the function obtained from a fit through the high coverage surfactant data (inverted turquoise triangles) results in a large error in the calculation of

Γ_{poly} at high c_{surf} values, with large negative values calculated, as we may have predicted from Figures 4.1 and 4.2. This function will therefore not be used. If we then turn to the PEO/SDS data in Figure 4.3 (b) we can see that the Γ_{poly} values calculated using the cubic function (green triangles) significantly exceed the diffusion controlled limit as marked by the solid black line, which is not physically possible. This function is then also dismissed. As the adsorption of polymer at low surfactant coverages has the greatest effect on the appropriate function used we might expect that the same function would be appropriate for both PEO/surfactant systems, however as their behaviour is different at high surfactant concentrations this may not be the case.

For both systems we are left with three systems to discuss; for PEO/C_{14}TAB the linear function fitted to the pure surfactant data (orange squares) and the line between the maximum and minimum coverages (blue diamonds), and the cubic function (green triangles), and for PEO/SDS the first two functions (orange squares and blue diamonds) remain along with the function from the high coverage data (turquoise triangles). The first notable difference between the remaining data sets for both systems is that Γ_{poly} is lower for the max-min line and for function from the high coverage data than it is for the remaining data. At low bulk surfactant concentrations, where the amount of surfactant at the interface is small compared to the amount of surface active polymer, we would expect that adsorption of polymer would be under diffusion control, as marked by the black line. We will therefore dismiss the max-min function for the PEO/C_{14}TAB system and both the max-min and the high coverage functions for the PEO/SDS system as they result in Γ_{poly} values lower than the diffusion controlled estimate.

For the PEO/SDS system we are therefore left with only the data calculated from the linear function through the pure surfactant data (orange squares), however for the PEO/C_{14}TAB system we are left with both the data from both the linear and cubic functions. Both of these remaining functions give physically reasonable values of Γ_{poly} at all surfactant concentrations, although with some differences, and either could be used in our analysis of the data in Chapter 5. For consistency with the PEO/SDS system I will choose to use the data arising from the linear function, however I will acknowledge in Chapter 5 that the choice of function used in the co-modelling of this system leads to errors in the values of and trends in the Γ_{poly} data.

It should be noted that in this approach we are ignoring any change occurring in the roughness contribution from the co-adsorption of polymer and surfactant at the interface. Increased roughness on the adsorption of a mixed layer would increase the ellipticity. If we neglect the change in roughness, the polymer surface excess we calculate will be less than the true surface excess, more especially at low surfactant concentrations. This error could perhaps be minimized by measurements of the surface tension of each polymer/surfactant system at the static interface, however such measurements were not

within the remit of the work in this thesis. To some extent the effect of the roughness is already compensated for by use of linear functions, which result in lower Γ_{poly} values at low surfactant concentration than we may expect in this region.

I will now move on to an examination of the effects of the function used on the interfacial composition calculated for mixtures of PSS/C_nTAB (discussed later in Chapters 6 and 7). As Figure 4.3 has shown, the surfactant surface excess is minimally affected by the function chosen to calculate the interfacial composition, hence in Figure 4.4 and Figure 4.5 only the polymer surface excesses are shown for clarity. In Figure 4.3 it was clear that using the function based on the gradient of the high coverage surfactant data and the y-intercept of pure water incurred significant errors in the polymer surface excess calculated. As a consequence this function will not be considered in the following discussion. Although the cubic function also incurred errors in the calculated Γ_{poly} values in Figure 4.3. it will still be examined for the other systems, as if Γ_{poly} is low at low surfactant coverages, a cubic function relating $\bar{\rho}$ and Γ for the surfactant may still be appropriate. As a consequence, Figures 4.4 and 4.5 show the effects of using functions obtained from a cubic or linear fit to the pure surfactant data or from a line joining the maximum and minimum coverage values, with the symbols consistent with those in Figure 4.3.

From Figures 4.4 and 4.5 we can see that the calculated values of Γ_{poly} are greatest when the cubic function is used, intermediate when the linear fit to the data is used and lowest for the max-min for all of the PSS/C_nTAB systems as they were for the PEO/surfactant mixtures. However, the difference in Γ_{poly} between the three calculation approaches is much smaller than it was for the PEO mixtures. As Γ_{poly} is low at low surfactant coverages, we cannot discount the values calculated using the cubic function, as it may still give the best physical approximation of the data at low coverages. Furthermore, the three methods of calculation cannot be distinguished by comparison of Γ_{poly} to the maximum value under diffusion control, 2 μmol m^{-2}, as all of the Γ_{poly} values in Figure 4.4 and Figure 4.5 are below this theoretical value.

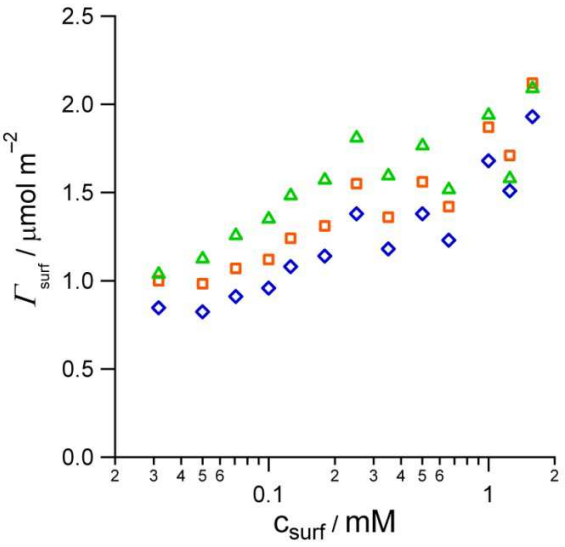

Figure 4.4. Surface excesses of PSS at the interface of the OFC from a mixed solution containing 100 ppm 17k PSS and increasing concentrations of C_{12}TAB, where the symbols are consistent with Figure 4.3, the green triangles are calculated using coefficients from a cubic fit to the pure surfactant $\bar{\rho}$ *v* Γ data, the orange squares from a linear fit, and the blue diamonds from a line between the values for the maximum and minimum coverages. Co-efficients are given in Table 4.1.

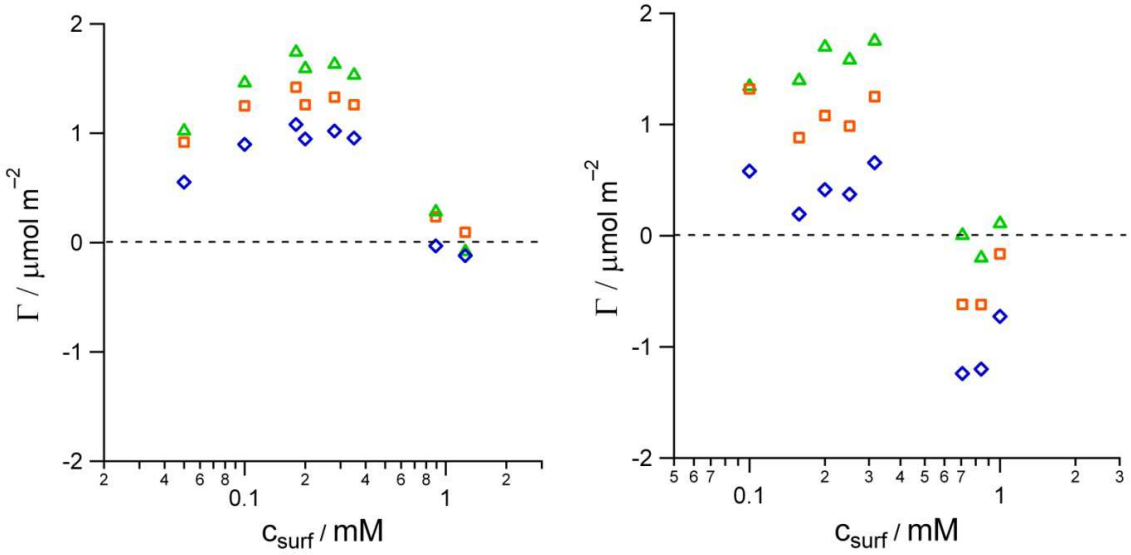

Figure 4.5. Surface excesses of PSS at the interface of the OFC from a mixed solution containg 100 ppm 17k PSS with (a) C_{14}TAB and (b) C_{16}TAB. The symbols are consistent with Figure 4.3 and Figure 4.4, the green triangles are calculated using coefficients from a cubic fit to the pure surfactant $\bar{\rho}$ v Γ data, the orange squares from a linear fit, and the blue diamonds from a line between the values for the maximum and minimum coverages. Co-efficients are given in Table 4.1.

From the PSS/C_{12}TAB and PSS/C_{14}TAB data, it is impossible to determine which calculation approach gives the most physically reasonable values of Γ_{poly}, however the PSS/C_{16}TAB data in Figure 4.5 (b) do allow the approaches to be distinguished. At the highest c_{surf} values measured, physically impossible

negative Γ_{poly} values are calculated using both the linear and min-max functions. On this basis, I will use the cubic function to obtain compositional data for all of the PSS/C_nTAB systems in Chapters 6 and 7. However, as the trends in Γ_{poly} are similar for all three systems using any of the three functions, it seems possible that any of the three functions could be the best to use in the co-modelling approach. As a consequence I will acknowledge the possible error in Γ_{poly} for these systems in all subsequent discussions.

The final system to examine is PEI/SDS at pH 10, which will be discussed in Chapter 8. For this system, the Γ_{poly} values calculated using all three approaches are given in Figure 4.6. The first thing we note from these data is that Γ_{poly} is very high at low surfactant coverages, which eliminates the need for a cubic function to account for the adsorption of surfactant at a bare interface. Either a linear fit or a cubic fit to the pure surfactant data results in an over-estimation of Γ_{poly} at the lowest surfactant concentrations measured, as the calculated Γ_{poly} values exceed the maximum value which would result from diffusion-controlled adsorption of the polymer (marked by the black arrow). As a consequence, I will use the max-min linear function for calculation of the interfacial composition for this system. Nevertheless, it should be noted that the function used to obtain the interfacial composition does not change the trend in Γ_{poly} with c_{surf} for this system, it only introduces a maximum difference in the calculated values of 1.5 μmol m^{-2}, and it has no effect on the qualitative interpretation of the trends in adsorption behaviour in Chapter 8.

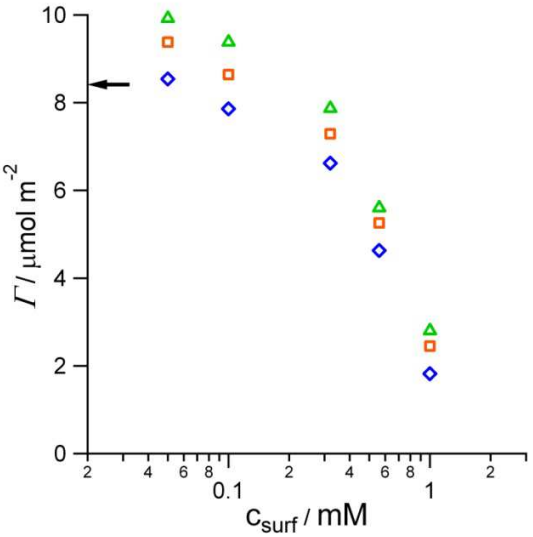

Figure 4.6. Surface excesses of PEI at the interface of the OFC from a mixed solution containg 100 ppm 750 k PEI and SDS at pH 10. The symbols are consistent with Figures 4.3, 4.4, and 4.5 the green triangles are calculated using coefficients from a cubic fit to the pure surfactant $\bar{\rho}$ *v* Γ data, the orange squares from a linear fit, and the blue diamonds from a line between the values for the maximum and minimum coverages. Co-efficient values are given in Table 4.1. The arrow marks the maximum Γ_{poly} value which can be reached under diffusion control.

In this section I have demonstrated that the choice of function used to calculate the interfacial composition has a significant effect on the calculated polymer surface excess for all of the polymer/surfactant systems studied in this thesis. The choice of function for a mixture cannot simply be predicted from that which is most appropriate for the pure surfactant, as changes in the optical properties of the surfactant layer at low coverage may not occur if a significant amount of polymer is co-adsorbed. For all of the polymer/surfactant systems in this thesis, the choice of function to approximate the relationship between $\bar{\rho}$ and Γ for the surfactant does not change the qualitative trends in the polymer coverage, it only affects the calculated values. For each system, the function which incurs the least physically impossible data points is chosen for use in the chapters which follow this one. Nevertheless, it should be noted that there may be some uncertainty in the values of Γ_{poly} from that presented in the following discussions. For a given polymer/surfactant system for which the full $\bar{\rho}$ v Γ calibration curve is not known, the only option is use of the function between $\Gamma_{surf} = 0$ and $\Gamma_{surf,max.}$ Although this function has not be chosen for use in the co-modelling of the systems above due to the presence of a full calibration curve, the errors are not sufficiently significant to make the method an unsatisfactory approach to the calculation of the interfacial composition of mixed systems. Furthermore, a reasonable first approach might be to use a cubic function in the situation where the polymer is not surface active and a linear function if the polymer is surface active, as this would work for all of the systems discussed above, and eliminates the need to measure NR data on the pure surfactant for every new system this approach is applied to.

4.4. Validation and Limitations of our Co-Modelling Approach

In order to apply our co-modelling methodology to determining the interfacial compositions of adsorbed layers we first need to be sure that the compositions we obtain from one isotopic contrast NR data and ellipsometry data are consistent with a data obtained on multiple isotopic NR contrasts when a plausible structural model is applied. Although measuring multiple isotopic contrasts as an approach to obtaining interfacial compositions of multiple systems is undesirable on the OFC due to the quantity of deuterated material required, we have recorded data on additional contrasts for several of the systems in this study in order to validate our approach. Data for PEO/SDS, PEO/C_{14}TAB, and PSS (100ppm 17k) /C_{12}TAB were recorded in two further isotopic contrasts, h-polymer/d-surfactant/D_2O and h-polymer/h-surfactant/D_2O. If our co-modelling methodology gives reasonable interfacial compositions, then we should be able to use these compositions to simulate fits to data obtained on multiple isotopic contrasts.

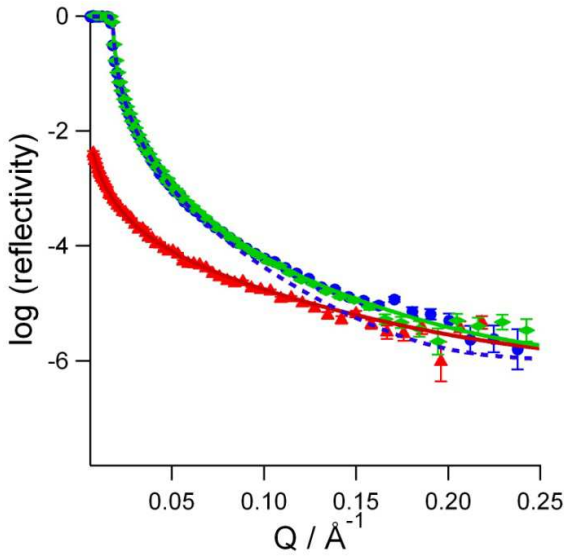

Figure 4.7. Neutron reflectivity profiles recorded in three isotopic contrasts, for the system PEO/SDS where c_{PEO} = 100 ppm and c_{SDS} = 0.5 mM. The red triangles are for h-polymer/d-surfactant/NRW, the blue circles for h-polymer/h-surfactant/D_2O, and the green diamonds for h-polymer/d-surfactant/D_2O. Simulated fits to these data using the surface compositions obtained from our co-modelling approach and a single 11 Å layer structure containing surfactant, polymer and solvent are shown as lines of corresponding colours.

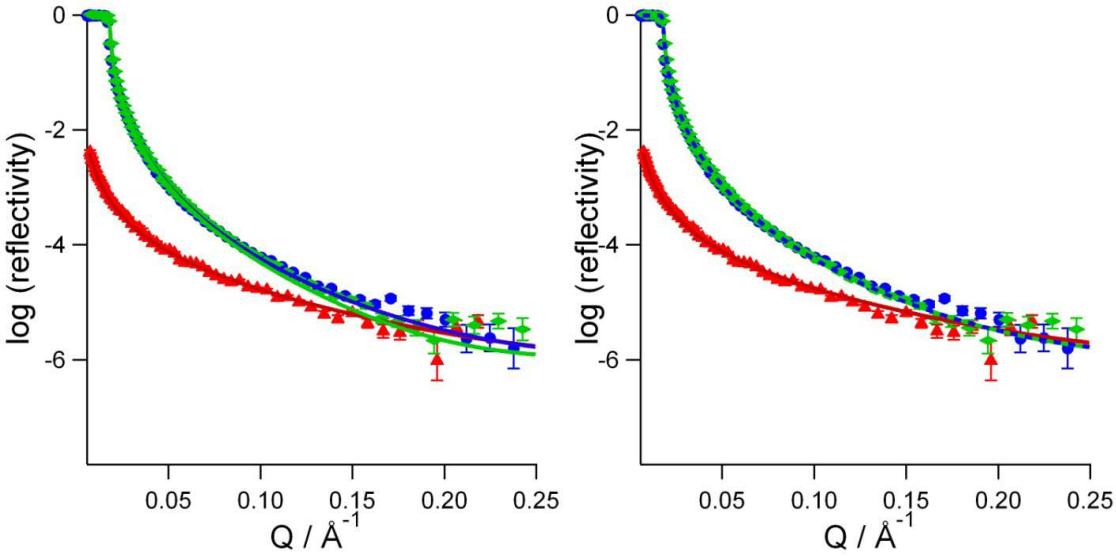

Figure 4.8. Neutron reflectivity profiles recorded in three isotopic contrasts, for the system PEO/SDS where c_{PEO} = 100 ppm and c_{SDS} = 0.5 mM. The symbols are identical to those in Figure 4.7. Simulated fits to these data using the surface compositions obtained from our co-modelling approach are shown as lines of colours corresponding to those of the data. For these simulations a 2-layer structure is used, where the top layer contains only surfactant chains and air and the bottom layer contains surfactant headgroups, polymers and solvent. (a) The chain layer density is varied with composition in the simulation, whilst its thickness is kept constant. (b) The chain layer thickness is varied with composition.

If we examine the data for the PEO/SDS system first, Figure 4.7 and Figure 4.8 show simultated fits to the NR data recorded on three isotopic contrasts using the surface compositions obtained from our co-modelling approach. In Figure 4.7, the simulated fits are for a single 11 Å mixed layer of polymer, surfactant and solvent, and in Figure 4.8 for a 2-layer arrangement where the top layer contains only surfactant chains and air and the bottom layer contains surfactant headgroups, polymer and solvent. These simple simulations assume that the compositions of a mixed layer containing polymer, surfactant and solvent can be calculated using an effective medium approximation.

From Figure 4.7 it is clear that the simulated fits to the data using the compositions obtained from our co-modelling approach and a single 11 Å mixed polymer/surfactant layer structure do not correspond well to the recorded data for all contrasts, with the simulation for the h-polymer/h-surfactant/D_2O contrast (dashed blue line) significantly outside the error bars of the corresponding data. Division of the surface structure into two layers improves the correspondance of the simulated fits to the data (Figure 4.8). The exact nature of the two-layer model used further affects the simulation; in Figure 4.8 (a) the hydrocarbon chain layer density was varied with Γ_{surf}, whilst in (b) the hydrocarbon layer thickness was varied. From Figure 4.8 (b) it is clear that when a varying chain layer thickness is employed, the simulations closely fit the recorded data for all three contrasts. I have therefore demonstrated that the compositions obtained using our co-modelling approach give a reasonable fit to NR data obtained on multiple isotopic contrasts for the PEO/SDS.

NR data recorded on multiple isotopic contrasts for the system PEO/C_{14}TAB are also consistent with the compositions obtained from our co-modelling approach when a reasonable structural model is employed. As previously, a single-layer model was found to be insufficient to fit the data. However, if the same structural model is used for this system as for PEO/SDS, with division of the adsorbed layer into a surfactant chain layer and a surfactant headgroup, polymer, and solvent layer, reasonable simulated fits to the data are obtained, as shown in Figure 4.9.

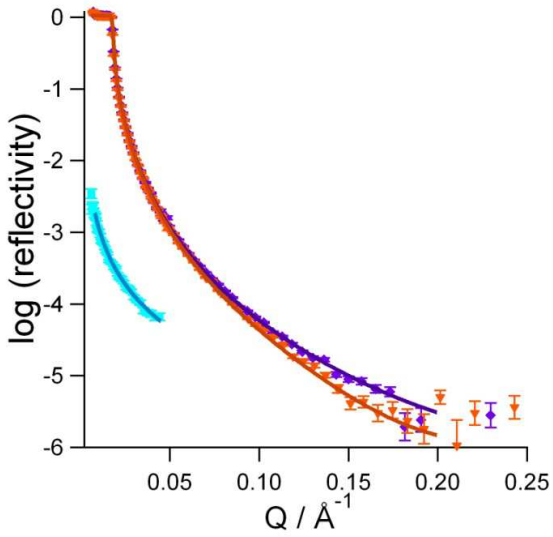

Figure 4.9 - Neutron reflectivity profiles recorded in three isotopic contrasts for the system PEO/C_{14}TAB where c_{PEO} = 100 ppm c_{surf} = 0.22 mM and c_{NaBr} = 0.1M. The turquoise squares are the h-polymer/d-surfactant/NRW data, the purple circles are the h-polymer/h-surfactant/D_2O data, and the orange inverted triangles h-polymer/d-surfactant/D_2O. Simulated fits to these data using the compositions obtained from our co-modelling approach and a two layer structure where the top layer consists of surfactant chains (of which the density is varied) and the sub layer consists of surfactant headgroups, polymer and solvent are shown in corresponding colours.

The third system for which NR data was obtained on multiple isotopic contrasts as part of the experimental work in this thesis is PSS/C_{12}TAB. Data was recorded on this system as well as the PEO/surfactant mixtures above in order to determine whether strong interactions between oppositely charged polymers and surfactants at the interface had any effect on the validity of our approach. Simulated fits to data obtained on all three contrasts are shown in Figure 4.10; (a) shows simulations using the same structure as that used for the PEO/surfactant mixtures, a two layer structure where the top layer consists of surfactant chains and the bottom a mix of headgroups, polymer and solvent, and (b) shows a single layer model containing a mixture of polymer and surfactant. From panel (a) we can see that that the two layer model does not give perfect fits to the data obtained on all three contrasts, although the simulated fits are close to the data. Panel (b) shows that a single layer model gives better simulated fits to the data in all three isotopic contrasts, suggesting that the polymer and surfactant are significantly intertwined at the interface. Although the model is different for this system, it is clear that satisfactory fits to NR data on multiple isotopic contrasts can be simulated using the compositions from our co-modelling approach, further validating our methodology.

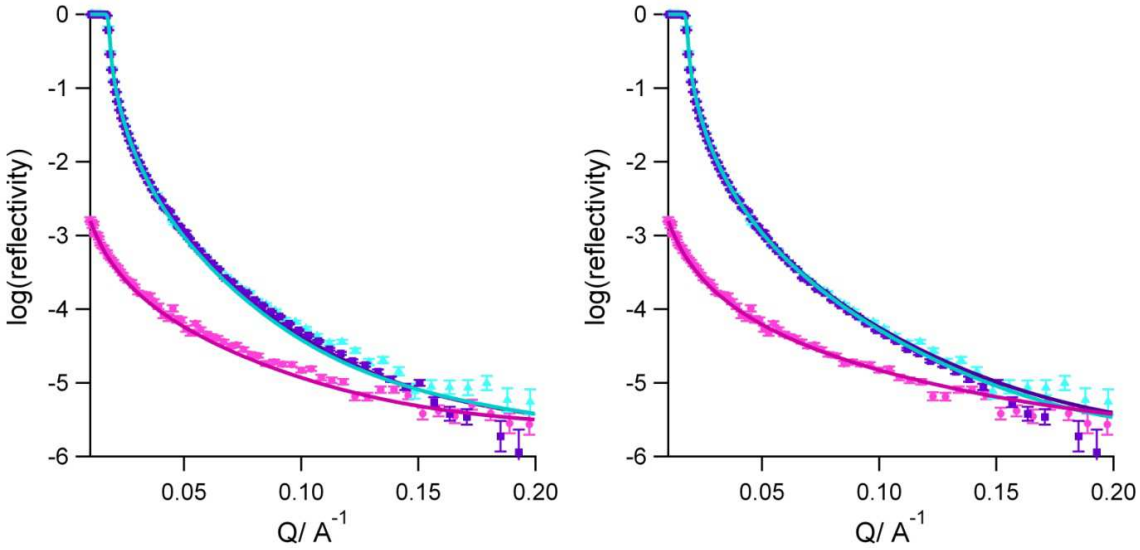

Figure 4.10. Neutron reflectivity profiles recorded in three isotopic contrasts, for the system PSS/C_{12}TAB where c_{PSS} = 100 ppm, c_{surf} =0.35 mM and c_{NaBr} =0.1M. The purple squares are the h-polymer/h-surfactant/ D_2O data, the pale blue triangles are the h-polymer/d-surfactant/D_2O data, and the pink circles h-polymer/d-surfactant/NRW. Panel (a) shows simulated fits using the compositions from our co-modelling approach and a two layer model where the top layer consists of only surfactant chains, and the thickness of which is varied, and the sub-layer consists of a mixture of surfactant headgroups, polymer chains, and solvent. Panel (b) shows simulated fits using the same compositions but a single layer model of 7 Å.

A further validation of our approach would be to use the NR data recorded on three isotopic contrasts to independently obtain consistent interfacial compositions, albeit using large quantities of deuterated materials. However, the similarity of all of the data recorded with a D_2O subphase to those for pure D_2O leads to large random errors for multiple neutron contrasts in the absence of any measurements containing deuterated PEO. For a thin adsorbed layer at the interface it is not surprising that the data recorded in a D_2O subphase are very similar to D_2O. Data on the h-polymer/h-surfactant/D_2O contrast show the change in solvent distribution at the interface by the adsorption of polymer and surfactant. If both components have minimal penetration into D_2O, the data will look very similar to that for pure D_2O, because the SLD of the adsorbed layer will only differ from D_2O when adsorbed polymer or surfactant headgroups displace D_2O at the interface resulting in a different SLD profile at the interface. Hence these data should give an indication of the adsorbed amount and spatial distribution of the polymer, although there is also a contribution from the deuterated surfactant chains and air layer which has an intermediate SLD.

In order to demonstrate the difficulty in independently determining the polymer surface excess from multiple isotropic contrast data, the simulated fits in Figure 4.8 (b) were refined with regards to polymer content using Motofit[33] by varying the solvent content in the second layer – equivalent to varying the polymer content. The polymer surface excesses obtained using this approach are shown in

Figure 4.11. The Γ_{poly} values obtained from refining the D_2O contrast fitting are extremely large, to the extent of being highly physically un-realistic. We have already shown that $\Gamma_{max,PEO}$ which can adsorb at the interface of the OFC by diffusion control is around 7 μmol m^{-2}, whilst the values in Figure 3 are around 20 times this value. Furthermore, these Γ_{poly} values are inconsistent with the data obtained for the h-polymer/d-surfactant/NRW contrast, and with the ellipsometry data. The derived polymer surface excesses are physically unrealistic due to the low sensitivity of NR to the quantity of a hydrogenated polymer with such a low scattering length density. In order to obtain accurate compositional information for this system from multiple isotopic contrast NR measurements we would need to use deuterated polymer.

The fact that Γ_{poly} cannot be accurately determined from our NR measurements on multiple isotopic contrasts demonstrates the strength of our co-modelling approach; even with NR data recorded on multiple isotopic contrasts we would not be able to determine reliably the interfacial composition unless we had deuterated polymer. Our co-modelling approach has a significantly enhanced sensitivity to the surface excesses of hydrogenated materials such as PEO, and may therefore be superior to NR measurements alone performed on multi-component systems for which not all components can be deuterated.

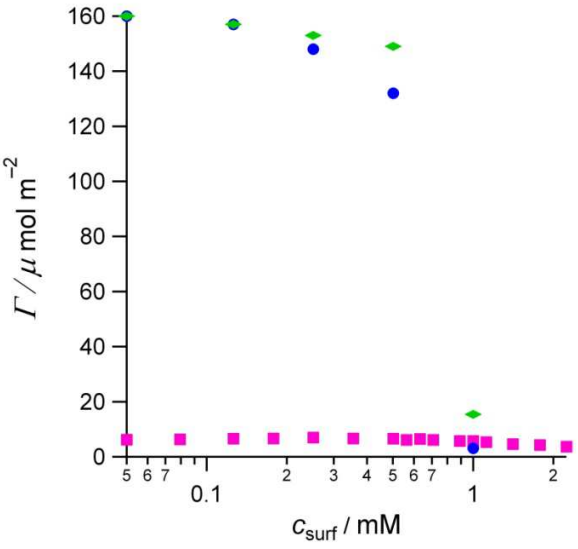

Figure 4.11. Surface excess of PEO in PEO/SDS as calculated using our co-modelling approach (pink squares), and as obtained from minimisations of the fits in Figure 2(b) for the h-polymer/d-surfactant/D_2O data (green diamonds) and the h-polymer/d-surfactant/D_2O data (blue circles).

In Figure 4.8, Figure 4.9 and Figure 4.10 I have shown that compositions obtained from our co-modelling approach are consistent with NR data when reasonable physical layer structures were used,

however in the case of systems where multiple contrast data are not available we do not know a priori the optimum structural model for the material at the interface. In order to apply our approach to a range of polymer/surfactant systems it will therefore be important to evaluate the effect of the structural model used in fitting the specular reflectivity profiles recorded on the h-polymer/d-surfactant/NRW contrast on the compositional data obtained. I will evaluate the effect of the layer model used on the value of $\sum_i \sigma_i \tau_i$ obtained for input into the co-modelling approach.

Figure 4.12 shows the effect of the fitting model used for the h-polymer/d-surfactant/NRW contrast data at low Q on the values of $\sum_i \sigma_i \tau_i$ obtained for the PEO/SDS system. It is clear from these data that the effect of the fitting model used on $\sum_i \sigma_i \tau_i$ is minimal, with the largest variation between data points at a given concentration being only around 5% of the value. As the values for a single 11 Å layer fit are within 5 % of those obtained from the two layer model, we will use the value of $\sigma \times \tau$ obtained from the single layer in the co-modelling even if the model would give a poor fit to data recorded on multiple isotopic contrasts, as it simplifies our approach.

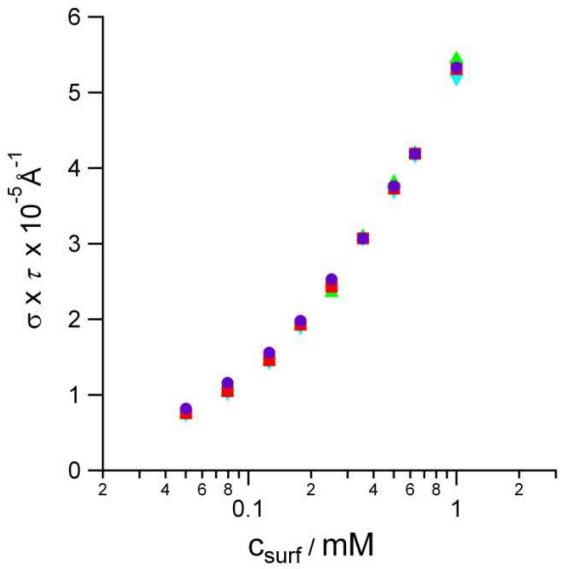

Figure 4.12. Product of the scattering length density and thickness, $\sigma \times \tau$, of the adsorbed layer of layers, obtained by fitting the NRW contrast using different structural models for the material at the interface for the PEO/SDS system. The structures used in fitting are one layer of 11 Å (inverted turquoise triangles), one layer of 20 Å (green triangles), a 2-layer model (red squares) and a 2 layer model with a diffuse sublayer (blue circles). Where the symbols are not distinguishable they are under the blue circles.

If we use the σ × τ values in Figure 4.12 to calculate the interfacial composition of the PEO/SDS system using our co-modelling approach (with the linear fit to the surfactant data used as the calibration plot), the data in Figure 4.13 are obtained.

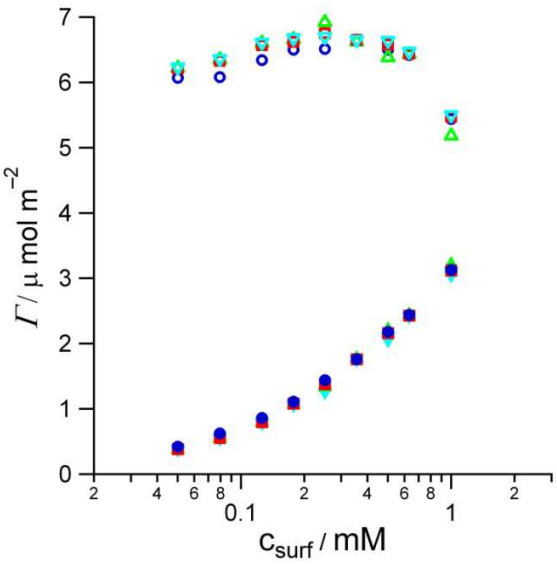

Figure 4.13. Surface excesses of PEO (empty symbols) and SDS (filled symbols) obtained using our co-modelling approach but with different structural models used in fitting the NR data, resulting in the $\sum_i \sigma_i \tau_i$ values in Figure 4.12. The symbols are consistent with the data in Figure 4.12.

From Figure 4.13 we can see that neither Γ_{surf} nor Γ_{poly} is measurably affected by the structural model used, with the biggest $\Delta\Gamma_{poly}$ between the different structures around 0.5 μmol m^{-2} and the biggest $\Delta\Gamma_{surf}$ = 0.15 μmol m^{-2}, and the trends in the data are not affected. Although only one structural model resulted in reasonable simulated fits to the NR data recorded in all three isotopic contrasts, use of any of the above structures gives values of the interfacial composition which vary by less than 5 % of the maximum value. As the simplest structural model is preferable, the single 11 Å layer approach will be used to fit data for this system for interpretation.

If we can use a single layer model to fit the specular reflectivity profiles at only low Q for all data recorded in the h-polymer/d-surfactant/NRW contrast without incurring significant errors in the calculated interfacial compositions, our simple co-modelling approach will be easily applicable to a range of polymer/surfactant systems. In order to evaluate whether this is the case I will now examine the effect of the fitting model used to obtain $\sum_i \sigma_i \tau_i$ on several other systems.

For the PSS/C_{12}TAB system, the simulated fits using compositions from our co-modelling approach which were closest to the data recorded on three isotopic contrasts were obtained using a single thin layer model as discussed above. Figure 4.14 shows the effect of the fitting model used on the fitted

values of $\sigma \times \tau$ or $\sum_i \sigma_i \tau_i$ for the data recorded on h-polymer/d-surfactant/NRW. It is clear from these data that despite there being an optimum structural model to fit the data from three isotopic contrasts, the error in $\sum_i \sigma_i \tau_i$ incurred by the fitting model used is never more than 5%.

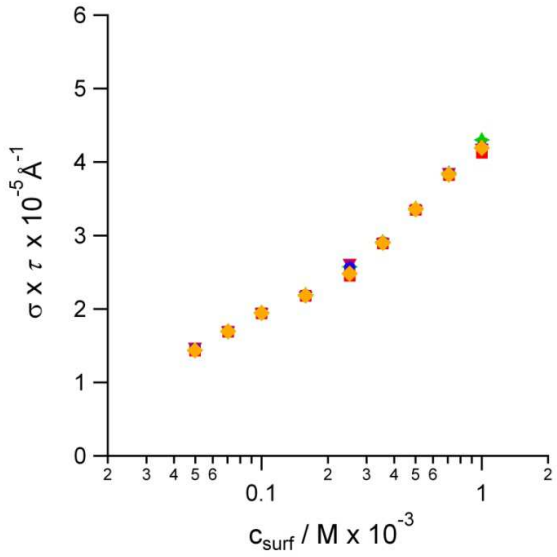

Figure 4.14. Sum of the products of the scattering length density, σ, and thickness, τ, ($\sum_i \boldsymbol{\sigma_i \tau_i}$) as fitted from NR data on the h-polymer/d-surfactant/NRW contrast using different structural models. Several models were used, a single 7 Å layer (red squares), a single 11 Å layer (yellow diamonds), a single 20 Å layer (green diamonds), two layers of 11 and 20 Å (blue circles) and two layers of 11 and 100 Å (pink triangles).

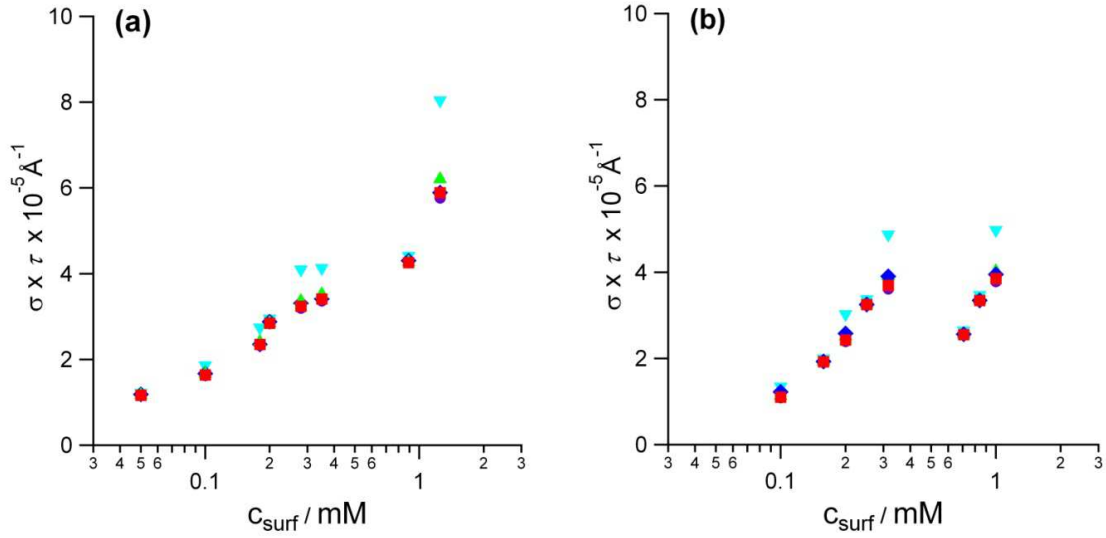

Figure 4.15. Product of the scattering length density, σ, and thickness τ (or sum of the values over more than one layer, $\sum_i \boldsymbol{\sigma_i \tau_i}$) obtained from fitting specular reflectivity profiles for (a) PSS/C_{14}TAB and (b) PSS/C_{16}TAB. The structural models used in fitting were a single layer of 11 Å (purple circles) of 14 Å (red squares) of 20 Å (green triangles) of 50 Å (turquoise inverted triangles) and a two layer structure with a top layer of 14 Å and a sub-layer of 20 Å (blue diamonds). The time-dependent data points (see below) are not shown in this figure.

For the PSS/C_{14}TAB and PSS/C_{16}TAB systems, the effect of the fitting model used to obtain $\sum_i \sigma_i \tau_i$ from the on h-polymer/d-surfactant/NRW contrast NR data is shown in Figure 4.15. For this system we do not have multiple isotopic contrast NR data, and the optimum layer model for determining $\sum_i \sigma_i \tau_i$ is assumed to be a single thin layer model as for the PSS/C_{12}TAB system. As C_{14}TAB and C_{16}TAB have longer hydrocarbon chains than C_{12}TAB, we would expect layers containing them to be thicker than those containing C_{12}TAB. For this reason I have also included a single 14 Å layer structure in the fitted structures, which gives a slightly better fit to the data at low Q. Figure 4.15 shows that the model used does not have a significant effect on the product of the scattering length density and thickness (σ x τ) obtained for either system, until thick layer models (50 Å, turquoise inverted triangles) are used. As a consequence, I will use the single 14 Å layer structure in fitting the data for the PSS/C_{14}TAB and PSS/C_{16}TAB systems.

As the layer structure used in fitting the h-polymer/d-surfactant/NRW contrast NR data has been demonstrated to have a minimal effect on both the values of $\sum_i \sigma_i \tau_i$ obtained and the interfacial compositions from co-modelling, I will use a single thin layer structure of fixed thickness to fit the NR data recorded for all polymer/surfactant systems in this thesis. However, it is important to note that the evaluatation of the effect of the fitting model on the data may be different for each polymer/surfactant system, especially if adsorption is at the static rather than the dynamic air/water interface if multilayer structures form or if particle like adsorption occurs. The brief evaluation of the effects of the fitting model on both $\sum_i \sigma_i \tau_i$ and the interfacial composition should therefore be undertaken for each system for which our co-modelling methodology is used in order to determine the errors in the calculated data.

4.5. Conclusions

We have developed and validated a new methodology for obtaining the interfacial composition of polymer/surfactant mixtures at the air/water interface. Our approach involves the co-modelling neutron reflectivity data recorded on only one NR contrast – hydrogenated (h-) polymer with deuterated (d-) surfactant in NRW – with optical data from ellipsometry measured using only hydrogenated materials. This approach is based on the different sensitivities of each technique to the amounts of polymer and surfactant in the adsorbed layer. The measured quantities for the two techniques, $\sum_i \sigma_i \tau_i$ and $\bar{\rho}$, can be approximated by equations relating them to the surface excesses of the two components. These equations can then be solved to obtain the surface excesses of the two components. The equation relating $\bar{\rho}$ and Γ for the surfactant is derived from a calibration plot. The choice of function used can lead to significant variation in the calculated interfacial composition if the selection is not made carefully, and must therefore be evaluated for every polymer/surfactant system. The choice of this function is one of the primary sources of uncertainty in the approach. The coefficients which relate $\sum_i \sigma_i \tau_i$ and Γ are obtained from the scattering lengths of both components.

In this chapter I have shown that the compositions calculated using our co-modelling approach can be used to simulate NR data obtained on multiple isotropic contrasts as long as an appropriate physical model is used. Furthermore, in the absence of deuterated polymer our co-modelling approach is more sensitive to the adsorbed amount of polymer than NR measurements on multiple isotropic contrasts, which cannot be used independently to obtain reasonable values of the polymer surface excess. I have also presented an evaluation of the effect of the structural model in fitting NR data obtained on the h-polymer/d-surfactant/NRW contrast contrast, and have shown for several systems that the error incurred from using the simplest physical model is only up to 5% of the maximum calculated value of Γ_{poly}.

Our new co-modelling approach has been shown to give reasonable values of the interfacial compositions of several different polymer/surfactant mixtures, to a greater degree of sensitivity for the polymer than is possible for multiple isotopic contrast NR measurements in the absence of deuterated polymer. We suggest that this methodology will be applicable to the adsorption of a wide range of polymer/surfactant mixtures at the air/water interface. Use of this approach, rather than multiple isotopic contrast neutron measurements will lead to significant savings in the use of deuterated materials and neutron beamtime, both valuable commodities. All of the interfacial compositions presented in this thesis are obtained using the methodology discussed in this chapter, and we hope that future studies will also take advantage of this approach.

4.6. References for Chapter 4

1. Zhang, J.; Thomas, R. K.; Penfold, J., *Soft Matter* **2005,** 1, (4), 310-318.
2. Penfold, J.; Tucker, I.; Thomas, R. K.; Taylor, D. J. F.; Zhang, J.; Zhang, X. L., *Langmuir* **2007,** 23, (7), 3690-3698.
3. Taylor, D. J. F.; Thomas, R. K., *Langmuir* **2002,** 18, (12), 4748-4757.
4. Taylor, D. J. F.; Thomas, R. K.; Hines, J. D.; Humphreys, K.; Penfold, J., *Langmuir* **2002,** 18, (25), 9783-9791.
5. Penfold, J.; Taylor, D. J. F.; Thomas, R. K.; Tucker, I.; Thompson, L. J. In *Adsorption of polymer/surfactant mixtures at the air-water interface: Ethoxylated poly(ethyleneimine) and sodium dodecyl sulfate*, Conference on Advances in the Study of Interfaes with Neutron Reflection, Grenoble, France, Oct 24-26, 2002; Amer Chemical Soc: Grenoble, France, 2002; pp 7740-7745.
6. Taylor, D. J. F.; Thomas, R. K.; Li, P. X., *Langmuir* **2003,** 19, (9), 3712-3719.
7. Campbell, R. A.; Yanez Arteta, M.; Angus-Smyth, A.; Nylander, T.; Varga, I., *J. Phys. Chem. B* **2011,** 115, (51), 15202-15213.
8. Thomas, R. K., *Annual Review of Physical Chemistry* **2004,** 55, 391-426.
9. Penfold, J. In *Specular Neutron Reflectivity: Applications to Soft Matter*, Neutron Reflectometry; A Probe for Materials Surfaces, Proceedings of a technical meeting Vienna, 2006, 2004; INTERNATIONAL ATOMIC ENERGY AGENCY: Vienna, 2004; pp 45-59.
10. Cooke, D. J.; Dong, C. C.; Lu, J. R.; Thomas, R. K.; Simister, E. A.; Penfold, J., *J. Phys. Chem. B* **1998,** 102, (25), 4912-4917.
11. Monteux, C.; Williams, C. E.; Meunier, J.; Anthony, O.; Bergeron, V., *Langmuir* **2004,** 20, (1), 57-63.
12. Monteux, C.; Llauro, M. F.; Baigl, D.; Williams, C. E.; Anthony, O.; Bergeron, V., *Langmuir* **2004,** 20, (13), 5358-5366.
13. Monteux, C.; Williams, C. E.; Bergeron, V., *Langmuir* **2004,** 20, (13), 5367-5374.
14. Asnacios, A.; Klitzing, R.; Langevin, D., *Colloids and Surfaces a-Physicochemical and Engineering Aspects* **2000,** 167, (1-2), 189-197.
15. Tonigold, K.; Varga, I.; Nylander, T.; Campbell, R. A., *Langmuir* **2009,** 25, (7), 4036-4046.
16. Campbell, R. A.; Ash, P. A.; Bain, C. D., *Langmuir* **2007,** 23, (6), 3242-3253.
17. Valkovska, D.; Wilkinson, K. M.; Campbell, R. A.; Bain, C. D.; Wat, R.; Eastoe, J., *Langmuir* **2003,** 19, (14), 5960-5962.
18. Ainalem, M. L.; Campbell, R. A.; Nylander, T., *Langmuir* **2010,** 26, (11), 8625-8635.
19. Kundu, S.; Langevin, D.; Lee, L. T., *Langmuir* **2008,** 24, (21), 12347-12353.
20. Vacklin, H. P.; Tiberg, F.; Fragneto, G.; Thomas, R. K., *Biochemistry* **2005,** 44, (8), 2811-2821.
21. Vandoolaeghe, P.; Rennie, A. R.; Campbell, R. A.; Thomas, R. K.; Höök, F.; Fragneto, G.; Tiberg, F.; Nylander, T., *Soft Matter* **2008,** 4, (11), 2267-2277.
22. Claesson, P. M.; Makuska, R.; Varga, I.; Mészáros, R.; Titmuss, S.; Linse, P.; Pedersen, J. S.; Stubenrauch, C., *Adv. Coll. Int. Sci.* **2010,** 155, (1-2), 50-57.
23. Battal, T.; Shearman, G. C.; Valkovska, D.; Bain, C. D.; Darton, R. C.; Eastoe, J., *Langmuir* **2003,** 19, (4), 1244-1248.
24. Manning-Benson, S.; Parker, S. R. W.; Bain, C. D.; Penfold, J., *Langmuir* **1998,** 14, (5), 990-996.
25. Valkovska, D. S.; Shearman, G. C.; Bain, C. D.; Darton, R. C.; Eastoe, J., *Langmuir* **2004,** 20, (11), 4436-4445.
26. Peron, N.; Campbell, R. A.; Nylander, T.; Vareikis, A.; Makuska, R.; Gilányi, T.; Mészáros, R., *J. Phys. Chem. B* **2008,** 112, (25), 7410-7419.
27. Bell, G. R.; Manning-Benson, S.; Bain, C. D., *J. Phys. Chem. B* **1998,** 102, (1), 218-222.
28. Day, J. P. R.; Campbell, R. A.; Russell, O. P.; Bain, C. D., *J. Phys. Chem. C* **2007,** 111, (25), 8757-8774.

29. Tyrode, E.; Johnson, C. M.; Rutland, M. W.; Day, J. P. R.; Bain, C. D., *The Journal of Physical Chemistry C* **2006,** 111, (1), 316-329.
30. Meunier, J., In *Light Scattering by Liquid Surfaces and Complementary Techniques*, Langevin, D., Ed. Dekker: New York, 1992.
31. Goates, S. R.; Schofield, D. A.; Bain, C. D., *Langmuir* **1999,** 15, (4), 1400-1409.
32. Borochov, N.; Eisenberg, H., *Macromolecules* **1994,** 27, (6), 1440-1445.
33. Nelson, A., *Journal of Applied Crystallography* **2006,** 39, 273-276.

Chapter 5. Poly(ethylene oxide) / Surfactant Systems

5.1 Introduction

Polymer/surfactant systems in which the two components interact either weakly or not at all are a good starting point for our survey of the effects of interactions in polymer/surfactant mixtures on adsorption kinetics. Comparison of the behavior of more complex polymer/surfactant mixtures to these weakly interacting systems will help us to elucidate the reasons for the behavior of the former systems. Mixtures of the non-ionic polymer poly(ethylene oxide) (PEO) with sodium dodecyl sulfate (SDS) or tetradecyltrimethylammonium bromide (C_{14}TAB) are the model systems upon which our current understanding of equilibrium properties of polymer/surfactant systems in the bulk and at interfaces was first built, [1, 2] and hence an examination of these systems seems a pertinent place to start.

PEO is a non-ionic polymer, and as a consequence can only interact weakly with charged surfactants either in the bulk or at the interface. PEO has been shown to be surface-active alone due to the hydrophobicity of the CH_2-CH_2 groups of the monomer segments, with a monolayer of polymer segments forming even at low bulk concentrations.[3-6] Due to the surface activity of both components, and the weak interactions between them, adsorption from a PEO/surfactant mixture is expected to primarily be competitive. On the OFC the species which dominate in a competitive adsorption situation is expected to be that which diffuses most quickly, in this case the surfactant. However, the rate of mass transport from the bulk solution is expected to control adsorption until free space limitations are reached.

PEO / C_{14}TAB is a good approximation to a non-interacting polymer/surfactant pair in the bulk solution, owing to the weakness of the hydrophobic interaction between PEO and hydrocarbon chains and the absence of any electrostatic attraction between the two species.[7] [8] At the static air/water interface, mixtures of PEO with C_{12}TAB show none of the deviations in the surface tension isotherms that are usually attributed to polymer/surfactant interactions in the bulk solution. Furthermore, measurements of the interfacial composition show that PEO is displaced from the interface by surfactant when c_{surf} is below the cac,[9] even though we would expect there to be no interaction between the two species in this region. Therefore on the OFC we would expect to see data indicative of a competitive adsorption mechanism for this system on the basis of excluded volume considerations.

Mixtures of PEO and SDS interact weakly in the bulk solution. Their interaction was traditionally attributed to hydrophobic bonding,[1] induced ion-dipole interactions, or interactions between the CH_2 groups of the polymer and the surfactant chains.[2] However, several more recent studies have suggested that the polymer/surfactant interaction is ionic in nature, mediated by metal cations complexed to the PEO chains.[8, 10, 11] The interaction between PEO and SDS leads to the formation of bulk complexes consisting of SDS micelles attached to individual polymer chains above the critical aggregation concentration (cac).[1, 2, 12-16]

Studies of the adsorption of PEO/SDS at the static air/water interface have shown that although polymer adsorbs at low bulk surfactant concentrations due to its inherent surface activity, it is displaced from the surface with increasing bulk surfactant concentration.[7] The adsorption of the two species is therefore commonly described as competitive.[9, 17, 18] However, the interaction between the two components means that there is also thought to be a co-operative component,[7] with a decrease in the free energy of the interface due to the mixing of the two components.[19] Inhibition of PEO adsorption by SDS has been attributed to increasing surface pressure on SDS adsorption, once the surface pressure exceeds that of a PEO monolayer, the adsorbed PEO layer thickens and collapses.[20] Alternatively, the formation of bulk polymer/surfactant complexes could decrease polymer adsorption,[21] however this seems unlikely as polymer has been suggested to be displaced from the air/water interface significantly below the cac.[7, 17] The recent simulations of Darvas *et al.*,[18] suggest that PEO and SDS adsorb competitively up until high surface coverages, with polymer segments displaced stepwise from the interface by the adsorption of surfactant molecules. In this model, polymer is not fully displaced from the interface until a monolayer of surfactant forms. We therefore expect to see that the adsorption behavior on the OFC is dominated by competitive adsorption, but this may not be as simple a mechanism as we expect for the PEO/C_{14}TAB mixture.

In this chapter I will explore the adsorption kinetics of both PEO/surfactant systems at the expanding interface of the OFC using a combination of ellipsometry, NR, co-modelling and LDV data, in order to examine the hypothesis that adsorption from both systems is controlled by a competitive adsorption mechanism. I will present our investigation into whether PEO adsorption is inhibited on the OFC at low surfactant concentrations where no bulk complexes form, or whether previous studies were limited by their sensitivity to polymer. Furthermore, I will determine whether the weak interaction between PEO and SDS results in qualitatively different behavior from the PEO/C_{14}TAB mixtures, and whether adsorption of either or both components in either or both systems is under diffusion or kinetic control. Use of several techniques including ellipsometry, NR and LDV to examine the interfacial adsorption will allow us to obtain a clear picture of the adsorption of PEO at the air/water interface, as each technique is sensitive to a different component or property of the system.

Materials and Methods

All of the measurements discussed in this chapter were recorded on solutions prepared in ultrapure water (Milli-Q; resistivity = 18 MΩ cm) for ellipsometry and LDV, or in D_2O (Euriso-top, C. E. Saclay, France) or null reflecting water (NRW) for NR measurements. The OFC and associated glassware were cleaned with a 2% solution of a strong alkaline detergent (Decon 90 or Gigapur) and rinsed thoroughly. SDS (Sigma, 99%) was purified by re-crystallisation three times from ethanol. C_{14}TAB (99%, Sigma) was purified by re-crystallisation three times from a mixture of ethanol and acetone. PEO (25k molecular weight, Sigma) was used as supplied. This polymer molecular weight was chosen in order to relate our data most easily to those of other studies which have used similar molecular weights[1, 7, 9, 14, 22] and in order to be above the threshold MW at which polymer behavior is no longer molecular weight dependent. [23, 24] Chain deuterated d-SDS and d-C_{14}TAB were kindly supplied by Dr R. K. Thomas from the Oxford Deuteration Facility. [25] All measurements involving C_{14}TAB were made in the presence of 0.1 M NaBr (Sigma Aldrich), and the measurements involving the involving SDS were made in the presence of 0.1 M NaCl (Sigma Aldrich).

For all polymer/surfactant measurements the polymer concentration was 100 ppm, and the surfactant concentration was varied. The first measurement for each system was made on a polymer and salt solution, or a salt solution in the case of surfactant measurements. To this solution, consecutive additions of stock surfactant solution were made in order to increase the bulk surfactant concentration stepwise from highly dilute to above the cmc of the mixture. Surfactant additions were made over a time period of several minutes, equivalent to several circulations of the system by the solution, and care was taken to ensure that the speed of addition and stock solution concentration had no effect on the measurements. For every addition of surfactant stock, salt and polymer were added to keep the bulk concentration of these components constant as the overall volume was increased.

5.2 PEO/C_{14}TAB

5.2.1. Results

5.2.1.1 Ellipsometry

Ellipsometry data recorded for the PEO/C_{14}TAB mixture and for pure C_{14}TAB are shown in Figure 5.1. Data were recorded at constant polymer and salt concentrations (100 ppm and 0.1 M, respectively) and are plotted with respect to the bulk surfactant concentration (c_{surf}). A dotted line indicates the value $\bar{\rho}_0$= 0.38 x 10^{-3} for pure water, and a dash-dot line indicates $\bar{\rho}$ for the polymer and salt solution in the absence of surfactant. Recall that for a pure surfactant a more negative ellipticity indicates a greater adsorbed amount, and that for a mixture the total ellipticity can be approximated by a linear combination of the ellipticities of the two components. PEO is surface-active alone: [3, 4, 24] 100 ppm of 25k PEO in 0.1 M inert electrolyte adsorbs at the surface of the OFC with a small negative ellipticity which corresponds to a Γ_{poly} of 6.4 μmol m^{-2}, less than half the value for the static air–water interface Γ_{poly} = 14.6 μmol m^{-2} (both values are calculated from $\bar{\rho}$ and dn/dc for PEO similarly to the calculation of $\bar{\rho}$ and dn/dc and Γ for polymer as discussed in Chapter 4). [26]

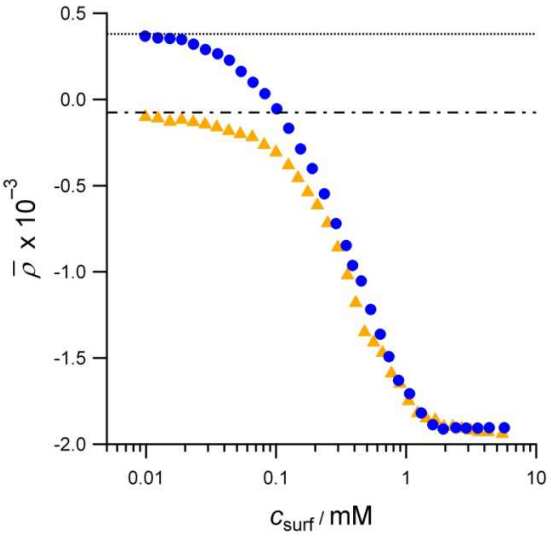

Figure 5.1. Coefficient of ellipticity ($\bar{\rho}$) at the surface of an OFC containing pure C_{14}TAB (blue circles) and C_{14}TAB in the presence of 100 ppm, 25k PEO (yellow triangles). Both measurements were made in the presence of 0.1 M NaBr. The upper dotted line is the ellipticity of the salt solution, and the lower dash-dot line is the ellipticity of the pure PEO and NaBr solution.

At low c_{surf}, $\bar{\rho}$ for the mixture is close to that of the polymer, whilst $\bar{\rho}$ for the surfactant solution is close to that of water. With increasing $c_{surf,}$ $\bar{\rho}$ becomes more negative for both PEO/C_{14}TAB and C_{14}TAB, whilst the difference between $\bar{\rho}$ for the mixture and that of the pure surfactant decreases, until the data sets converge. At c_{surf} ~ 1 mM, $\bar{\rho}$ in the presence of the polymer is the same as that of the pure surfactant. These two data sets were measured consecutively with the same instrument calibration, hence the overlap at high c_{surf} is real. It is tempting to draw conclusions about the composition of the interface from Figure 5.1, however we note that the surface expansion rates (θ) are not necessarily the same in the presence and absence of polymer, and that we cannot simply ascribe the difference between the two curves to polymer alone, since the surface excess of surfactant may be different. In order to draw conclusions about the composition of the interface we need NR data, and in order to hypothesise about the adsorption mechanism in action in this system we also need LDV data.

5.2.1.2. Laser Doppler Velocimetry

Measurements of the surface expansion rate (θ) using LDV can enable us to model quantitatively the kinetics of adsorption. For pure monomeric surfactants under diffusion control, the shape of θ *v* c_{surf} is typically a volcano plot, [27] as seen for C_{14}TAB in Figure 5.2. The presence of surfactant in solution induces surface tension gradients (Marangoni effects). The largest gradients - and hence the largest values of θ - occurring at c_{surf} values where small changes in Γ lead to big surface tension changes, and small gradients occurring at either low or very high surfactant coverages. Further details on the principles of LDV can be found in Chapter 2. For a pure surfactant solution, deviations from a volcano plot may arise from kinetic barriers to adsorption, which prevent the surface from reaching local equilibrium. For a polymer/surfactant mixture, interactions between the two components at the interface will alter θ compared to a pure surfactant system.

The expansion rate of PEO/C_{14}TAB in Figure 5.2 does not have the standard volcano plot form; instead a minimum in θ occurs at intermediate c_{surf}. The occurrence of two peaks in θ suggests that there may be two different mechanisms at work in different c_{surf} ranges. From considerations of mass balance at the surface, we would expect that for a given bulk concentration, a lower value of θ would correspond to a higher value of Γ. If we inspect the ellipsometry data in Figure 5.1 (an indicator of the total surface excess), we see a slight discontinuity occurs in $\bar{\rho}$ at c_{surf} = 0.5 mM, corresponding to the local minimum in the θ *v* c_{surf} plot in Figure 5.2. This dip may correspond to a higher total surface excess of the system in the region of the minimum in θ, however NR measurements are necessary to confirm this. The possible explanations of this local minimum will be discussed in greater length below. At high c_{surf} (>1

mM), θ is very similar for the surfactant and polymer/surfactant mixtures. In the same c_{surf} region in Figure 5.1, the values of $\bar{\rho}$ also co-incide for the systems.

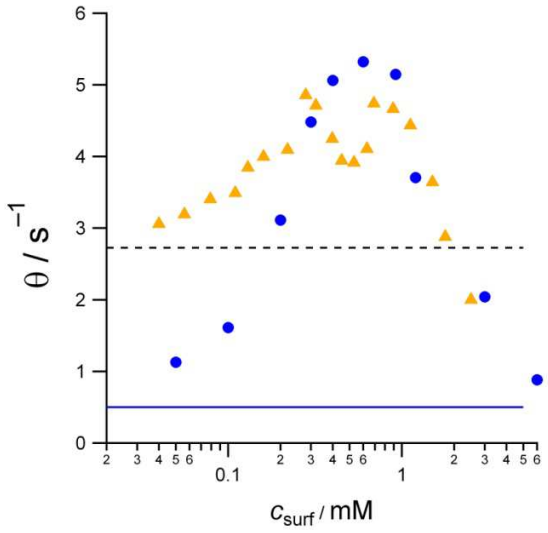

Figure 5.2. Surface expansion rate as a function of C_{14}TAB concentration for pure C_{14}TAB (blue circles) taken from reference 27 and C_{14}TAB in the presence of 100 ppm, 25k PEO (yellow triangles). Both measurements were in the presence of 0.1 M NaBr. The dashed line indicates θ for the pure polymer solution and the solid line for the pure salt solution.

5.2.1.3 Neutron Reflectivity

In Chapter 4 we showed that a two-layer model consisting of a top layer of surfactant chains of variable thickness and a sub-layer of surfactant headgroups, polymer chains, and solvent was necessary to fit the NR data recorded for this system with three isotopic contrasts. However, we also demonstrated that a simple single-layer model could be used in fitting data recorded on the h-polymer/d-surfactant/NRW contrast in order to obtain robust model independent values of $\sum_i \sigma_i \tau_i$ for use in our co-modelling approach. Figure 5.3 shows the $\sigma \times \tau$ values obtained from these fits using a single layer of 11 Å for the PEO/C_{14}TAB system.

Figure 5.3 plots $\sigma \times \tau$ for PEO/C_{14}TAB (yellow triangles) and pure C_{14}TAB (blue circles) against c_{surf}. At low c_{surf}, $\sigma \times \tau$ for the mixture is lower than that for the pure surfactant, as would be expected from the higher surface expansion rates in Figure 5.2. As c_{surf} increases, $\sigma \times \tau$ for PEO/C_{14}TAB quickly rises to the pure surfactant value. What appears to be a small overshoot at c_{surf} = 0.4 mM corresponds to the dip in the surface expansion rate of the mixture (a lower expansion rate leading to a larger surface excess), but the difference is close to the random error in the data. The values of $\sigma \times \tau$ in Figure 5.3 are

determined from NR data measured on the h-polymer/d-surfactant/NRW contrast, in which the deuterated surfactant has a much greater neutron scattering length than the polymer. Therefore, to a very good approximation these data tell us about the amount of adsorbed surfactant. Co-modelling of ellipsometry and NR measurements then allows us to determine the amount of adsorbed polymer.

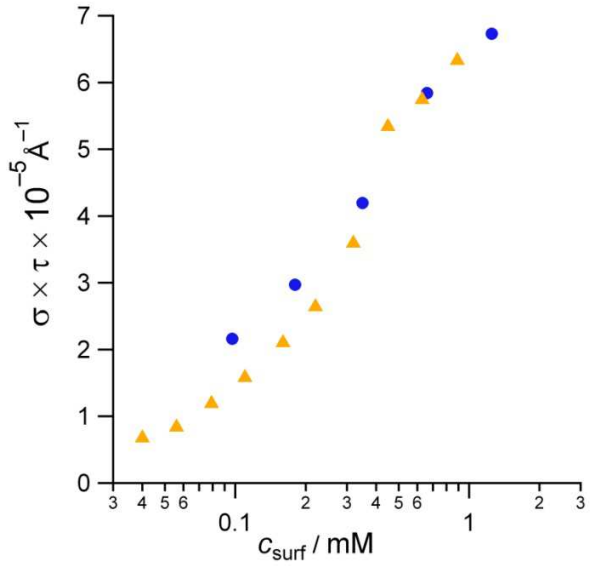

Figure 5.3. Product of the scattering length density, σ, and thickness, τ, $\sigma \times \tau$ as fitted from NR data. The blue circles are the C_{14}TAB data, and the yellow triangles the PEO/C_{14}TAB data. The data were fitted using a single 11 Å layer. All measurements were made in the presence of 0.1M NaBr.

The NR data in Figure 5.3 are co-modelled with the ellipsometry data in Figure 5.1 using the approach discussed in Chapter 4, and the resulting interfacial composition is shown in Figure 5.4.

5.2.2. Adsorption Kinetics

The interfacial composition of the PEO/C_{14}TAB mixture at a range of bulk compositions is compared with that for C_{14}TAB in the presence of 0.1 M NaBr in Figure 5.4; green squares are the amount of polymer at the interface in terms of moles of monomer, the turquoise diamonds are C_{14}TAB in the mixture and the blue circles the pure C_{14}TAB data. The solid green line gives the upper limit to the polymer coverage which can be reached by diffusion controlled adsorption, $\Gamma_{poly,max}$. This value is calculated from Equation 2.5 $\left(\Gamma_{dyn} = \sqrt{\frac{2D}{\pi\theta}}\,(c - c_s)\right)$ using the surface expansion rate data in Figure 5.2, with $c_s = 0$ and $D_{poly} = 4.3 \times 10^{-11}$ $m^2 s^{-1}$.[14] Thus, this curve represents the diffusion-controlled limit for polymer adsorption in the absence of adsorbed surfactant molecules, at the experimental expansion rates. This calculated diffusion controlled value of $\Gamma_{poly,max}$ is less than 50% of the equilibrium surface excess (as shown later in Figure 5.10 or by Gilányi *et al.*[24]). If polymer adsorbs under diffusion control, the bulk polymer concentration limits Γ_{poly}, and a larger bulk polymer concentration would give Γ_{poly} closer to the equilibrium value for a static interface.

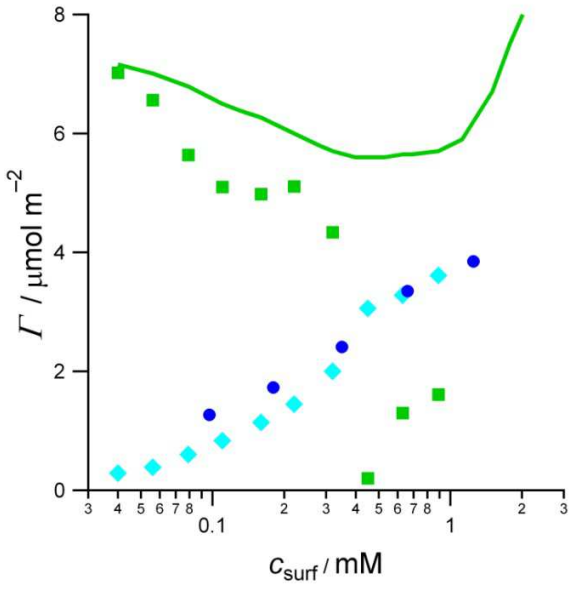

Figure 5.4. Surface excesses of PEO (green squares) and C_{14}TAB (turquoise diamonds) adsorbing from a mixture of C_{14}TAB and 100 ppm, 25k PEO as determined by co-modelling of ellipsometry and NR data, using a linear function to account for the contribution of surfactant to $\overline{\rho}_{mix}$ as discussed in Chapter 4. Also shown for comparison are the data for pure C_{14}TAB (blue circles) from NR. All measurements were in the presence of 0.1 M NaBr. The solid green line is the diffusion-controlled limit for polymer adsorption with $c_s = 0$. The surface expansion rate is taken from Figure 5.2 and the monomer and micelle diffusion coefficients are 4.3 x 10^{-10} m^2 s^{-1} and 1 x 10^{-10} m^2 s^{-1}, respectively.[27]

In Figure 5.4 we can see that at the lowest bulk surfactant concentrations measured the polymer surface coverage is within error of $\Gamma_{poly,max}$. Polymer is adsorbing under diffusion control, as we would expect considering its strong driving force for adsorption.[24] As the surfactant concentration is increased, at $c_{surf} < 0.3$ mM, Γ_{poly} in Figure 5.4 starts to deviate more significantly from the maximum diffusion controlled value. Note that if Γ_{poly} were calculated using the cubic function, which was not dismissed as a reasonable approach in Chapter 4 (Figure 4.3 a), Γ_{poly} would be close to the diffusion controlled limit until $c_{surf} \approx 0.3$ mM. In the same region, Γ_{surf} is low, less than the pure surfactant value. It is most likely that competitive adsorption is occurring in this region, with surfactant adsorption limiting the amount of polymer which can adsorb due to free space considerations. This is a reasonable expectation in a region where both Γ_{poly} and Γ_{surf} are at around 50% of their maximum values. This would therefore suggest that the values of Γ_{poly} in Figure 5.4, as calculated using the linear function in Chapter 4, are the most physically appropriate.

An alternative explanation for the adsorption of both components at less than their diffusion controlled surface excesses at low surfactant concentrations is the higher surface expansion rate of the mixture in this region compared to that of either component alone, which would decrease Γ. In order to determine whether competitive adsorption or increased surface expansion limits adsorption we need to determine the subsurface concentration, c_s, of surfactant and compare it with the expected value if the interface were at local equilibrium.

The sub-surface concentration of pure surfactant can be calculated from Equation 2.5 (as reproduced above) using the Γ and θ data in Figure 5.4 and Figure 5.2 respectively. The diffusion coefficient used for monomeric surfactant is $D_{surf} = 4.3 \times 10^{-10}$ m^2 s^{-1},[27] and at concentrations above the cmc of the system, D is obtained according to the method described by Valkovska *et al.*[27] The values thus calculated are shown in Figure 5.5. Valkovska *et al.* showed that both the dynamic and equilibrium adsorption of C_{14}TAB in the presence of 0.1 M NaBr obeys the Volmer isotherm[27] as given in Equation. 5.1. The Volmer isotherm is a simplified version of the Van der Waals isotherm which neglects the interaction between the molecules (in fact fitting the Van der Waals isotherm gave an interaction parameter of zero).

$$K\, a_s = \frac{\alpha\Gamma}{1-\alpha\Gamma}\, exp\left[\frac{\alpha\Gamma}{1-(\alpha\Gamma)}\right] \qquad (5.1.)$$

where a_s is the activity of the molecule, and can be approximated to c_s (the subsurface concentration or simply the bulk concentration at a static interface), K is the standard free energy of adsorption of the surfactant ions, and α is the excluded area per molecule at the interface. When surfactant adsorption is under diffusion-control the surface is in local equilibrium, and $\Gamma_{dyn}(c_s)$ should follow the Volmer

isotherm, where the constants in Equation 5.1 are obtained from $\Gamma_{eq}(c_b)$. The previous study showed excellent agreement between the calculated isotherm and the dynamic data on the OFC; C_{14}TAB in the presence of 0.1 M NaBr is diffusion controlled. The pure surfactant data recorded as part of this thesis and shown in Figure 5.5 (purple triangle) also show good agreement with the same theoretical Volmer isotherm (purple line).

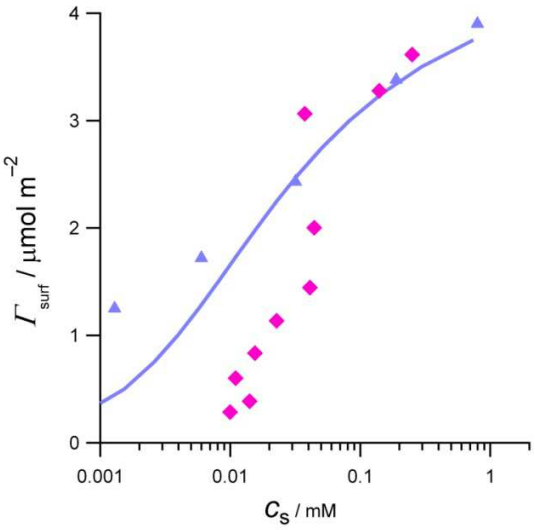

Figure 5.5. Γ_{dyn} *v* c_s data for pure C_{14}TAB (purple triangles) and C_{14}TAB in the presence of 100 ppm, 25k PEO (pink diamonds). Both measurements were made in the presence of 0.1 M NaBr. The purple line marks $\Gamma_{dyn}(c_s)$ calculated from the Volmer adsorption isotherm for the pure surfactant. Note that c_s is on a logarithmic scale so the differences in c_s between the experimental data and the theoretical curve at low Γ are small on an absolute scale and arise from errors in D, θ and c_b; any kinetic barriers would cause the experimental data to lie to the right of the theoretical line, not the left.

We cannot determine whether C_{14}TAB in a mixture with PEO adsorbs under diffusion control using the same method as for pure C_{14}TAB as we do not have the static data required for the isotherm calculations. As a simple alternative we can calculate c_s for C_{14}TAB in the mixture from Equation 2.5 as for the pure surfactant on the assumption that there are no polymer/surfactant interactions in the bulk solution which would influence the mass transport of the surfactant. [8] These calculated c_s values are then compared to the Volmer isotherm for the pure surfactant in Figure 5.5, in order to determine whether the adsorption of polymer has an effect on surfactant adsorption. If adsorption of C_{14}TAB from the mixture were totally unaffected by the presence of polymer at the surface, then $\Gamma_{dyn}(c_s)$ would fall on the purple line in Figure 5.5, as adsorption would be identical to that for the pure surfactant. Favourable interactions between the two components, as previously seen for the non-ionic/anionic surfactant mixture octaethyleneglycol n-decyl ether ($C_{10}E_8$) with APFN, [28] would cause the data to fall

above the purple line. Excluded volume effects or unfavorable interactions would cause the data to fall below the purple line.

From Figure 5.5, it is clear that for $\Gamma_{surf} \leq 2$ μmol m^{-2}, i.e. $c_{surf} < 0.3$ mM, c_s is systematically higher at a given Γ_{surf} for the surfactant in the mixture than in the pure surfactant solution, and the data fall below the purple line. The simplest explanation is a competitive adsorption mechanism due to excluded volume effects, which may have an additional contribution from any repulsive interactions between the components. If only excluded volume effects limited surfactant adsorption, we would expect that at low coverages (in the Henry law limit) Γ_{surf} at a given c_s would be proportional to the free surface area, i.e. the fraction not covered with polymer. Above, we mentioned that the maximum value of Γ_{poly} on the OFC is less than half of the maximum value at equilibrium, therefore if only excluded volume effects limited surfactant adsorption we would expect c_s for surfactant in the mixture to be not more than twice that of c_s for the pure surfactant at a given Γ_{surf}-value. However, in Figure 5.5 it is clear that the difference in c_s at low coverages is a factor of 5-10, which suggests that the adsorption of polymer may also cause a kinetic barrier to the adsorption of surfactant in the low c_{surf} region.

At intermediate c_{surf} (≈ 0.4 mM) the polymer surface excess in Figure 5.4 drops sharply to zero over a narrow concentration range. In the same c_{surf} region, a minimum is observed in the surface expansion rate in Figure 5.2. These two features are not simply co-incident as the minimum in θ occurs due to the decrease in surface tension gradient generated by polymer adsorption. Note that at this point Γ_{surf} for the mixture is higher than for the pure surfactant, but this difference can be ascribed to the lower surface expansion rate. At higher c_{surf} values polymer no longer adsorbs. However $\Gamma_{poly} \neq 0$ in this region in Figure 5.4, which is most probably due to errors in the co-modelling methodology as discussed in Chapter 4, as use of the cubic function in the co-modelling approach results in much smaller residual values of Γ_{poly}. As polymer no longer adsorbs surfactant adsorption is no longer inhibited. As a consequence θ increases again due to the adsorption of free surfactant molecules. Γ_{surf} also increases up to the pure surfactant value by $c_{surf} = 0.6$ mM, whilst θ reaches the pure surfactant data at around $c_{surf} = 1$ mM. The ellipsometric data, which is the most fine-grained and most precise of the three techniques, shows the pure surfactant and polymer/surfactant curves converging between $c_{surf} = 0.4$ and 0.8 mM and then tracking each other at higher concentrations. We can therefore confidently conclude from all these measurements that at surfactant concentrations above 0.8 mM, there is no PEO remaining at the surface.

We are therefore left with the following intriguing question; why is the polymer adsorption switched off over such a narrow range of bulk surfactant concentrations: from diffusion-controlled adsorption at 0.3 mM to no adsorption at all at 0.8 mM? Over the same c_{surf} range, Γ_{surf} only increases from 2 to 3

μmolm^{-2}. The sharpness of the transition is in part a consequence of the mass transport in the OFC: the equilibrium surface excess of polymer would in fact decrease for values of Γ_{surf} below 2 μmolm^{-2}, but we do not observe this on the OFC because the polymer adsorption is mass-transport limited.

The sharpness of the fall-off in Γ_{poly} is not a feature that we have been able to capture with a simple competitive Volmer isotherm for any reasonable values of the isotherm parameters, and the decrease in polymer adsorption at low surfactant coverages is unexpected. A possible (qualitative) explanation is that as the surface coverage of surfactant increases, fewer segments per polymer molecule are able to adsorb to the surface and therefore the adsorption energy of the polymer molecules (and the hence the equilibrium constant, K, that appears in competitive adsorption isotherms) decreases. This decrease in K with increasing Γ_{surf} has a similar effect to a repulsive interaction between the surfactant and the polymer, which disfavours mixed monolayers and leads to a sharpening of the transition between adsorbed polymer and adsorbed surfactant.

5.3 PEO/SDS

5.3.1. Results & Co-Modelling

5.3.1.1 Ellipsometry

The ellipsometry data recorded on the PEO/SDS mixture (shown in Figure 5.6) share many of the features of the ellipsometry data for PEO/C_{14}TAB in Figure 5.1. $\bar{\rho}$ for the mixture starts close to the pure polymer value at low c_{surf}, and becomes increasingly negative as c_{surf} is increased. The difference between the ellipticities of the mixture and the pure surfactant persists to higher surfactant concentrations for PEO/SDS than it did for PEO/C_{14}TAB, which suggests that behavior at the interface may be different in this system. For the PEO/C_{14}TAB system $\bar{\rho}$ for the mixture converges with that for the pure surfactant at high c_{surf} values. From Figure 5.6 it is not clear whether this also happens for PEO/SDS due to the small 'hump' in $\bar{\rho}$ for the mixture at high c_{surf}. An independent measurement of $\bar{\rho}$ at high c_{surf}, performed by adding polymer to 4 mM SDS found that the PEO/SDS solution had a more negative ellipticity than the pure SDS (but only by about 5×10^{-5} at 100 mM). Thus we conclude that the cross-over in Figure 5.6 is an artefact due to the use of different instrument calibrations for the SDS and PEO/SDS measurements.

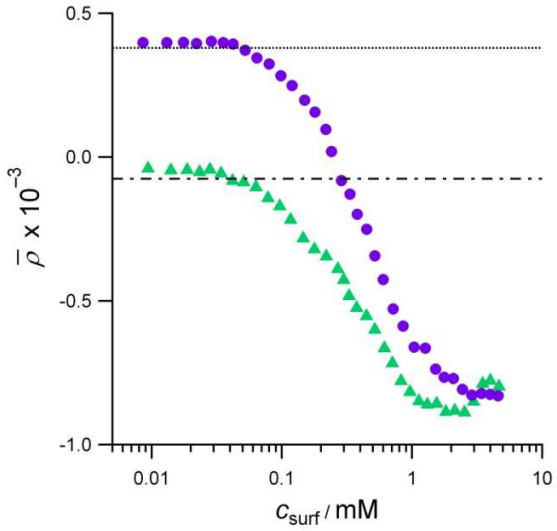

Figure 5.6. Coefficient of ellipticity at the surface of an OFC containing pure SDS (circles) and SDS in the presence of 100ppm, 25k PEO (triangles). Both measurements were in the presence of 0.1 M NaCl. The upper dotted line is the ellipticity of the salt solution, and the lower dash-dot line is the ellipticity of the pure PEO and NaCl solution.

As previously, we note here that although it is tempting to draw conclusions from the data in Figure 5.6, especially from comparisons to the PEO/C_{14}TAB data in Figure 5.1, we need LDV and NR data in order to resolve the interfacial composition and adsorption mechanism of this system.

5.3.1.2. LDV

Although LDV data for the PEO/C_{14}TAB system (Figure 5.2) did not have a classic volcano plot shape, data for the PEO/SDS system (Figure 5.7) do, with only a single peak in the data, similar to that for a pure surfactant. The main difference between the data for PEO/SDS and that for pure SDS is that θ is significantly higher at low to intermediate c_{surf} values for the mixture due to the surface activity of the pure polymer. The data for the mixture and the pure surfactant cross at c_{surf} = 0.8 mM, a concentration where the ellipticity is still much more negative (indicative of a higher surface excess) in the presence of PEO. Since it is implausible that complexation of SDS with PEO could accelerate diffusion of SDS to the surface, this observation provides strong evidence that PEO remains at the surface at least at concentrations up to ~ 1 mM SDS. However, use of ellipsometry and LDV cannot give us the full picture of the adsorption behavior of these systems, for this we need the interfacial composition information which can be obtained from our co-modelling approach.

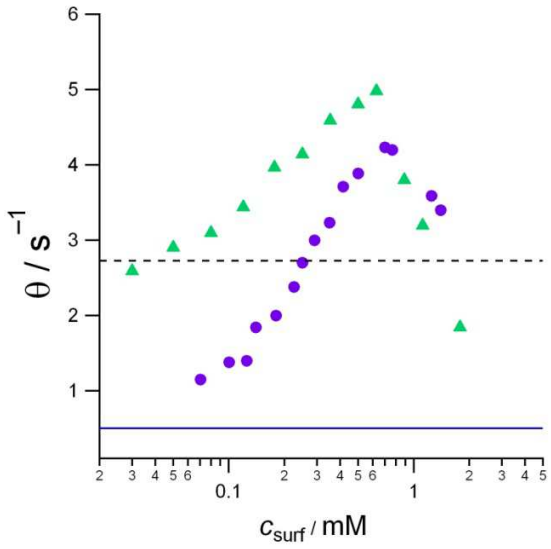

Figure 5.7. Surface expansion rate as a function of SDS concentration for pure SDS (purple circles) and SDS in the presence of 100 ppm, 25k PEO (green triangles). Both measurements were in the presence of 0.1 M NaCl. The dashed line indicates θ for the pure polymer solution and the solid line for the pure salt solution.

5.3.1.3 NR

The same single 11 Å layer model was used to fit the NR data obtained on the h-polymer/d-surfactant/NRW contrast to obtain $\sigma \times \tau$ as for the PEO/C_{14}TAB mixture above. Figure 5.8 plots the values of $\sigma \times \tau$ obtained from these fits for PEO/SDS (green triangles) against those for pure SDS (purple circles): $\sigma \times \tau$ for the mixture is below that of the pure surfactant data over the whole range of c_{surf} values measured. As only the surfactant is deuterated in the h-polymer/d-surfactant/NRW contrast and the SLD of PEO is low, surfactant dominates $\sigma \times \tau$ for the mixture, hence to a first approximation the amount of adsorbed surfactant in the mixture is less than for the pure surfactant over the whole c_{surf} range measured. This is unlike the data for the PEO/C_{14}TAB system, for which data for the mixture and the pure surfactant (Figure 5.3) coincided at intermediate c_{surf} values when polymer adsorption was inhibited. This suggests that perhaps the polymer adsorption behavior is different in this system. Co-modelling of the ellipsometry data with the data in Figure 5.8 will allow us to determine the adsorption behavior of the polymer over the same c_{surf} range.

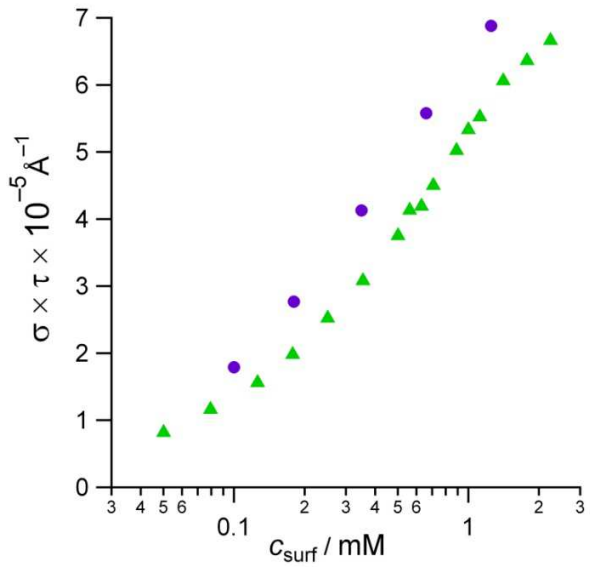

Figure 5.8. Product of the scattering length density, σ, and thickness, τ, as fitted from NR data using an single 11 Å layer model. The purple circles are the SDS data, and the green triangles the PEO/SDS data. All measurements were made in the presence of 0.1M NaCl.

The NR data in Figure 5.8 are co-modelled with the ellipsometry data in Figure 5.6 using the approach discussed in Chapter 4. The interfacial composition thus obtained for the PEO/SDS mixture on the OFC is shown in Figure 5.11.

5.3.1.5. Static Data

In order to facilitate modelling of the adsorption kinetics of PEO/SDS in the following sections, data were also recorded on this system at the static air/water interface using both ellipsometry and neutron reflectometry. The ellipsometry data in Figure. 5.9 (a) are remarkably insensitive to changes in c_{surf} over the whole range studied, whilst the NR data in Figure. 5.9 (b) show a clear increase in $\sum_i \sigma_i \tau_i$ with c_{surf}. The surface composition data obtained by co-modelling the data in Figure. 5.9 (a) and (b) are shown in Figure 5.10. Γ_{surf} increases and Γ_{poly} decreases with increasing c_{surf}; it appears that adsorption is classically competitive, although we might not expect Γ_{poly} to decrease to zero.

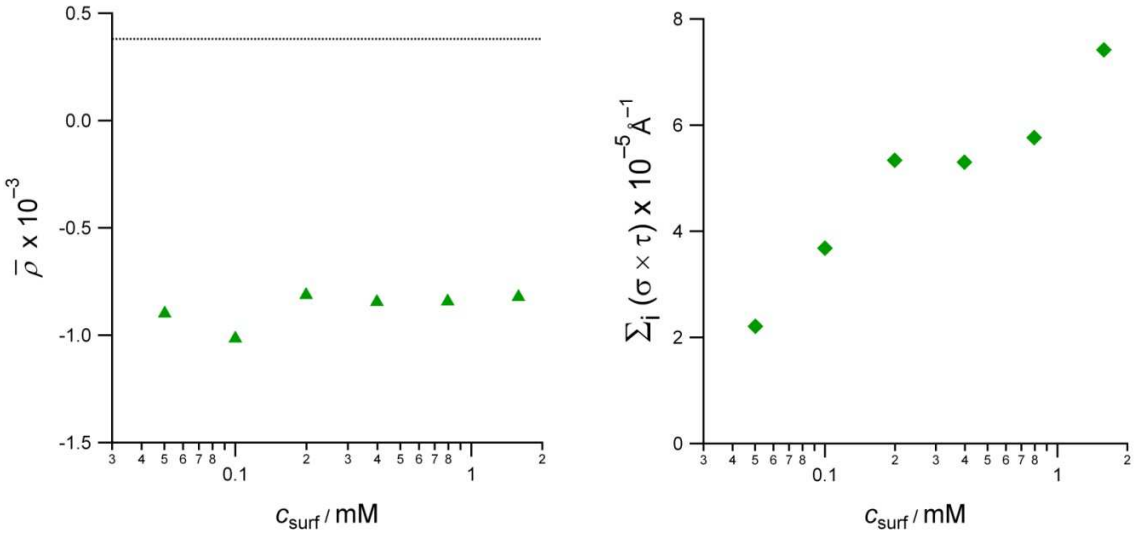

Figure. 5.9. (a) Coefficient of ellipticity at the surface of PEO/SDS/NaCl/H_2O solutions at the static air/water interface. The horizontal line marks the ellipticity of pure salt solution. (b) $\sum_i \sigma_i \tau_i$ for the adsorbed layer for PEO/SDS at the static air/water interface, as fitted from NR data using a single 11 Å layer model.

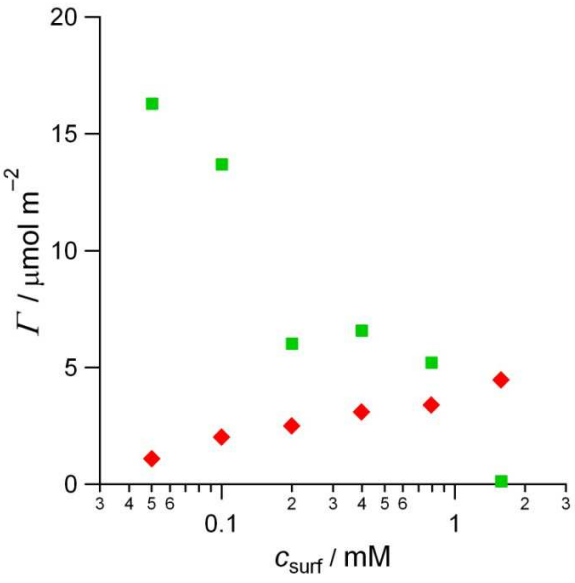

Figure 5.10. Surface excesses of PEO (green squares) and SDS (red diamonds) adsorbing from a mixture of SDS and 25k 100 ppm PEO at the static air/water interface as determined by co-modelling of ellipsometry and NR data. All measurements were made in the presence of 0.1 M NaCl.

5.3.2. Adsorption Kinetics

The interfacial composition of the PEO/SDS mixture, calculated from co-modelling the ellipsometry and NR data is compared with that for pure SDS in the presence of 0.1 M NaCl in Figure 5.11. As for the PEO/C_{14}TAB system above, the solid green line gives the upper limit to the polymer coverage which can be reached by diffusion controlled adsorption, $\Gamma_{\text{poly,max}}$, as calculated from $\Gamma_{dyn} = \sqrt{\frac{2D}{\pi\theta}}(c - c_s)$ using the surface expansion rate data in Figure 5.7, with $c_s = 0$ and $D_{\text{poly}} = 4.3 \times 10^{-11}$ m^2s^{-1}.[14] Polymer adsorbs at close to the diffusion controlled limit up until the region of the cac of the system at ≈ 0.7 mM SDS. [12] It therefore appears that polymer adsorbs under diffusion control despite the presence of surfactant until around the bulk compositions where polymer/surfactant complexes form, which will have a larger size and surface charge than the PEO molecules. However, even at surfactant concentrations below the cac Γ_{surf} is lower than that of the pure surfactant. This may be due to either competitive adsorption (which appears not to be affecting Γ_{poly}) or the higher surface expansion rate of the mixture, or a combination of the two factors. Whether or not surfactant is adsorbing under diffusion control will be assessed later by comparison of the data to those predicted using an adsorption isotherm.

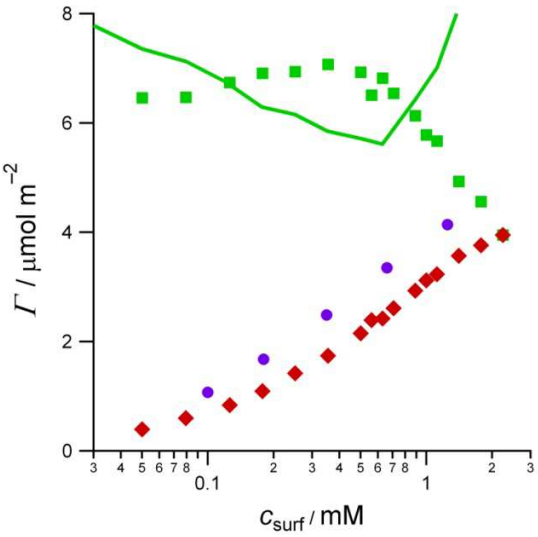

Figure 5.11. Surface excesses of PEO (green squares) and SDS (red diamonds) adsorbing from a mixture of SDS and 25k 100 ppm PEO as determined by co-modelling of ellipsometry and NR data, using a linear function to account for the contribution of surfactant to $\overline{\rho}$. Also shown for comparison are the data for pure SDS (purple circles) as measured using NR. All measurements were made in the presence of 0.1 M NaCl. The solid green line is an approximation to the diffusion controlled maximum polymer surface excess $\Gamma_{\text{poly,max}}$ as calculated from Equation 2.5 and the θ data in Figure 4 with $c_s = 0$.

The surface excess of PEO only starts to decrease in the region of the cac, at around c_{surf} = 0.7 mM, and once the surfactant excess has reached at least 50% of its maximum value. The decreasing values of Γ_{poly} with increased surfactant concentration beyond this point could therefore be attributed to either the slower mass transport of polymer/surfactant complexes above the cac, or to competitive adsorption at the interface. The rate of decline in Γ_{poly} in this region is much more gradual than in the presence of C_{14}TAB, and polymer continues to adsorb at all bulk compositions measured. In the same region, the surface expansion rate in Figure 5.7 reaches a maximum and then declines monotonically with increasing c_{surf}. This also indicates a more gradual change in the adsorption behavior of PEO/SDS compared to the sharp change in the PEO/C_{14}TAB system which caused the local minimum in θ.

At the bulk cmc (2.6 mM), Γ_{poly} is still 4 μmol m^{-2} and Γ_{surf} remains 10% below its saturation value. In order to check that the fact that polymer remains at the surface is not an artifact of the co-modelling methodology, independent ellipsometry measurements were made in this region (as discussed above), and proved that polymer does continue to adsorb at the interface. This behaviour is very different to that of the PEO/C_{14}TAB mixture, where PEO adsorption was inhibited from $c_{surf} > 0.4$ mM (Figure 5.4) and Γ_{surf} in the mixture = Γ_{surf} of the pure surfactant at intermediate to high surfactant concentrations.

It is conceivable that the decrease in Γ_{poly} at high c_{surf} could be due to a decreasing D_{poly} as bulk complexes form, however for this to be the case, D_{poly} would have to decrease to around $1/5^{th}$ of its original value, which is not indicated by any bulk studies.[22, 29, 30] Therefore, diffusion-controlled adsorption of polymer/surfactant complexes is unlikely to explain the observed decrease in Γ_{poly} at high c_{surf}. Furthermore, although the point at which Γ_{PEO} begins to decrease coincides with the bulk cac of the PEO/SDS system (0.7 mM), this is probably coincidental as the subsurface concentration of surfactant (c_s) is still well below the cac in this region: the subsurface concentration does not reach the cac until $c_{surf} \sim 1$ mM as shown later in Figure 5.14. Therefore the formation of bulk complexes in the PEO/SDS system cannot fully explain the adsorption behavior of the system on the OFC. It therefore we can conclude that synergistic interactions between polymer and surfactant at the interface determine the adsorption behavior at high c_{surf}.

The more gradual inhibition of PEO adsorption in the presence of SDS compared with C_{14}TAB must be due to the different interactions between the polymer and the two oppositely charged surfactants. Previous studies have suggested that there is a favorable interaction between PEO and SDS, either due to electrostatic attraction between the charged groups of SDS and the charge distribution of the moderately polar PEO monomer units[2] or to ionic interactions mediated by metal cations.[8, 10, 11] This positive interaction gives rise to a co-operative element to the adsorption,[7] favouring a mixed layer, and to bulk complexation of PEO and SDS, the effect of which is discussed above. A favourable interaction

between the two components at the interface would increase the coverage of one or both of them, increase the overall coverage compared to the non-interacting case, and the composition would move towards a more mixed monolayer. However, a favourable interaction between competitively adsorbing components may still lead to a decrease in surface excess compared to the two components alone.

In order to determine whether a synergistic interaction gives rise to the continued presence of polymer at the interface at high surfactant coverages in the OFC, we need to compare the experimental data to those calculated from an adsorption isotherm. For PEO/SDS we have static Γ v c_{surf} data for the mixture (as previously shown in Figure 5.10), hence a full analysis of the mixture by comparison to isotherms is possible. As a simple approximation for the mixture we use a Volmer isotherm to approximate the composition of the interface, which is equivalent to the van der Waals isotherm for a two component system as derived by Kralchevsky,[31] but neglecting the interaction between the two components and neglecting the effect of the counterions, as discussed for pure C_{14}TAB. The equation for a mixture is thus:

$$K_1 a_{1s} = \frac{\alpha_{11}\Gamma_1}{1-\alpha(\Gamma_1+\Gamma_4)}\ exp\left[\frac{(2\alpha_{11}-\alpha)\Gamma_1+(2\alpha_{14}-\alpha)\Gamma_4}{1-\alpha(\Gamma_1+\Gamma_4)}\right] \quad (5.2.)$$

where the subscript 1 denotes the surfactant, and subscript 4 denotes the polymer; a is the activity of the molecule, and can be approximated to c_s (the subsurface concentration or simply the bulk concentration at a static interface), K is the standard free energy of adsorption of the surfactant ions, and α is the excluded area per molecule at the interface, and average excluded volume, $\alpha_{14} = \left(\frac{\sqrt{\alpha_{11}}+\sqrt{\alpha_{44}}}{2}\right)^2$.

SDS has not been examined in a previous OFC study, and hence we do not know if its adsorption is diffusion controlled, and we do not have any theoretical isotherm parameters to use in Equation.5.2 Therefore in order to use the isotherm in Equation. 5.2 on the mixture we first need to determine the values of K and α for SDS by fitting data for SDS in the presence of 0.1 M NaCl recorded at the static interface by Penfold *et al.*[32] as shown in Figure. 5.12 As previously for C_{14}TAB we did this using a Volmer isotherm for a one component system, which is a simplification of Equation 5.1. The Volmer isotherm gives a good fit to the data in Figure. 5.12 without inclusion of an interaction parameter.

The least squares fit in Figure. 5.12 gives values of the constants for the surfactant K_1 = 1.15 x 10^4 and α_{11} = 1.5 x 10^5. As $\alpha \approx 1/\Gamma_{max}$, for polymer α_{44} = 1/(1.5 x 10^{-5}) = 6.67 x 10^4 or 3 x 10^7 in terms of polymer molecules. If these constants for the pure polymer and surfactant are used in the equation for the Volmer isotherm of the mixture to calculate c_s for the surfactant in the mixture at the static interface, and the values are plotted against Γ_{surf} and Γ_{poly}, the turquoise lines in Figure 5.13 are

obtained. From Figure. 5.12 and Figure 5.13 it is clear that at the static interface both the pure SDS and PEO/SDS data can be adequately fitted by a Volmer adsorption isotherm. With these isotherms in hand, we can now analyze the adsorption kinetics of both pure SDS and PEO/SDS on the OFC (Figure 5.14).

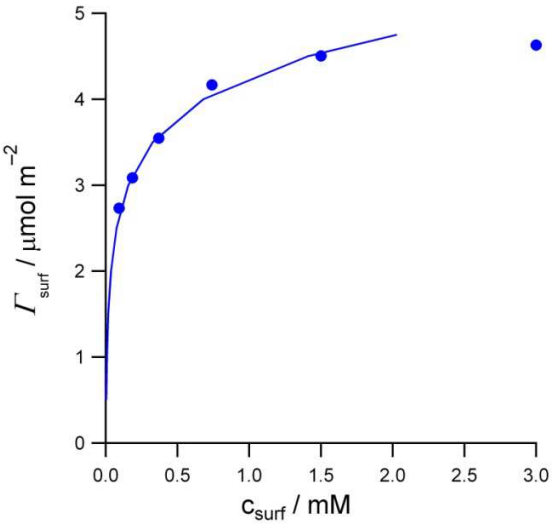

Figure. 5.12. Surface excess of pure SDS solutions at the static air/water interface in the presence of 0.1 M NaCl. Data are taken from Penfold *et al*., reference 32.

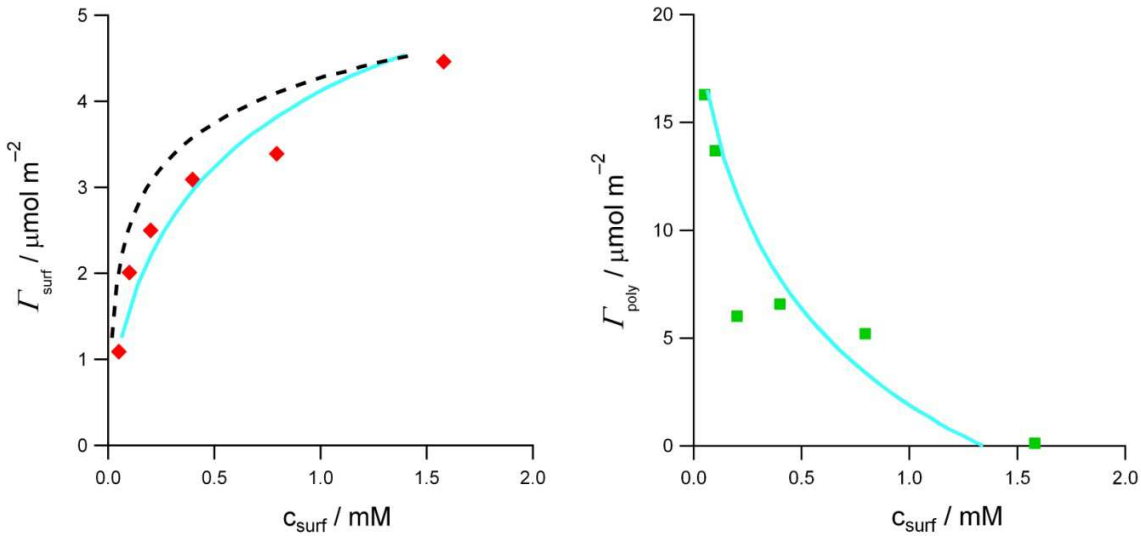

Figure 5.13. Surface excesses of (a) SDS and (b) PEO at the static air/water interface adsorbed from a mixture of SDS and 100 ppm, 25 k PEO and 0.1 M NaCl, calculated using our co-modelling approach, as shown previously in Figure 5.10, but separated here for clarity. The dashed line in (a) is the surface excess of pure surfactant at the same bulk surfactant concentration as extracted from Penfold *et al*.,[33] previously shown as data points in Figure. 5.12. The solid turquoise line in both (a) and (b) is the theoretical prediction of $\Gamma(c_{surf})$ from the Volmer isotherm for the mixture.

Adsorption of pure SDS on the OFC will be confirmed to be under diffusion control if the experimental data are a good fit to those calculated using the isotherm parameters obtained from the static data in Figure. 5.12. For pure SDS, experimental values of the subsurface concentration (c_s) are calculated from Equation 2.5 using D_{SDS} = 4.3 x 10^{-10} m s^{-1} [14], surface expansion rates from Figure 5.7, and surface excesses from Figure 5.11. These c_s values are plotted against Γ_{surf} in Figure 5.14 as purple circles, and the values calculated using the isotherm parameters determined from Figure. 5.12 are shown as a green dashed line. The excellent agreement between the experimental data and the values calculated using the Volmer isotherm shows that pure SDS adsorption is diffusion controlled.

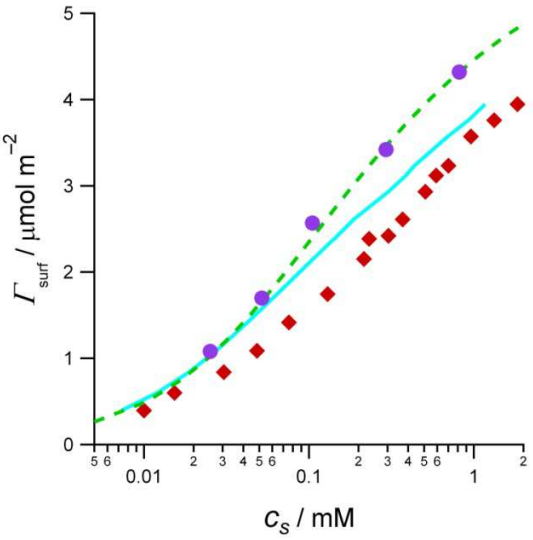

Figure 5.14. Γ_{dyn} v c_s data for SDS in the presence (red diamonds) and absence (purple circles) of 100 ppm, 25 k PEO. Both measurements were made in the presence of 0.1 M NaCl. The dashed green line marks $\Gamma_{dyn}(c_s)$ calculated from the Volmer adsorption isotherm for the pure surfactant and the solid turquoise line is $\Gamma_{dyn}(c_s)$ calculated from the Volmer isotherm for the mixture.

In order to determine whether adsorption of SDS in the mixture is diffusion controlled we firstly have to take into account the fact that the diffusion co-efficient of both species changes above the cac due to bulk complexation. In order to account for this we can use the methodology employed by Valkovska *et al.* [27]for surfactant solutions above the cmc in order to estimate how the overall diffusion co-efficients of the species change. Values of c_s for SDS in the mixture can then be determined, and these are plotted as red diamonds in Figure 5.14. Calculation of c_s from Equation 5.2. using the isotherm parameters for the mixture (exactly as in Figure 5.13 for the static data) results in the solid turquoise line in Figure 5.14. Comparison of the theoretical isotherm values with those obtained experimentally shows us that for a given value of Γ, the subsurface concentration, c_s for the surfactant in the mixture is greater than both that of the pure surfactant and that predicted by the Volmer isotherm for the mixture.

As for PEO/C_{14}TAB the presence of PEO causes a barrier to the adsorption of surfactant. It is important to note here that these conclusions are not reached due to the choice of a simplified isotherm model; if we included a parameter to account for favourable interactions between PEO and SDS the difference between the experimental and calculated values would in fact be increased. The data therefore suggest that a favorable interaction between PEO and SDS does not lead to enhanced adsorption at the interface.

Although favourable interactions between PEO and SDS at the interface do not enhance the adsorption of surfactant, they still have a large effect on the adsorption behaviour. In the PEO/SDS mixture a very high surfactant coverage is necessary to inhibit adsorption of PEO, much greater than that required in the PEO/C_{14}TAB mixture. Even once the surfactant coverage is very high and the vast majority of polymer segments are prevented from adsorbing at the interface, polymer can still adsorb, most probably due to a favorable interaction with the surfactant headgroups at the interface. Darvas *et al*.[18] suggested that the synergistic effect of SDS on PEO was due to a combination of the electrostatic attraction between the components and an increase in the conformational entropy of PEO in the presence of SDS. Furthermore, they suggested that PEO was only inhibited from adsorbing at the interface when the last monomer unit was prevented from adsorbing by surfactant, i.e. when a complete surfactant monolayer had adsorbed. Our results at the dynamic air/water interface are fully consistent with the conclusions of these simulations.

5.4 Conclusions

The adsorption behavior of mixtures of the non-ionic polymer PEO with cationic C_{14}TAB or anionic SDS has been evaluated in order to understand the factors which affect adsorption from polymer/surfactant mixtures at the interface of the OFC. These systems were chosen as model systems to which adsorption from more complex mixtures can be compared due to their weak polymer/surfactant interactions, a result of the non-ionic nature of the polymer.

For both systems at low c_{surf} values, polymer adsorption is under diffusion control, and is independent of the nature or concentration of the surfactant. $\Gamma_{poly,max}$ is significantly below the equilibrium value on the OFC, as it is limited by diffusion. In the same c_{surf} region, the surface excess of surfactant in both mixtures is reduced compared to that in the absence of polymer. In part the reduction in surfactant adsorption in this region is due to mass transport effects, as the surface expansion rate is higher in the presence of polymer, but there is also evidence that the adsorbed PEO causes a kinetic barrier to surfactant adsorption.

At intermediate c_{surf} values, when the surfactant surface excess reaches a threshold value of around 2 μmol m^{-2}, adsorption of polymer begins to be inhibited in both systems. Whilst this inhibition can be explained largely in terms of competition between the polymer and surfactant for space at the interface, there are significant differences in the behavior of the two surfactants. In the mixture with C_{14}TAB, PEO adsorption becomes fully inhibited over a narrow surfactant concentration range (in terms of both the bulk and interfacial compositions). However in the mixture with SDS, inhibition of PEO adsorption occurs over a much wider bulk surfactant concentration range. Furthermore, for PEO/SDS there is evidence from ellipsometry that a small amount of polymer is still adsorbed at saturation coverage of the surfactant (when the subsurface concentration exceeds the cmc).

The sharp displacement of PEO by C_{14}TAB is explained in terms of the cooperative nature of polymer adsorption (a small adsorption energy from each of a large number of adsorbed segments): once the polymer has to compete for space with the surfactant, the number of adsorbed segments decreases and hence so does the adsorption energy per molecule. This change in adsorption energy has the same effect as an unfavorable interaction parameter between the polymer and surfactant, sharpening the adsorption isotherm and disfavoring mixed layers. In contrast, there is known to be a favorable interaction between PEO and SDS which is ascribed either to a charge-dipole interaction or to a Coulombic interaction mediated by binding of metal cations to PEO. Although adsorption at the interface is not synergistic for PEO/SDS to the extent of enhancing the adsorption of surfactant, the continued adsorption of PEO at high SDS coverages suggests the influence of a favourable interaction

between the two components at the interface. Our data in this region are consistent with the simulations of Darvas *et al*.,[18] who suggest that due to electrostatic interactions and an increase in the conformational entropy of PEO in the presence of SDS, PEO adsorption is only completely inhibited when a full surfactant monolayer has adsorbed.

5.5. References for Chapter 5

1. Jones, M. N., Interaction of Sodium Dodecyl Sulfate with Polyethylene Oxide. *J. Colloid Interface Sci.* **1967,** 23, (1), 36-42.
2. Goddard, E. D., Polymer Surfactant Interaction .1. Uncharged Water-Soluble Polymers and Charged Surfactants. *Colloid Surf.* **1986,** 19, (2-3), 255-300.
3. Rennie, A. R.; Crawford, R. J.; Lee, E. M.; Thomas, R. K.; Crowley, T. L.; Roberts, S.; Qureshi, M. S.; Richards, R. W., Adsorption of poly(ethylene oxide) at the air-solution interface studied by neutron reflection. *Macromolecules* **1989,** 22, (8), 3466-3475.
4. Lu, J. R.; Su, T. J.; Thomas, R. K.; Penfold, J.; Richards, R. W., The determination of segment density profiles of polyethylene oxide layers adsorbed at the air-water interface. *Polymer* **1996,** 37, (1), 109-114.
5. Mahn Won, K., Surface activity and property of polyethyleneoxide (PEO) in water. *Colloid. Surf. A* **1997,** 128, (1-3), 145-154.
6. Darvas, M.; Gilányi, T.; Jedlovszky, P., Adsorption of Poly(ethylene oxide) at the Free Water Surface. A Computer Simulation Study. *J. Phys. Chem. B* **2010,** 114, (34), 10995-11001.
7. Cooke, D. J.; Dong, C. C.; Lu, J. R.; Thomas, R. K.; Simister, E. A.; Penfold, J., Interaction between poly(ethylene oxide) and sodium dodecyl sulfate studied by neutron reflection. *J. Phys. Chem. B* **1998,** 102, (25), 4912-4917.
8. Wang, Y. L.; Han, B. X.; Yan, H.; Cooke, D. J.; Lu, J. R.; Thomas, R. K., Interaction between poly(ethylene oxide) and dodecyl sulfates with different monovalent metal counterions studied by microcalorimetry. *Langmuir* **1998,** 14, (21), 6054-6058.
9. Cooke, D. J.; Blondel, J. A. K.; Lu, J.; Thomas, R. K.; Wang, Y.; Han, B.; Yan, H.; Penfold, J., Interaction between Poly(ethylene oxide) and Monovalent Dodecyl Sulfates Studied by Neutron Reflection. *Langmuir* **1998,** 14, (8), 1990-1995.
10. Maltesh, C.; Somasundaran, P., Effect of Binding of Cations to Polyethylene-Glycol on Its Interactions with Sodium Dodecyl-Sulfate. *Langmuir* **1992,** 8, (8), 1926-1930.
11. Dubin, P. L.; Gruber, J. H.; Xia, J. L.; Zhang, H. W., The Effect of Cations on the Interaction between Dodecyl-Sulfate Micelles and Poly(Ethyleneoxide). *J. Colloid Interface Sci.* **1992,** 148, (1), 35-41.
12. Mészáros, R.; Varga, I.; Gilányi, T., Effect of polymer molecular weight on the polymer/surfactant interaction. *J. Phys. Chem. B* **2005,** 109, (28), 13538-13544.
13. Varga, I.; Gilányi, T.; Mészáros, R., Characterisation of ionic surfactant aggregates by means of activity measurements of a trace probe electrolyte. In *Adsorption and Nanostructure*, Springer Berlin / Heidelberg: 2002; Vol. 117, pp 136-140.
14. Pettersson, E.; Topgaard, D.; Stilbs, P.; Soderman, O., Surfactant/nonionic polymer interaction. a NMR diffusometry and NMR electrophoretic investigation. *Langmuir* **2004,** 20, (4), 1138-1143.
15. Bernazzani, L.; Borsacchi, S.; Catalano, D.; Gianni, P.; Mollica, V.; Vitelli, M.; Asaro, F.; Feruglio, L., On the interaction of sodium dodecyl sulfate with oligomers of poly(ethylene glycol) in aqueous solution. *J. Phys. Chem. B* **2004,** 108, (26), 8960-8969.
16. Nagarajan, R., *Polym. Prepr. Am. Chem. Soc. Polym. Chem.* **1982,** 23, 41.
17. Peron, N.; Mészáros, R.; Varga, I.; Gilányi, T., Competitive adsorption of sodium dodecyl sulfate and polyethylene oxide at the air/water interface. *J. Colloid Interface Sci.* **2007,** 313, (2), 389-397.
18. Darvas, M.; Gilányi, T.; Jedlovszky, P., Competitive Adsorption of Surfactants and Polymers at the Free Water Surface. A Computer Simulation Study of the Sodium Dodecyl Sulfate Poly(ethylene oxide) System. *J. Phys. Chem. B* **2011,** 115, (5), 933-944.
19. Lu, J. R.; Thomas, R. K.; Penfold, J., Surfactant layers at the air/water interface: structure and composition. *Adv. Coll. Int. Sci.* **2000,** 84, (1-3), 143-304.

20. Henderson, J. A.; Richards, R. W.; Penfold, J.; Thomas, R. K.; Lu, J. R., Organization of poly(ethylene oxide) monolayers at the air-water interface. *Macromolecules* **1993,** 26, (17), 4591-4600.
21. Ramachandran, R., Kennedy, G.J., , *Colloids Surf* **1991,** 54, 261.
22. Gjerde, M. I.; Nerdal, W.; Hoiland, H., Interactions between poly(ethylene oxide) and sodium dodecyl sulfate as studied by NMR, conductivity, and viscosity at 283.1-298.1 K. *J. Colloid Interface Sci.* **1998,** 197, (2), 191-197.
23. Peron, N.; Campbell, R. A.; Nylander, T.; Vareikis, A.; Makuska, R.; Gilányi, T.; Mészáros, R., Competitive adsorption of neutral comb polymers and sodium dodecyl sulfate at the air/water interface. *J. Phys. Chem. B* **2008,** 112, (25), 7410-7419.
24. Gilányi, T.; Varga, I.; Gilányi, M.; Mészáros, R., Adsorption of poly(ethylene oxide) at the air/water interface: A dynamic and static surface tension study. *J. Colloid Interface Sci.* **2006,** 301, (2), 428-435.
25. Simister, E. A.; Thomas, R. K.; Penfold, J.; Aveyard, R.; Binks, B. P.; Cooper, P.; Fletcher, P. D. I.; Lu, J. R.; Sokolowski, A., Comparison of Neutron Reflection and Surface-Tension Measurements of the Surface Excess of Tetradecyltrimethylammonium Bromide Layers at the Air-Water-Interface. *J. Phys. Chem.* **1992,** 96, (3), 1383-1388.
26. Venohr, H.; Fraaije, V.; Strunk, H.; Borchard, W., Static and dynamic light scattering from aqueous poly(ethylene oxide) solutions. *European Polymer Journal* **1998,** 34, (5-6), 723-732.
27. Valkovska, D. S.; Shearman, G. C.; Bain, C. D.; Darton, R. C.; Eastoe, J., Adsorption of ionic surfactants at an expanding air-water interface. *Langmuir* **2004,** 20, (11), 4436-4445.
28. Day, J. P. R.; Campbell, R. A.; Russell, O. P.; Bain, C. D., Adsorption kinetics in binary surfactant mixtures studied with external reflection FTIR spectroscopy. *J. Phys. Chem. C* **2007,** 111, (25), 8757-8774.
29. Yuan, H. Y.; Luo, L. L.; Zhang, L. Z.; Zhao, S. Z.; Mao, S. M.; Yu, J. Y.; Shen, L. S.; Du, Y. D., Aggregation of sodium dodecyl sulfate in poly(ethylene glycol) aqueous solution studied by H NMR spectroscopy. *Colloid & Polymer Science* **2002,** 280, (5), 479-484.
30. Barhoum, S.; Yethiraj, A., An NMR study of macromolecular aggregation in a model polymer-surfactant solution. *J. Chem. Phys.* **2010,** 132, (2), 9.
31. Kralchevsky, P. A.; Danov, K. D.; Kolev, V. L.; Broze, G.; Mehreteab, A., Effect of Nonionic Admixtures on the Adsorption of Ionic Surfactants at Fluid Interfaces. 1. Sodium Dodecyl Sulfate and Dodecanol. *Langmuir* **2003,** 19, (12), 5004-5018.
32. Penfold, J.; Taylor, D. J. F.; Thomas, R. K.; Tucker, I.; Thompson, L. J., Adsorption of polymer/surfactant mixtures at the air-water interface: Ethoxylated poly(ethyleneimine) and sodium dodecyl sulfate. *Langmuir* **2003,** 19, (19), 7740-7745.
33. Penfold, J.; Tucker, I.; Thomas, R. K.; Taylor, D. J. F.; Zhang, J.; Zhang, X. L., The impact of electrolyte on the adsorption of sodium dodecyl sulfate/polyethyleneimine complexes at the air-solution interface. *Langmuir* **2007,** 23, (7), 3690-3698.

Chapter 6. Adsorption Kinetics of Mixtures of PSS and $C_{12}TAB$

6.1 Introduction

In the previous two chapters I introduced our new co-modelling approach to obtaining the surface composition and applied it to some 'base-line' systems, PEO/surfactant mixtures. In this chapter I will apply our approach to the adsorption kinetics of an oppositely charged polymer/surfactant system, poly(styrene sulfonate) [PSS] with dodecyltrimethylammonium bromide ($C_{12}TAB$). Taylor et al. classified PSS/$C_{12}TAB$ as a 'Type 1' polymer/surfactant system,[1, 2] exhibiting multilayer formation at the static air/water interface at intermediate surfactant concentrations, and no 'cliff edge peak' in the surface tension. Investigation of this system is complementary to the study of PDMDAAC/SDS on the OFC which precedes this thesis,[3] as PDMDAAC/SDS was classified as 'Type 2' by Taylor et al,[4] with only monolayer adsorption and a peak in the surface tension.[5, 6]

In the bulk solution PSS forms stable complexes with $C_{12}TAB$ from very low surfactant concentrations[7] (cac ≈ 0.015 mM),[8] orders of magnitude below the cmc of $C_{12}TAB$ (cmc ≈ 4 mM in the presence of 0.1 M NaBr), [2, 8] due to a combination of electrostatic interactions between the charged moieties on the two species and the hydrophobicity of the polymer. Stable complexes are formed due to the penetration of the phenyl groups of the polymer into the surface of the complexed surfactant micelle,[8-10] causing the micelles to be more densely packed than in pure surfactant solution. In many polymer/surfactant mixtures, complexes aggregate and precipitate close to charge equivalence. Several studies of PSS/$C_{12}TAB$ mixtures have shown that minimal phase separation occurs compared to other oppositely charged polymer/surfactant mixtures,[9, 11] although others have demonstrated that the system becomes turbid at around molar equivalence.[10] It is quite possible that the mixing methodology used in sample preparation has an effect on the bulk phase behaviour of PSS/$C_{12}TAB$ mixtures, as it has been to shown to in several other polymer/surfactant systems including PSS/$C_{16}TAB$[12] in which precipitation may only occur when gentle mixing methodologies are employed.

At the static air/water interface, adsorption in PSS/$C_{12}TAB$ mixtures has been shown to exhibit a sharp increase with increasing surfactant concentration.[1, 2, 7, 13] In the presence of salt (as in the experiments presented in this chapter), this transition occurred in the region of 1.6 – 2 mM $C_{12}TAB$.[2, 7] Taylor et al.[1, 2] attributed the high adsorbed amount to multilayer formation, whereas Monteux et al. demonstrated that the adsorbed layer was a heterogeneous microgel containing polymer/surfactant aggregates.[7] Monteux et al. attributed the presence of aggregates at the interface to the onset of aggregation of

polymer/surfactant complexes, first at the interface and then in the bulk. Bulk aggregation caused the adsorbed amount to fall at 4 mM C_{12}TAB.[7, 13] In dynamic elasticity studies, Noskov et al. recorded dense regions of polymer and surfactant of low net charge at the interface, which they described as 2-dimensional complexes containing entangled PSS molecules, whilst the surrounding film had a significantly lower elasticity.[14-16]

In this chapter I will use measurements on the OFC to try to determine how the adsorption of each species (polymer or surfactant) is affected by the presence of the other. Adsorption of the two species may be competitive due to free space considerations (as in Chapter 5), synergistic due to the attractive interactions between the species at the interface, or the adsorption of one species may inhibit the adsorption of the other. As PSS is not surface-active alone, it can only adsorb at the interface by interacting with C_{12}TAB, so synergistic adsorption must occur. We expect that adsorbed surfactant electrostatically attracts polyelectrolyte which consequently acts as a sublayer. This is in contrast to the PEO/surfactant mixtures in Chapter 5 in which PEO was surface active alone, and the weak interations between the neutral polymer and the surfactant molecules did not lead to significant synergy. The OFC can also be used to determine whether bulk phase separation (if it occurs in this system) has an effect on interfacial adsorption. If aggregates form in the bulk solution at high surfactant concentrations, we would expect to see a decrease in the adsorbed amount due to their slower diffusion on the OFC timescale.

The dynamic adsorption of PSS/C_{12}TAB is examined here as a function of both polymer concentration, molecular weight, and surfactant concentration. From simple mass transport considerations, we might expect that an increased polymer molecular weight will lead to a decreased polymer surface excess due to slower diffusion of polymer molecules and polymer/surfactant complexes, and may also decrease the adsorption of surfactant from complexes. Increasing the concentration of a polymer of a given size should increase the amount of polymer which can reach the interface, up to a threshold amount dictated by the surfactant concentration and steric constraints at the air/water interface.

Data recorded on several PSS/C_{12}TAB systems using NR, ellipsometry and LDV are presented in this chapter, along with an examination of the adsorption kinetics of this system using a basic model of the adsorption from a complex-forming polymer/surfactant system.

Materials

Solutions were made in ultrapure water (Milli-Q; resistivity = 18 mΩ.cm) for ellipsometry, or in D_2O (Euriso-top, C. E. Saclay, France) or NRW for NR measurements. The OFC and associated glassware were cleaned with a 2% solution of a strong alkaline detergent (Decon 90 or Gigapur) and rinsed thoroughly. C_{12}TAB (99%, Sigma) was purified by re-crystallisation three times from a mixture of ethanol and acetone. PSS (17k, 150k and 2.6M molecular weight, Sigma) was used as supplied. dC_{12}TAB was kindly supplied by Dr R. K. Thomas from the Oxford Deuteration Facility. [17] 0.1 M NaBr (Sigma Aldrich) was used for all experiments.

6.2 Results

6.2.1. Ellipsometry

Figure 6.1 and Figure 6.2 show the coefficient of ellipticity, $\bar{\rho}$, as a function of C_{12}TAB concentration (c_{surf}) for pure C_{12}TAB and two series of PSS/C_{12}TAB mixtures, all in the presence of 0.1 M NaBr. Figure 6.1 shows measurements made at a range of bulk polymer concentrations from 0 to 400 ppm of 17k PSS, and Figure 6.2 shows measurements on systems containing different polymer molecular weights from 17k to 2.6M PSS, at all 100 ppm. The dashed line shows the ellipticity of pure water which is indistinguishable from the ellipticity of polymer and salt solutions in the absence of surfactant, since PSS is not surface-active.[1] The ellipsometry data are the most fine-grained of the data I recorded and consequently give us the most subtle information about the adsorption behaviour.

At low surfactant concentrations, $\bar{\rho}$ is more negative, corresponding to a larger total surface excess, for the mixtures than for the pure surfactant. In interacting polymer/surfactant systems, enhanced adsorption at low surfactant concentrations has been seen in several previous studies, and attributed to synergistic adsorption of polymer and surfactant at the interface.[1, 18, 19] At the lowest values of c_{surf} (<0.02 mM), the ellipsometry data for all of the systems in Figure 6.1 and Figure 6.2 are very similar, despite the different polymer concentrations and molecular weights, suggesting that in this region adsorption at the interface is determined by the surfactant rather than the polymer.

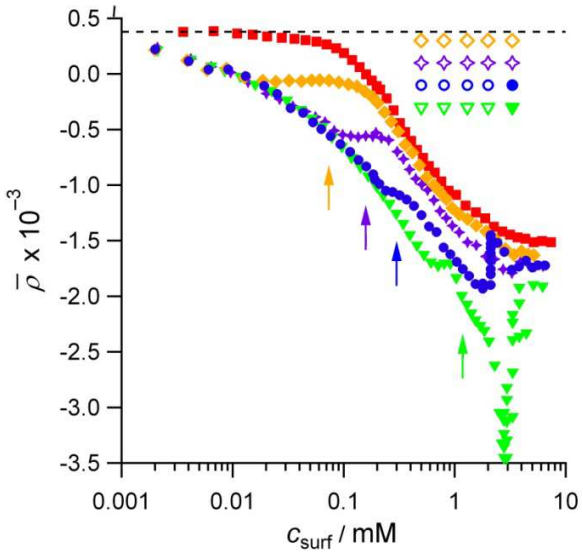

Figure 6.1. Coefficient of ellipticity at the surface of an OFC containing C_{12}TAB and different concentrations of PSS (at a constant molecular weight of 17k), where the red squares at 0 ppm PSS, the yellow diamonds are 20 ppm, the purple crosses 50 ppm, the blue circles 100 ppm, and the green triangles 400 ppm. All measurements were made in the presence of 0.1 M NaBr. The upper dotted line is the ellipticity of the salt solution, and of the polymer and salt solution. The symbols in the top right corner represent UV-vis measurements on various PSS/C_{12}TAB samples, where symbols are empty until the O.D. at 450 nm > 0.1. The upward pointing arrows below the data represent the point at which we predict the formation of single polymer/micelle complexes will be complete.

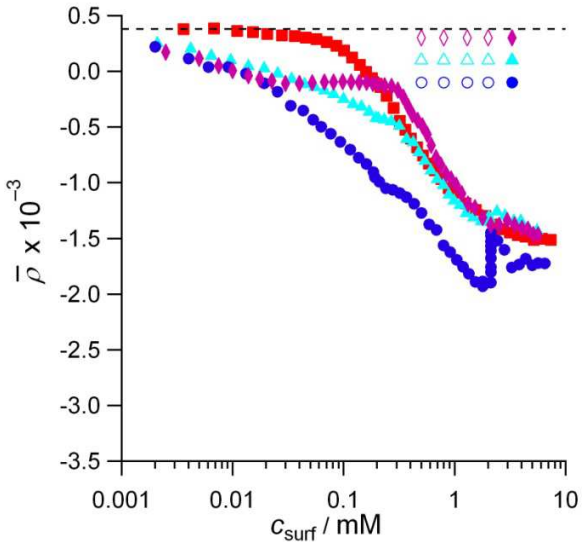

Figure 6.2. Coefficient of ellipticity at the surface of an OFC containing C_{12}TAB and different PSS molecular weights (at a constant concentration of 100 ppm). The red squares at 0 ppm PSS, the blue circles are 17k (as in Figure 5), the turquoise triangles are 150k, and the pink diamonds are 2.6M. All measurements were made in the presence of 0.1 M NaBr. The upper dotted line is the ellipticity of the salt solution, and of the polymer and salt solutions. The symbols in the top right corner represent UV-vis measurements on various PSS/C_{12}TAB samples, where symbols are empty until the O.D. at 450 nm > 0.1.

As the surfactant concentration is increased further, $\bar{\rho}$ is similar for all systems containing 17k PSS (Figure 6.1), until each system successively reaches a turning point which precedes a plateau in $\bar{\rho}$. The surfactant concentrations corresponding to both the start and end of the plateau increase with increasing bulk polymer concentration, suggesting that these changes in adsorption behaviour may be attributable to key polymer:surfactant ratios being reached, either in the bulk or at the interface. Although the plateau in $\bar{\rho}$ may be suggestive of a constant surface composition, I will show below that the surface excess of one component increases whilst simultaneously the surface excess of the other component decreases. It is therefore important not to over-interpret such ellipsometry data alone; we have to examine the interfacial composition obtained from co-modelling the ellipsometry and NR data before we can reach conclusions about the origin of the turning points and plateaus in the ellipsometry data.

For the systems containing the same polymer concentration but different molecular weights (Figure 6.2) the three data sets are very similar at low surfactant concentrations (to within errors caused by cleanliness issues with these systems) but deviate from each other at $c_{surf} \approx 0.02$ mM. As c_{surf} is increased beyond this point, $\bar{\rho}$ varies with molecular weight, with lower molecular weight polymer resulting in more negative $\bar{\rho}$ values (indicative of higher surface excesses). As the ellipticity is related to the total surface excess, it is not surprising that the recorded values of $\bar{\rho}$ suggest lower total surface excesses for systems containing slower diffusing polymer molecules. In Figure 6.2, unlike Figure 6.1, only the 2.6 M PSS system displays a defined plateau in $\bar{\rho}$ at intermediate c_{surf} values. This may help us to examine the reasons behind the plateau.

At the end of the plateau, the gradient in $\bar{\rho}$ increases again, and in the majority of the systems the gradient, or even the value, of $\bar{\rho}$ tracks that of the pure surfactant. The value of c_{surf} corresponding to this turning point depends on the bulk polymer concentration but not on its molecular weight (Figure 6.1 and Figure 6.2).

At the highest c_{surf} values measured in Figure 6.1, $\bar{\rho}$ for the mixtures is close to the pure surfactant values. However for the 100 and 400 ppm systems, before this point is reached, time-dependent changes in $\bar{\rho}$ were recorded. These changes are displayed as multiple values of $\bar{\rho}$ for a given value of c_{surf}. Over time the values of $\bar{\rho}$ become less negative. Since the sensitivity of ellipsometry to the adsorption of the two components is similar, these changes in $\bar{\rho}$ are large enough that they must correspond to a decrease in the amount of one of the components adsorbing at the interface and cannot be due just to a change in composition. Due to the flowing nature of the OFC, a significant change in the total surface excess at a constant bulk composition must indicate a change in the mass transport of this species to the interface, which we attribute to aggregation of polymer/surfactant complexes. Large

aggregates cannot reach the interface on the timescale of surface expansion, hence material in them cannot contribute to adsorption. Aggregation causes increased turbidity of the solution, hence our hypothesis that aggregation explains the time dependent data is supported by the O.D. data in Figure 6.1 which show that the same is initially turbid in this region. Although the data did not observably change with time for the other systems in Figure 6.1 and Figure 6.2, all of the systems containing polymer concentrations of 100 ppm or more exhibit turbid solutions in this region, hence we conclude that bulk phase aggregation also occurs in these systems, but it may not occur in the systems containing low polymer concentrations.

6.2.2. NR

The specular reflectivity profiles recorded on the h-polymer/d-surfactant/NRW contrast were fitted using a single 11 Å layer model in order to obtain the values of $\sigma \times \tau$ shown in Figure 6.3. This was determined to be the optimum fitting model for the data in Chapter 4, where it was demonstrated that use of a more complicated model or a thicker single layer resulted in a worse fit to NR data recorded on three isotopic contrasts. Figure 6.3 shows that the amount of material at the interface, as indicated by $\sigma \times \tau$, is relatively independent of the polymer concentration and polymer molecular weight, except for the highest MW (2.6M) at low c_{surf}, despite the markedly different $\bar{\rho}$ data in Figure 6.2.

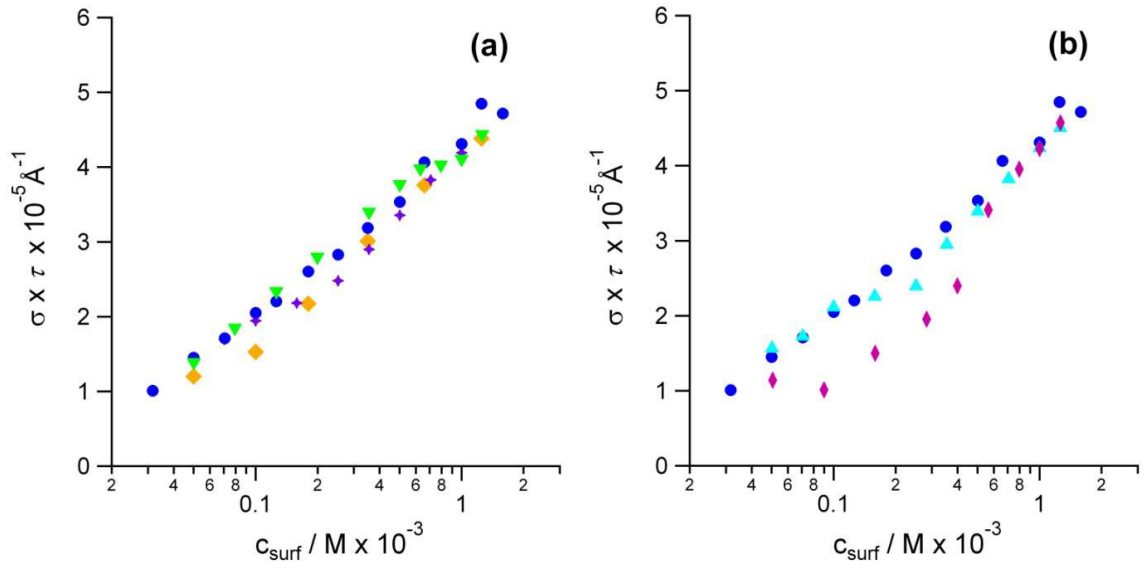

Figure 6.3. Product of the scattering length density and thickness fitted to an 11 Å single layer model for a range of PSS/C_{12}TAB systems, which vary by (a) polymer concentration and (b) polymer molecular weight, with symbols corresponding to those in Figure 6.1 and Figure 6.2.

The $\sigma \times \tau$ values in Figure 6.3 (a) vary remarkably little with polymer concentration considering the significant differences between the ellipsometry data of these systems in Figure 6.1 and the very different amounts of polymer in the bulk solution. As these data are obtained from NR measurements on the isotopic contrast h-polymer/d-surfactant/NRW, the primary contribution usually comes from the deuterated surfactant. However, PSS has a relatively high neutron scattering length density per segment for a hydrogenated polymer, 1.85×10^{-6} v 5.12×10^{-6} Å^{-2} for $dC_{12}TAB$, hence the data in Figure 6.3 cannot simply be attributed to the surfactant surface excess as it was in Chapter 5. We therefore cannot assume that the similarity of $\sigma \times \tau$ for the different systems in Figure 6.3 (a) is indicative of similar Γ_{surf} values for all of the systems, as it may be due to changing proportions of the two components at the interface.

As $\sigma \times \tau$ cannot be assumed to be linearly related to Γ_{surf} for this system as it can for other polymer/surfactant systems (see Chapter 4), further interpretations of the adsorption behaviour cannot be reached from the NR data alone. Co-modelling of these data with the ellipsometry data in Figure 6.1 and Figure 6.2 will allow us to determine the interfacial compositions of the mixtures.

6.2.3. Interfacial Compositions from Co-modelling

The function used to account for the contribution of surfactant to $\bar{\rho}$ for the mixture in our co-modelling approach was shown in Chapter 4 to have a minimal effect on both the trends in the data and the surfactant surface excess, but to cause variations in the calculated polymer surface excess. A cubic function was chosen for consistency with the other PSS/C_nTAB systems, as discussed in Chapter 7.

The effect of polymer concentration and molecular weight on the interfacial composition of PSS/C_{12}TAB mixtures is shown in Figure 6.4 and Figure 6.5, respectively, with Γ_{surf} in panel (a) and Γ_{poly} in panel (b). Γ_{surf} is remarkably insensitive to changes in either the polymer concentration or molecular weight, with only the highest molecular weight polymer causing a large deviation from the Γ_{surf} data for the other systems, although there is also a small plateau in the 400 ppm Γ_{surf} data at high c_{surf}. At low c_{surf}, the surfactant surface excess in the mixture is greater than that of the pure surfactant, which is, in general terms, consistent with synergistic adsorption of polymer and surfactant in this region. At higher c_{surf}, $\Gamma_{surf,mix}$ drops slightly below the pure surfactant value, which may be due to a change in the adsorption mechanism, as discussed later.

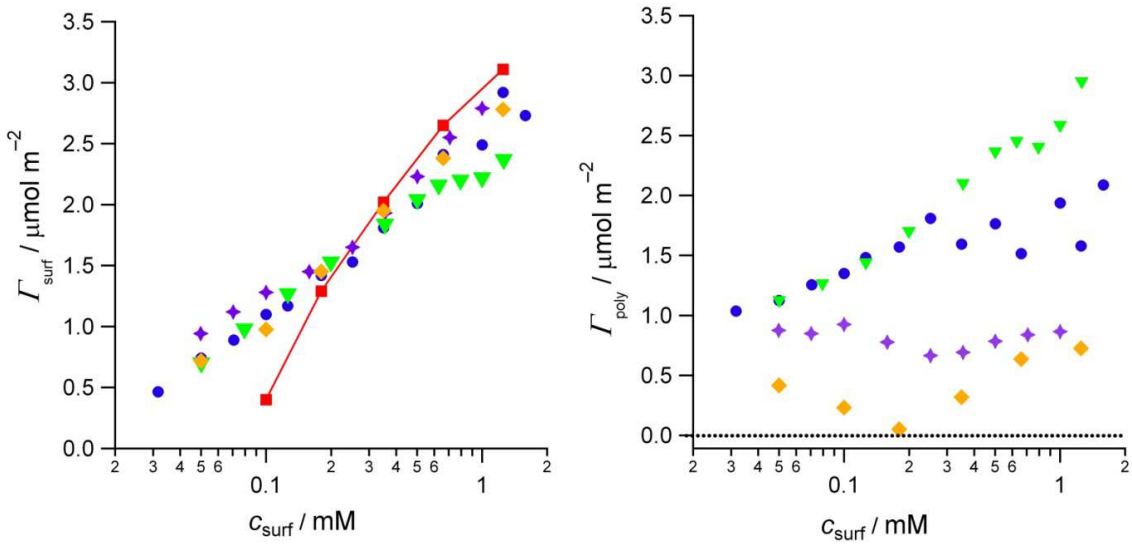

Figure 6.4. Surface excesses of (a) C_{12}TAB and (b) PSS adsorbing from mixtures of the two components, as calculated using our co-modelling methodology. The different data sets are different polymer concentrations (constant molecular weight of 17k), with symbols consistent with the other figures in this chapter, where the red squares are 0 ppm PSS, the yellow diamonds are 20 ppm, the purple crosses 50 ppm, the blue circles 100 ppm, and the green triangles 400 ppm. All measurements were made in the presence of 0.1 M NaBr. The red line is only added as a guide to the eye.

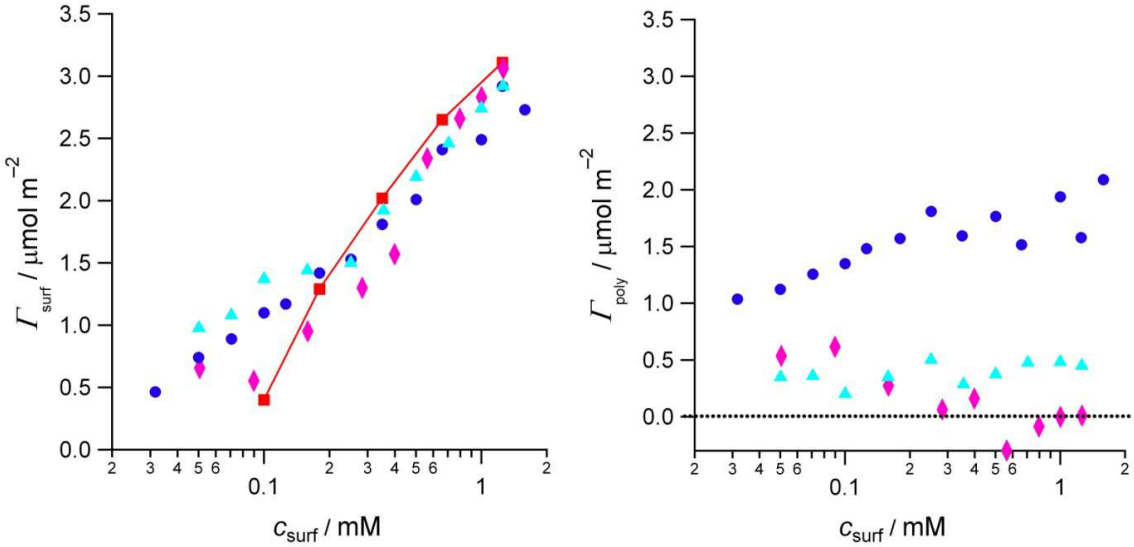

Figure 6.5. Surface excesses of (a) C_{12}TAB and (b) PSS adsorbing from mixtures of the two components, as calculated using our co-modelling methodology. The different data sets are different polymer molecular weights (constant polymer concentration of 100 ppm) , where the red squares at 0 ppm PSS, the blue circles are 17k (as in Figure 5), the turquoise triangles are 150k, and the pink diamonds are 2.6M. All measurements were made in the presence of 0.1 M NaBr. The red line is only added as a guide to the eye.

Γ_{poly} varies significantly with both polymer concentration and polymer molecular weight, as seen in Figure 6.4 (b) and Figure 6.5 (b). Largely, Γ_{poly} increases with increasing bulk polymer concentration,

and decreases with polymer molecular weight. However Γ_{poly} is not simply related to either the polymer concentration or molecular weight, suggesting that other factors also influence interfacial adsorption.

There are several noteworthy features in the Γ_{poly} data in Figure 6.4 (b) and Figure 6.5 (b). Firstly, Γ_{poly} is very similar for the 100 and 400 ppm systems until $c_{surf} \approx 0.2$ mM, suggesting that Γ_{poly} is independent of the polymer concentration in this range at low $c_{surf.}$ Furthermore, the maximum value of Γ_{poly} for the 400 ppm system is not 4 × that of the 100 ppm system, polymer adsorption is limited by something other than polymer concentration in this system. Secondly, Γ_{poly} is within experimental precision of zero for both the 20 ppm system in Figure 6.4 (b) and for the 2.6 M system in Figure 6.5 (b Thirdly, the Γ_{poly} data for the 150 k PSS/C_{12}TAB system in Figure 6.5 (b) do not fall within the predicted trend of decreasing Γ_{poly} with increasing molecular weight. This is unexpected, and may be due to experimental errors. I will discuss this point further later.

6.2.4. LDV

The surface expansion rates, θ, obtained from LDV measurements allow us to analyse the adsorption kinetics of the PSS/C_{12}TAB systems in a quantitative way. As discussed in Chapter 2, plots of θ v c_{surf} for pure surfactants have a volcano [20] shape, as seen for pure C_{12}TAB (red squares) in Figure 6.6. For polymer/surfactant mixtures however the data may deviate from this shape if the adsorption mechanism changes, as seen for PEO/C_{14}TAB in Chapter 5. Furthermore, the co-adsorption of polymer and surfactant at the interface at low surfactant concentrations can cause θ to remain close to the pure water value, as observed in the study of the adsorption of PDMDAAC/SDS on the OFC.[3] In order for θ to be at the pure water value despite the non-zero value of Γ_{surf}, material must adsorb in a way which does not support surface tension gradients at the interface, perhaps due to interactions between polymer and surfactant molecules at the interface or to the direct adsorption of polymer/surfactant complexes at the interface. Both the data in Chapter 5 and the previous study of PDMDAAC/SDS have shown us that surface expansion rate data can give us valuable clues about adsorption behaviour. To see if this is also the case for PSS/C_{12}TAB mixtures, data recorded at different polymer concentrations and polymer molecular weights are shown in Figure 6.6 (a) and (b) respectively.

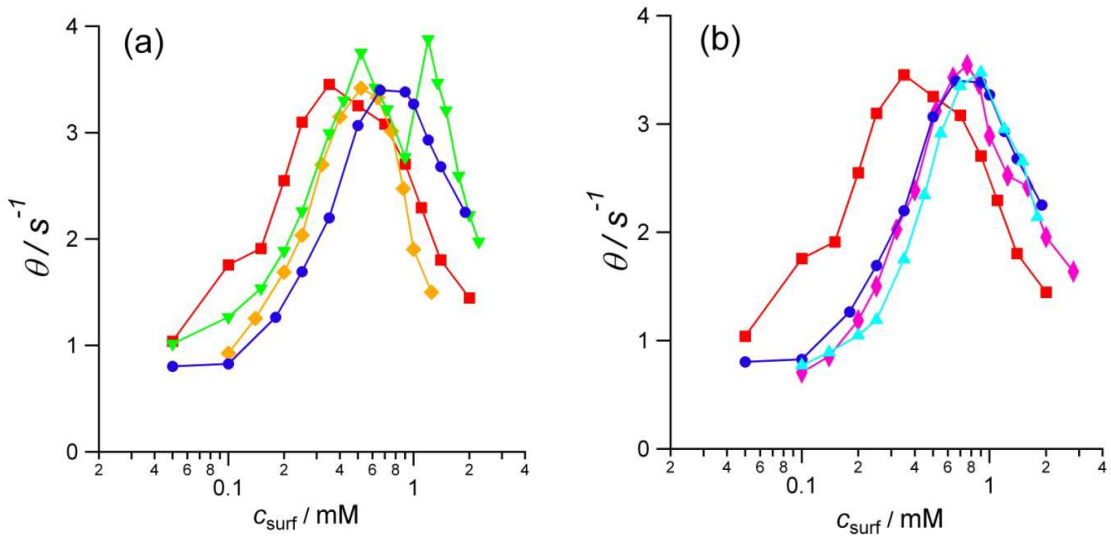

Figure 6.6. Surface expansion rate as a function of C_{12}TAB concentration for samples with (a) a varying polymer concentration, with the symbols corresponding to those in Figure 6.4, and (b) a varying polymer molecular weight, with the symbols corresponding to those in Figure 6.5.

The surface expansion rate data for all of the PSS/C_{12}TAB data in Figure 6.6 (apart from that for the system containing 400 ppm PSS) are of the standard volcano shape.. If we disregard the 400 ppm data for the moment, we can see that there is a shift in the volcano plot to higher c_{surf} compared to the pure surfactant. The shift is greater for the 100 ppm than the 20 ppm system (Figure 6.6 (a)), but almost independent of the polymer molecular weight (Figure 6.6 (b)). This latter observation is remarkable if we consider that we would expect such differently sized species to exhibit quite different adsorption behaviour.

The shift in θ to higher c_{surf} is most marked at low c_{surf} values. For a pure surfactant system, a decrease in θ at a given c_{surf} may be indicative of an increased surfactant surface excess. For all of the PSS/C_{12}TAB systems we can see from Figure 6.4 and Figure 6.5 that $\Gamma_{surf,mix} > \Gamma_{surf}$, hence the decreased value of θ must be due to interactions between the polymer and surfactant at the interface or the adsorption of polymer/surfactant complexes, as discussed above. The shift in θ to higher c_{surf} values is not as marked as it was in the previous study of PDMDAAC/SDS.[3].

The 400 ppm system exhibits quite different θ v c_{surf} data than the other systems, with a local minimum in θ at intermediate c_{surf} values. A minimum in θ was previously observed in the PEO/C_{14}TAB system, and attributed to Marangoni effects caused by polymer adsorption at low c_{surf} and surfactant adsorption at high c_{surf}. However Figure 6.4 shows that there is no significant decrease in the surface excess of either component in this region, although there is a very slight plateau in Γ_{poly}, so the same explanation cannot account for the minimum in θ for this system. If we examine the $\bar{\rho}$ data in Figure 6.1 we can see

that the plateau in $\bar{\rho}$ and the local minimum in θ occur at very similar surfactant concentrations. It therefore seems likely that both features have the same explanation, a switch over in the species dominating adsorption.

6.2.5. Static Data

In order to make comparisons between adsorption at the static and dynamic interfaces, and ultimately to enable us to use adsorption isotherms in our calculations of the adsorption kinetics of these systems, data for several PSS/C_{12}TAB systems (20 ppm, 100 ppm and 400 ppm 17k PSS) were also recorded at the static air/water interface using FIGARO's adsorption troughs and a petri dish for ellipsometry measurements. Data were recorded only at c_{surf} < 1.25 mM in order to minimize the production of kinetically-trapped aggregates which occurs when mixing the components for solutions of higher $c_{surf,}$ as discussed in the following section. The ellipsometry and NR data are shown in Figure 6.7. Both $\bar{\rho}$ and $\sigma \times \tau$ are relatively constant with increasing c_{surf}, although $\sigma \times \tau$ increases slightly for the 400 ppm system and decreases slightly for the 20 ppm system.

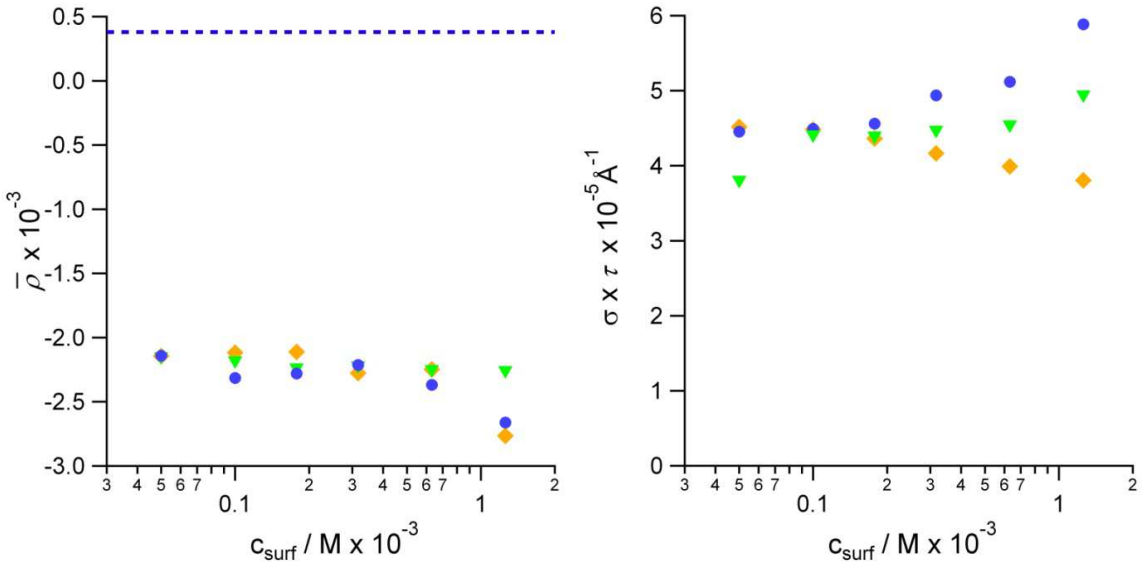

Figure 6.7. (a) Ellipticity and (b) product of the fitted scattering length and thickness of adsorbed layers from several PSS/C_{12}TAB systems at the static air/water interface: 20 ppm (yellow diamonds), 100 ppm (blue circles), 400 ppm (green triangles). All measurements were made with 17k PSS in the presence of 0.1 M NaBr.

The results of co-modelling the data in Figure 6.7 are shown in Figure 6.8. As expected from the ellipsometry and NR data, the interfacial excess of neither polymer nor surfactant varies in a clear way

with the bulk concentration of either polymer or surfactant. Furthermore, the maximum Γ_{surf} and Γ_{poly} values in Figure 6.8 are close to the maximum values measured on the OFC in Figure 6.4.

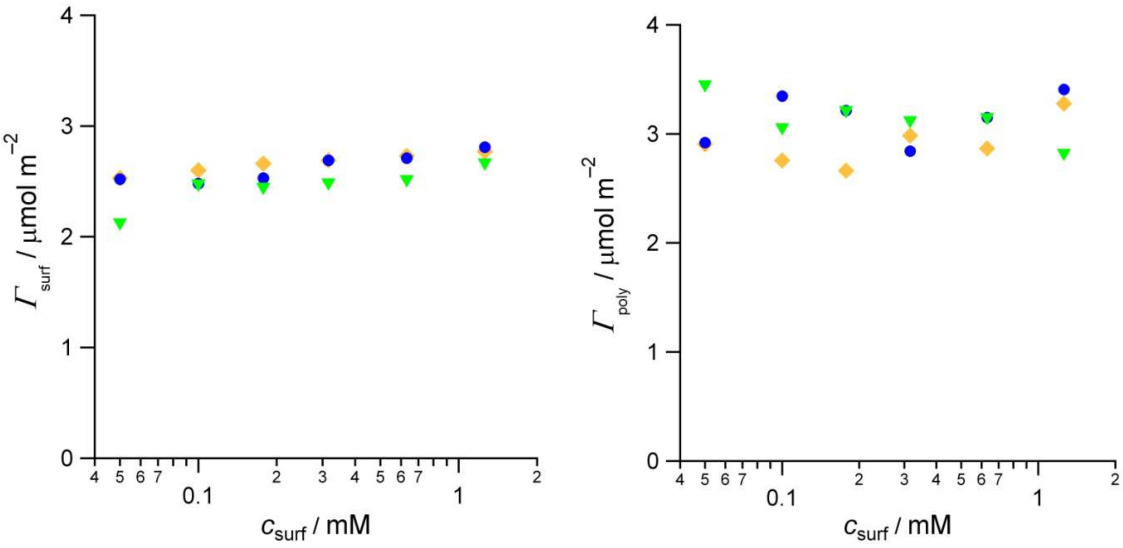

Figure 6.8. Surface excesses of (a) C_{12}TAB and (b) PSS adsorbing from mixtures of the two components at the static air/water interface, as calculated using our co-modelling methodology and the data in Figure 6.7. The symbols correspond to those in Figure 6.7.

6.2.6. Time-dependence at high c_{surf}

Figure 6.1 shows that around c_{surf} = 2 mM $\bar{\rho}$ time-dependent is for both the 100 and 400 ppm systems. For the 100 ppm system $\bar{\rho}$ becomes less negative from -2×10^{-3} to -1.4×10^{-3} (indicative of a decreasing total surface excess) over a period of 2 hours. NR data were recorded as a function of time at the same bulk solution composition, and the resultant $\sigma \times \tau$ values are shown in Figure 6.9 (a).

Co-modelling these data (Figure 6.9 b) shows that Γ_{poly} decreases significantly with time whilst Γ_{surf} stays relatively constant. For the dynamic surface excess of any species to decrease at constant bulk composition, the simplest explanation is that its mass transport becomes slower. In polymer/surfactant systems, such a situation is consistent with the formation of bulk aggregates which diffuse slowly on the timescale of the OFC due to their size. Hence it seems likely that the time dependence in Figure 6.9 can be attributed to the progressive formation of bulk polymer/surfactant aggregates.

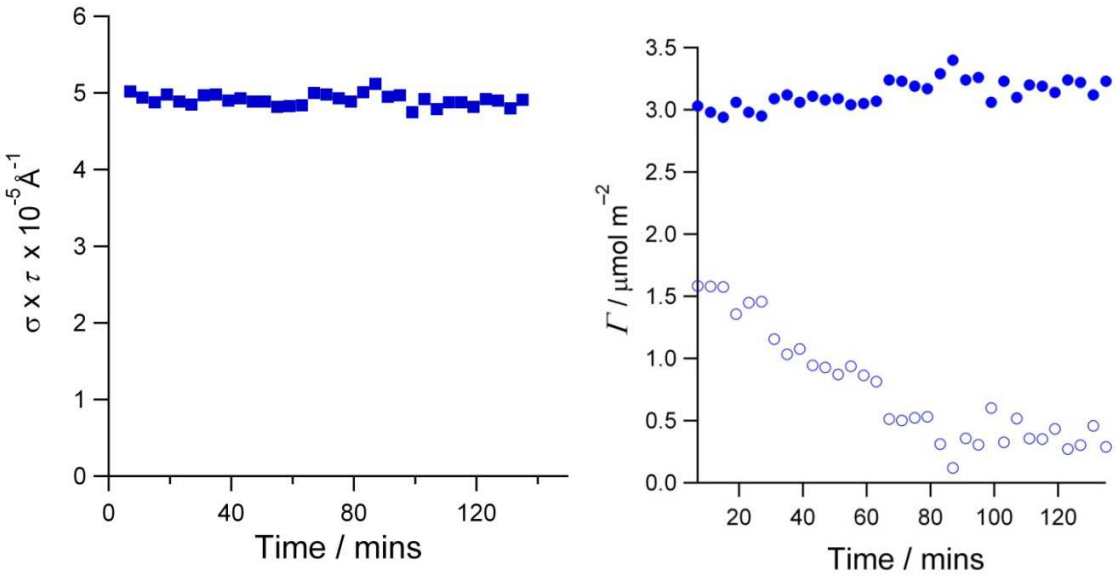

Figure 6.9. (a) The product of the fitted scattering length density and thickness, $\sigma \times \tau$, as determined by NR measurements on 100 ppm 17k PSS and 2 mM C_{12}TAB (in the presence of 0.1 M NaBr). (b) The calculated surface excesses of C_{12}TAB (filled blue circles) and PSS (empty blue circles) adsorbing at the interface of the OFC from the same solution, as obtained using our co-modelling approach.

6.3 Discussion

6.3.1. Bulk Characteristics

It is clear from the ellipsometry, NR, and LDV data presented above, as well as the calculated interfacial compositions, that the adsorption kinetics of PSS/C_{12}TAB are complicated, with changes in the behaviour occurring with increasing c_{surf}. Before attempting to interpret these interfacial data it is first pertinent to discuss the bulk species present in PSS/C_{12}TAB mixtures, as their formation will have an influence on adsorption at the air/water interface.

At a critical aggregation concentration (cac) significantly below the cmc for the pure surfactant (≈ 4 mM in the presence of 0.1 M NaBr[2, 8]) polymer/surfactant complexes form in the bulk solution. Few studies have reported values of the cac for PSS/C_{12}TAB in the presence of NaBr. Taylor et al. stated a value of 0.037 mM for 140 ppm 17k PSS/C_{12}TAB,[2] however this value was determined from surface tension measurements, which are highly challenging for strongly interacting polymer/surfactant mixtures, leading to great uncertainty in the value. Kogej et al. stated a lower value of 0.015 mM from fluorescence spectroscopy measurements on 70k PSS/C_{12}TAB.[8] Although the polymer used in the latter study is longer than the shortest polymer used in the experiments in this thesis, which may lower the cac due to increased conformation flexibility, the cac value of Kogej et al is used in the discussions and calculations which follow as it was determined from bulk rather than surface measurements. It is important to bear in mind however that we can only approximate the cac to be in the region of 0.015 mM C_{12}TAB. For the purposes of these discussions we will assume the conventional model in which the surfactant and polymer are unassociated in dilute solutions below the cac, while the polymer stabilises micelles of the surfactant above the cac.

In dilute solutions of the pure surfactant C_{12}TAB forms approximately spherical micelles with a reported aggregation number, N = 49, for 40 mM C_{12}TAB in 20 mM NaBr.[21] The higher salt concentration and lower surfactant concentration in our experiments will tend to increase and decrease the aggregation number, respectively, so in the absence of a direct measurement we will assume N = 49 in our experiments also.

Polymer/surfactant complexes in mixtures of 17k PSS and C_{12}TAB are likely to consist of a single polymer molecule bound to a single surfactant micelle, as 17k PSS is a short polymer with around 80 styrene sulfonate monomers. PSS is also a relatively stiff polymer, due to steric interactions and electrostatic repulsions between the side chains. The characteristic ratio of PSS will depend on the electrolyte concentration, but even for pure polystyrene the characteristic ratio is 10 suggesting that

PSS consists only of 8 or so equivalent segments. The polymer therefore lacks the conformational flexibility to bind effectively to more than one micelle per polymer chain, in addition to having insufficient charge on a single chain to balance the charge on two micelles. Literature values of the aggregation number of C_{12}TAB in a complex with PSS vary between 40 and 63.[9, 22] As these values were not recorded under the conditions used in the experiments in this thesis we will assume in the absence of direct measurements that the aggregation number is the same as that of the pure surfactant, 49. When higher MW PSS is used more than one micelle can condense on each chain, and the chain may be flexible enough to wrap around them. There will be a statistical distribution in the number of micelles bound to each polymer.

Since our best estimate of the cac of PSS/C_{12}TAB is nearly two orders of magnitude lower than the cmc, the stabilisation afforded by the polymer is substantial ($Nk_BTln(cac/cmc) \sim -200\ k_BT$). The primary source of this stabilisation is the entropy of the bromide counterions released when polymer associates with the micelle. For example, assuming that, say, 80% of the counterions are bound to a free micelle and that the local concentration of bound counterions is ~5 M, the entropic stabilisation from replacing the bound Br^- counterions by the polymer chain is $\sim -170\ k_BT$. For PSS/C_{12}TAB complexes there is also likely to be a hydrophobic component to the stabilization of the complexes due to the penetration of aromatic groups of the polymer into the surface of the surfactant micelle.[9] A study of monolayers of $C_{16}TA^+$ p-tosylate$^-$ at the air/water interface showed that 80% of the counterions were associated with the monolayer,[23, 24] hence it is likely that a large proportion of the aromatic groups in the polymer insert into the micelle surface.

As the surfactant concentration is increased above the cac the concentration of polymer/surfactant complexes increases, whilst the free surfactant concentration (and hence the chemical potential of the surfactant) remains approximately constant, and the concentration of free polymer (and hence the chemical potential of the polymer) decreases. Theoretically, once there is one surfactant micelle associated with every polymer molecule, complexation can be regarded as 'complete'. For ease, I will call this point c_{comp}. For each system, the surfactant concentration calculated to correspond to c_{comp} is indicated by an arrow in Figure 1. It should be noted that these values are only calculated from the bulk surfactant concentration necessary for each polymer molecule to be associated with 49 surfactant molecules, they are not obtained from bulk measurements. This estimation of c_{comp} may incur significant errors in our model, however we are using it as a starting point in the absence of the appropriate bulk measurements. In this model we expect that above c_{comp} increases in c_{surf} have no effect on the polymer/surfactant complexes, and their concentration remains constant, only the concentration of free surfactant increases. In this simple model, we assume that the size of the micelles in the polymer/surfactant complexes remains constant, though in reality an increase in the chemical

potential of the free surfactant will lead to an increase in the size of the bound micelles and a decrease in the chemical potential of the polymer (due to better charge neutralisation).

6.3.2 Accounting for Polymer/Surfactant Complexes in a Model of Adsorption Kinetics

In order to model quantitatively the effects of polymer/surfactant complexes on adsorption kinetics in the OFC, we need to account for their mass transport and adsorption. The presence of complexes affects the adsorption kinetics in two primary ways; firstly, the rate of mass transport of complexes may be slower than that of molecular species if their size is greater, and, secondly, complexes must break down on the timescale of surface expansion in order to deliver material to the interface. Valkovska et al. developed a model of adsorption from micellar surfactant systems which handled the diffusion of monomers and micelles separately under the assumption of fast micellar breakdown.[20] As a first approach, I will use an adaptation of that model to account for the diffusion of polymer and surfactant molecules and complexes. As we have defined individual complexes of 17k PSS to contain only a single surfactant micelle and a single surfactant molecule, we can treat these systems very similarly to the way that Valkovska treated surfactant systems above the cmc. Although a more involved model will eventually be necessary, as this model cannot account for the adsorption behaviour above c_{comp}, such a model has not been developed to date, hence the simple model presented here is used as a first approximation.

Several assumptions are implicit in our adsorption model. As for micelles and monomers of short chain surfactants such as C_{12}TAB, we will assume that equilibration between polymer, surfactant, and polymer/surfactant complexes in solution is fast. This means that the chemical potential of the polymer and surfactant in the PS complexes will always be equal to the chemical potential of the free polymer and free surfactant at the same distance from the surface. We will also assume that complex breakdown is fast on the timescale of the OFC, and that therefore the presence of complexes does not cause a kinetic barrier to the adsorption of either species. Furthermore, we will assume that adsorption kinetics are fast, so that the material at the surface is in local equilibrium with the polymer, surfactant, and polymer/surfactant complexes in the sub-surface. The question of whether adsorption proceeds through free polymer and surfactant or through polymer/surfactant complexes is then immaterial, since the only factor that determines the surface composition is the chemical potentials of the polymer and surfactant in the subsurface (which may be lower or higher than those in the bulk). Further assumptions to simplify the model include treating the cac as a sharply defined point below which no complexes

exist in solution and above which the surfactant monomer concentration is constant, and treating the adsorbing material as neutral in order to avoid the complication of electric double layers.

Below the cac, there are no complexes in solution and only molecular species will affect adsorption. Free polymer and free surfactant diffuse to the surface with transport rates that obey the convective-diffusion equation, and the resultant surface excess is given by equation 2.5, reproduced here as Equation 6.1

$$\Gamma = \sqrt{\frac{2D}{\pi\theta}}\,(c_b - c_s) \tag{6.1}$$

where D is the diffusion coefficient, c_b the bulk concentration and c_s the subsurface concentration. For the free surfactant, $D_{mon} = 4.6 \times 10^{-10}$ m^2s^{-1}.[20] Wang measured $D_{poly} = 6.5 \times 10^{-11}$ m^2s^{-1} for 24k PSS and also showed that the radius of gyration of the polymer follows the Flory-Huggins scaling law for a good solvent, $R_g \propto M^{0.6}$, where M is the molecular weight.[25] Consequently, for 17k PSS, we will use a value of $D_{poly} = 8.0 \times 10^{-11}$ m^2s^{-1}.

Below the cac, the concentration profiles of both polymer and surfactant as a function of the distance from the surface into the bulk, z, are obtained from[20]

$$c = c_s + (c_b - c_s)ERF\left(z\sqrt{\frac{\theta}{2D}}\right) \tag{6.2}$$

where c_s is obtained from Equation 6.1. Figure 6.10 shows a schematic concentration profiles of polymer (blue line) and surfactant (red line) at $c_{surf} < c_{cac}$.

Above the cac, the diffusion of polymer/surfactant complexes also has to be accounted for in our model. The formation of complexes decreases the concentration of free polymer molecules in the solution, and the concentration of free surfactant molecules will stay constant at $c_{surf,free}$ = cac. The amount of surfactant in complexes is given by $c_{surf,complex} = c_{b,surf} - c_{cac}$, and the amount of polymer in complexes is given by $c_{poly,complex} = 82/49 \times c_{surf,complex}$.

Although the bulk surfactant concentration is above the cac, mass transport considerations mean that the sub-surface concentration is below the cac. This means that although PS complexes in the bulk solution affect the transport of material to the interface, the subsurface contains only free polymer and surfactant. The region below the surface is a 'complex-free zone', similar to the micelle-free zone of Valkovska et al.[20] The complex-free zone ends at a distance h from the surface at which the surfactant concentration reaches the cac (Figure 6.12). At $z < h$ surfactant transport is only in the form of

molecular species, at $z > h$ surfactant transport is only in the form of polymer/surfactant complexes (green line in Figure. 6.12).

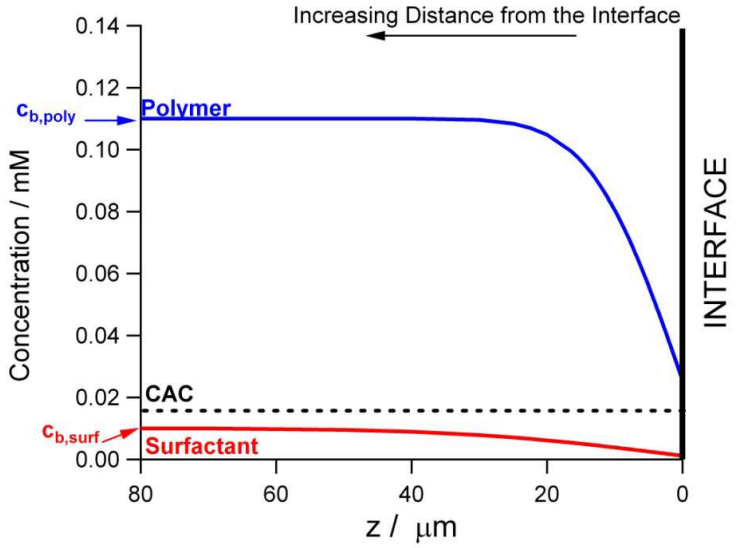

Figure 6.10. Schematic diagram of the concentration profiles of the molecular species in the diffusion layer of an expanding surface at $c_{surf} < c_{cac}$. The horizontal dashed line denotes the cac of the system.

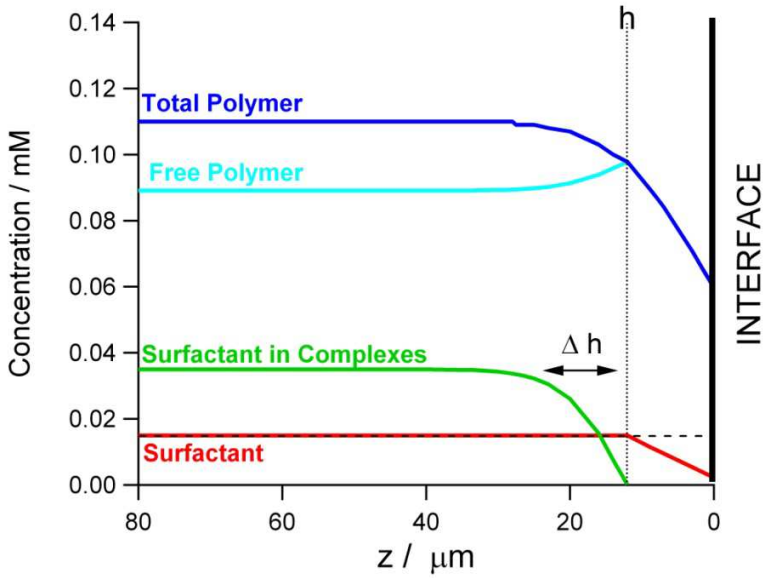

Figure 6.11. Schematic diagram of the concentration profiles of the species at $c_{surf} < c_{cac}$, with the distance h which denotes the edge of the complex-free zone marked as a vertical dotted line, and the cac marked by a horizontal dashed line. Δ h marks the region in which polymer/surfactant complexes are breaking down into free polymer and monomeric surfactant.

We do not know the value of the diffusion coefficient of the complexes, D_{PS}, a priori. On the one hand, binding of the polymer to the micelle is likely to lead to a more compact conformation of the polymer

and hence a larger diffusion coefficient; on other hand, D_{PS} must be less than that of a C_{12}TAB micelle (~1.0×10^{-10} m^2s^{-1} from the Stokes-Einstein formula). Hence we will assume that for 17k PSS, $D_{PS} = D_{poly} = 8 \times 10^{-11}$, although this assumption will be tested later. For $z < h$, the polymer diffuses with the free polymer diffusion coefficient, $D_{poly.}$ For $z > h$, the polymer diffusion coefficient is in general a weighted mean of the diffusion coefficients of the free polymer and the polymer/surfactant complex, D_{PS}. Since we are assuming $D_{PS} = D_{poly}$ for 17k PSS, the polymer mass transport obeys Equation 6.1.

If we assume infinitely fast complex breakdown, the diffusion equations for surfactant monomers and complexes in the centre of the OFC take the form

$$D_{surf}\frac{d^2c_{surf,free}}{dz^2} + z\theta\frac{dc_{surf,free}}{dz} = 0 \qquad (6.3.a)$$

$$D_{PS}\frac{d^2c_{surf,complex}}{dz^2} + z\theta\frac{dc_{surf,complex}}{dz} = 0 \qquad (6.3.b)$$

From the work of Valkvoska, the value of h for a given system composition can be calculated from the experimental data for the surface expansion rate, θ, and the surface composition using

$$\frac{c_{b,surf}-c_{cac}}{c_{cac}-c_{s,surf}} = \sqrt{\frac{D_{surf}}{D_{PS}}}\cdot\frac{exp\left(\frac{-\theta h^2}{2D_{surf}}\right)}{erf\left(h\sqrt{\frac{\theta}{2D_{surf}}}\right)}\cdot\frac{erfc\left(h\sqrt{\frac{\theta}{2D_{PS}}}\right)}{exp\left(\frac{-\theta h^2}{2D_{PS}}\right)} \qquad (6.4)$$

And the flux of monomers to the interface at z =0 (to obtain $c_{s,mon}$) is:

$$\theta\Gamma = D_{surf}\frac{dc}{dz_0} = (c_{cac}-c_s)\sqrt{\frac{2\theta D_{surf}}{\pi}}\left[erf\left(h\sqrt{\frac{\theta}{2D_{surf}}}\right)\right]^{-1} \qquad (6.5)$$

The concentration profile of surfactant monomers at $z < h$ as a function of z (red line) is then obtained by solving the diffusion equation, Equation 3.a, using the following boundary conditions: at z =0 $c_{surf} = c_{s,surf}$, and at $z = h$, $c_{surf,free} = c_{cac}$, resulting in

$$c - c_{s,surf} = \left(c_{cac}-c_{s,surf}\right)\frac{erf\left(z\sqrt{\frac{\theta}{2D_{mon}}}\right)}{erf\left(h\sqrt{\frac{\theta}{2D_{mon}}}\right)} \qquad (6.6)$$

The concentration profile of surfactant in complexes (green line) is obtained from the solution of equation 6.3.b with the boundary conditions: at $z = h$ $c_{surf,complex} = 0$ and at $z = \infty$, $c_{surf,complex} = c_{surf,complex,\infty} = c_{surf}$. This gives the equation

$$c_{surf,complex} = c_{surf,complex,\infty}\left[1-\frac{erfc\left(z\sqrt{\frac{\theta}{2D_{PS}}}\right)}{erfc\left(h_1\sqrt{\frac{\theta}{2D_{PS}}}\right)}\right] \qquad (6.7)$$

The total polymer concentration is still obtained from Equation 6.2, and the concentration of free polymer molecules due to complexation (purple line) $c_{poly,free} = c_{poly} - 49/82 \times c_{surf,complex}$.

There will only be a complex-free zone below the interface until a threshold bulk surfactant concentration. For a pure surfactant, $h = 0$ once c_{surf} is a certain amount above the cmc. [26] For complexes, there is not a direct relationship between the cac and the point where $h = 0$, and the appropriate c_{surf} can be calculated from Equation 6.5. Above this point, the sub-surface surfactant concentration, $c_s >$ cac.

For polymer/surfactant mixtures this approach will describe the mass transport of the bulk species until $c_{surf} = c_{comp}$, as at that point the formation of complexes will be complete, and the concentration of free surfactant molecules in bulk solution will increase whilst the concentration of complexes stays constant. There will now be two distances in the mass transport model: h_1 defining the edge of the complex-free zone, h_2, beyond which surfactant monomers again contribute to mass transport, and all the polymer is in the form of complexes. However, a model which can account for this behaviour is yet to be fully developed, hence we only model mass transport for $c_{surf} < c_{comp.}$.

Now that I have discussed a basic theoretical model of the mass transport in complexing polymer/surfactant systems, I will move on to discuss the data obtained for the PSS/C_{12}TAB systems (in the results section above) in the context of this model.

6.3.3. PSS/C_{12}TAB Systems Containing Different Concentrations of Polymer

At very low surfactant concentrations (c_{surf} < 20 μM) the ellipsometric data are independent of both the concentration of the 17k PSS (Figure 6.1) and the molecular weight of the polymer chain (Figure 6.2). This observation implies that the total adsorbed amount is independent of the mass transport or adsorption kinetics of the polymer, as we would expect when the polymer is in excess. We would therefore expect that adsorption is limited by surfactant diffusion at low c_{surf}. From data at the static air/water interface (Figure 6.8) the polymer and surfactant are strongly adsorbed at the interface, and the equilibrium value of the bulk concentration, c_b, at the values of Γ measured on the OFC will be very small, hence from the condition for diffusion control, $\Gamma_{dyn}(c_s) = \Gamma_{eq}(c_b)$, c_s will be very small in our measurements, much smaller than c_b. We would therefore expect that $c_{s,surf} = 0$ if surfactant adsorption is diffusion controlled, and we can test whether our data are consistent with this hypothesis. Unfortunately, we do not have surface composition or expansion rate data at c_{surf} < cac for any of the systems studied, and we can only estimate the values by extrapolation. For the 100 ppm system, at 0.01 mM, $\bar{\rho} \approx 5 \times 10^{-5}$, $\theta \approx 0.7$ s^{-1} and $\Gamma_{surf} \approx 0.2$ μmolm^{-2} (by extrapolation). If we calculate the maximum value of Γ_{surf} under diffusion control using Equation 6.1 with $c_s = 0$, we obtain a value of $\Gamma_{surf,max} = 0.2$ μmolm^{-2}. It therefore appears that surfactant adsorption is under diffusion control. By extrapolation of the data in Figure 6.4 (b) $\Gamma_{poly} \approx 0.8$ μmolm^{-2}. Using equation 6.1 to determine the maximum possible value under diffusion control yields $\Gamma_{poly,max} = 4.7$ μmolm^{-2}. Therefore we conclude that polymer adsorption is not diffusion controlled in this region, which is what we would expect when polymer is in excess in solution and its adsorption depends on interactions with adsorbed surfactant.

As c_{surf} is increased further we would expect adsorption to become polymer mass transport limited. If this is the case and the polymer adsorbs under diffusion control, the subsurface polymer concentration, $c_{s,poly}$, would drop to a value close to zero. We can calculate $c_{s,poly}$ from Equation 6.1. and the experimental data in Figure 6.4 and Figure 6.6. As we are assuming $D_{PS} = D_{poly}$, polymer diffusion is not affected by complex formation. As a reminder however, the estimated values of c_{comp} for the three systems are 0.08 mM, 0.3 mM and 1.3 mM respectively. The calculated values of $c_{s,poly}$ for all three systems are shown in Figure 6.12. Note that at all of the surfactant concentrations in Figure 6.12 polymer/surfactant complexes form as the surfactant concentration is always above the cac.

From Figure 6.12 we can see that $c_{s,poly} > 0$ for all three systems, polymer adsorption is not diffusion controlled over a wide range of c_{surf} values. Although $c_{s,poly}$ does tend to zero for the 20 and 100 ppm systems at high c_{surf} (for the 20 ppm system $c_{s,poly} \approx 0$ from $c_{surf} = 0.4$ mM), implying polymer adsorption is diffusion controlled at high c_{surf}, it remains non zero until well above c_{comp} for both

systems (0.08 mM and 0.3 mM for the 20 and 100 ppm systems respectively). Polymer can get to the sub-surface by diffusion of individual molecules or polymer/surfactant complexes, but this does not result in a large amount of polymer at the interface (see Figure 6.4). This implies the presence of a barrier to the adsorption of polymer in all three systems. We would expect there to be a barrier to polymer adsorption (and therefore a high value of $c_{s,poly}$) at very low c_{surf}, as although polymer molecules can reach the sub-surface by diffusion, polymer only adsorbs at the interface due to interactions with adsorbed surfactant, and Γ_{surf} is low. However, as c_{surf} and hence Γ_{surf} is increased we would expect Γ_{poly} to increase accordingly (and $c_{s,poly}$ to decrease), which does not happen. The continuing high values of $c_{s,poly}$ could be attributable to steric barriers to the adsorption of polymer. However, it is unlikely that steric barriers have a significant effect in this region due to the low polymer coverage. It is only for the 400 ppm system that steric barriers have an effect on the polymer adsorption, for this system the maximum value of Γ_{poly} reached on the OFC (Figure 6.4 (b)) is close to the value at the static air/water interface (Figure 6.6 (b)). Alternatively, slow complex breakdown may limit adsorption of polymer. However, we would expect slow complex breakdown to limit Γ_{surf} as well, which is not seen in the data. It is therefore not clear what controls polymer adsorption in these systems.

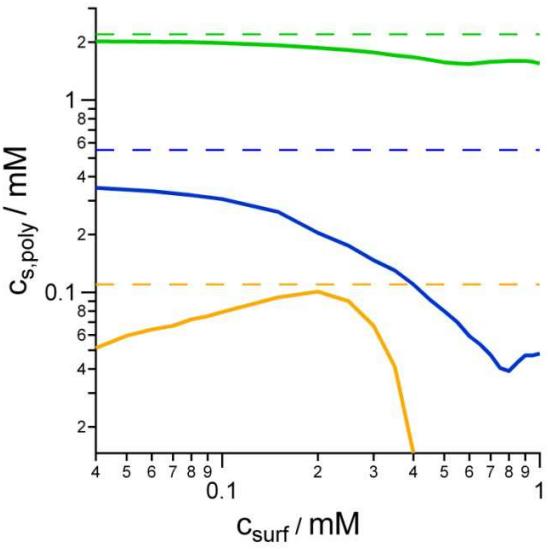

Figure 6.12. Calculated values of the subsurface concentration of polymer ($c_{s,poly}$) as a function of bulk surfactant concentration. The yellow line is $c_{s,poly}$ for the 20 ppm system, the blue line for the 100 ppm system, and the green line for the 400 ppm system. The dashed lines denote the bulk polymer concentration for each system.

At high bulk surfactant concentrations, where there is no longer a complex free zone and complexes can be in the sub-surface layer, polymer adsorption approaches diffusion control for the 20 and 100 ppm systems. As polymer is primarily in complexes in this region (the estimated values of c_{comp} for the

20 ppm and 100 ppm systems are 0.08 mM and 0.3 mM) perhaps it is not that the complex dissociation rate limits polymer adsorption. Polymer adsorption appears to be diffusion controlled in this region yet does not reach the surface excesses observed at the static interface, as we might expect. We expect that future development of the adsorption model will help to explain these data.

There is a minimum rate at which complexes would have to dissociate for the assumptions of our diffusion model with complex-free zone (Figure 6.11) to hold. This rate can be estimated from the maximum flux of surfactant in complexes at $z > h$, (green line in Figure 6.11), as calculated from Equation 6.6. Δh is the region below the complex-free zone below where complexes are breaking down. By analogy with the way one calculates the thickness of diffusion layers in electrochemistry, we define the thickness of the region, Δh, by the ratio of the concentration of surfactant in complexes, $c_{surf,comp}$, to the diffusive flux of surfactant in complexes at $z = h$, that is the maximum gradient of the green line. The breakdown time is then obtained from $\Delta h/h\theta$, where $h\theta$ is the value of v_z at $z = h$. At low c_{surf} the breakdown must be fast, with breakdown times of around 0.7 s for the 20 and 100 ppm systems at $c_{surf} = 0.06$ mM, and 0.4 s for the 400 ppm system. At higher c_{surf}, the lifetime can be up to 2 s and the fast breakdown model will still hold.

Calculated values of the sub-surface concentration of surfactant are shown in Figure 6.13 scaled to the bulk surfactant concentration, which shows that $c_s \approx 0$ for all three systems over the majority of the concentration range, except at the lowest surfactant concentrations measured. As θ is lower for the mixtures than the pure surfactant there is more time for the surfactant to adsorb, and as Γ_{surf} for the mixtures is similar to the pure surfactant values it is unsurprising that the calculated subsurface concentrations of surfactant are low. Adsorption of surfactant at the interface is not limited by the formation of complexes despite the fact that the majority of surfactant in the solution is in the form of bulk complexes (cac is at lower c_{surf} than shown on the graph for all three systems). It is therefore unlikely that slow complex dissociation limits polymer adsorption, as if it did surfactant adsorption would also be limited. Hence there must be another barrier to the adsorption of the polymer. Alternatively, it is possible that complexes can shed sufficient surfactant monomers to maintain surfactant adsorption, but they cannot fully dissociate to allow polymer to adsorb.

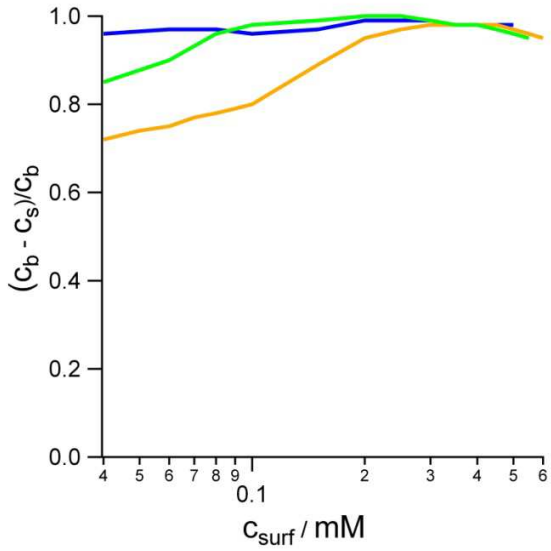

Figure 6.13. Calculated values of the sub-surface concentration of surfactant, c_s, from Equation 6.6, scaled to the bulk surfactant concentration. The colours of the lines correspond to those in Figure 6.12.

If we now return to our examination of the ellipsometry data in Figure 6.1, we can see that with increasing c_{surf} the ellipsometry data for all four polymer concentrations follow almost the same curve until, successively, they show a kink in the ellipticity and peel off from the main curve. We suspected that this kink in the ellipsometry data might be due to the switch over from adsorption limited by surfactant mass transport to that limited by polymer mass transport, however it is clear from Figure 6.12 and Figure 6.13 that this is not the case and that there must be another explanation of these turning points. In order to determine the origin of these and other features in the ellipsometry data in Figure 6.1 I will now examine each of the systems containing different polymer concentrations in turn, starting with the 20 ppm system.

For the 20 ppm system, the first kink in $\bar{\rho}$ is in the region of the cac of the system, 0.015 mM. It therefore seems possible that the gradient of $\bar{\rho}$ changes because the mass transport regime has changed and surfactant adsorption is slowed down by the formation of PS complexes. Above the cac, there is a plateau in $\bar{\rho}$. One might think that a plateau in the ellipticity would correspond to a constant surface composition. In the previous study of PDMDAAC/SDS, plateaus in the ellipticity were ascribed to the diffusion-controlled adsorption of polymer/surfactant complexes,[3] which gave rise to a constant interfacial composition. However, if there is a complex-free zone for the PSS/C_{12}TAB mixtures ($h_1 > 0$ until $c_{surf} > 0.5$ mM), then there are no complexes at the interface to adsorb. Furthermore, in principle the presence of a complex-free zone would mean that complexes have no effect on θ, unlike in the PDMDAAC/SDS study, where the presence of complexes at the interface caused a significant decrease in θ relative to the pure surfactant value.

Figure 6.4 shows that the surface composition is not constant in the plateau for 20 ppm PSS; in the region up to the end of the plateau ($c_{surf} \approx 0.1$ mM) Γ_{surf} increases and Γ_{poly} decreases (although Γ_{poly} is close to the limit of resolution of our approach in this region) with increasing bulk surfactant concentration. At first this result appears paradoxical as we would expect an increase in Γ_{surf} to enhance the interfacial binding of an oppositely charged polymer, not diminish it. However, if we consider that at cac (0.015 mM) < c_{surf} < c_{comp} (0.081 mM) the concentration of polymer/surfactant complexes is increasing and therefore the concentration of free polymer is decreasing, the behaviour can be explained by free polymer molecules controlling polymer adsorption in this region. If polymer molecules can adsorb quickly to the interface from the sub-surface they will control adsorption until their concentration is limited due to slow breakdown of polymer/surfactant complexes. This hypothesis is supported by the fact that as the concentration of free polymer decreases, so does Γ_{poly}. Γ_{surf} continues to go up in this region, which must be because some of the polymer/surfactant complexes can supply surfactant (but not polymer) to the interface either by completely breaking down or by the release of a small number of surfactant molecules.

In our proposed model, the formation of bulk complexes is complete in the 20 ppm system at $c_{comp} \approx$ 0.08 mM, as marked by the leftmost arrow in Figure 6.1. As c_{surf} is increased beyond c_{comp}, the concentration of free surfactant molecules in solution increases. In the same region, a gentle change in the gradient of $\bar{\rho}$ occurs, with values becoming more negative. It is unclear why an increase in the free surfactant concentration in the bulk solution should mark the end of the plateau if there is still a complex-free zone near the interface, however it is clear that the two do coincide. One possibility is that the calculated value of c_{comp} is far from the actual value at which bulk complexation is complete, as we have not used bulk measurements to determine c_{comp}. Future measurements of the bulk properties of this system or refinements to the adsorption model may be able to explain this inconsistency.

As c_{surf} is increased further the ellipsometry data track the pure surfactant as the free surfactant concentration increases. The slight difference in $\bar{\rho}$ values between the data for the 20 ppm system and the pure surfactant are due to the continued adsorption of PSS at the interface. The continued difference between the values at high c_{surf}, where a surfactant monolayer is adsorbed for the pure surfactant solution, suggests that PSS can continue to adsorb at the interface even at high surfactant coverages. This is not unexpected, as polymer is not surface active alone, and adsorbs by association with the surfactant at the interface. For the 20 ppm system, the complex-free zone vanishes at $c_{surf} = 0.5$ mM, however this has no apparent effect on adsorption at the interface. One possible inference is that the presence of a complex-free zone has no effect on adsorption, because diffusion of molecular species to the interface is not the rate-determining step in the adsorption process.

Now that I have discussed the adsorption of the 20 ppm system, I will turn to the mixtures containing higher polymer concentrations. Although the kink in the ellipsometry data at low bulk surfactant concentrations coincides with the point where c_{surf} = cac for the 20 ppm system, this cannot be the explanation for the systems containing higher polymer concentrations, for which the kink occurs at progressively higher c_{surf} values. For the 50 ppm system the kink occurs at c_{surf} = 0.1 mM, nearly an order of magnitude higher concentration than for the 20 ppm system, and well above the cac. For the 100 ppm system the kink occurs at c_{surf} = 0.2 mM, exactly double the 50 ppm value. For both the 50 and 100 ppm systems this kink is in the region cac < c_{surf} < c_{comp} (c_{comp} is calculated to be 0.16 and 0.3 mM for the 50 and 100 ppm systems, respectively). It is unclear why there would be a change in the adsorption behaviour in the middle of the region where the concentration of complexes increases and that of free polymer decreases. For both the 50 and 100 ppm systems Γ_{poly} stops increasing and reaches a constant value at the kink (Figure 6.4), suggesting that the kink can primarily be attributed to a change in the polymer adsorption, although it is not clear what causes this change.

As c_{surf} is increased past the first kink in $\bar{\rho}$, there is a plateau in the $\bar{\rho}$ data for the 50 ppm system but not the 100 ppm system. The end of the plateau for the 50 ppm system occurs at $c_{surf} \approx 0.2$ mM, which is only slightly above c_{comp} = 0.16 mM. Therefore the end of the plateau appears to correspond to the region in which we estimate that bulk complexation is complete, as it did for the 20 ppm system. In the 100 ppm system there is no clear plateau, but there is a region of lower gradient in $\bar{\rho}$ between c_{surf} = 0.2 and 0.33 mM, with the latter value again close to c_{comp} = 0.3 mM, after which the gradient of $\bar{\rho}$ v c_{surf} increases. Up until c_{comp} the concentration of slowly dissociating complexes is increasing and that of free polymer is decreasing, and the polymer adsorption rate falls. From this model we would expect Γ_{poly} to reach a constant value at c_{comp}, which it does for the 50 and 100 ppm systems (Figure 6.4), which may suggest that our estimated c_{comp} values are close to the true values. The change in the polymer adsorption may contribute to the kink in $\bar{\rho}$ in this region. If there were no complex free zone, the kink would be best explained by the increased adsorption of fast diffusing free surfactant molecules at $c_{surf} > c_{comp}$, however in our adsorption model the subsurface surfactant concentration cannot exceed the cac as $h_2 \neq 0$, and free surfactant cannot significantly affect adsorption at the interface. Nevertheless, in the region of c_{comp} the gradient of Γ_{surf} increases for both systems. It is clear that our adsorption model needs to be further developed in the future to explain the adsorption behaviour in this region.

The ellipsometry data for the 400 ppm system also exhibit a plateau in $\bar{\rho}$ at intermediate c_{surf}, however in this case it occurs between c_{surf} = 0.6 and 0.9 mM, well below c_{comp} for the system (1.2 mM). The

completion of complexation is therefore not related to the plateau for this system. Instead, the first kink in the ellipticity co-incides with the c_{surf} value at which h tends to zero, 0.6 mM, above which there is no longer a complex-free zone below the interface. Once there is no longer a complex-free zone, the sub-surface concentration of surfactant $c_{s,surf}$ > cac, and the chemical potential does not increase any further until all the polymer in the subsurface is in the form of complexes, hence a plateau occurs in $\overline{\rho}$, as well as in both Γ_{poly} and Γ_{surf}.

The disappearance of the complex-free zone affects the adsorption behaviour of the 400 ppm system, despite not having had an effect on the systems containing lower polymer concentrations, because c_{surf} < c_{comp} in this region, the concentration of complexes has not yet reached its maximum value. In all of the other systems, the complex-free zone disappears, and $h_2 = 0$, at c_{surf} = 0.6 mM, but this value is sufficiently above c_{comp} to ensure that the free surfactant concentration is high, and hence no significant effect on the adsorption behaviour is observed. Working on the theory that the first kink in the ellipticity at 0.6 mM is where the sub-surface concentration of surfactant reaches the cac, we can calculate a value of D_{PS} from equation 1 from Γ_{surf} = 2.15 and θ = 3.5 with c_s= cac, which gives 8 x 10^{-11} m^2s^{-1}, identical to the polymer diffusion coefficient we assumed earlier.

The unusual shape of the θ data for the 400 ppm system in Figure 6.6 can be attributed to the overlap in c_{surf} of the complex-free zone vanishing and the concentration of complexes continuing to increase. For all of the systems containing different polymer concentrations, a maximum in θ is reached in the same region, as the interface becomes saturated at high Γ_{surf}. This may or may not be related to the disappearance of the complex-free zone in this region. This maximum in θ is reached for the 400 ppm system as the complex-free zone vanishes, at the point corresponding to the beginning of the plateau in $\bar{\rho}$. The subsequent decrease in θ can be attributed to the same explanation as the plateau in $\bar{\rho}$, the chemical potential of the surfactant cannot increase any further in this region. θ increases again at a c_{surf} value corresponding to the end of the plateau in the ellipticity as the concentration of complexes increases, and the surface excesses of polymer and surfactant reach the maximum values as limited by the rates of complex dissociation and kinetic barriers to adsorption. Γ_{poly} is limited in this system, at close to the maximum value at the static interface in Figure 6.8. A second maximum in θ is reached at c_{surf} = c_{comp}, as now the sub-surface region is saturated with complexes. The double maximum in θ can be therefore rationalised, similarly to in Chapter 5, to overlapping volcano plots for two different species which dominate interfacial adsorption in different c_{surf} ranges.

For both the 100 and 400 ppm systems time dependent changes in the adsorption behaviour occur at high surfactant concentrations, c_{surf} = 2 mM, as indicated by the ellipsometry data in Figure 6.1. The 100 ppm system has been studied as a function of time in this region using both ellipsometry and NR.

Over a period of more than two hours, $\bar{\rho}$ becomes less negative, and Γ_{poly} decreases significantly whilst Γ_{surf} stays constant (Figure 6.4). If the total concentration of both components in the system remains constant, the surface excess of material at a steady state expanding air/water interface can only decrease if the material can diffuse to the sub-surface on the timescale of the OFC reduce in concentration. Such a situation is consistent with the formation of bulk aggregates that diffuse more slowly on the timescale of the OFC. This explanation is supported by the turbidity data in Figure 6.1, only the 100 and 400 ppm solutions become turbid, and only in the region of the time dependent change in the interfacial composition.

It is notable that aggregation occurs in these systems only at high c_{surf}, and at the same c_{surf} despite the fact that c_{comp} is estimated to be 0.3 mM and 1.3 mM for the 100 and 400 ppm systems respectively. As we have compositional data for the 100 ppm system we will discuss this first. Due to the low aggregation number of the micelle in a PSS/C_{12}TAB aggregate, the complexes are far from neutral at c_{comp} and will not therefore lose their colloidal stability and aggregate. As c_{surf} is increased above our estimated value of c_{comp} we would expect that increases in the free energy of the surfactant would increase the micelle size, neutralising the complex and causing aggregation. However, as aggregation does not occur until much higher surfactant concentrations this cannot be occurring to a sufficient extent to neutralise the aggregates. It is not clear from our model why aggregation does not occur until around 2 mM on the OFC and charge neutrality is not reached until 4.8 mM.[27] It is possible that the high charge of the complexes prevents them from aggregating until high surfactant concentrations. It is also possible that our model in which c_{comp} occurs at a defined point is incorrect, and that bulk complexation continues to occur with increasing bulk concentration and is only nearly completion in the region of c_{surf} = 2 mM. In order to determine whether this latter hypothesis is the case, complementary bulk phase measurements of species size and mobility would be necessary.

Despite bulk aggregation of polymer/surfactant complexes in the time dependent region, Γ_{surf} stays constant (Figure 6.4). We suggest that this is because the free surfactant concentration is high, either because c_{comp} is at a low significantly lower surfactant concentration, or because the bulk free surfactant concentration increased with the bulk complex concentration up until 2 mM. Whichever is the case it is clear that c_{surf} is sufficiently high to give rise to close to monolayer adsorption alone in the region of time dependence. Indeed the slight increase in the surface excess of surfactant with time is consistent with the loss of polymer which was electrostatically bound polymer to the surfactant headgroups, taking up space in the headgroup layer and slightly limiting the surface excess of surfactant due to steric hindrance, i.e., slightly higher surfactant coverage is possible when the amount of adsorbed polymer decreases, as is discussed in a recent study of PDADMAC/SDS layers at the static air/water interface.[28]

A reduction in the polymer surface excess at the static surface (Figure 6.9) as a consequence of the formation of aggregates in the bulk solution would be consistent with the effect of aggregation on adsorption from polymer/surfactant mixtures at the static water interface demonstrated by Campbell *et al*. for PDADMAC/SDS.[28, 29] However, we note that the study of Taylor et al recorded the presence of interfacial multilayers at the interface, rather than a depleted adsorbed amount, at similar bulk surfactant concentrations.[2] The most recent work of Campbell *et al*. [30] on the effect of gravity on the formation of multilayers, leads us to tentatively postulate an explanation for this apparently contradictory behaviour; the aggregates which form in a PSS/C_{12}TAB solution have a low density, enabling them to reach the static interface under gravity. Such an eventuality would resolve any inconsistency in the experimental data of Taylor et al and that presented in this chapter, although it must be emphasised that the mechanism of interfacial multilayer formation at the static air/water interface is related to a different mechanism to that at due to self assembly at the static interface. nvestigations of Campbell et al on the effect of aggregation on the adsorption behaviour of PSS/C_{12}TAB systems are ongoing, however initial results have shown that the formation of both thick gel like interfacial layers and a surface tension peak can be found for the same system, and rationalised by dynamic changes in the bulk phase behaviour as they were for PDADMAC/SDS.[31]

6.3.4. PSS/C_{12}TAB Systems Containing Different Polymer Molecular Weights

If we increase the molecular weight (MW) of the polymer at constant solution composition, a change in the dynamic adsorption is expected as large polymers diffuse more slowly. Extrapolating from the measurements of Wang et al[25] we estimate values of the polymer diffusion coefficient, D_{poly} = 8.0, 2.1 and 0.39 × 10^{-11} m^2s^{-1} for 17k, 150k and 2.6M PSS, respectively. Again, in the absence of any experimental measurement of D_{PS}, I will assume that $D_{PS} = D_{poly}$, for all three surfactant chain lengths. From first principles, we would predict that the difference between the adsorption behaviour of these three systems will be dominated by the slower diffusion of polymer and polymer/surfactant complexes with increasing molecular weight.

If we examine the turning points in the ellipsometry data for the three systems containing different molecular weight polymers (Figure 6.2), we can see that $\bar{\rho}$ is similar for all three for c_{surf} < 0.02 mM. The proximity of this kink in the data to the cac previously calculated for the 17k system suggests that the cac is minimally affected by the polymer chain length. At this concentration the 2.6M system shows a pronounced kink, leading to a plateau in $\bar{\rho}$ at higher bulk surfactant concentrations. At c_{surf} > 0.02 mM the 17k and 150k data curve gently downwards, however $\bar{\rho}$ is less negative (corresponding to a lower surface excess) with increasing polymer chain length.

A second turning point in $\bar{\rho}$ occurs for all three systems at around c_{surf} = 0.3 mM, which corresponds to the estimated value of c_{comp}, the surfactant concentration where complexation is complete, for the 17k system. It is remarkable that a turning point occurs at the same bulk surfactant concentration for all three systems, as this suggests that complexation is 'complete' in the same region despite the formation of multi-micellar complexes for the long chain PSS molecules, in which we might expect complexation to continue until the complex is neutralised. This is not unexpected in light of previous studies of the PSS/C_nTAB systems which have shown that complexation occurs up to a surfactant:polymer ratio of around 0.65, regardless of the polymer molecular weight,[9, 22] but is nevertheless difficult to explain. As in the section above, we note that our assumptions about the bulk behaviour of the system, particularly c_{comp} have a significant impact on our interpretations of the adsorption model, and this should be born in mind throughout the following discussion.

Although Γ_{surf} is lower at low c_{surf} for the 2.6M system than for the systems containing lower MW polymers, Γ_{surf} is still slightly larger than the pure surfactant value. Therefore we suggest that the low value of Γ_{poly} limits synergistic adsorption in this system, resulting in a lower value of Γ_{surf}. If complex formation and dissociation had a significant effect on Γ_{surf}, the value would lie below that of the pure surfactant.

In order to determine whether there is a barrier to polymer adsorption for the systems containing different molecular weight polymers, we can again calculate the sub-surface concentration of polymer, $c_{s,poly}$ from Equation 6.1, the experimental data and the diffusion coefficients above (similarly to in Figure 6.12), as shown in Figure 6.14.

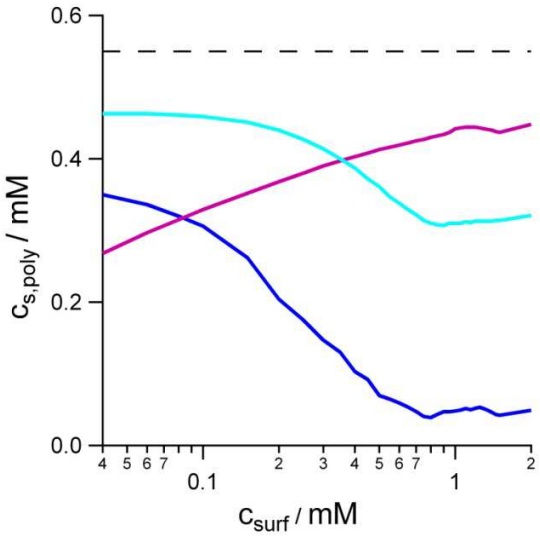

Figure 6.14. Calculated values of the subsurface concentration of polymer, $c_{s,poly}$, in terms of monomers, as a function of bulk surfactant concentration. The blue line is $c_{s,poly}$ for the 17k system, the turquoise line for the 150k system, and the purple line for the 2.6M system. The dashed line denotes the bulk polymer concentration.

From Figure 6.14 we can see that that polymer adsorption is not under diffusion control (as indicated by $c_{s,poly} \neq 0$) at any c_{surf} value measured for the 150k and 2.6M systems, and that it only approaches diffusion control at high c_{surf} for the 17k system. It is therefore clear that the limited values of Γ_{poly} in Figure 6.5 (b) cannot simply be attributed to the slower diffusion of larger polymer molecules and polymer/surfactant complexes as we might have expected from the conclusions reached above for the 17 k system. The amount of polymer that can go to the sub-surface (or to the edge of the complex-free zone) by diffusion is high in all three systems as shown by Figure 6.14, but this polymer cannot adsorb at the interface. There must therefore be a barrier to polymer adsorption in all three systems, similar to that demonstrated for the systems containing different polymer concentrations in Figure 6.12.

In order to determine whether the complex dissociation rate may limit the adsorption of polymer and surfactant, we can again work out how fast breakdown kinetics would have to be for our adsorption model in Figure 6.11 to hold. For the 2.6 M system, the necessary breakdown time at $c_{surf} = 0.15$ mM is

0.12 s, for the 150 k system it is 0.37, and 2.4 s for the 17 k system. The formation of multi-micellar complexes for long chain polymers may slow down the kinetics of dissociation to some extent, but this may not be significant if micelles dissociate independently of each other. It is however important to remember that a system which forms multi-micellar complexes will behave differently to a system which forms complexes consisting of single polymers and micelles. We expect that at low bulk surfactant concentrations all of the polymer molecules are complexed to a small number of micelles, with the number of micelles increasing up until c_{comp} rather than the concentration of complexes.

At $c_{surf} > c_{comp}$ the ellipsometry data track those for the pure surfactant, as they did for the PSS/C_{12}TAB systems at different polymer concentrations, and adsorption can be attributed to the increasing free surfactant concentration in solution. At around 2 mM, small steps in $\overline{\rho}$ are observed in Figure 6.2 for both the 150 k and 2.6 M systems, and the systems become turbid; aggregation occurs. The fact that the surfactant concentration at which aggregation occurs is the same for all polymer molecular weights supports either or both of the hypothesis given earlier; firstly that the high net charge of the complexes at c_{comp} cannot be neutralised until significantly higher concentrations, and secondly that bulk complexation continues until the aggregation region despite our prediction that c_{comp} occurs at around 0.3 mM surfactant.

Although the decrease in $\overline{\rho}$ is smaller than that for the 17 k system, this difference in magnitude may simply be due to the smaller decrease in $\overline{\rho}$ when Γ_{poly} is low before aggregation occurs. However, without further time dependent NR studies in this region we cannot examine how the interfacial composition changes in this region, and further data would have a minimal effect on the conclusions reached here.

The surface expansion rate data in Figure 6.6 (b) vary minimally with polymer molecular weight, despite the differences in interfacial composition and $\bar{\rho}$ for the three systems. The data for all three systems are shifted to higher c_{surf} values than the pure surfactant data, but maintain the same volcano plot shape. As discussed above, the presence of a complex-free zone means that the shift to higher c_{surf} values of the volcano plot cannot be due to delivery of material to the interface by complexes, but rather to the co-adsorption of polymer and surfactant at the interface or the reduced amount of free surfactant in the bulk solution. The fact that θ varies so little with polymer molecular weight, despite the differences in Γ_{poly}, suggests that in these systems surfactant adsorption controls θ. In turn, the greater variation of θ for the systems containing different polymer concentrations in Figure 6.6 (a) suggests that polymer concentration has a greater effect on θ than polymer molecular weight. The domination of θ by Γ_{surf} is further re-inforced by both the co-incidence of the maxima in θ, despite the

fact that the complex-free zone vanishes at increasing c_{surf} as polymer molecular weight is increased, and by the similarity of the θ data to that of the pure surfactant at high c_{surf} for all three systems.

6.4. Conclusions

From the results and discussion presented in this chapter it is clear that the adsorption kinetics of mixtures of PSS and C_{12}TAB are much more complex than those of the weakly interacting systems discussed in Chapter 5. Although we have postulated a simple model of the adsorption kinetics of interacting polymer/surfactant systems in this chapter, the model does have limitations as it does not allow us to fully explain the data, and a more complex model will be required in the future. However, I have used key points of this initial model along with features of the data to try to determine the adsorption mechanism in action in these systems.

At surfactant concentrations below the cac, synergistic adsorption of polymer and surfactant occurs at the surface in all of the systems studied. At concentrations above the cac (0.015 mM), the formation of polymer/surfactant complexes has a significant effect on the adsorption behaviour, with a variety of features observed in the fine-grained ellipsometry data. For mixtures of 17k PSS and C_{12}TAB, complexes consisting of a single polymer molecule and single surfactant micelle form, due to the small number of polymer segments per molecule. From the number of polymer segments and the micellar aggregation number we can estimate the bulk surfactant concentration at which each polymer molecule will be associated with a micelle.

The formation of complexes as the surfactant concentration is increased above the cac causes the concentration of free polymer in the solution to decrease, and this causes a change in the adsorption behaviour of the majority of the PSS/C_{12}TAB mixtures studied. Polymer cannot reach the interface from complexes in this region, instead we propose a mechanism whereby the diffusion of free polymer to the interface controls polymer adsorption in the region between the cac and the point at which bulk complexation is complete.

A kink in the ellipsometry data is observed at the surfactant concentration at which we predict that complex formation is complete, c_{comp}. Once complex formation is complete, we expect that increases in the bulk surfactant concentration will increase the concentration of free surfactant or the micelle size in the complexes, and the free polymer concentration is zero. However, our initially postulated adsorption model does not allow for the flux and therefore subsurface concentration of free surfactant molecules

to increase until there is no complex free zone, at c_{surf} = 0.6 mM. The model therefore appears to be inconsistent with the data recorded, as increases in the surfactant concentration beyond c_{comp} cause increases in the ellipsometry and surfactant surface excess data, which follow the trends of the free surfactant; it is clear the model needs some development. It is possible that both this inconsistency, and the significantly difference between the estimated value of c_{comp} and the observed bulk aggregation, can be accounted for by errors in the estimation of c_{comp}, which is not a measured value. Other studies have shown that bulk polymer surfactant complexation does not always occur as predicted theoretically, and without complementary bulk measurements we cannot tell whether our the values of c_{comp} used in our model are correct.

A barrier to the adsorption of polymer appears to exist for all of the polymer/surfactant systems. As surfactant adsorption is unaffected it is unlikely that this barrier is due to slow complex dissociation, unless complexes can shed surfactant monomers without fully dissociating to release polymer molecules. Furthermore, the barrier cannot be steric, as there are barriers to adsorption even at low surface coverage. Steric barriers do limit the maximum polymer excess reached by the 400 ppm system however, as the coverage cannot be higher than that at the static air/water interface. It is possible that kinetic barriers control polymer adsorption, however it is not yet clear what these comprise.

Measurements using higher molecular weight polymers follow similar patterns to those of the 17 k polymer; the formation of multi-micellar complexes rather than single-micelle complexes has little effect on the adsorption behaviour. Despite the fact that we might expect complexation to continue until the polymer is neutralised by micelles, behaviour indicative of complexation being complete at the same concentrations as for the 17 k polymer is observed. The polymer surface excess is the only thing notably affected by the polymer molecular weight. As polymer adsorption is not under diffusion control this is not just due to the slower mass transport of larger polymer molecules and complexes, there must be another factor limiting polymer adsorption, which further work is required to resolve.

At high surfactant concentrations (2 mM), significant aggregation of the polymer/surfactant complexes occurs for the systems containing high polymer concentrations. The formation of aggregates removes surface active molecules and complexes from the bulk solution, preventing them from affecting the interfacial adsorption behaviour as aggregates cannot reach the interface on the timescale of the OFC due to their large size. However surfactant adsorption is not depleted by the formation of bulk aggregates, as aggregation does not occur until surfactant concentrations significantly above the point where we predict that complex formation is complete (we estimate c_{comp} = 0.3 mM for the 100 ppm system), and hence the free surfactant concentration is high. Furthermore, as the polymer surface excess decreases in this region the surfactant surface excess increases due to removal of the bulky

polymer groups from the interface. Aggregation occurs at surfactant concentrations far above $c_{comp,}$ which is not entirely unexpected, as the low micellar aggregation number in the complexes means that the complexes are far from neutralised at c_{comp}. The complexes cannot become neutralised and hence do not aggregate until much higher surfactant concentrations. However, an alternative explanation is that bulk complexation continues as the surfactant concentration is increased above our estimated value of c_{comp}, and in this region the complexes become gradually more neutralised, whilst the free surfactant concentration also increases due to the low favourability of the surfactant adding to the complexes. Without bulk measusrements we cannot determine which of these possibilities is the case.

Whilst at the dynamic interface we observe a reduction in the surface excess of both components due to aggregation, Taylor et al recorded the presence of multilayers, rather than a decreased adsorbed amount at the static interface in the same region. This inconsistency between the two studies can be resolved if we hypothesise that the aggregates which form in PSS/C_{12}TAB mixtures have a low density, enabling them to reach the static air/water interface under gravity, whilst they cannot diffuse to the dynamic air/water interface of the OFC on the timescale of surface expansion.

6.5. References for Chapter 6

1. Taylor, D. J. F.; Thomas, R. K., The adsorption of oppositely charged polyelectrolyte/surfactant mixtures: Neutron reflection from dodecyl trimethylammonium bromide and sodium poly(styrene sulfonate) at the air/water interface. *Langmuir* **2002,** 18, (12), 4748-4757.
2. Taylor, D. J. F.; Thomas, R. K.; Hines, J. D.; Humphreys, K.; Penfold, J., The adsorption of oppositely charged polyelectrolyte/surfactant mixtures at the air/water interface: Neutron reflection from dodecyl trimethylammonium bromide/sodium poly(styrene sulfonate) and sodium dodecyl sulfate/poly(vinyl pyridinium chloride). *Langmuir* **2002,** 18, (25), 9783-9791.
3. Campbell, R. A.; Ash, P. A.; Bain, C. D., Dynamics of adsorption of an oppositely charged polymer-surfactant mixture at the air-water interface: Poly(dimethyldiallylammonium chloride) and sodium dodecyl sulfate. *Langmuir* **2007,** 23, (6), 3242-3253.
4. Taylor, D. J. F.; Thomas, R. K.; Penfold, J., Polymer/surfactant interactions at the air/water interface. *Adv. Coll. Int. Sci.* **2007,** 132, (2), 69-110.
5. Staples, E.; Tucker, I.; Penfold, J.; Warren, N.; Thomas, R. K.; Taylor, D. J. F., Organization of polymer-surfactant mixtures at the air-water interface: Sodium dodecyl sulfate and poly(dimethyldiallylammonium chloride). *Langmuir* **2002,** 18, (13), 5147-5153.

6. Staples, E.; Tucker, I.; Penfold, J.; Warren, N.; Thomas, R. K. I., Organization of polymer-surfactant mixtures at the air-water interface: Poly(dimethyldiallylammonium chloride), sodium dodecyl sulfate, and hexaethylene glycol monododecyl ether. *Langmuir* **2002,** 18, (13), 5139-5146.
7. Monteux, C.; Williams, C. E.; Meunier, J.; Anthony, O.; Bergeron, V., Adsorption of oppositely charged polyelectrolyte/surfactant complexes at the air/water interface: Formation of interfacial gels. *Langmuir* **2004,** 20, (1), 57-63.
8. Kogej, K.; Skerjanc, J., Fluorescence and conductivity studies of polyelectrolyte-induced aggregation of alkyltrimethylammonium bromides. *Langmuir* **1999,** 15, (12), 4251-4258.
9. Almgren, M.; Hansson, P.; Mukhtar, E.; Van Stam, J., Aggregation of alkyltrimethylammonium surfactants in aqueous poly(styrenesulfonate) solutions. *Langmuir* **1992,** 8, (10), 2405-2412.
10. Hansson, P.; Almgren, M., Interaction of Alkyltrimethylammonium Surfactants with Polyacrylate and Poly(Styrenesulfonate) in Aqueous-Solution - Phase-Behavior and Surfactant Aggregation Numbers. *Langmuir* **1994,** 10, (7), 2115-2124.
11. Hayakawa, K.; Kwak, J. C. T., Surfactant Poly-Electrolyte Interactions .1. Binding of Dodecyltrimethylammonium Ions by Sodium Dextran Sulfate and Sodium Poly(Styrenesulfonate) in Aqueous-Solution in the Presence of Sodium-Chloride. *J. Phys. Chem.* **1982,** 86, (19), 3866-3870.
12. Pojjak, K.; Bertalanits, E.; Mészáros, R., Effect of Salt on the Equilibrium and Nonequilibrium Features of Polyelectrolyte/Surfactant Association. *Langmuir* **2011,** 27, (15), 9139-9147.
13. Monteux, C.; Llauro, M. F.; Baigl, D.; Williams, C. E.; Anthony, O.; Bergeron, V., Interfacial microgels formed by oppositely charged polyelectrolytes and surfactants. 1. Influence of polyelectrolyte molecular weight. *Langmuir* **2004,** 20, (13), 5358-5366.
14. Akentiev, A. V.; Bilibin, A. Y.; Zorin, I. M.; Lin, S. Y.; Loglio, G.; Miller, R.; Noskov, B. A., Scanning probe microscopy of adsorption layers of sodium polystyrenesulfonate/dodecyltrimethylammonium bromide complexes. *Colloid Journal* **2011,** 73, (4), 437-444.
15. Noskov, B. A.; Loglio, G.; Miller, R., Interaction between sodium poly(styrene sulfonate) and dodecyltrimethylammonium bromide at the air/water interface. *Mendeleev Communications* **2005**, (2), 63-65.
16. Noskov, B. A.; Loglio, G.; Miller, R., Dilational viscoelasticity of polyelectolyte/surfactant adsorption films at the air/water interface: Dodecyltrimethylammonium bromide and sodium poly(styrenesulfonate). *J. Phys. Chem. B* **2004,** 108, (48), 18615-18622.
17. Simister, E. A.; Thomas, R. K.; Penfold, J.; Aveyard, R.; Binks, B. P.; Cooper, P.; Fletcher, P. D. I.; Lu, J. R.; Sokolowski, A., Comparison of Neutron Reflection and Surface-Tension Measurements of the Surface Excess of

Tetradecyltrimethylammonium Bromide Layers at the Air-Water-Interface. *J. Phys. Chem.* **1992,** 96, (3), 1383-1388.
18. Asnacios, A.; Langevin, D.; Argillier, J. F., Complexation of cationic surfactant and anionic polymer at the air-water interface. *Macromolecules* **1996,** 29, (23), 7412-7417.
19. Penfold, J.; Tucker, I.; Thomas, R. K.; Zhang, J., Adsorption of polyelectrolyte/surfactant mixtures at the air-solution interface: Poly(ethyleneimine)/sodium dodecyl sulfate. *Langmuir* **2005,** 21, (22), 10061-10073.
20. Valkovska, D. S.; Shearman, G. C.; Bain, C. D.; Darton, R. C.; Eastoe, J., Adsorption of ionic surfactants at an expanding air-water interface. *Langmuir* **2004,** 20, (11), 4436-4445.
21. Rodenas, E.; Dolcet, C.; Valiente, M.; Valeron, E. C., Physical Properties of Dodecyltrimethylammonium Bromide (DTAB) Micelles in Aqueous Solution and Their Behavior as the Reaction Medium. *Langmuir* **1994,** 10, (7), 2088-2094.
22. Fundin, J.; Brown, W., Polymer/Surfactant Interactions - Sodium Poly(Styrenesulfonate) and Ctab Complex-Formation - Light-Scattering Measurements in Dilute Aqueous-Solution. *Macromolecules* **1994,** 27, (18), 5024-5031.
23. Bell, G. R.; Bain, C. D.; Li, Z. X.; Thomas, R. K.; Duffy, D. C.; Penfold, J., Structure of a Monolayer of Hexadecyltrimethylammonium p-Tosylate at the Airâ˜Water Interface. *Journal of the American Chemical Society* **1997,** 119, (42), 10227-10228.
24. Bell, G. R.; Li, Z. X.; Bain, C. D.; Fischer, P.; Duffy, D. C., Monolayers of Hexadecyltrimethylammonium p-Tosylate at the Airâ˜Water Interface. 1. Sum-Frequency Spectroscopy. *J. Phys. Chem. B* **1998,** 102, (47), 9461-9472.
25. Wang, L. X.; Yu, H., Chain Conformation of Linear Poly-Electrolyte in Salt-Solutions - Sodium Poly(Styrene Sulfonate) in Potassium-Chloride and Sodium-Chloride Solutions. *Macromolecules* **1988,** 21, (12), 3498-3501.
26. Song, Q.; Couzis, A.; Somasundaran, P.; Maldarelli, C., A transport model for the adsorption of surfactant from micelle solutions onto a clean air/water interface in the limit of rapid aggregate disassembly relative to diffusion and supporting dynamic tension experiments. *Colloids and Surfaces A: Physicochemical and Engineering Aspects* **2006,** 282â€“283, (0), 162-182.
27. Varga, I., Personal Communication. In September 2012.
28. Campbell, R. A.; Yanez Arteta, M.; Angus-Smyth, A.; Nylander, T.; Varga, I., Effects of Bulk Colloidal Stability on Adsorption Layers of Poly(diallyldimethylammonium Chloride)/Sodium Dodecyl Sulfate at the Air/ater Interface Studied by Neutron Reflectometry. *J. Phys. Chem. B* **2011,** 115, (51), 15202-15213.
29. Campbell, R. A.; Angus-Smyth, A.; Arteta, M. Y.; Tonigold, K.; Nylander, T.; Varga, I., New Perspective on the Cliff Edge Peak in the Surface Tension of

Oppositely Charged Polyelectrolyte/Surfactant Mixtures. *J. Phys. Chem. Letts.* **2010,** 1, (20), 3021-3026.
30. Campbell, R. A.; Yanez Arteta, M.; Angus-Smyth, A.; Nylander, T.; Varga, I., Multilayers at Interfaces of an Oppositely Charged Polyelectrolyte/Surfactant System Resulting from the Transport of Bulk Aggregates under Gravity. *The Journal of Physical Chemistry B* **2012,** 116, (27), 7981-7990.
31. Campbell, R. A., Personal Correspondance. In August 2012.

Chapter 7. Adsorption Kinetics of Mixtures of PSS and C_nTABs

7.1. Introduction

In Chapter 6 I discussed the dynamic adsorption behaviour of PSS/C_{12}TAB, and in this chapter I will go on to examine the effect of the length of the alkyl chain of the surfactant on adsorption at the expanding interface of the OFC. Increasing the alkyl chain length of a surfactant increases its hydrophobicity, which increases the driving force for both interfacial adsorption and micellisation in a pure surfactant solution, lowering the cmc and increasing the micelle aggregation number.[1, 2] PSS forms stable complexes with all of the C_nTABs due to the electrostatic interactions between the charge moieties, and due to the hydrophobicity of the polymer, the sidegroups of which penetrate into the surface of the surfactant micelle on complexation.[2-4] Furthermore, this causes the polymer molecule to wrap around the micelle, shielding the hydrophobic parts of the polymer and surfactant and releasing counterions, which further favours aggregation.[2] Increasing the hydrophobicity of the surfactant will increase the co-operative interaction between the surfactant and the hydrophobic moieties of the (PSS) chain, which will decrease the critical aggregation concentration of the system.[3, 5] Several studies of the bulk phase behaviour of PSS/C_nTAB systems have shown that precipitation occurs in these systems as the ratio of polymer charges to surfactant in the bulk solution approaches unity.[4, 6-9] As increasing the surfactant hydrophobicity leads to stronger interactions between the polymers and micelles, it also increases the size of the two-phase region, and precipitation becomes more likely for longer chain surfactants.

The variation in adsorption behaviour of PSS/C_nTAB systems at the static air/water interface with surfactant chain length has been investigated by Taylor *et al*.[10] and Monteux *et al*.[11] Both studies show that adsorption is most favoured for PSS/C_nTAB systems containing short chain surfactants, despite the fact that in the absence of polymer the driving force for adsorption is much greater for surfactants with long alkyl chains. Taylor *et al*. showed that C_nTABs with n = 10, 12, 14 undergo mono to multilayer transitions at the air/water interface, whilst when n =16, only monolayer adsorption occurs.[10] Within their adsorption model[12, 13] they attributed this difference in behaviour to the greater favourability of formation of bulk species than of sub-layer species. However, Taylor *et al*. found that they were unable

to categorise PSS/C_{14}TAB using their adsorption model as it exhibited both multilayer adsorption and a peak in the surface tension, properties of their 'Type 1' and 'Type 2' systems respectively.

In a simpler explanation of the decreased adsorbed amount for systems containing longer chain surfactants, Monteux *et al*. attributed it directly to bulk precipitation of polymer and surfactant.[11] Furthermore, in another study Kristen *et al*. demonstrated that although the addition of PSS to a C_{12}TAB foam film increased stability, addition of C_{14}TAB completely destabilized the film at the isoelectric point,[14] which is consistent with bulk phase precipitation occurring in this region.

Bulk aggregation is expected to be more favoured for mixtures of PSS with longer chain surfactants, due to the stronger cooperative interaction between the two components. As discussed previously, on the OFC aggregation is generally expected to decrease the adsorbed amount at the interface due to the slow diffusion of aggregates. We would therefore expect that the effects of precipitation on adsorption at the dynamic interface of the OFC would become more pronounced with increasing chain length. In this chapter I aim to use measurements on the OFC to determine the link between the bulk phase behaviour of PSS/C_nTAB mixtures and their adsorption at a dynamic air/liquid interface.

As in the two previous chapters, I will first present and discuss measurements made on the PSS/C_nTAB systems using ellipsometry, NR, and LDV, as well as the compositional information obtained by co-modelling ellipsometry and NR data. I will then move on to a more in depth discussion of the data, and I will try to elucidate whether it is possible to model the adsorption kinetics of the mixtures containing longer chain surfactants in the same way as it was possible to do so for the PSS/C_{12}TAB system in Chapter 6.

Materials

Solutions were made in ultrapure water (Milli-Q; resistivity = 18 mΩ.cm) for ellipsometry, or in NRW for NR measurements. The OFC and associated glassware were cleaned with a 2% solution of a strong alkaline detergent (Decon 90 or Gigapur) and rinsed thoroughly. C_{12}TAB, C_{14}TAB and C_{16}TAB (99%, Sigma) was purified by re-crystallisation three times from a mixture of ethanol and acetone. PSS (17k, molecular weight, Sigma) was used as supplied. Deuterated surfactants were kindly supplied by Dr R. K. Thomas from the Oxford Deuteration Facility. [15] 0.1 M NaBr (Sigma Aldrich) was used for all experiments.

7.2 Results

7.2.1 Ellipsometry

Figure 7.1 shows ellipsometry data as a function of bulk surfactant concentration for pure C_{14}TAB and C_{16}TAB, and for the PSS/C_{14}TAB and PSS/C_{16}TAB mixtures, whilst Figure 7.2 compares the ellipsometry data for all three PSS/C_nTAB mixtures. Data were recorded at constant polymer and salt concentrations (100 ppm and 0.1 M, respectively) and are plotted with respect to the bulk surfactant concentration (c_{surf}). A dashed line indicates the value $\overline{\rho}_0$ = 0.38 x 10^{-3} for pure water, which is indistinguishable from the value recorded for solutions of PSS and NaBr in the absence of surfactant, as PSS is not surface active alone, as mentioned in Chapter 6.

At low bulk surfactant concentrations, $\overline{\rho}$ is more negative (corresponding to a higher total surface excess) for all of the polymer/surfactant mixtures than for the corresponding pure surfactants; more or different material adsorbs at the interface when polymer is added to the solution. In Chapter 6 we saw that for PSS/C_{12}TAB, synergistic adsorption of polymer and surfactant occurred in the low surfactant concentration regime, with the adsorption of both components enhanced compared to their adsorption alone.

As the surfactant concentration is increased, $\overline{\rho}$ for PSS/C_{14}TAB tracks that of PSS/C_{12}TAB, whereas $\overline{\rho}$ for PSS/C_{16}TAB is less negative (indicative of a lower total surface excess) and closer to the pure surfactant values. At c_{surf} = 0.15 mM the ellipsometry data for PSS/C_{16}TAB changes slope, and $\overline{\rho}$ tends back towards that of the other two mixtures. If we bear in mind the explanations for the kink in the $\overline{\rho}$ data for the PSS/C_{12}TAB systems which were discussed in Chapter 6, it is probable that a change in the adsorption behaviour of the PSS/C_{16}TAB mixture occurs in this region.

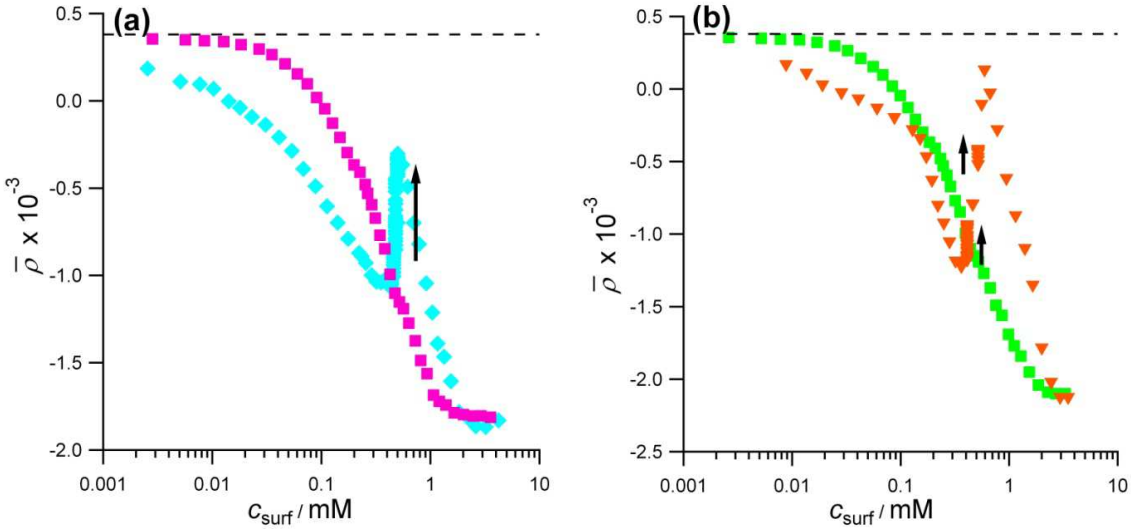

Figure 7.1. Coefficient of ellipticity at the surface of an OFC containing (a) C_{14}TAB (pink squares) and a mixture of PSS and C_{14}TAB (turquoise diamonds), and (b) C_{16}TAB (lime green squares) and a mixture of PSS and C_{16}TAB (orange triangles). All measurements were made in the presence of 0.1 M NaBr. The arrows indicates the direction of change of the time-dependent change in the ellipticity at intermediate c_{surf}. The dotted line is the ellipticity of the salt solution, and of the polymer and salt solution.

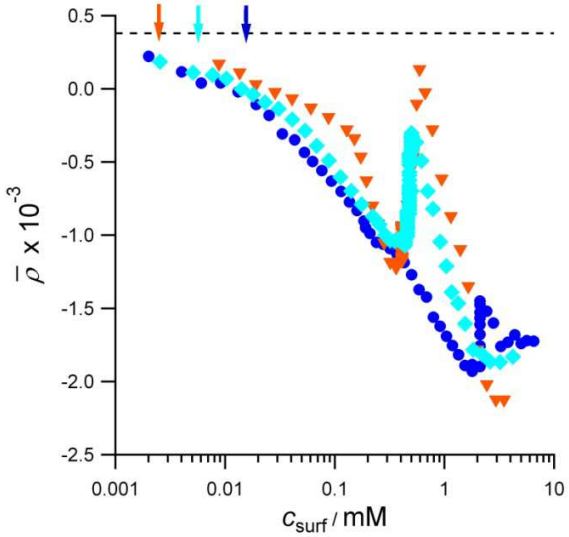

Figure 7.2. Coefficient of ellipticity at the surface of an OFC containing PSS with C_{12}TAB (blue circles), C_{14}TAB (turquoise diamonds) and C_{16}TAB (inverted orange triangles). Some of these data are re-produced from Figure 7.1 and from Chapter 6, but are shown here to facilitate comparison of the effects of surfactant chain lengths. All measurements were made in the presence of 0.1 M NaBr. The dotted line is the ellipticity of the salt solution, and of the polymer and salt solution. The downward pointing arrows mark the cacs of the three systems (given later), with the colours corresponding to those of the data sets.

At $c_{surf} \approx 0.4$ mM, both the PSS/C_{14}TAB and PSS/C_{16}TAB systems exhibit marked changes in the value of $\overline{\rho}$ as a function of time, shown as multiple data points at a given value of c_{surf} in this region, with the direction of the change denoted by arrows in Figure 7.1. Over a period of several hours, $\overline{\rho}$ for both systems increased by at least 1×10^{-3}, and in the case of the PSS/C_{16}TAB system the final value of $\overline{\rho}$ in this region is close to the pure water value. These changes in $\overline{\rho}$ correspond to a reduction in the total surface excess with time, and at the expanding interface of the OFC this must be due to changes occurring in the bulk solution. These changes are similar to, but much more pronounced than, the time dependence in $\overline{\rho}$ observed for the PSS/C_{12}TAB system at c_{surf} = 2 mM. In Chapter 6, this time-dependent behaviour for PSS/C_{12}TAB was attributed to the aggregation of polymer/surfactant complexes in the bulk solution which led to decreased adsorption of both components at the interface. By analogy, it follows that the time dependent behaviour observed for the PSS/C_{14}TAB and PSS/C_{16}TAB systems can also be attributed to aggregation of polymer/surfactant complexes in the bulk solution, although aggregation occurs at much lower c_{surf} for these two systems than for PSS/C_{12}TAB.

At high c_{surf}, $\overline{\rho}$ becomes more negative (indicative of a higher total surface excess) again for all three systems eventually tending to the pure surfactant values at the highest concentrations measured. Once bulk aggregation is complete, further addition of surfactant increases the free surfactant concentration and adsorption, but NR data is necessary to confirm the composition of the interface in this region.

7.2.2 NR

The specular reflectivity profiles obtained from NR measurements on the h-polymer/d-surfactant/NRW contrast were fitted using a single 14 Å layer model as discussed in Chapter 4. The product of σ and τ is shown in Figure 7.3 as a function of bulk surfactant concentration for both PSS/C_{14}TAB (turquoise diamonds) and PSS/C_{16}TAB (orange triangles), compared with pure C_{14}TAB (turquoise solid line) and pure C_{16}TAB (orange dashed line). The calculated surface excesses for the two polymer/surfactant mixtures are very similar at low bulk surfactant concentrations, and are close to the pure surfactant values for both systems. Although these measurements are made using deuterated surfactant and hydrogenated polymer, we cannot assume that $\sigma \; x \; \tau$ is determined predominantly by adsorbed surfactant as we did in Chapter 5, as the neutron scattering length density of PSS is 1.85 x 10^{-6} $Å^{-1}$ (see Chapter 6).

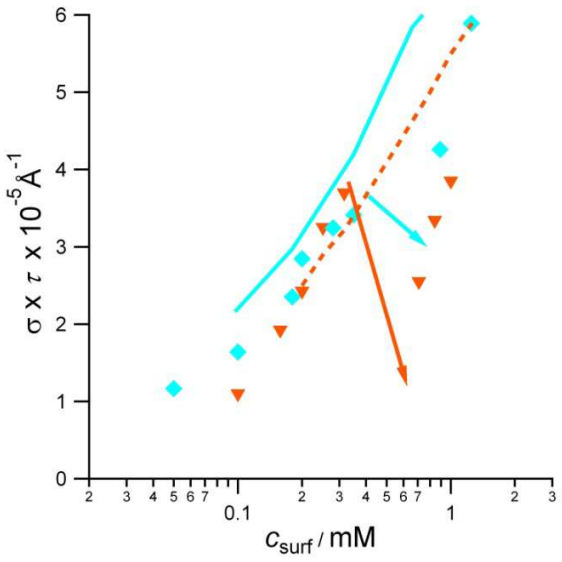

Figure 7.3. Product of the scattering length density, σ, and thickness, τ, of the adsorbed layer, as obtained from fits to the specular reflectivity profiles using a single 14 Å layer, for PSS/C_{14}TAB (turquoise diamonds) and PSS/C_{16}TAB (orange triangles). The solid turquoise line indicates the pure C_{14}TAB data and the dashed orange line the C_{16}TAB data. The arrows represent the decrease in $\sigma \times \tau$ with time which occurs in the intermediate surfactant concentration region. These data are shown separately as function of time at several different c_{surf} in Figure 7.4.

When 0.4 mM < c_{surf} < 0.6 mM $\sigma \times \tau$ decreases with time for both PSS/C_{14}TAB and PSS/C_{16}TAB, which indicates a decreased adsorbed amount at the interface. For both systems this decrease in $\sigma \times \tau$ occurs in a similar region to the decrease in $\overline{\rho}$ seen in Figure 7.1 and Figure 7.2. These data are not displayed in Figure 7.3 for clarity, with the region affected denoted instead by an arrow, however Figure 7.4 (a) and (b) show the decrease in $\sigma \times \tau$ which occurs with time for both systems at several successive surfactant concentrations. The total decrease in $\sigma \times \tau$ is both smaller in magnitude and occurs over a larger range of c_{surf} for PSS/C_{14}TAB than PSS/C_{16}TAB, 1.5×10^{-5} Å^{-1} over 0.26 mM for the former compared to 3×10^{-5} Å^{-1} over 0.16 mM for the latter. In order to determine the compositions of these systems and further discuss the adsorption behaviour, we need to co-model these NR data with the ellipsometry data in Figure 7.1 and Figure 7.2.

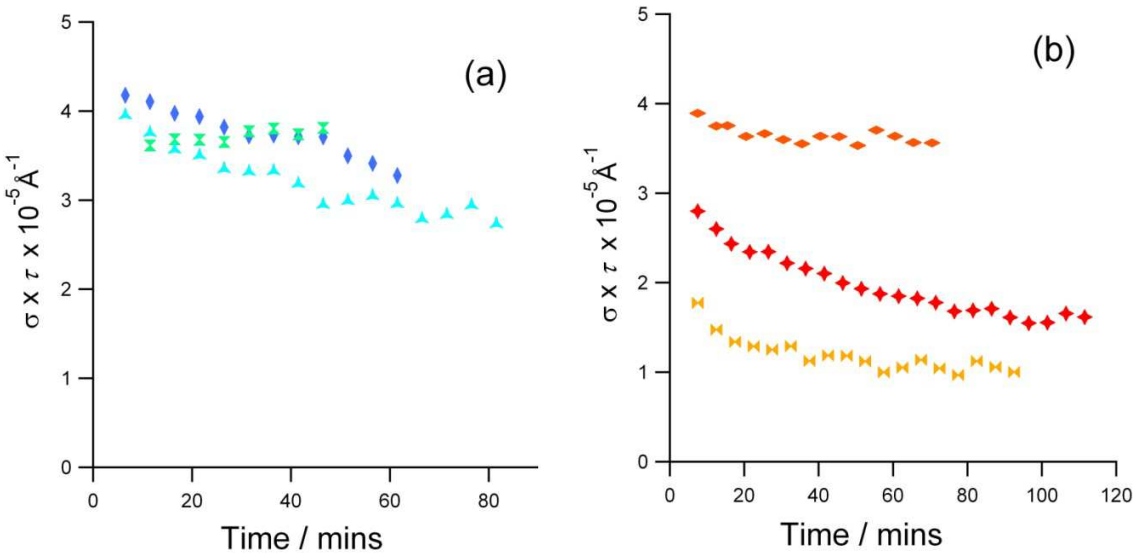

Figure 7.4. Product of the scattering length density, σ, and thickness, τ, of the adsorbed layer as function of time for (a) the intermediate c_{surf} values of the PSS/C_{14}TAB system, c_{surf} = 0.4 mM (green bows) , 0.5 mM (blue diamonds) and 0.66 mM (turquoise triangles) and (b) the PSS/C_{16}TAB system where c_{surf} = 0.4 mM (orange diamonds), 0.5 mM (red crosses) and 0.56 mM (yellow bows).

7.2.3. Calculated Interfacial Compositions

The calculated interfacial compositions obtained from our co-modelling approach for both PSS/C_{14}TAB and PSS/C_{16}TAB are shown in Figure 7.5, and the data sets are compared in Figure 7.6 to enable the effects of surfactant chain length on the interfacial composition to be easily distinguished. A cubic function was used to relate $\overline{\rho}$ and Γ for the reasons discussed in Chapter 4.

From Figure 7.5 we can see that the trends in adsorption behaviour with increasing surfactant concentration are very similar for PSS/C_{14}TAB and PSS/C_{16}TAB. At c_{surf} < 0.4 mM Γ_{surf} is close to, but below, the pure surfactant value. Γ_{surf} increases with c_{surf} whilst Γ_{poly} is relatively constant. For the PSS/C_{12}TAB system Γ_{surf} for the mixture exceeded that of the pure surfactant, suggesting synergistic adsorption of both components, however for C_{14}TAB and C_{16}TAB surfactant adsorption is not enhanced.

When 0.4 mM < c_{surf} < 0.6 mM where both the ellipsometry and NR data (Figure 7.2 and Figure 7.4) are time-dependent , Γ_{poly} drops to within experimental error of zero for both systems, whilst Γ_{surf} also decreases. It is very difficult to co-model the time-dependent data, the systems would need to be identical time dependent states of bulk aggregation during separate measurements using the two

methodologies, and this is not realistic due to the time dependence of the data. Small mis-matches in the aggregation states of the two systems with time can result in very different calculated surface compositions. Although co-modelling of the data in the time dependent region was attempted for the PSS/C_{12}TAB system in Chapter 6, much more pronounced aggregation is evident for the PSS/C_{14}TAB and PSS/C_{16}TAB systems, so co-modelled compositions are not shown for these systems. If further controlled measurements were recorded on these systems it may be possible to co-model the data to obtain interfacial composition, however I think that this will be unlikely unless ellipsometry and NR measurements can be performed simultaneously. Although interfacial compositions at long times could equally be given, recent studies (on other systems) have shown that even the end states of the system may not be identical unless many factors are strictly controlled.[16, 17] As a consequence I have simply denoted the changes in interfacial composition in the time dependent region by arrows in Figure 7.5.

At $c_{surf} > 0.6$ mM the experimental data are no longer time dependent, and Γ_{poly} is calculated to be zero (Figure 7.5); polymer does not adsorb in this region. This supports the hypothesis that the time dependent behaviour is attributable to aggregation of polymer/surfactant complexes in the bulk solution which cannot then diffuse to the interface on the timescale of adsorption. Furthermore it implies that there is no further re-dissolution of the particles with further surfactant addition, which is often suggested to occur in polymer/surfactant mixtures.[8] In this region Γ_{surf} increases as the bulk surfactant concentration is increased, whilst Γ_{poly} remains at zero.

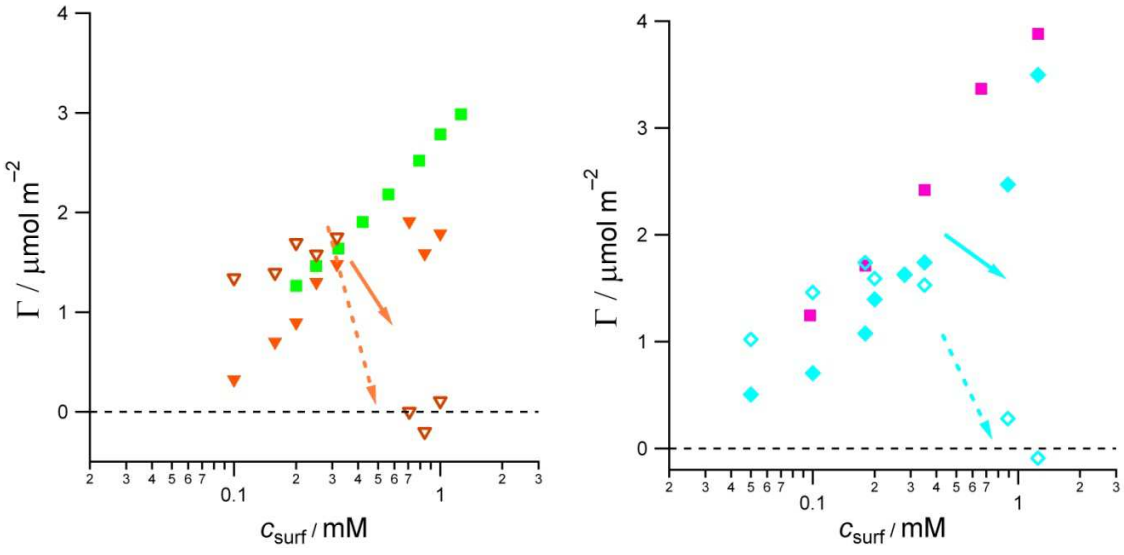

Figure 7.5. Surface excesses on the OFC of (a) C_{14}TAB from a pure C_{14}TAB solution (pink squares), and of C_{14}TAB and PSS from a mixture of the two components (filled and empty turquoise diamonds respectively), and (b) of C_{16}TAB from a pure C_{16}TAB solution (green squares), and of C_{16}TAB and PSS (100 ppm and 17 k) from a mixture of the two components (filled and empty orange inverted triangles respectively). All measurements were made in the presence of 0.1 M NaBr. The time compositional changes in the time dependent region are denoted by arrows, solid for Γ_{surf} and dashed for Γ_{poly}.

If we examine Figure 7.6, which compares Γ_{surf} and Γ_{poly} for the systems with different surfactant chain lengths, we can see that for $c_{surf} < 0.4$ mM, Γ_{poly} is almost identical for all three systems, whilst Γ_{surf} is not. The similarity of the Γ_{poly} values may suggest that polymer adsorption is controlled by the same mechanism in all three systems, however in order to evaluate whether or not this is the case we need to examine the surface expansion rate data obtained from LDV measurements. Furthermore, as Γ_{surf} varies between the mixtures in this region it appears that polymer adsorption does not depend on the surfactant surface excess despite the fact that PSS is not surface active alone.

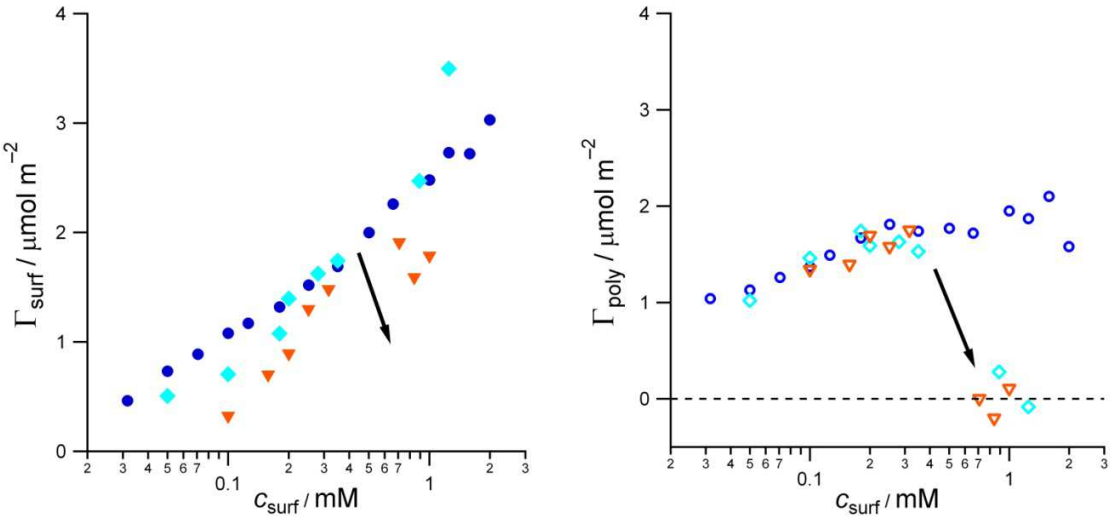

Figure 7.6. Summary of the surface excesses of (a) C_nTAB and (b) PSS adsorbing from mixtures of the two components, as calculated using our co-modelling methodology. The different data sets are different surfactant chain lengths (constant polymer concentration of 100 ppm and MW of 17 k) , where the blue circles are the mixture containing C_{12}TAB, the turquoise diamonds C_{14} TAB, and the orange inverted triangles are C_{16}TAB. These data are reproduced from Figure 6.5 and Figure 7.5 for comparison purposes. The time dependent region (for the PSS/C_{14}TAB and PSS/C_{16}TAB systems is denoted by a black arrow in both figures.

In the region where Γ_{poly} is very similar for all three systems, Γ_{surf} decreases with increasing surfactant chain length. If the mass transport of complexes dominates adsorption of both components we would expect that Γ_{surf} would be very similar for all three systems if Γ_{poly} is. However, if the adsorption of polymer at the interface is not under diffusion control, as in Chapter 6, it is possible that the same barrier to polymer adsorption could affect surfactant adsorption, and that the effect may increase with surfactant chain length. These possibilities will be discussed further below.

7.2.4. LDV

As in the previous chapters, surface expansion rate data enables us to begin to quantitatively consider the adsorption kinetics of the PSS/C_nTAB systems. For pure monomeric surfactants under diffusion control (such as C_{14}TAB and C_{16}TAB in Figure 7.7) the plot of θ v c_{surf} is a typically a volcano plot. For the PSS/C_{12}TAB system, the θ data shown in Figure 6.7, also have a volcano shape, although the volcano plot is shifted to slightly higher c_{surf} for the mixtures. The surface expansion rate data for the PSS/C_{14}TAB and PSS/C_{16}TAB data in Figure 7.7 do not exhibit a simple volcano shape over the whole range of surfactant concentrations. At low surfactant concentrations, there is a marked shift of the data to higher c_{surf} values for the PSS/C_{14}TAB system and not the PSS/C_{16}TAB system. This is unexpected, as if the same adsorption mechanism is happening in all three systems, at least at low surfactant concentrations we would expect to see similar θ behaviour. However, this difference in θ in comparison to the pure surfactant values may be partially explained by the low Γ_{surf} of the PSS/C_{14}TAB mixture as compared to the pure surfactant in Figure 7.5.

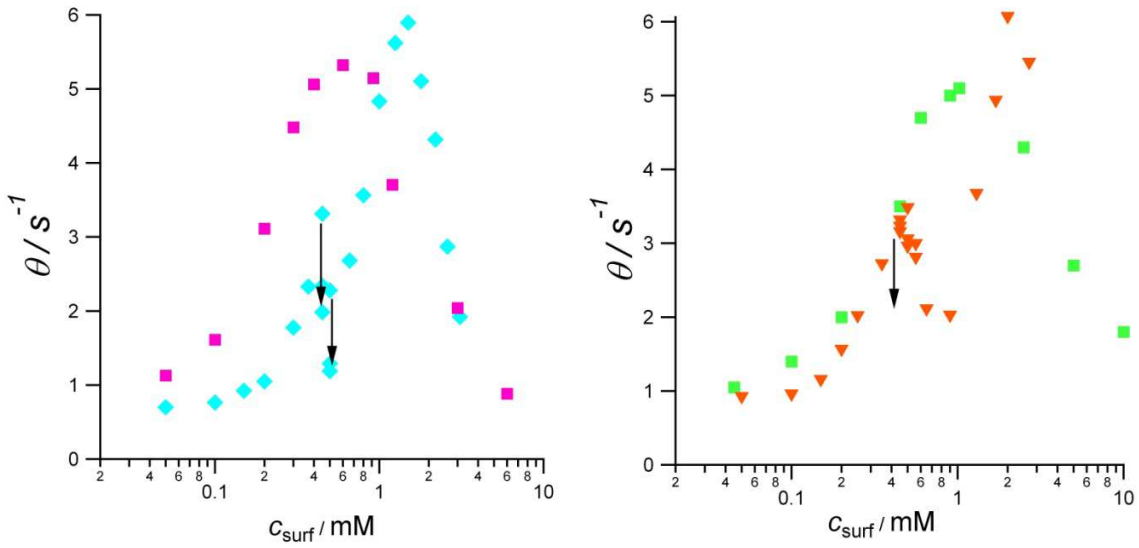

Figure 7.7. Surface expansion rate on the OFC as a function of (a) C_{14}TAB concentration for bulk solutions containing pure C_{14}TAB [from reference [18]] (pink squares) or PSS/C_{14}TAB (turquoise diamonds) and (b) C_{16}TAB concentration for bulk solutions containing pure C_{16}TAB [from reference [18]] (green squares) or PSS/ C_{16}TAB (orange inverted triangles). Arrows denote the direction of change for bulk compositions at which a time dependence of the surface expansion rate was observed, in these regions data were recorded every 30 minutes. Both measurements were performed in the presence of 0.1 M NaBr.

If instead of comparing the θ data for the mixtures to the relevant pure surfactant data, we compare the data from all three mixtures with each other as in Figure 7.8 a much more striking result is seen; for c_{surf} < 0.4 mM), the θ v c_{surf} data are almost identical for all three systems. In this region, the same

mechanism may therefore control the surface expansion rate in all three systems, leading to the very similar interfacial compositions seen in Figure 7.6, although there may equally be different physical explanations of the values of θ in the three systems.

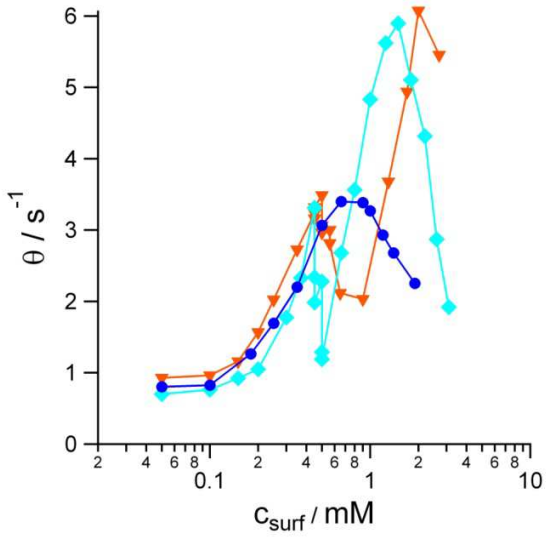

Figure 7.8. Surface expansion rate of PSS/C_{12}TAB (blue circles), PSS/C_{14}TAB (turquoise diamonds) and PSS/C_{16}TAB (orange triangles) as a function of bulk surfactant concentration. All measurements were made in the presence of 0.1 M NaBr and the polymer concentration was 100 ppm. These data are reproduced from Figure 7.7 and Figure 6.7 for the purposes of comparison.

At intermediate bulk surfactant concentrations, close to where time-dependent changes were observed in both the ellipsometry and NR data, θ also decreases with time for both the PSS/C_{14}TAB and PSS/C_{16}TAB systems at several consecutive values of c_{surf}. The bulk process which causes a decrease in the adsorbed amount of both components unsurprisingly causes a decrease in the Marangoni flows. The decrease in θ causes a local minimum in θ v c_{surf} for both the PSS/C_{14}TAB and PSS/C_{16}TAB systems. Local minima in θ have been seen previously in this study for the PEO/C_{14}TAB systems and 400 ppm PSS/C_{12}TAB systems in Chapters 5 and 6, and were attributed to changes in the species which dominated the adsorption behaviour. For the PSS/C_nTAB systems the local minima can be attributed to aggregation of polymer/surfactant complexes.

As the surfactant concentration is increased past the time dependent region, θ increases. If only free surfactant is adsorbing at the interface after aggregation removes the polymer, we would expect the data to follow the pure surfactant curve, but translated along the c_{surf} axis to allow for the surfactant removed as polymer/surfactant aggregates. The higher maximum values of θ reached suggest that other species are present at the interface, although it is possible that they were recorded due to errors incurred by the presence of aggregates in solution.

7.3. Discussion

7.3.1. Bulk Species and Interactions

As in Chapter 6, before discussion of the adsorption mechanism for the PSS/C_nTAB systems, I will first consider what we know about the species present in the bulk solution and how they vary with surfactant concentration.

The critical micelle concentration (cmc) of the C_nTAB surfactants in the absence of polymer decreases with increasing chain length due to the increased hydrophobicity of the surfactant. In the presence of PSS, micellisation will occur in all three systems at a critical aggregation concentration (cac) well below the free cmc due to the stabilization of the surfactant micelle by interaction with the polymer. Furthermore, the difference between the cac and the cmc decreases with increasing chain length.[19] The cac values given by Kogej *et al*. for the mixtures with increasing surfactant chain length are 0.015 mM, 0.0057 mM and 0.0025 mM. Although the cmc of the pure surfactant is lowered by the presence of salt, the cac is expected to increase as the electrostatic interactions between the polymer and surfactant are shielded. However, the cac increases only slightly with salt for the PSS/C_nTAB systems.[3, 4] The cmc of surfactant in a mixture with polymer will be slightly higher than the pure surfactant values as micelles can only form in solution once all of the polymer is saturated with surfactant. Kogej *et al*. give values of the cmc for the pure surfactants as 3.66 mM for C_{12}TAB to 0.33 mM for C_{14}TAB and 0.034 mM for C_{16}TAB in the presence of 0.1 M NaBr.[3] In polymer/surfactant mixtures the cmc will be slightly higher than in the pure surfactant system due to the formation of polymer/surfactant complexes, and it will increase with increasing amounts of surfactant bound to the polymer in complexes.

For the pure C_nTAB surfactants in 0.1 M KBr, the shape of the micelles which form in solution also changes with alkyl chain length, C_{12}TAB and C_{14}TAB form spherical micelles in solution, whilst C_{16}TAB can form rodlike micelles.[6, 20] In polymer/surfactant complexes, interaction of the surfactant with the polymer inhibits the formation of threadlike micelles, and favours that of spherical micelles,[4] however the work of Nause *et al*. observed a transition of the shape of the micelles in complexes from spherical to rodlike with increasing surfactant concentration.[21]

The aggregation number (N_{agg}) of the surfactant in a micelle is determined by the length of its hydrocarbon chain. For the pure surfactants, Roelants *et al*. give N_{agg} as 65 for pure C_{12}TAB, 97 for pure C_{14}TAB, and 104 for pure C_{16}TAB in the absence of salt,[22] whilst Imae *et al*. give the values as

53, 71, and 91 in the presence of salt.[20] However, the micellar aggregation number of surfactants is usually smaller in polymer/surfactant complexes.[23] In complexes with PSS, the insertion of the polymer phenyl groups into the micelle surface[2] will hinder micellar growth compared to that in the free surfactant solution, and previous studies have shown that the aggregation number can be reduced by up to half compared to the free micelle values.[2, 6] Using long chain PSS and in the absence of salt, Almgren et al showed that N_{agg} for PSS/C_{16}TAB varies between 79 and 60 with increasing bulk surfactant concentration, with the micellar size decreasing rather than increasing with surfactant concentration.[2] The higher salt concentration and lower surfactant concentration in our experiments will tend to increase and decrease the aggregation number, respectively, so in the absence of a direct measurement we will assume N = 79 in our experiments also. This is significantly larger than the value for PSS/C_{12}TAB, given as 49 in Chapter 6. No measurements of the micellar aggregation number for PSS/C_{14}TAB surfactants under the conditions used here exist in the literature. For the purposes of our calculations we estimate that N_{agg} for PSS/C_{14}TAB is intermediate between that of the other two surfactants, as suggested by the N_{agg} values of the pure surfactant, and the fact that the difference in N_{agg} still exists for complexes.[2, 23] I will therefore use a value of N_{agg} = 65 although this approximate value may incur errors in the following analysis.

The polymer/surfactant complexes which form in mixtures of 17 k PSS (which contains only 82 monomer units) and C_nTAB surfactants above the cac, consist of single polymer molecules complexed to a single surfactant micelle, as discussed in Chapter 6. If the micellar aggregation number is smaller than the number of monomer units in the polymer, the polymer charge will not be entirely compensated by the micelle and the complex will not be neutral. We estimate that the formation of these complexes will be complete at $c_{surf} = c_{comp}$, where c_{comp} is the concentration at which each polymer molecule in solution is associated with a surfactant micelle. Further increases in the bulk surfactant concentration above this point are assumed not to change the complexes, but instead to increase the free surfactant concentration.

If neutral polymer/surfactant complexes have formed by c_{comp} we would theoretically expect bulk aggregation of complexes to occur, as the lack of charge means that the complexes lose their colloidal stability. However, aggregation is unlikely to occur if the complexes are still charged, and will not occur until bulk solution compositions around the charge neutrality point of the complex.

The surfactant concentration at which polymer/surfactant complex formation will be complete, c_{comp}, can be estimated from the ratio of the micellar aggregation number in the complex to the number of monomers in a polymer molecule (82 for 17 k PSS). For PSS/C_{12}TAB in Chapter 6 we estimated that there is one micelle per polymer molecule at $c_{comp} = 49/82 \times c_{poly}$+ cac, which resulted in c_{comp} = 0.3

mM. For PSS/C_{14}TAB and PSS/C_{16}TAB, c_{comp} will be higher, at 0.39 and 0.47 mM respectively. The uncertainty in N_{agg} for each system (as mentioned above) leads to an uncertainty in c_{comp}, however we do have a good indication of the surfactant concentration region in which c_{comp} is reached. Furthermore, as discussed in Chapter 6, without bulk measurements we cannot be sure that complexation will be complete in the region in which we theoretically expect it to be, hence we will try not to over-interpret the data in the region of our estimated c_{comp} values.

In order to model the adsorption kinetics of these systems quantitatively we need values of the diffusion coefficient of the polymer/surfactant complexes, D_{PS}. For the PSS/C_{12}TAB system we estimated that D_{PS} was the same as D_{poly} = 8 x 10^{-11} ms^{-1}, as the free surfactant micelle had a diffusion coefficient of around 1.1 x 10^{-10} ms^{-1},[24] which is consistent with a micellar radius of 22 Å[25] if we calculate D using the Stokes Einstein relationship, $D = k_B T/6\pi\eta R_g$ (where k_B is Boltzmann's constant, η is the solution viscositiy and R_g is the radius of gyration). In order to calculate D_{PS} assuming the diffusion coefficient of the complexes is the same as that of the surfactant micelles, D_{mic}, for the PSS/C_{14}TAB and PSS/C_{16}TAB mixtures we need to estimate how N_{agg} varies with the micellar aggregation number. If C_{12}TAB forms micelles of N_{agg} = 53[20] and r_H = 22 Å[25], and C_{14}TAB forms micelles of N_{agg} = 71[20] and the hydrodynamic radius, r_H = 27 Å[25], we can estimate that for C_{14}TAB micelles of N_{agg} = 65 and C_{16}TAB micelles of N_{agg} = 79, r_H = 26 and 30 Å respectively. As a check, these radii are consistent with the approach of Roelants et al who estimate the radius of a micelle from the number of carbons in the tail group.[22] The complex diffusion coefficients D_{PS} calculated from these radii and the Stokes-Einstein equation are 1 x 10^{-10}, 0.93 x 10^{-10} and 0.83 x 10^{-10} ms^{-1} for PSS/C_{12}TAB, PSS/C_{14}TAB, and PSS/C_{16}TAB complexes respectively. The micellar aggregation number has a minimal effect on the size of the complex or its diffusion rate in solution.

In Chapter 6 a simple model of the adsorption kinetics in complex forming systems was suggested as an extension of that proposed by Valkovska *et al*. for micellar surfactant systems.[18] This basic model is based on the idea that a complex-free zone forms in the sub-surface region, and that transport from the edge of the complex-free zone to the interface is only in the form of molecular species. It is likely that a complex-free zone will also form in the PSS/C_{14}TAB and PSS/C_{16}TAB systems. In the following section we will explore whether the measured data is consistent with the formation of a complex free zone, and whether or not polymer and surfactant in the bulk solution can adsorb under diffusion control in the concentration region before bulk aggregation occurs.

7.3.2. Kinetic Adsorption Behaviour

I will now discuss and interpret the experimental data presented in the results section in light of what we know about the PSS/C_nTAB systems. First I will focus on the ellipsometry data as it is the most fine-grained of the experimental methodologies employed, and data have furthermore been recorded over the largest range of surfactant concentrations. However I will also discuss what the NR, compositional and LDV data can tell us.

At c_{surf} < 0.02 mM, the ellipsometry data in Figure 7.1 and Figure 7.2 are relatively independent of the surfactant chain length, with $\overline{\rho}$ very similar for all three data sets at the lowest concentrations measured. For all three systems, at the lowest c_{surf} values $\overline{\rho}$ is higher (corresponding to a lower total surface excess) for the mixture than for the pure surfactant, which exhibits negligible adsorption in this region. This, along with the fact that polymer is not surface active alone, leads us to conclude that synergistic adsorption enhances the surface excess of one or both components in this region.

In the surfactant concentration range between the cac and the estimated c_{comp} , the concentration of complexes in the bulk solution increases, as does their effect on the interfacial adsorption behaviour. Over this surfactant concentration range Γ_{poly} is identical for all three systems, the surfactant chain length has no observable effect on polymer adsorption. Polymer adsorption may therefore be controlled by the same mechanism in all three systems, the mass transport of free polymer molecules to the interfacial region. However, in Chapter 6 it was clear that polymer adsorption was not under diffusion control for any PSS/C_{12}TAB mixtures, polymer reached the sub-surface by mass transport but then could not adsorb at the interface. If we calculate the sub-surface polymer concentration for all three PSS/C_nTAB systems using $\Gamma = \sqrt{\frac{2D}{\pi\theta}}(c_b - c_s)$, the experimental Γ_{poly} data in Figure 7.6 and θ data in Figure 7.8 and the very similar D_{PS} values calculated above, very similar subsurface polymer concentrations, $c_{s,poly}$, values will be obtained for all three systems, as shown in Figure 7.9. Although $c_{s,poly} > 0$ at all bulk surfactant concentrations measured before aggregation occurs (c_{surf} < 0.4 mM), this does not necessarily mean that adsorption is not under diffusion control, as this can only be determined from comparison of c_s to c_{eq} for the same surface composition (data we do not have). However, the high values of $c_{s,poly}$ suggest that there may be a barrier to adsorption of polymer from the sub-surface to the interface.

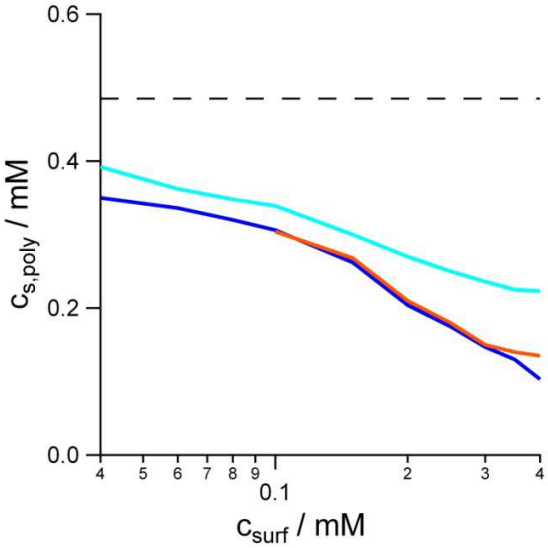

Figure 7.9. Calculated trends in the sub-surface concentration of polymer, $c_{s,poly}$, as a function of bulk surfactant concentration for PSS/C_{12}TAB (blue line), PSS/C_{14}TAB (turquoise line), and PSS/C_{16}TAB (orange line). The horizontal dashed line denotes the bulk polymer concentration.

What is most remarkable about the polymer surface excess in these systems is that it is essentially independent of the surfactant surface excess despite the fact that PSS is not surface active alone. Γ_{surf} varies with surfactant chain length but Γ_{poly} is almost identical for all three systems (Figure 7.6). At low bulk surfactant concentrations polymer is in excess in the bulk, and we would expect that although polymer can get to the sub-surface by diffusion it would not be able to adsorb as it is limited by interaction with adsorbed surfactant, and Γ_{surf} is low. This results in a high $c_{s,poly}$ at low c_{surf} (as seen in Figure 7.9). However, as c_{surf} and hence Γ_{surf} is increased we would expect Γ_{poly} to increase proportionally, and we do not observe this. Furthermore, if Γ_{poly} is controlled by Γ_{surf} we would expect there to be a difference in Γ_{poly} between the three systems even at low bulk surfactant concentrations, which we do not see.

To explain the adsorption behaviour of these systems at $c_{surf} < 0.4$ mM we first need to consider why Γ_{surf} for the mixtures on the OFC decreases with increasing surfactant chain length. In PSS/C_nTAB mixtures, the cac is low, so the majority of surfactant is in the form of polymer/surfactant complexes which consist of a single surfactant micelle and polymer molecule. The concentration of complexes at a given c_{surf} will decrease with increasing chain length due to the larger micellar aggregation number, but this would not affect Γ_{surf} if the complexes can get to the interface by diffusion as the amount of surfactant per complex is higher. The size and therefore the diffusion rate of these complexes varies

minimally with surfactant chain length, and it is therefore unexpected that Γ_{surf} is not more similar at a given c_{surf} for all three systems, as we assume that surfactant adsorption controlled by the mass transport of complexes. This could suggest that surfactant adsorption is not under complex mass transport control, perhaps due to the slow dissociation of complexes in the sub-surface region. Slow complex dissociation does not however explain the similar values of Γ_{poly} for the three systems.

At $c_{surf} < c_{comp}$ (0.4 mM) polymer is in excess in solution, and can reach the sub-surface in the form of molecules or complexes. At $c_{surf} > 0.1$ mM, the surface expansion rate increases sharply for all three systems, and Γ_{poly} increases a little, hence $\Gamma_{poly}\theta$ is increasing sharply as well. The combination of these factors suggests that polymer adsorption is controlled by the mass transport of free polymer in this region, and hence that it is not affected by the rate of complex breakdown, unlike surfactant adsorption.

Once $c_{surf} \approx c_{comp}$ (0.4 mM), we assume in our model that all of the polymer molecules are complexed to a single surfactant micelle, and there are no more free polymer molecules in the solution. In this region Γ_{surf} and Γ_{poly} are strikingly similar for all three systems (Figure 7.6). In this model polymer adsorption can no longer be controlled by the mass transport of free polymer, and both components must reach the interface in polymer/surfactant complexes. It is not clear if this supports the hypothesis of adsorption limited by the rate of complex breakdown, as in this case polymer adsorption is not more limited than it was when under polymer molecule diffusion control. However, the similarity of the data for the three systems suggests that once complex formation is complete the value of Γ_{surf} determines the polymer adsorption.

One final thing to note in the $c_{surf} < 0.4$ mM region is that Γ_{poly} does not reach either the maximum value predicted from diffusion control, or the lower maximum value measured at the static air water interface ≈ 3 μmol m^{-2} (as discussed in Chapter 6) for any of these systems, despite the fact that Γ_{surf} is close to the value at the static surface (2.5 μmol m^{-2}). Polymer adsorption cannot be sterically limited in this region, as the coverage of both components is significantly below the maximum possible value, and the high value of Γ_{surf} shows that Γ_{poly} cannot be limited by surfactant adsorption. Although repulsion between charged species at the interface and in the sub-layer could limit adsorption, this effect will be screened by the presence of electrolyte in these solutions. It is therefore not possible to conclude from the data what controls polymer adsorption in these systems at $c_{surf} < 0.4$ mM.

At 0.4 mM < c_{surf} < 0.6 mM time-dependent changes in the ellipsometry, NR, and LDV data indicative of decreases in the adsorbed amounts of both components, were recorded for PSS/C_{14}TAB and PSS/C_{16}TAB. In Chapter 6, similar time-dependent changes in the measured data were observed for the PSS/C_{12}TAB system at concentrations well above the estimated value of c_{comp}, and were attributed

to the aggregation of polymer/surfactant complexes in the bulk solution. For a polymer/surfactant solution at constant bulk composition the only way in which the adsorption of polymer and surfactant can decrease is if their mass transport rates are decreased due to the formation of large bulk species: aggregates. We therefore also attribute the time dependent changes in the data for the PSS/C_{14}TAB and PSS/C_{16}TAB systems to bulk aggregation processes. Aggregation occurs at bulk compositions around the charge neutrality point of the complexes.

For the PSS/C_{14}TAB and PSS/C_{16}TAB systems time dependent changes in the adsorption behaviour indicative of bulk phase aggregation occur at in the region c_{surf} = 0.4 - 0.6 mM, and in this region the solutions are turbid. Aggregation occurs very close to our estimated values of c_{comp}, the point at which we predict that every polymer molecule is associated with a surfactant micelle (0.39 mM and 0.47 mM for PSS/C_{14}TAB and PSS/C_{16}TAB respectively). From our calculated values of the aggregation numbers for C_{14}TAB and C_{16}TAB micelles in the presence of PSS, the complexes are not entirely neutral at our estimated c_{comp} values. However, when the surfactant concentration is increased above c_{comp} the surfactant chemical potential increases, increasing the size of the micelles in the polymer/surfactant complexes and neutralising the complex, leading to aggregation. As the cac for these systems is so low, only a small amount of surfactant has to be added above c_{comp} to have a big effect on the surfactant chemical potential, and hence aggregation will occur at surfactant concentrations close to c_{comp}. Small sequential additions of surfactant above c_{comp} will cause an increasing proportion of the complexes to become neutralised, hence the continued aggregation at several successive surfactant concentrations.

One problem arises with our interpretation however, as aggregation occurs in the PSS/C_{16}TAB system at $c_{surf} \approx 0.4$ mM, below the estimated c_{comp} value of 0.47 mM. A reasonable explanation for this is the uncertainty in our estimation of c_{comp}, arising from use of approximate N_{agg} values, and c_{comp} may instead occur at a surfactant concentration close to the start of aggregation. This is possible considering that literature values of the micellar aggreagation number of C_{16}TAB with PSS vary as low as 60 (rather than the highest value of 79 which was used), which would give a c_{comp} value of 0.35 mM. Furthermore, as mentioned above, the values of c_{comp} are only estimated from theoretical values rather than obtained from bulk measurements, which will inherently incur errors in the interpretation of a model based on these values.

Charged polymer/surfactant complexes may also be neutralised if the formation of small aggregates in solution, dimers and trimers etc is favoured and these species are stable. The concentration of these oligomeric complexes is in equilibrium with the monomeric polymer/surfactant complexes and is therefore very sensitive to the concentration of complexes in solution. Once there are enough of the

oligomeric complexes in solution, the growth of aggregates proceeds quickly. Without bulk studies to correspond with the conditions of our experiments we cannot dismiss this possibility, however it seems probable that in the PSS/C_{14}TAB and PSS/C_{16}TAB systems aggregation occurs due to the neutralisation of single polymer molecule/surfactant micelle complexes by the addition of further free surfactant.

In the PSS/C_{12}TAB system bulk phase separation does not occur in the region of c_{comp} (0.3 mM) as it does for PSS/C_{14}TAB and PSS/C_{16}TAB, it occurs at much higher bulk surfactant concentrations, around c_{surf} = 2 mM. This behaviour was discussed in Chapter 6, however I will discuss it again here for clear comparison with the other systems. If we consider the small value of the micellar aggregation number in the complex, which may in fact be considerably lower than our estimated value of 49 (as low as 30-40),[2] it is clear that at $c_{surf} \approx c_{comp}$ the PSS/C_{12}TAB complex is far from neutral. Recent bulk studies have shown that not only does aggregation not occur until around 2 mM (as in our measurements) the charge neutrality point is not reached in this system until very high surfactant concentrations, around 5 mM.[26] As discussed in Chapter 6, for aggregation not to occur until surfactant concentrations so far above c_{comp} the increase in the surfactant chemical potential above c_{comp} must not lead to neutralisation of the complexes until much higher surfactant concentrations, or alternatively bulk complexation must continue well past the estimated c_{comp} value, with aggregation occurring once the complexes become close to neutral.

Bulk aggregation is a dynamic process, occurring over a period of several hours, and at successive surfactant concentrations. Once aggregation is complete in all three systems there are no polymer/surfactant complexes or free polymer molecules remaining in the solution, they are all sequestered in aggregates which cannot diffuse to the interface on the timescale of the OFC due to their large size. Polymer therefore no longer adsorbs at the interface of the OFC (Figure 7.6). Γ_{surf} is also decreased by aggregation for the PSS/C_{14}TAB and PSS/C_{16}TAB systems as a significant proportion of the surfactant molecules in solution are also sequestered in aggregates, but not for the PSS/C_{12}TAB system as aggregation only occurs when the free surfactant concentration is high. For PSS/C_{14}TAB and PSS/C_{16}TAB, increasing c_{surf} past the point at which aggregation occurs only increases the free surfactant concentration and therefore Γ_{surf}. The difference in free surfactant concentrations in the aggregation region explains why aggregation has a minimal effect on θ of the PSS/C_{12}TAB system, but a significant effect on the other two systems in Figure 7.8, as aggregation removes a large proportion of the material which can supports Marangoni flows from the solution. If the LDV data were more extensive in the high surfactant concentration region it is possible that we would be able to estimate the

free surfactant concentration and hence the composition of the aggregates, however this is not possible with the current data.

As the formation of aggregates causes a decrease in the adsorbed amount of polymer and surfactant available for adsorption on the OFC, we would expect that it would have a similar effect on measurements performed at the static air/water interface unless the aggregates can reach the interface. The work of Monteux *et al*.[11] and Kristen *et al*.[14] did suggest that reduced adsorbed amounts in these systems at the static air water interface resulted from bulk aggregation. However, the work of Taylor *et al*. showed that multilayer adsorption occurs in the phase separation region for PSS/C_{12}TAB and PSS/C_{14}TAB but not for PSS/C_{16}TAB.[10] With reference to the recent work of Campbell *et al*. we suggest that the difference in their data could be attributed either to different transport of aggregates under gravity in the two systems,[17] or to an inconsistency in the way in which the samples are prepared for measurements on the three systems.[8, 16, 27] The controlled measurements at the static interface which would be necessary to test this hypothesis were not within the scope of this thesis, however we hope that they will be performed in the near future.

7.4. Conclusions

In mixtures of PSS and C_nTAB surfactants on the OFC, synergistic adsorption occurs at low to intermediate surfactant concentrations, where $c_{surf} < c_{comp}$, the point at which each polymer molecule is associated with a surfactant micelle. Polymer adsorbs at the air/water interface despite not being surface active alone due to interactions with surfactant at the interface. Despite this, the amount of polymer which adsorbs at the interface is independent of the surfactant surface surface excess. This is demonstrated by the independence of the polymer surface excess on the surfactant chain length despite the fact that the surfactant surface excess varies. Furthermore the maximum value of Γ_{poly} reached for the PSS/C_{14}TAB and PSS/C_{16}TAB systems is lower than both the diffusion controlled maximum value and that at the static interface. We therefore suggest that at surfactant concentrations below c_{comp} adsorption of polymer is controlled by that of free polymer molecules in the solution, whilst adsorption of surfactant, which is all in complexes, is limited by slow complex breakdown.

In all three PSS/C_nTAB systems aggregation of polymer/surfactant complexes occurs, and this leads to a depletion in the adsorbed amount of both components as a function of time. In the PSS/C_{14}TAB and

PSS/C_{16}TAB systems aggregation occurs close to the estimated value of c_{comp}, as large surfactant micelles are associated with each polymer molecule and the complex is almost neutral when c_{comp} is reached. Small increases in surfactant concentration above c_{comp} increase the surfactant chemical potential enough for the micelles to increase in size and the complexes to become neutralised, and hence aggregate. Alternatively, it may be that our estimated c_{comp} value is simply close to the neutralisation point for this system, at which complexation would naturally be complete and aggregation occur. Future complementary bulk measurements would enable us to determine the true bulk phase behaviour in this region. For the PSS/C_{12}TAB system charge neutrality is much further from c_{comp}, and bulk phase separation does not occur until surfactant concentrations nearly an order of magnitude above the estimated value of c_{comp}. We attribute this to the smaller micelle aggregation number in the PSS/C_{12}TAB complexes, which theoretically leaves the complexes far from neutral at our estimated value of c_{comp}, and aggregation would only be able to occur once the complexes could be neutralised. It may be that for this system complexation continues with increasing surfactant concentration well beyond the predicted c_{comp} value, and aggregation only occurs once the complexes are close to neutralised. For all three systems, at surfactant concentrations above the aggregation region, polymer no longer adsorbs as it is sequestered in aggregates, and increases in the surfactant concentration only increase the concentration of free surfactant molecules in solution, and therefore the surfactant surface excess.

The data presented in this chapter have shown that an understanding of the bulk phase behaviour is critical to understanding the adsorption from strongly interacting polymer/surfactant mixtures at a dynamic interface. This has wide ranging implications for mixtures of surfactants and polyelectrolytes which are used under dynamic conditions and for which bulk phase behaviour occurs.

7.5. References for Chapter 7

1. Zana, R., Ionization of Cationic Micelles - Effect of the Detergent Structure. *J. Colloid Interface Sci.* **1980,** 78, (2), 330-337.
2. Almgren, M.; Hansson, P.; Mukhtar, E.; Van Stam, J., Aggregation of alkyltrimethylammonium surfactants in aqueous poly(styrenesulfonate) solutions. *Langmuir* **1992,** 8, (10), 2405-2412.
3. Kogej, K.; Skerjanc, J., Fluorescence and conductivity studies of polyelectrolyte-induced aggregation of alkyltrimethylammonium bromides. *Langmuir* **1999,** 15, (12), 4251-4258.
4. Fundin, J.; Brown, W., Polymer/Surfactant Interactions - Sodium Poly(Styrenesulfonate) and Ctab Complex-Formation - Light-Scattering Measurements in Dilute Aqueous-Solution. *Macromolecules* **1994,** 27, (18), 5024-5031.
5. Chu, D. Y.; Thomas, J. K., Effect of Cationic Surfactants on the Conformational Transition of Poly(Methacrylic Acid). *Journal of the American Chemical Society* **1986,** 108, (20), 6270-6276.
6. Hansson, P.; Almgren, M., Interaction of Alkyltrimethylammonium Surfactants with Polyacrylate and Poly(Styrenesulfonate) in Aqueous-Solution - Phase-Behavior and Surfactant Aggregation Numbers. *Langmuir* **1994,** 10, (7), 2115-2124.
7. Thalberg, K.; Lindman, B.; Karlstrom, G., Phase-Behavior of Systems of Cationic Surfactant and Anionic Polyelectrolyte - Influence of Surfactant Chain-Length and Polyelectrolyte Molecular-Weight. *J. Phys. Chem.* **1991,** 95, (8), 3370-3376.
8. Pojjak, K.; Bertalanits, E.; Mészáros, R., Effect of Salt on the Equilibrium and Nonequilibrium Features of Polyelectrolyte/Surfactant Association. *Langmuir* **2011,** 27, (15), 9139-9147.
9. Estrela-Lopis, I.; Ramos, J. J. I.; Donath, E.; Moya, S. E., Spectroscopic Studies on the Competitive Interaction between Polystyrene Sodium Sulfonate with Polycations and the N-Tetradecyl Trimethyl Ammonium Bromide Surfactant. *Journal of Physical Chemistry B* **2010,** 114, (1), 84-91.
10. Taylor, D. J. F.; Thomas, R. K.; Li, P. X., Adsorption of oppositely charged polyelectrolyte/surfactant mixtures. Neutron reflection from alkyl trimethylammonium bromides and sodium poly(styrenesulfonate) at the air/water interface: The effect of surfactant chain length. *Langmuir* **2003,** 19, (9), 3712-3719.
11. Monteux, C.; Williams, C. E.; Bergeron, V., Interfacial microgels formed by oppositely charged polyelectrolytes and surfactants. Part 2. Influence of surfactant chain length and surfactant/polymer ratio. *Langmuir* **2004,** 20, (13), 5367-5374.
12. Taylor, D. J. F.; Thomas, R. K.; Penfold, J., Polymer/surfactant interactions at the air/water interface. *Adv. Coll. Int. Sci.* **2007,** 132, (2), 69-110.
13. Taylor, D. J. F.; Thomas, R. K., The adsorption of oppositely charged polyelectrolyte/surfactant mixtures: Neutron reflection from dodecyl trimethylammonium bromide and sodium poly(styrene sulfonate) at the air/water interface. *Langmuir* **2002,** 18, (12), 4748-4757.
14. Kristen, N.; Vullings, A.; Laschewsky, A.; Miller, R.; von Klitzing, R., Foam Films from Oppositely Charged Polyelectolyte/Surfactant Mixtures: Effect of Polyelectrolyte and Surfactant Hydrophobicity on Film Stability. *Langmuir* 26, (12), 9321-9327.
15. Simister, E. A.; Thomas, R. K.; Penfold, J.; Aveyard, R.; Binks, B. P.; Cooper, P.; Fletcher, P. D. I.; Lu, J. R.; Sokolowski, A., Comparison of Neutron Reflection and Surface-Tension Measurements of the Surface Excess of Tetradecyltrimethylammonium Bromide Layers at the Air-Water-Interface. *J. Phys. Chem.* **1992,** 96, (3), 1383-1388.
16. Campbell, R. A.; Yanez Arteta, M.; Angus-Smyth, A.; Nylander, T.; Varga, I., Effects of Bulk Colloidal Stability on Adsorption Layers of Poly(diallyldimethylammonium Chloride)/Sodium Dodecyl Sulfate at the Air/ater Interface Studied by Neutron Reflectometry. *J. Phys. Chem. B* **2011,** 115, (51), 15202-15213.

17. Campbell, R. A.; Angus-Smyth, A.; Arteta, M. Y.; Tonigold, K.; Nylander, T.; Varga, I., New Perspective on the Cliff Edge Peak in the Surface Tension of Oppositely Charged Polyelectrolyte/Surfactant Mixtures. *J. Phys. Chem. Letts.* **2010,** 1, (20), 3021-3026.
18. Valkovska, D. S.; Shearman, G. C.; Bain, C. D.; Darton, R. C.; Eastoe, J., Adsorption of ionic surfactants at an expanding air-water interface. *Langmuir* **2004,** 20, (11), 4436-4445.
19. Goddard, E. D., Ananthapadmanabhan K.P. Eds. , *Interactions of Surfactants with polymers and protein*. Bocan Rotan: CRC Press: 1993.
20. Imae, T.; Ikeda, S., Sphere-rod transition of micelles of tetradecyltrimethylammonium halides in aqueous sodium halide solutions and flexibility and entanglement of long rodlike micelles. *The Journal of Physical Chemistry* **1986,** 90, (21), 5216-5223.
21. Nause, R. G., Hoadland, D.A., Strey, H.H., Structural Evolution of Complexes of Poly(styrenesulfonate) and Cetyltrimethylammonium Chloride. *Macromolecules* **2008,** 41, 4012-4019.
22. Roelants, E., De Schryver, F.C. , Parameters Affecting Aqueous Micelles of CTAC, TTAC, and DTAC probed by fluorescence quenching. *Langmuir* **1986,** 3, 209-214.
23. Dubin, P. L.; Gruber, J. H.; Xia, J. L.; Zhang, H. W., The Effect of Cations on the Interaction between Dodecyl-Sulfate Micelles and Poly(Ethyleneoxide). *J. Colloid Interface Sci.* **1992,** 148, (1), 35-41.
24. Mandal, A. B., Self-diffusion studies on various micelles using ferrocene as electrochemical probe. *Langmuir* **1993,** 9, (7), 1932-1933.
25. Candau, S. J. H., E., Zana, R. , New Aspects of the behaviour of alkyltrimethylammonium bromide micelles: light scattering and viscosimetric studies. *J Physique* **1984,** 45, 1263-1270.
26. Varga, I., Personal Communication. In September 2012.
27. Campbell, R. A., Personal Correspondance. In August 2012.

Chapter 8: Mixtures of Poly(ethylene imine) and SDS at High and Low pH

8.1 Introduction

Poly(ethylene imine) [PEI] is a widely studied polymer due to its use in a range of industrial applications including the cosmetics, paper, mining, and pharmaceutical industries.[1] PEI is an interesting polymer in that its charge density can be controlled by varying the solution pH; at low pH PEI has a high charge density, whilst at high pH it has a low charge density.[2, 3] This ability to vary the polymer charge density means that mixtures of poly(ethylene imine) [PEI] and sodium dodecyl sulfate (SDS) have been widely studied, as they can be used to examine the effects of both electrostatic and hydrophobic interactions between the polymer and surfactant on the behaviour of the system. Mixtures containing PEI are also interesting for several other reasons; first the polymer architecture can be easily varied,[2, 3] second the polymer molecular weight affects the physical properties,[4] and a large range of molecular weights are commercially available, and third, ionic strength is known to affect the behaviour of the mixture.[4]

PEI forms complexes with SDS at both low and high solution pHs, despite the fact that it has a low charge density at high pH. The mechanism of binding in PEI/SDS complexes has been the subject of numerous recent studies, primarily using indirect methods. SDS has been shown to have a large binding affinity for PEI regardless of the solution pH.[5] Furthermore, the process of PEI/SDS complexation itself causes a change in the solution pH due to the release of OH^- ions[6, 7] Winnick *et al*. proposed a thermodynamic model to describe the variation of pH with SDS concentration at a fixed PEI concentration, which takes into account the positive feedback of binding on the protonation equilibrium of the amine groups,[8] and also rationalizes the high binding capacity of PEI at high pH, which is similar to the value at lower pH.[7]

Li *et al*. proposed a two-step mechanism for PEI/SDS binding in the bulk solution with changing bulk surfactant concentration, consisting of monomer binding at low surfactant concentrations followed by cooperative binding of micelle-like surfactant aggregates with increasing bulk surfactant concentration.[5] Mészáros *et al*. proposed a more involved two-step mechanism based on a thermodynamic model, which occurs for PEI/SDS regardless of the solution pH,[8, 9] At low surfactant concentrations, SDS monomers bind to PEI forming PEI/SDS complexes, and the system is a thermodynamically stable solution of the polymer/surfactant complexes. Once a threshold amount of surfactant has bound, these complexes collapse and a kinetically unstable dispersion of complexes is

formed. These complexes can coagulaulate as the electric potential of the particles is too small to stabilize the dispersion in this concentration region. At a given polymer concentration the critical surfactant concentration for coagulation increases with decreasing solution pH, due to the greater charge density of PEI at low pH. As the surfactant concentration is further increased adsorption of SDS onto the outside of the collapsed PEI/SDS particles leads to charge reversal. This phase can be considered as a stable colloidal dispersion of collapsed PEI/SDS particles.[10]

Mészáros *et al*. have demonstrated that the formation of polymer/surfactant aggregates is not an equilibrium process, and that the mixing methodology employed can determine the bulk phase behaviour at low pH but not at high pH.[11] At surfactant concentrations well below the two-phase region, Meszaros *et al*. demonstrated that kinetically trapped aggregates can be formed according to the mixing methodology used, but only to a significant extent in PEI/SDS mixtures at low pH.[10-12] This aggregation of complexes before the two-phase region (i.e. at low surfactant concentrations) was shown to be most likely when the protonation degree of the PEI molecules is high (low pH) and when the net charge of the primary complexes is low due to strong electrostatic interactions with the surfactant. The effects of mixing can be understood in terms of the local rate of coagulation of the polymer/surfactant particles, which is related to concentration gradients present during mixing.[10,13] Furthermore, the surfactant concentration range over which the two-phase region occurs depends on the concentration of added electrolyte, which decreases the stability of charge-stabilized complexes and enhances coagulation.[10]

Characterisation of the size and form of the PEI/SDS complexes has shown that their hydrodynamic radius is largely independent of the solution pH, but it can be controlled by the mixing methodology to a significant extent at low solution pH.[11] Despite this, binding isotherm measurements have shown that more surfactant is bound to each polymer molecule at low pH, as we would expect for polymer molecules with a higher charge density.[9] Bastardo *et al*. examined the size and shape of the PEI/SDS complexes at both high and low pHs using a combination of SAXS and SANS.[14, 15] They found that PEI molecules adopt elongated flat ellipsoid structures in solution, to which SDS binds without changing the molecular conformation of the PEI . With increasing surfactant concentration these complexes stack on top of each other to form aggregates. At low pH the internal structure of the aggregates is ordered, whereas at high pH it is not.

Penfold *et al*. have studied the adsorption from PEI/SDS mixtures at the air/water interface using NR meausurements. They showed that adsorption is most pronounced at high pH, with Bragg diffraction peaks indicating interfacial multilayers observed, especially in the region of charge neutralisation, whilst at low pH only monolayer adsorption was observed.[2, 4] Multilayers at high pH were initially

attributed to hydrophobic interactions between the two species at the interface, but were subsequently attributed to the combined effect of a dipole-dipole interaction between the surfactant headgroup and the charged nitrogens and a co-operative interaction between the chains of the attached surfactants.[16] Surface tension measurements in the same studies revealed a 'cliff edge peak' in the data at low solution pH, whilst at high pH the data resembled that of a weakly interacting polymer/surfactant mixture. The same studies showed that adsorption from PEI/SDS mixtures was strongly dependent on polymer architecture,[2] polymer molecular weight,[2, 4] and the ionic strength of the bulk solution.[4] Interfacial multilayers were favored by use of the hyperbranched polymer of low molecular weight in solutions with added inert electrolyte.

Although both the bulk phase behavior and the interfacial properties of PEI/SDS mixtures have been extensively studied, few authors have made systematic connections between the two. The only study which has examined the connection between bulk and interfacial behaviour is that of Tonigold *et al*.[17] who investigated the effects of bulk aggregates on adsorption layers at the air/water interface with respect to the solution pH and the sample history using ellipsometry. They observed both a high interfacial excess and significant fluctuations in the optical signal for the system at high pH, both of which were attributed to the presence of bulk aggregates in the adsorption layer. These aggregates were shown to have originated from the bulk solution, as filtration of the sample caused the fluctuations to disappear initially, although they later reappeared. At low pH, no such aggregates were present at the interface after the interface was cleaned to remove aggregates trapped at the interface during sample preparation and handling, which showed that the aggregates do not adsorb spontaneously at low pH. The presence of bulk aggregates at the interface at high pH, but not at low pH for aspirated samples, was attributed to the lower surface charge density of the aggregates at high pH, and the consequent decreased repulsion between the aggregates and the interface. It should be noted that this bulk study of Tonigold *et al*. was performed using significantly higher polymer molecular weights than in the work of Penfold *et al*.

If we consider the recent work of Campbell *et al*. relating the bulk and interfacial behaviour of the Pdmdaac/SDS system,[18-20] we can begin to hypothesise how the formation of bulk phase aggregates in a polymer/surfactant system such as PEI/SDS may affect adsorption. Campbell *et al*. demonstrated that the surface tension[18] and surface excess[19] of well-equilibrated samples depended on how the samples were handled, due to the redispersion of kinetically-trapped aggregates. Furthermore, they went on to show that interfacial multilayers at the static air/liquid and solid/liquid interfaces originate not from a self-assembly process at the interface itself but from the transport of bulk aggregates to the interface under gravity.[20] Conversely, if aggregates are transported away from an interface of given orientation also under gravity then interfacial multilayers were absent.

In this chapter I will examine how the bulk phase behaviour of PEI/SDS mixtures at both high and low pHs affects the dynamic surface excess of the PEI/SDS system at the air/water interface, using the steady-state expanding interface of the OFC. Once we understand how the bulk aggregates present in the phase separation region of these systems affect the dynamic surface excess we can begin to further explain the adsorption behaviour previously observed at static air/water interfaces. As in the previous chapters a combination of ellipsometry and NR data will be presented in order to discuss the changing interfacial compositions of mixtures of PEI and SDS. Measurements have been made at two extreme solution pHs, pH 10 where PEI is 5% charged, and pH 4 where around 67% of the polymer monomers are charged, in order to determine the effect of polymer charge on the adsorption behaviour at the dynamic interface. It will become clear from the discussions in this chapter that the dynamic adsorption behaviour of PEI/SDS mixtures is very different at pH 4 and pH 10, and the reasons for this will be explored.

The format of this chapter is slightly different to those which preceed it, as it is divided into two sections in which the behaviour of PEI/SDS mixtures are examined at the two different solution pHs, with the results and discussion of each system presented in the relevant section. PEI/SDS mixtures at both pHs have been examined using both NR and ellipsometry measurements, for measurements made at pH 10 interfacial compositions are obtained from these measurements using our comodelling approach, whilst at pH 4 unusual ellipsometry data precluded use of our co-modelling methodology. As a consequence, the focus for the pH 4 systems is on determining the physical reason for these data.

Materials

As previously, all of the measurements in this chapter were recorded on solutions prepared in ultrapure water (Milli-Q; resistivity = 18 MΩ cm) for ellipsometry, or NRW for NR meausurements, and all experimental equipment was cleaned with a 2 % solution of a strong alkaline detergent (Decon 90 or Gigapur). Hydrogenated SDS (Sigma, 99%) was purified by re-crystallization three times from ethanol. PEI (750k molecular weight, Sigma) was used as supplied. This polymer molecular weight was chosen in order to relate our data most easily to those of other studies which have used similar molecular weights.[10, 11, 14, 15, 17] Chain deuterated d-SDS was kindly supplied by Dr R. K. Thomas from the Oxford Deuteration Facility.[21] 0.1 M NaCl (Sigma Aldrich) was used in all measurements.

As a consequence of the documented effects of the mixing methodology on the phase behaviour of the system[11] and the interfacial properties,[17] these systems were not recorded by adding consecutive aquilots of surfactant to the polymer solution as in two previous chapters. Instead each solution was

freshly prepared using a standard mixing approach.[17] Equal quantities (750 ml) of polymer and surfactant at double their intended measurement concentration were poured quickly into an empty beaker, resulting in a total solution volume of 1.5 l. The solution was then immediately added to the empty OFC system and measured. The maximum delay time between mixing the components and starting the measurements was around one minute for ellipsometry measurements and 4 minutes for NR measurements. Measurements were made over short time periods (not longer than 30 minutes) at pH 10, as the alkaline solutions were found to change in pH with time due to the adsorption of carbon dioxide from the atmosphere.[22] As the pH of the solution decreases, so does the charge density of PEI and the strength of the polymer/surfactant interaction, which will affect the interfacial excess measured by both NR and ellipsometry. During the 30 minute measurement time, the change in pH is < 0.4.

All ellipsometry measurements presented in this chapter were recorded on a 1 s timebase rather than the 5 s timebase used elsewhere in this thesis due to the interesting nature of the data recorded. The optical density (OD) at 450 nm of PEI/SDS/NaCl/H_2O solutions was measured using a Jasco V-630 spectrophotometer in a quartz cell with a 10-mm path length to determine the sample turbidity. As neither the polymer nor the surfactant has an adsorption band above 350 nm, the optical density gives a measure of the quantity and density of the aggregates suspended in the solution.

8.2. PEI/SDS at pH 10

At high pH, previous studies at static air/water interfaces observed thick adsorbed layers[2, 4] or layers containing embedded aggregates[17] in or close to the phase separation region. Using the OFC we can build on the work of Tonigold *et al.*[17] to further elucidate the effects of aggregate formation in the phase separation on dynamic adsorption at the interface, and hence to determine the mechanism by which large adsorbed amounts can reach the static interface. Before starting this discussion it is important to note that under the conditions used in this experiment PEI is not surface active alone, as determined by independent ellipsometry measurements.

Figure 8.3 (a) plots $\sigma \times \tau$ as a function of time for five h-PEI/d-SDS/NRW solutions with different bulk surfactant concentrations. $\sigma \times \tau$ is obtained from fits to the recorded specular reflectivity profile using a single layer model, as discussed in Chapter 4. As the scattering length of the deuterated surfactant (2.76×10^{-3} Å) is much higher than that of a PEI segment (3.76×10^{-5} Å), NR measurements in null-reflecting water are most sensitive to the surface excess of the deuterated surfactant. The increase of $\sigma \times \tau$ with c_{surf} (except at the highest concentration measured) therefore tells us that the surfactant surface

excess also increases with c_{surf}. However, the values of $\sigma \times \tau$ for the mixture bare no clear relationship to those for of the pure surfactant (marked as coloured dashes next to the y-axis), with $\sigma \times \tau$ for the mixture greater than the pure surfactant at the lowest c_{surf} and lower at the highest c_{surf}. Adsorption is not occurring as in a pure surfactant solution.

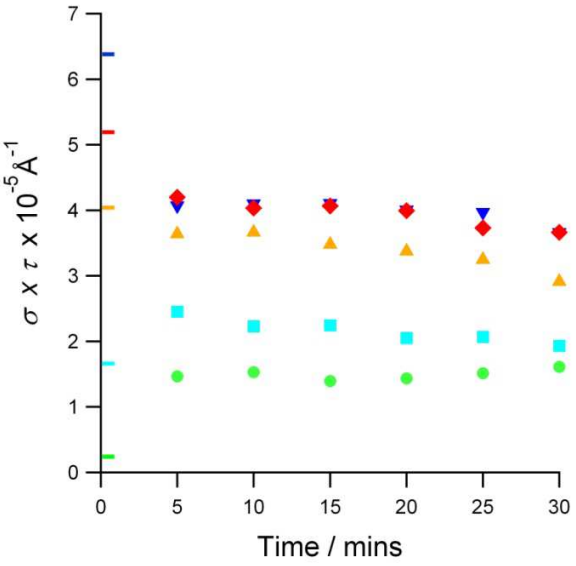

Figure 8.1. Product of the scattering length density and thickness of the adsorbed layer, $\sigma \times \tau$, obtained from fitting specular reflectivity profiles obtained during NR experiments to a single layer model. Data were recorded as a function of time and measurements were made at SDS concentrations of 0.05 mM (green circles), 0.1 mM (turquoise squares) , 0.32 mM (yellow triangles) , 0.56 mM (red diamonds) and 1 mM (blue inverted triangles) with 100 ppm PEI and 0.1 M NaCl at pH 10 in the OFC. The dashed markers down the y-axis denote the value of $\sigma \times \tau$ for pure SDS and 0.1 M NaCl at the same concentrations.

The specular reflectivity profiles for these PEI/SDS systems at pH 10 do not exhibit Bragg peaks indicative of multilayer adsorption on the OFC or at the static air/water interface of an adsorption trough as shown in Figure. 8.2. These data are in keeping with the findings of Penfold *et al*. who showed that multilayer formation is more pronounced with polymers of low molecular weight,[2, 4] and with the results of Bastardo, who found that PEI/SDS aggregates did not have an ordered structure at high pH. These data confirm that the scope of this investigation concerns the effects of bulk aggregates on the interfacial properties rather than the reasons for multilayer formation.

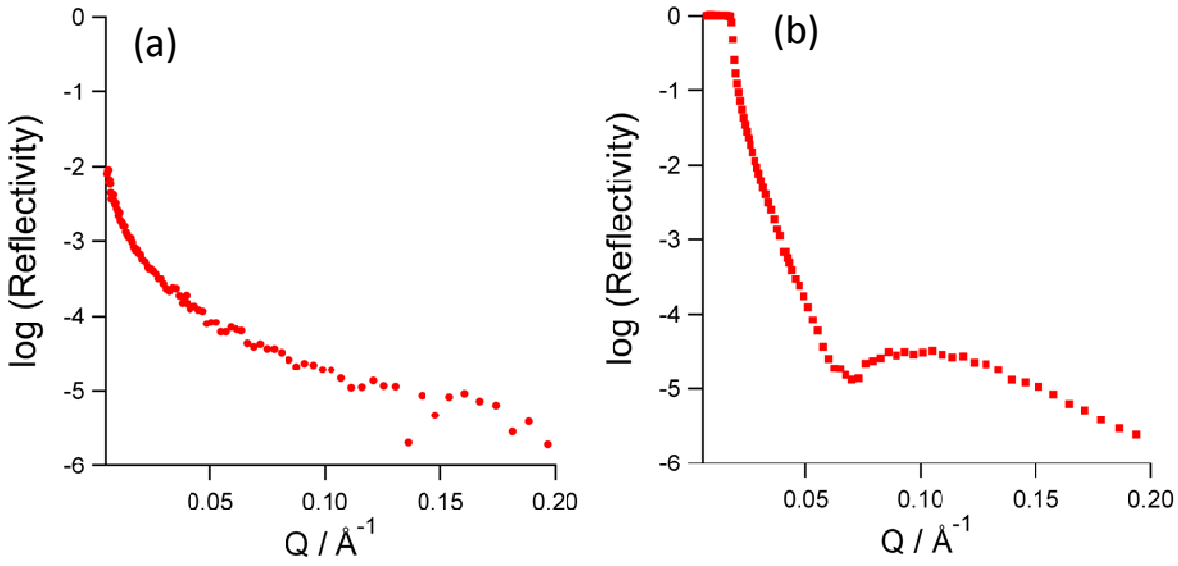

Figure. 8.2. Specular neutron reflectivity profiles recorded on PEI/SDS at pH 10 at both the dynamic and static air/water interfaces. (a) is data recorded on the OFC where the concentration of SDS is 0.56 mM and the isotopic contrast is h-polymer/d-surfactant/NRW,and (b) is data recorded at the static interface where the concentration of SDS is 0.66 mM and the isotopic contrast is h-polymer/h-surfactant/D_2O. The data in (b) was kindly donated by R. Campbell and I. Varga.

Ellipsometry data recorded on five solutions with the same bulk compositions as those measured using NR are shown in Figure 8.3. Recall that for a single component solution such as a pure surfactant a more negative ellipticity is equivalent to a greater adsorbed amount at the interface. For a mixture such as PEI/SDS the sensitivity of ellipsometry to the adsorption of the two components is similar (see Chapter 4) and a more negative value of the ellipticity can only be attributed to a change in the total adsorbed amount (Γ_{tot}). The ellipsometry data in Figure 8.3 suggests that Γ_{tot} remains relatively constant compared to the change in Γ_{surf} indicted by Figure 8.1, until high surfactant concentrations where Γ_{surf} no longer increases and $\bar{\rho}$ becomes less negative. Furthermore, $\bar{\rho}$ is significantly more negative than the equivalent pure surfactant value or the monolayer value (close to the blue dash) at all but the highest concentrations measured, indicating the adsorption of a significant amount of polymer or more than a monolayer of surfactant. The latter possibility can be discounted by reference to Figure 8.1, therefore there must be a significant amount of polymer adsorbed at the interface.

The ellipsometry data for all of the solutions shown in Figure 8.3 exhibit both spikes and drifts in the $\bar{\rho}$ values. The spikes are likely to originate from large polymer/surfactant aggregates passing through the refracted laser beam. Drifts with time, also seen in the $\sigma \times \tau$ data from NR in Figure 8.1, are probably due to small changes in pH of the solution due to CO_2 absorption.

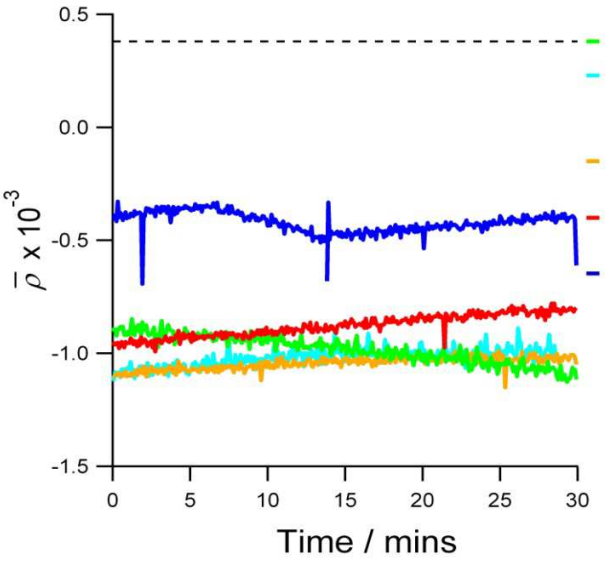

Figure 8.3. Ellipticity, $\bar{\rho}$, recorded as a function of time for five PEI/SDS solutions with identical compositions to those measured using NR in Figure 8.1. These are SDS concentrations of 0.05 mM (green), 0.1 mM (turquoise) , 0.32 mM (yellow) , 0.56 mM (red) and 1 mM (blue) with 100 ppm PEI and 0.1 M NaCl at pH 10 in the OFC. The black dashed line indicates the ellipticity of pure water or of PEI and NaCl, which has the same ellipticity. The coloured dashes down the right hand side of the figure show the ellipticities of pure SDS solutions containing the same concentrations of SDS.

The interfacial compositions of PEI/SDS solutions on the OFC, calculated by co-modelling the NR and ellipsometry data from Figure 8.1 and Figure 8.3 using the approach discussed in Chapter 4, are shown in Figure 8.4 (a), along with the data for pure SDS. Γ_{poly} is highest at the lowest c_{surf} despite the lack of inherent surface activity of the polymer, which implies that polymer is present at the interface solely due to its interaction with adsorbed surfactant. From Figure 8.4 (a), there appear to be two distinct regions of behaviour with a transition between 0.32 and 0.5 mM. At low c_{surf} the total surface excess is constant and the surfactant excess is increasing, whilst the polymer excess decreases slightly. At higher c_{surf}, the surfactant excess is constant and the polymer excess is decreasing.

The optical density of the samples in Figure 8.4 (b) also undergoes a transition at intermediate surfactant concentrations from clear to turbid samples, as marked by the vertical dashed line. Changes in the optical density of the solution are indicative of changes in the bulk phase behaviour, and increasing optical density is indicative of aggregation in the bulk phase. On the right side of the boundary the polymer/surfactant complexes have aggregated either during mixing because of the local concentration gradients generated, or they have a lack of colloidal stability due to their low surface charge. This vertical line is extended upwards into Figure 8.4 (a) where it appears to mark the transition between the two distinct regions of adsorption behaviour mentioned above.

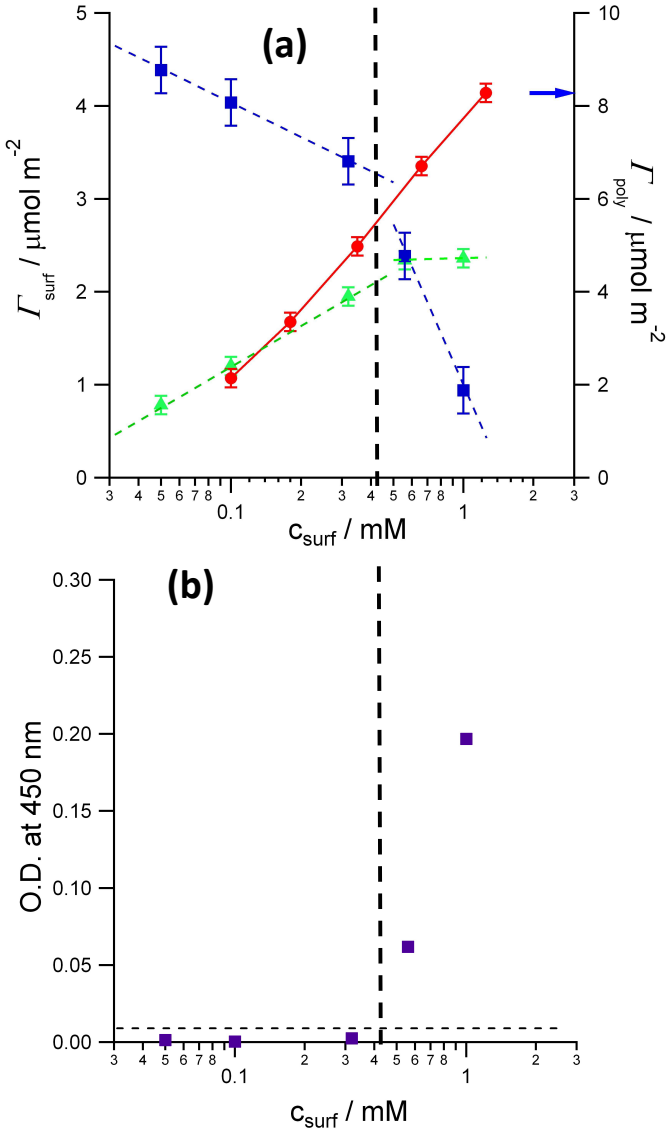

Figure 8.4 . (a) Surface excesses of pure SDS (red squares), SDS in a mixture with PEI at pH 10 (green triangles) and PEI in the same mixture (blue squares) and **(b)** Optical density at 450 nm of several mixtures of PEI/SDS at pH 10. In panel (a) the red line serves simply as a guide to the eye, the blue arrow on the right hand side denotes $\Gamma_{poly,max}$ adsorbed under diffusion control, and the vertical dashed line denotes the point at which turbidity increases above 0.01 .

At the lowest c_{surf} values, polymer adsorbs at close to its estimated diffusion controlled limit, as denoted by the blue arrow in Figure 8.4 (a). This estimate of the maximum possible amount of PEI which can adsorb under diffusion control is obtained (as previously) from $\Gamma = \sqrt{\frac{2D}{\pi\theta}}(c - c_s)$ in the situation where c_s, the subsurface polymer concentration is zero, and at low c_{surf} values θ is estimated to be close to the pure water value of 0.5 s^{-1}. The diffusion coefficient is estimated to be $D = 1 \times 10^{-11}$ m^2s^{-1} from the hydrodynamic radius reported by Mezei *et al.*[10, 11] and the stokes Einstein equation

($D = k_B T/6\pi\eta R_G$ where k_B is the Boltzmann constant, T is the temperature, and η is the solution viscosity).

As c_{surf} is increased below the vertical dashed line in Figure 8.4, Γ_{poly} decreases below the maximum value it can reach under diffusion control. A decrease in polymer adsorption with increasing surfactant coverage was observed for the weakly interacting systems PEO/C_{14}TAB and PEO/SDS on the OFC in Chapter 5, and was attributed to competitive adsorption of the two components at the air/water interface.[23] In a competitive adsorption model, inhibition of the adsorption of one component coincides with increased adsorption of the other. However, it is probable that the decrease in Γ_{poly} in this region is simply due to increases in the surface expansion rate with increasing surfactant adsorption. The progressive formation of polymer/surfactant complexes in the bulk solution in this region (before the phase boundary) will decrease the chemical potential of the polymer, reducing the driving force for it to adsorb to the surfactant monolayer. This will result in an increased subsurface polymer concentration, which from the equation above will decrease the polymer surface excess.

As c_{surf} is increased further between 0.3 and 1 mM SDS Γ_{poly} drops steeply, from 7.3 to 2.5 μmol m^{-2}. This drop in polymer adsorption occurs when c_{surrf} is in the region of the vertical dashed line in Figure 8.4. If we consider that at pH 10 around 6% of the PEI monomers are charged, this equates to around 0.14 mM of charged monomers for a 100 ppm solution. At c_{surf} values slightly above 0.14 mM, charge equivalence, we would expect that PEI/SDS complex formation will be complete, however the measured charge neutralisation point will be at a slightly higher c_{surf} due to co-operative binding in this system. Further surfactant added to the bulk solution once complex formation is complete will be in the form of free surfactants (as seen for other systems in Chapters 6 and 7). From the work of Meszaros *et al*. we would expect that aggregation of complexes would occur once complexation is complete due to the formation of an unstable colloidal dispersion of particles.[8, 10-12] We therefore attribute both the sharp drop in Γ_{poly} and the simultaneous increase in turbidity of the system at intermediate c_{surf} values to the formation of polymer/surfactant aggregates in the bulk solution which cannot diffuse to the interface of the OFC on the timescale of surface expansion.

In the same c_{surf} region as the sharp decrease in Γ_{poly} (between 0.3 and 1 mM SDS), the change in Γ_{surf} is small, increasing from 2.0 to 2.4 μmol m^{-2}, whilst the surface excess of the pure surfactant almost doubles. Bulk aggregation of polymer/surfactant complexes will remove surfactant from the liquid phase, hence we would expect Γ_{surf} to decrease in the aggregation region. However, the concentration of free surfactant molecules in solution will increase with c_{surf} once complexation is complete, and this will increase the amount of surfactant which can adsorb at the interface. From Figure 8.4 it appears that these two effects effectively cancel each other out, and the surfactant surface excess stays relatively

constant. Furthermore, the surface expansion rate (for which we do not have data) will change in this region due to the aggregation of complexes, which will also affect Γ_{surf}. Although the effects of bulk phase aggregation dominate the adsorption behaviour in this region, we do not observe a simple correlation between aggregate formation and Γ_{surf}.

Formation of large bulk phase aggregates in mixtures of PEI and SDS at pH 10 limits the amount of both polymer and surfactant which can adsorb at the interface of the OFC in the phase separation region, although free surfactant adsorption can also occur. Tonigold *et al*. showed that these bulk phase aggregates can reach the static air/water interface,[17] which we would not necessarily expect from our data on the OFC, as aggregates on the nm scale would not be expected to adsorb to an expanding liquid interface on the sub-second timescale of the OFC due to their slow diffusion to the subsurface. If we consider the recent work of Campbell *et al*. however,[20] it is possible that the bulk phase aggregates may reach the static air/water interface due to transport under gravity, i.e. they are less dense than the solution. Examination of the adsorption of PEI and SDS at the static interface is outside the remit of the work performed in this thesis, however the hypothesis of aggregates which deplete the system of polymer/surfactant complexes but can float to the static air/water interface could explain both our data on the OFC and those of Tonigold *et al*.[17] and Penfold *et al*.[2, 4] at the static air/water interface, and this is currently under investigation by Campbell and Varga.

8.3. PEI/SDS at pH 4

For PEI/SDS mixtures at low pH, the proportion of protonated amine groups is much greater than at high pH (an increase in charge density from 5% to 68% from pH 10 to pH 4),[14] resulting in a stronger electrostatic interaction between PEI and SDS. A stronger interaction causes more surfactant to bind to the polymer, and increases the favourability of aggregate formation even in the pre-precipitation region when gentle mixing methodologies are employed.[10, 11] At the static air/water interface, lower adsorbed amounts were observed at low pH than at high pH.[2, 4, 17] If we link together the increased favourability of aggregation and the lower adsorbed amounts at the static interface we would expect to see that the formation of bulk aggregates limits the adsorbed amount on the OFC to a greater extent at pH 4 than at pH 10, unless another adsorption mechanism is in action.

Turbidity measurements in Figure 8.6 (a) show that at pH 4 the solution becomes turbid at lower c_{surf} values than at pH 10 (0.2 mM and 0.5 mM respectively); bulk aggregation occurs at lower surfactant

concentrations. Figure 8.6 (b) shows the $\sigma \times \tau$ values obtained from NR data for several PEI/SDS mixtures at pH 4. For all of the solutions measured, $\sigma \times \tau$ decreases with time despite the fact that CO_2 has no effect on the polyelectrolyte charge density at pH 4 and therefore cannot be responsible for the time dependence. This situation is quite different to the almost constant values of $\sigma \times \tau$ recorded at pH 10 (Figure 8.4). On the OFC, with a steady state expanding interface of < 1 s, changes in the adsorbed amount as a function of time must be attributed to changes in the bulk solution, as we have seen previously for the PSS/C_nTAB systems in Chapters 6 and 7. As discussed above, the negligible neutron scattering length density of PEI compared to d-SDS means that to a first approximation $\sigma \times \tau$ can be assumed to represent the surfactant surface excess. We therefore conclude from Figure 8.6 that Γ_{surf} decreases as a function of time for all of the compositions measured. The most logical explanation is that Γ_{surf} decreases due to the slow formation of bulk aggregates which cannot adsorb at the interface on the OFC timescale.

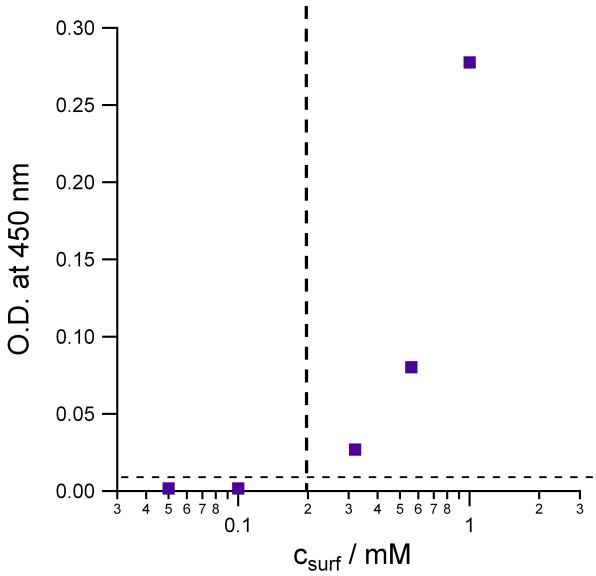

Figure 8.5. Optical density at 450 nm of PEI/SDS at pH 4 as a function of surfactant concentration recorded immediately after mixing. The vertical dashed line denotes the point at which turbidity increases above 0.01.

If we consider the turbidity and $\sigma \times \tau$ data together it becomes clear that time dependence in $\sigma \times \tau$ is seen even when the solution is clear, which is outside the equilibrium phase separation region hence in an equilibration context we would expect no aggregation to occur. However, previous studies have shown that kinetically trapped aggregates can form even outside the phase separation region in PEI/SDS mixtures at pH 4 due to the concentration gradients present during mixing.[10, 11, 17] Furthermore, the formation of such kinetically trapped aggregates is favoured when gentle mixing is used, as it is here.[11] The flow system of the OFC continuously gently stirs the solution, and this may lead to the kinetically trapped aggregates formed on mixing acting as nucleation sites for further

aggregation under non-equilibrium flow conditions. The resulting loss of small bulk complexes into large aggregates may explain the reduction in Γ_{surf} with time due to the slow diffusion of large aggregates.

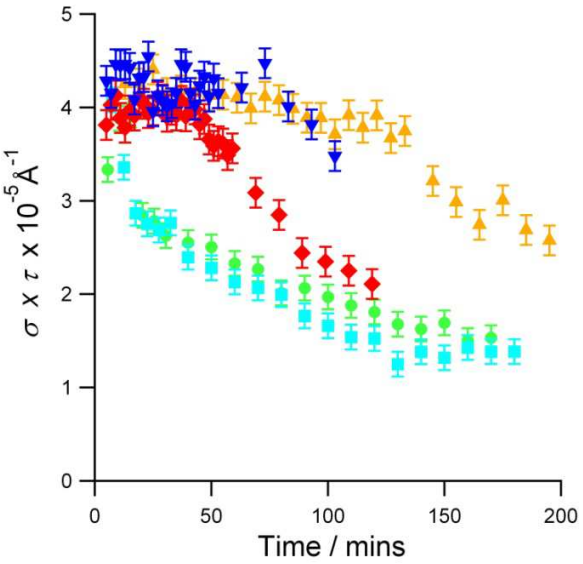

Figure 8.6. NR data (shown as the fitted quantity $\sigma x \tau$) as a function of time for 0.05 mM (green), 0.1 mM (turquoise) , 0.32 mM (yellow) , 0.56 mM (red) and 1 mM (blue) SDS with 100 ppm PEI and 0.1 M NaCl at pH 4.

The rate of decrease in $\sigma \times \tau$ due to time dependent aggregation varies with the bulk surfactant concentration as shown in Figure 8.6. As aggregation progresses, the concentration of surface active species will decrease, which will in turn affect the aggregation rate. At low bulk surfactant concentrations the decrease in Γ_{surf} due to bulk aggregation is observed immediately as the remaining concentration of free surfactant in the system is not sufficient to maintain Γ_{surf} at the same value. At high surfactant concentrations, there is a time-lag before the start of the reduction in $\sigma \times \tau$ as the interface is initially saturated with surface-active material; the surface excess remains constant until the bulk solution becomes sufficiently depleted of monomers and small complexes that adsorption becomes diffusion-limited.

In Chapters 6 and 7 for PSS/C_nTAB mixtures bulk aggregation led to decreased adsorbed amounts of both components (unless the concentration of free surfactant was high). In order to determine the effect of aggregation on interfacial adsorption for PEI/SDS at pH 4 we initially sought to co-model the NR and ellipsometry data (Figure 8.6 and Figure 8.7 respectively). However, in contrast to all of the ellipsometry data presented in this thesis up to this point, the ellipsometry data recorded on PEI/SDS at pH 4 fluctuate wildly and do not approach a steady-state even after several hours, as shown in Figure 8.7. It is clear from the high standard deviation of these data that it would be quite impractical to

proceed with our co-modelling approach to determine the composition of the adsorbed layer. The ellipsometry data would need to be averaged in order to do so, and the method used to average the data would be arbitrary in the absence of a physical understanding of the processes occurring. Furthermore, NR and ellipsometry measurements on these systems are likely to have different sensitivities to the material at the interface if bulk aggregates are present in the interfacial layer, due to the fact that their diameter is much greater than the thin film limit, and co-modelling the data does not take this into account. Consequently, we will not attempt to co-model the data in Figure 8.6 and Figure 8.7, however instead we will undertake a thorough investigation of the reasons for the fluctuations in the ellipsometry data.

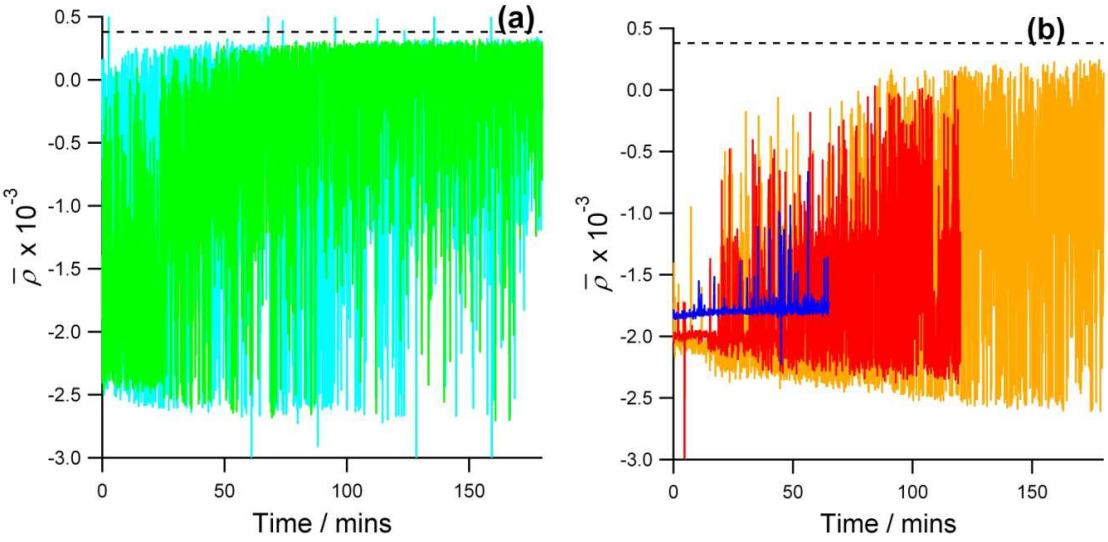

Figure 8.7. Ellipticity, $\bar{\rho}$, of PEI/SDS at pH 4 at (a) 0.05 mM (turquoise) and 0.1 mM (green) and (b) 0.32 mM (purple), 0.56 mM (red) and 1 mM (blue) SDS. All measurements made in the presence of 0.1 M NaCl and shown in two separate panels for clarity.

The first important point to notice about the fluctuations in the ellipsometry data in Figure 8.7 is that they occur within well defined upper and lower limits. The lower coverage bound is close but not equal to zero, indicative of an almost but not quite bare surface. A low concentration of free molecules could account for this value. The upper coverage limit in $\bar{\rho}$ of around -2.5 x 10^{-3} is much higher than that corresponding to an SDS monolayer, $\bar{\rho} \approx$ -0.8 x 10^{-3}, suggestive of a large total adsorbed amount including polymer at the interface.

In order to compare this value with the data of Tonigold *et al.*,[17] who's ellipsometry data were constant over a wide range of c_{surf} for this system, we first need to convert the measured values of Δ from the work of Tonigold *et al.* to values of $\bar{\rho}$. As the values of Ψ are not given in the work of Tonigold *et al.* due to the insensitivity of the parameter at the air/water interface we cannot use the equation $\bar{\rho} =$

$tan\Psi sin\Delta$ to obtain Δ. Instead we can convert Δ to η, the ellipsometric thickness using the following relationships,[24]

$$\delta\Delta = g(\varphi)\frac{\eta}{\lambda} \tag{8.1}$$

Where $g(\varphi)$ is a function which depends only on the bulk properties (the refractive indices of air, 1, and water, 1.33) and the angle of incidence of the ellipsometry measurements φ = 53.1°

$$g(\varphi) = \frac{4\pi n_{air} {n_{soln}}^2 cos\varphi sin^2\varphi}{({n_{soln}}^2 - {n_{air}}^2)[({n_{soln}}^2 + {n_{air}}^2)cos^2\varphi - {n_{air}}^2]} \tag{8.2}$$

η is then converted into $\bar{\rho}$ using Equation 2.19, repeated here for clarity:

$$\bar{\rho} = \frac{\pi}{\lambda}\frac{\sqrt{\varepsilon_1+\varepsilon_2}}{\varepsilon_1-\varepsilon_2}\eta \tag{8.3}$$

where ε_1 and ε_2 are the relative permittivities of air and water, and λ is the wavelength of light.

The minimum value of $\bar{\rho}$ for PEI/SDS at pH 4 corresponding to the largest surface excess at the static air/water interface from the work of Tonigold is then -2.5 x 10^{-3}, which is very close to the lower limit of the spikes in $\bar{\rho}$ in Figure 8.7.

For all five solutions measured, the proportion of measured $\bar{\rho}$ values corresponding to high coverages decreases with time, with more values falling near to the pure water value at long times. This upward trend in values mirrors the decrease in $\sigma \times \tau$ obtained by NR measurements which average over both temporal and spatial inhomogeneities in Figure 8.6. Interestingly, for the 0.32 and 0.56 mM SDS solutions the initial value of $\bar{\rho}$ is relatively stable at around 80% of the minimum in $\bar{\rho}$ (maximum coverage), although fluctuations quickly develop. With time the upper and lower limits of the fluctuations increase for both systems, until the entire $\bar{\rho}$ range stated above is covered. For the 1 mM system $\bar{\rho}$ remains relatively constant at a value below the minimum in $\bar{\rho}$ (maximum coverage) for the other systems, but even for this solution there were some sharp spikes in the ellipticity. Although the data cannot be co-modelled over the whole time range measured due to the fluctuations in $\bar{\rho}$, for the higher c_{surf} systems the relatively constant initial values of $\bar{\rho}$ enable us to co-model the data in this region with the initial values in Figure 8.6. The resultant surface compositions are Γ_{surf} = 2.4 – 2.7 μmolm^{-2}, and Γ_{poly} = 13 μmolm^{-2} for the 0.32 and 0.56 mM systems decreasing to 11 μmolm^{-2} at 1 mM SDS. These Γ_{surf} values are not dissimilar to those seen for the system at pH 10 in Figure 8.4, however the Γ_{poly} values exceed the calculated maximum diffusion controlled values given above, which is not possible for polymer transported to the material in the form of polymer molecules. This reminds us that

we need to understand the origin of the spikes in the ellipsometry data before we co-model the data for this system.

I will now consider and discuss the plausibility of five possible explanations for the fluctuations in the ellipsometric data for the PEI/SDS systems at pH 4. The first possibility is that the fluctuations are caused by bubbles in the solution which are stabilized by the polymer and surfactant. The second is that bulk aggregates pass through the laser beam at the interface scattering light. The third is that bulk aggregates transported to the interface by diffusion and/or convection remain intact at or near the interface, and the recorded ellipticity would be an average of the aggregate and monolayer values. The fourth is that bulk aggregates adsorb directly to the interface and rearrange to form multilayer structures analogous to those found at high pH in the NR experiments of Penfold *et al*. The fifth and final possibility is that aggregates reach the interface, and that the a combination of the expanding interface and the resultant local surface tension causing Marangoni effects causes the aggregates to spread laterally across the interface to form patches of monolayer thickness.

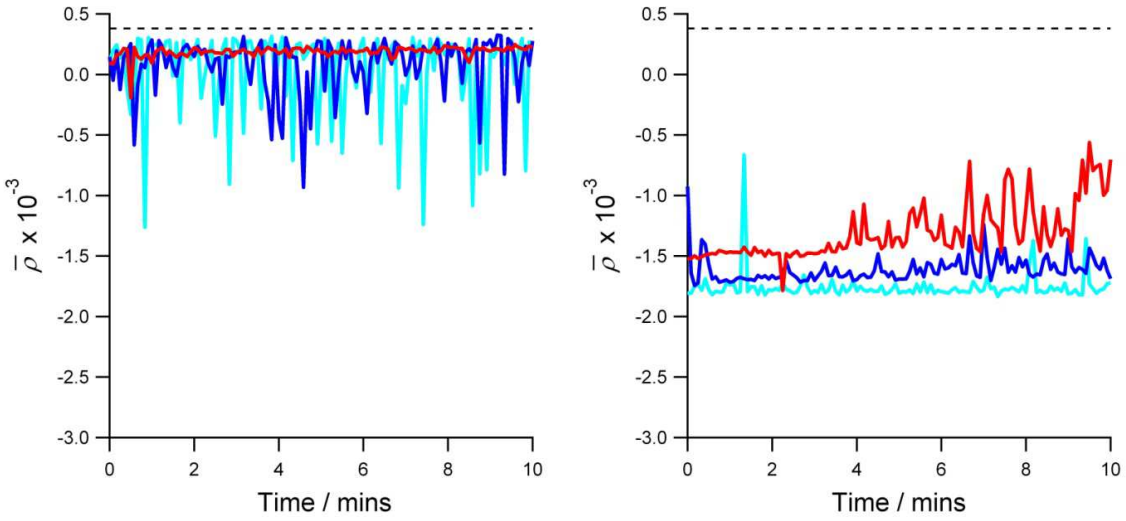

Figure 8.8. Ellipticity, $\bar{\rho}$, of PEI/SDS at pH 4, **(a)** The turquoise data is the last 10 minutes from the 0.1 mM PEI/SDS at pH 4 shown in figure 4. The blue data is the same solution filtered through 25 µm filter paper (Whatman grade 4), and the red is filtered through 2.5 µm filter paper (Whatman grade 5).(**b)** Colours correspond to the same processes as in (a), but the SDS concentration is 1 mM

First, in order to assess whether the fluctuations in $\bar{\rho}$ resulted from aggregates or bubbles, two of the solutions from Figure 8.7 were filtered through a 25 μm filter and then a 2.5 μm, and the ellipticity on the OFC was re-measured after filtering (Figure 8.8). For the PEI and 0.1 mM SDS system (Figure 8.8 (a)) removal of micron sized bulk species eliminates the downward spikes in the ellipsometry data. For the PEI and 1 mM SDS solution, removal of micron-sized species results in the appearance of many

more upward spikes in $\bar{\rho}$. Micron sized bubbles are generated in the flow system and cannot be removed by filtration, furthermore bubbles are present in other polymer/surfactant mixtures which do not exhibit spikes in $\bar{\rho}$. We can therefore discount bubbles as the primary cause of the fluctuations in the ellipsometry data, instead attributing them to the presence of micron sized aggregates in solution.

The next possibility is that aggregates in the flow system pass through the laser beam, scattering light and resulting in random perturbations of the ellipsometry signal. As ellipsometry measures the change in the polarisation of the reflected beam rather than its intensity, we would not expect light scattering by particles to have a major effect on the measured ellipticity. Nevertheless, to conclusively eliminate this possibility we recorded ellipsometry measurements on solutions containing 100-nm and 5-μm diameter silica particles in the OFC. No spikes were observed with either system and $\bar{\rho}$ remained within experimental error of the value for pure water. Therefore we can discount this possibility as well.

The third possibility is that aggregates remain intact at the surface or in the near surface region, and rather than scattering light they give rise to coherent reflections which are averaged with those of the surrounding monolayer leading to temporal fluctuations. In order for these aggregates to result in only negative spikes in $\bar{\rho}$ rather than spikes in both directions they will have to be within a defined size range.

We have simulated the response of $\bar{\rho}$ to the presence of a layer of PEI/SDS at the interface using the Film Wizard software,[25] an optical matrix model of stratified interfaces (Figure 8.9). PEI/SDS aggregates have been shown by Bastardo *et al*. to be lamellar with a d-spacing of 37 Å[15]. To calculate the refractive index of the aggregates we need an estimation of the bilayer thickness in the lamellae. For an SDS monolayer NR measurements made as part of this thesis give a layer thickness of 11 Å. Although previous studies have used thicker layers of around 18 Å,[26] such a layer structure was not compatible with our experimental data. The thickness of the SDS bilayers in the lamellae may then be taken as 22 Å, resulting in a volume fraction of SDS in the aggregates, Φ_{SDS}, of 0.595. This equates to a number of moles of SDS in the layer, from which the number of moles of PEI monomers can be calculated, as at pH 4 67% of the PEI monomers will be associated with an SDS molecule. This allows us to calculate a volume fraction of PEI in the layer of Φ_{PEI} = 0.159, and the volume fraction of water Φ_{H2O} is then 0.246. The refractive index of the aggregates, n_{agg} than then be calculated from

$$n_{agg} = (\Phi_{SDS} \times n_{SDS}) + (\Phi_{PEI} \times n_{PEI}) + (\Phi_{H_2O} \times n_{H_2O}) = 1.44 \quad (8.4)$$

where n_{H2O} = 1.331, n_{PEI} = 1.52,[27, 28] and n_{SDS} is calculated from the refractive index increment dn/dc_{SDS} =0.1195,[29] and the density of SDS, ρ_{SDS}, calculated from V_m = 403Å^3 [30, 31] =0.1094 gcm^{-3} as n_{SDS} =

1.46. The refractive index of the aggregates, n_{agg}, can then be used to simulate the effect of the layer thickness, d, on the measured ellipticity $\bar{\rho}$, resulting in Figure 8.9.

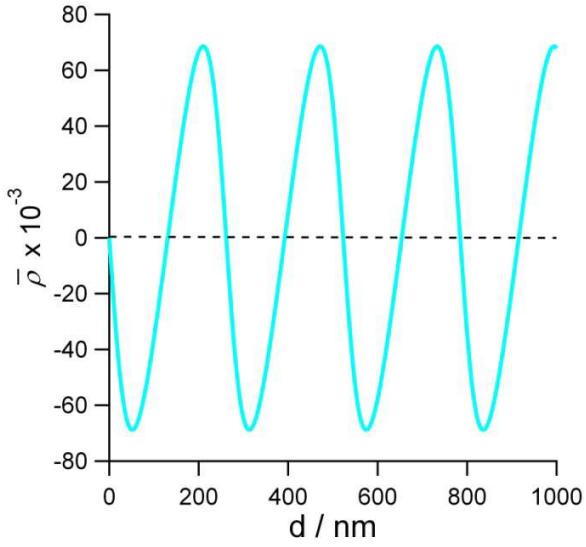

Figure 8.9. Simulation of $\bar{\rho}$ at the Brewster angle for light of λ = 632.8 nm interacting with an air/water interface with a layer n = 1.44[15] and a subphase n = 1.331 with respect to the layer thickness d. Details of the simulation are given below.

The ellipsometric response to layer thickness in Figure 8.9 varies sinusoidally, with a periodicity of 260 nm. Note that $\bar{\rho}$ not only takes on values much larger than the experimental readings but also has positive values for patches between 130 and 260 nm in thickness, and negative values for patches between 260 and 390 nm in thickness etc. From the filtration experiments discussed above (Figure 8.8) it is clear that the aggregates are polydisperse, and can be more than 25 μm in diameter. If such polydisperse aggregates were at the interface, the fluctuations in $\bar{\rho}$ would be both positive and negative and have larger values than those in Figure 8.7. We can therefore conclude that the delivery of intact aggregates by convection, and the coherent averaging of the monolayer and the aggregates by ellipsometry is not the correct mechanism to explain the spikes in the data. The fact that the data all fall within tight boundaries, points to the presence of intermittent patches of material at the interface with a well-defined thickness.

The fourth possibility is that aggregates which reach the interface rearrange to form patches of a lamellar structure. If these patches had a range of sizes and thicknesses similar to the polydispersity of the bulk aggregates again fluctuations which are both negative and positive would result as predicted by Figure 8.9. In order for patches of multilamellar structures to give rise to the data in Figure 8.9 they would need to consistently have a thickness < 130 nm. In order for polydisperse aggregates with diameters which may exceed 25 μm to supply such thin patches they would have to rearrange on the timescale of the OFC. Such a rearrangement was just possible for single polymer molecule/micelle

complexes on the nanometer scale of PSS/C_{12}TAB in Chapter 6, but it will clearly not be possible for a multi-polymer multi-micelle aggregate on the scale of many microns in this PEI/SDS solution. We can therefore exclude the possibility of aggregates rearranging to contribute multi-lamellar patches at the dynamic interface.

Finally we consider the situation where aggregates reach the surface by convection and are broken up and low surface tension material is spread laterally across the surface aided by Marangoni flows, resulting in the presence of intermittent patches which have a thickness corresponding to a polymer/surfactant layer. At high aggregate concentrations, these patches merge to form a continuous layer. Such a mechanism would be consistent with the fact that all the ellipsometry data recorded fall between well-defined boundaries corresponding to low coverage and almost full monolayer coverage respectively. To test this hypothesis, we recorded data with different data acquisition rates of 1 s (as above) and 0.1 s, as shown in Figure 8.10. If the convection/spreading mechanism were responsible for the spikes then data sampled at a faster rate would be expected to fall within the same boundaries of surface coverage, whereas if the rate of data sampling were limiting the range of values (i.e. fluctuations were being averaged as a result of the acquisition time being considerably greater than the frequency of the discrete events) then data sampled on a shorter timebase would be expected to have more extreme limiting values of $\bar{\rho}$.

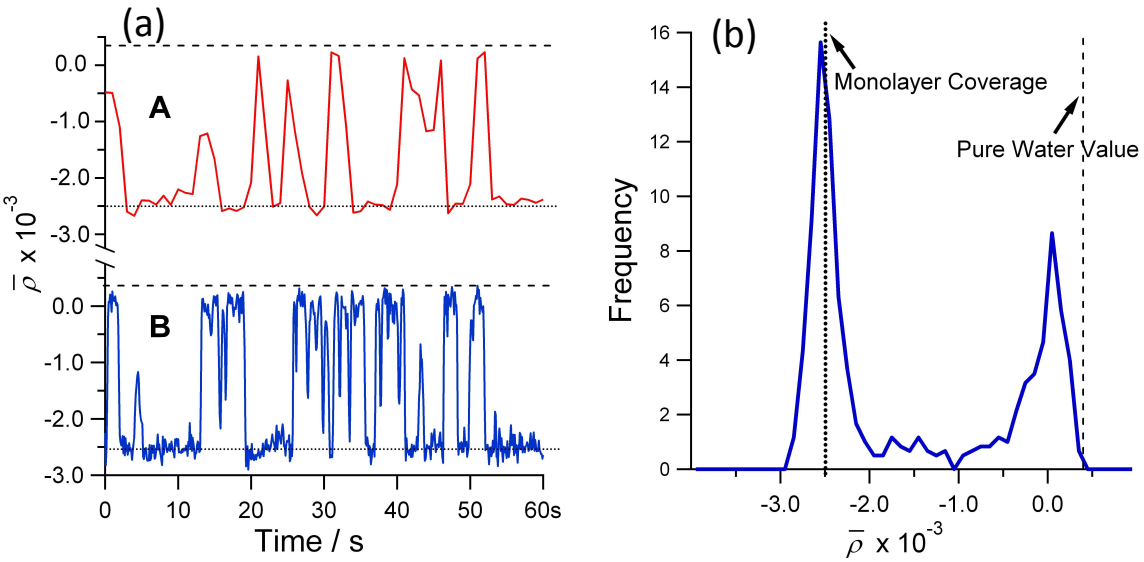

Figure 8.10. (a) $\bar{\rho}$ recorded at a sampling rate of 1 s (as elsewhere in this study; red line) and 0.1 s (blue line) for PEI/SDS mixtures at pH 4 where c_{SDS} =0.1 mM. The data in panel (a) are offset vertically from each other for clarity**. (b)** Histogram of the data recorded at a sampling rage of 0.1 s from panel (a) in bins of width 0.0001 in $\bar{\rho}$, which shows the frequency of occurrence of a given value of $\bar{\rho}$ recorded over 1 min (600 data points in total). In both panels the dashed line indicates the pure water value, which corresponds to an empty interface, and the dotted line corresponds to the maximum coverage value -2.5 × 10^{-3} as calculated above from the work of Tonigold *et al*.[17]

Data acquired using a shorter timebase exhibit fluctuations between the same limiting values as those acquired on a lower timebase. It is therefore clear that the occurrence of limiting values is not an artefact of the averaging of many events on the timescale of the measurements. Figure 7 (b) presents a histogram of the data recorded in Figure 8.10 (a) with the fast sampling rate. Figure 7 (b) shows that the optical excess of measured by ellipsometry is at one of the two limits for around 90% of the time, with only a small number of data points falling at intermediate values. The majority of the data points fall close to the values related to low and high interfacial coverages of a thin adsorption layer of polymer and surfactant at the interface (as calculated above by comparison to the work of Tonigold *et al*.[17]). We interpret the intermediate spikes as arising during moments of partial coverage, i.e. from domains (or holes). As a plausibility check, a domain the size of the laser spot that has a thickness of 2 nm contains the same amount of material as a spherical aggregate with a diameter of 10 μm, which falls in the size range that we have shown (Fig 5) to be responsible for the spikes in the surface excess.

Now that the underlying mechanism which supplies material to the interface of the OFC from PEI/SDS mixtures at pH 4 has been determined, I will briefly return to the ellipsometry data in Figure 8.7 to discuss how this mechanism explains the changes in the ellipsometry observed with increasing c_{surf}. At low surfactant concentrations (Figure 8.7 a) such as 0.1 mM SDS, the bulk composition is on the edge of the phase separation region and the concentration of aggregates in solution is low. Despite this there are initially many negative spikes in the data due to discrete 'events', defined as polymer/surfactant aggregates delivering a monolayer of material across the interface after they reach the interface by convection and re-organise. The number of these 'events' decreases with time as aggregation progresses and large aggregates form in solution which cannot reach the interface of the OFC. Filtration (Figure 8.8 a) also decreases the quantity of aggregates, further reducing the frequency and magnitude of the spikes.

For the sample at 1 mM SDS, the system is well inside the phase separation region (close to the charge neutrality point of the system) and the concentration of aggregates in solution is much higher. As a consequence the number of 'events' is so high that the resultant interfacial coverage is almost constant on the timescale of the measurements (Figure 8.7 b). This coverage has been calculated to equal that of a PEI/SDS monolayer at the static air/water interface by reference to Tonigold *et al*.[17] Bulk aggregation with time and filtration reduce the quantity of aggregates in the bulk solution, but the number of aggregates is so large, and they are so polydisperse, that only occasional, intermittent reductions in the coverage occur. At 0.32 and 0.56 mM the initial aggregate concentration is lower than at 1 mM, and progressive aggregation decreases the concentration of aggregates which can reach the interface to the extent that the number of 'events' decreases significantly with time and spikes form.

Although we have determined the mechanism for interfacial adsorption for PEI/SDS mixtures at pH 4 which is consistent with all of the data for these systems, one key question remains: why is this mechanism predominant at pH 4 but not at pH 10? Possible answers to this question can be obtained from a consideration of the effect of the higher polymer charge density at pH 4 on the bulk and interfacial behaviours of the systems. Firstly, at pH 4 the concentration of both equilibrium and kinetically trapped aggregates in solution is significantly higher than at pH 10. Secondly, a much larger amount of surfactant is bound to each polymer molecule at low pH making the aggregates more hydrophobic. Thirdly, the internal structure of the aggregates is more ordered at pH 4 than pH 10 as demonstrated by Bastardo *et al*.[14, 15] Any of these factors could be key to the difference in mechanisms at different solution pHs, although there may also be other considerations such as film elasticity or the dynamics of the complex dissociation. Evidently it will take a systematic assessment of the probability of the occurrence of this mechanism in a range of polymer/surfactant systems which have varying aggregate concentrations, compositions and structures in order to assess its significance to polyelectrolyte/surfactant systems in general

In Chapters 6 and 7, time dependent decreases in the total surface excesses for the PSS/C_nTAB systems were attributed to bulk aggregation, whilst for PEI/SDS at pH 4 aggregates can reach the interface by convection and intermittently spread patches of a thin layer of nanometer thickness by Marangoni flow. The simplest explanation of this difference in behaviour is that bulk aggregates can only supplement the coverage by this mechanism if they are present (or form) in a large number in a region where the amount of molecular material which adsorbs at the interface is very low. This effect would be expected to be greatest in the region of charge neutrality and at long timescales where the majority of the material is in bulk aggregates and the concentration of molecular material is small. However, measurements at long times in the region of charge neutrality for the PSS/C_nTAB systems did not exhibit spikes in the ellipsometry data, despite the fact that for mixtures of PSS and C_{16}TAB the surface coverage of molecular species after bulk aggregation was low. This suggests that a low concentration of molecular species is not crucial to the occurrence or otherwise of this mechanism, which in turn suggests that the structure of the aggregates or the material at the interface is decisive.

8.4 Conclusions

The study of the interfacial properties of PEI/SDS mixtures at the dynamic interface of the OFC has demonstrated how bulk aggregate formation can have very different effects on the dynamic adsorption behaviour when the polymer charge density is altered by pH variation. Bulk aggregation occurs to a significant extent in PEI/SDS at both high and low solution pHs, although kinetically trapped aggregates can also form on mixing at low surfactant concentrations outside the phase separation region at pH 4. Nevertheless, the effects of aggregation on the dynamic adsorption at the air/water interface change significantly with solution pH; at pH 10 bulk aggregate formation probably depletes the solution of material which can adsorb on the OFC timescale, whereas at pH 4 aggregates supplement the interfacial mechanism b a convection and spreading mechanism.

At pH 10 the formation of bulk aggregates depletes the solution of free surfactant, free polymer, and small polymer/surfactant complexes which can otherwise diffuse to the sub-surface and adsorb at the interface on the timescale of the OFC. Furthermore, the concentration and hence the effect of aggregates increases with bulk surfactant concentration; at high bulk surfactant concentrations the polymer surface excess is small. This behaviour is very similar to that observed for the PSS/C_nTAB systems in Chapters 6 and 7, and follows the predicted effect of bulk aggregation on dynamic interfacial adsorption. Nevertheless, this behaviour is contrary to that observed at the static air/water interface, where high adsorbed amounts were recorded in or near the phase separation region. The most likely explanation of this is that aggregates which cannot reach the interface of the OFC can reach the static air/water interface either by surface self-assembly or under gravity and contribute to an observed high adsorbed amount.

At pH 4 the effects of bulk aggregation on the dynamic interfacial behaviour are much more complicated. A dynamic aggregation process occurs in the bulk solution over several hours, leading to a reduction in the surface excess of surfactant similar to that observed at pH 10 due to the decreasing concentration of small species in solution. However, in this system the aggregates can also reach the interface by convection where they reorganise and spread material across the surface in the form of patches of polymer/surfactant thin film by Marangoni flows. If the number of aggregates arriving at the surface on the timescale of surface expansion is relatively low, and if the interfacial coverage from adsorption of monomeric species is low, then discrete events are seen as fluctuations in the ellipsometry signal. If the concentration of aggregates in the solution is sufficiently high the number of events is much larger, and the interface can become saturated with material supplimented by aggregates. This mechanism is caused by some or all of the following factors: a high number density of

aggregates, a low surface coverage from the adsorption of monomeric species, and the structure or order of the aggregates.

The dynamic adsorption mechanism determined in this chapter for the PEI/SDS system at pH 4 is remarkably different to the mechanism which we would previously have predicted to occur in an aggregating polymer/surfactant mixture. The discovery of this adsorption mechanism may have wide ranging implications for the preparation and use of formulations containing mixtures of polymers and surfactants in which phase separation occurs. Furthermore, it suggests that there is a clear need to develop the current models of adsorption from polymer/surfactant mixtures under non-equilibrium conditions to account for the effects of aggregates such as those in the PEI/SDS system at pH 4, as well as to account for the disparity between the dynamic and static adsorption behaviour in the PEI/SDS system at pH 10.

8.5. References

1. Meszaros, R.; Thompson, L.; Bos, M.; de Groot, P., Adsorption and electrokinetic properties of polyethylenimine on silica surfaces. *Langmuir* **2002,** 18, (16), 6164-6169.
2. Penfold, J.; Tucker, I.; Thomas, R. K.; Zhang, J., Adsorption of polyelectrolyte/surfactant mixtures at the air-solution interface: Poly(ethyleneimine)/sodium dodecyl sulfate. *Langmuir* **2005,** 21, (22), 10061-10073.
3. Wang, H.; Wang, Y. L.; Yan, H.; Zhang, J.; Thomas, R. K., Binding of sodium dodecyl sulfate with linear and branched polyethyleneimines nn aqueous solution at different pH values. *Langmuir* **2006,** 22, (4), 1526-1533.
4. Penfold, J.; Tucker, I.; Thomas, R. K.; Taylor, D. J. F.; Zhang, J.; Zhang, X. L., The impact of electrolyte on the adsorption of sodium dodecyl sulfate/polyethyleneimine complexes at the air-solution interface. *Langmuir* **2007,** 23, (7), 3690-3698.
5. Li, Y.; Ghoreishi, S. M.; Warr, J.; Bloor, D. M.; Holzwarth, J. F.; Wyn-Jones, E., Binding of sodium dodecyl sulfate to some polyethyleneimines and their ethoxylated derivatives at different pH values. Electromotive force and microcalorimetry studies. *Langmuir* **2000,** 16, (7), 3093-3100.
6. Winnik, M. A.; Bystryak, S. M.; Siddiqui, J., Interaction of pyrene-labeled poly(ethylene imine) with sodium dodecyl sulfate in aqueous solution. *Macromolecules* **1999,** 32, (3), 624-632.
7. Winnik, M. A.; Bystryak, S. M.; Chassenieux, C.; Strashko, V.; Macdonald, P. M.; Siddiqui, J., Study of interaction of poly(ethylene imine) with sodium dodecyl sulfate in aqueous solution by light scattering, conductometry, NMR, and microcalorimetry. *Langmuir* **2000,** 16, (10), 4495-4510.
8. Mészáros, R.; Thompson, L.; Bos, M.; Varga, I.; Gilányi, T., Interaction of sodium dodecyl sulfate with polyethyleneimine: Surfactant-induced polymer solution colloid dispersion transition. *Langmuir* **2003,** 19, (3), 609-615.
9. Mezei, A.; Meszaros, R., Novel method for the estimation of the binding isotherms of ionic surfactants on oppositely charged polyelectrolytes. *Langmuir* **2006,** 22, (17), 7148-7151.
10. Mezei, A.; Abraham, A.; Pojjak, K.; Meszaros, R., The Impact of Electrolyte on the Aggregation of the Complexes of Hyperbranched Poly(ethyleneimine) and Sodium Dodecyl Sulfate. *Langmuir* **2009,** 25, (13), 7304-7312.
11. Mezei, A.; Meszaros, R.; Varga, I.; Gilanyi, T., Effect of mixing on the formation of complexes of hyperbranched cationic polyelectrolytes and anionic surfactants. *Langmuir* **2007,** 23, (8), 4237-4247.
12. Mészáros, R., The thermodynamic stability of the mixtures of hyperbranched poly(ethyleneimine) and sodium dodecyl sulfate at low surfactant-to-polyelectrolyte ratios. *J. Colloid Interface Sci.* **2009,** 338, (2), 444-449.
13. Mezei, A. l.; PojjaÌ k, K.; MeÌ szaÌ ros, R. b., Nonequilibrium Features of the Association between Poly(vinylamine) and Sodium Dodecyl Sulfate: The Validity of the Colloid Dispersion Concept. *The Journal of Physical Chemistry B* **2008,** 112, (32), 9693-9699.
14. Bastardo, L. A.; Meszaros, R.; Varga, I.; Gilanyi, T.; Cleasson, P. M., Deuterium isotope effects on the interaction between hyperbranched polyethylene imine and an anionic surfactant. *Journal of Physical Chemistry B* **2005,** 109, (33), 16196-16202.
15. Bastardo, L. A.; Garamus, V. M.; Bergstrom, M.; Claesson, P. M., The structures of complexes between polyethylene imine and sodium dodecyl sulfate in D2O: A scattering study. *Journal of Physical Chemistry B* **2005,** 109, (1), 167-174.
16. Penfold, J.; Thomas, R. K.; Zhang, X. L.; Taylor, D. J. F., Nature of Amine-Surfactant Interactions at the Air-Solution Interface. *Langmuir* **2009,** 25, (7), 3972-3980.
17. Tonigold, K.; Varga, I.; Nylander, T.; Campbell, R. A., Effects of Aggregates on Mixed Adsorption Layers of Poly(ethylene imine) and Sodium Dodecyl Sulfate at the Air/Liquid Interface. *Langmuir* **2009,** 25, (7), 4036-4046.

18. Campbell, R. A.; Angus-Smyth, A.; Arteta, M. Y.; Tonigold, K.; Nylander, T.; Varga, I., New Perspective on the Cliff Edge Peak in the Surface Tension of Oppositely Charged Polyelectrolyte/Surfactant Mixtures. *J. Phys. Chem. Letts.* **2010,** 1, (20), 3021-3026.
19. Campbell, R. A.; Yanez Arteta, M.; Angus-Smyth, A.; Nylander, T.; Varga, I., Effects of Bulk Colloidal Stability on Adsorption Layers of Poly(diallyldimethylammonium Chloride)/Sodium Dodecyl Sulfate at the Airâ€“Water Interface Studied by Neutron Reflectometry. *J. Phys. Chem. B* **2011,** 115, (51), 15202-15213.
20. Campbell, R. A.; Yanez Arteta, M.; Angus-Smyth, A.; Nylander, T.; Varga, I., Multilayers at Interfaces of an Oppositely Charged Polyelectrolyte/Surfactant System Resulting from the Transport of Bulk Aggregates under Gravity. *The Journal of Physical Chemistry B* **2012,** 116, (27), 7981-7990.
21. Simister, E. A.; Thomas, R. K.; Penfold, J.; Aveyard, R.; Binks, B. P.; Cooper, P.; Fletcher, P. D. I.; Lu, J. R.; Sokolowski, A., Comparison of Neutron Reflection and Surface-Tension Measurements of the Surface Excess of Tetradecyltrimethylammonium Bromide Layers at the Air-Water-Interface. *J. Phys. Chem.* **1992,** 96, (3), 1383-1388.
22. Star, A. H., T-R., Joshi, V., Gabriel, J.-C.P., Gruner, G. , *Adv. Mater.* **2004,** 16, 2049.
23. Angus-Smyth, A.; Campbell, R. A.; Bain, C. D., Dynamic Adsorption of Weakly Interacting Polymer/Surfactant Mixtures at the Air/Water Interface. *Langmuir* **2012**.
24. Peron, N.; Campbell, R. A.; Nylander, T.; Vareikis, A.; Makuska, R.; Gilányi, T.; Mészáros, R., Competitive adsorption of neutral comb polymers and sodium dodecyl sulfate at the air/water interface. *J. Phys. Chem. B* **2008,** 112, (25), 7410-7419.
25. Scientific Computing International, C., CA, Film Wizard. In 1999.
26. Lu, J. R.; Purcell, I. P.; Lee, E. M.; Simister, E. A.; Thomas, R. K.; Rennie, A. R.; Penfold, J., The Composition and Structure of Sodium Dodecyl-Sulfate Dodecanol Mixtures Adsorbed at the Air-Water-Interface - a Neutron Reflection Study. *J. Colloid Interface Sci.* **1995,** 174, (2), 441-455.
27. Yan, L.; Huck, W. T. S.; Zhao, X. M.; Whitesides, G. M., Patterning thin films of poly(ethylene imine) on a reactive SAM using microcontact printing. *Langmuir* **1999,** 15, (4), 1208-1214.
28. Halthur, T. J.; Claesson, P. M.; Elofsson, U. M., Stability of polypeptide multilayers as studied by in situ ellipsometry: Effects of drying and post-buildup changes in temperature and pH. *Journal of the American Chemical Society* **2004,** 126, (51), 17009-17015.
29. Mysels, K. J., Princen, L.H., *J Phys Chem* **1959,** 63, 1696.
30. Vass, S.; Torok, T.; Jakli, G.; Berecz, E., Sodium Alkyl Sulfate Apparent Molar Volumes in Normal and Heavy-Water - Connection with Micellar Structure. *Journal of Physical Chemistry* **1989,** 93, (17), 6553-6559.
31. Marcus, Y., *Ion Properties*. Marcel and Dekker: New York, 1997.

Chapter 9. Conclusions & Future Work

The work presented in this thesis had three initial aims; to commission and install an OFC on FIGARO at the ILL, to develop a method of determining the interfacial composition of adsorbed polymer/surfactant layers composition of an adsorbed layer by co-modelling data from NR and ellipsometry, and to examine the adsorption kinetics of several systems on the OFC using this co-modelling approach.

Installation of the OFC on FIGARO involved several refinements to the standard system. The main two refinements made were moving the cylinder closer to the final collimation slits in order to reduce the effects of gravity on the measured data, and the installation of a pump cut-out mechanism in order to prevent floods in aggregating systems. The OFC is now a standard sample environment on FIGARO which is offered to external users. We have already attracted one external user, and will surely attract interest from the wider academic and industrial communities in the coming years.

In this thesis I have presented work on the development and validation of a new quantitative methodology for obtaining the composition of the adsorbed layer at the air/water interface from mixtures of polymers and surfactants. The approach involves co-modelling neutron reflectivity data recorded on only one isotopic contrast – hydrogenated polymer with deuterated surfactant in NRW – with optical data from ellipsometry. The measured quantities from the two techniques can be related to the surface excesses of both components by use of a pair of simultaneous equations. For a given polymer/surfactant system, the function used in the ellipsometry calculation can have a significant effect on the calculated polymer surface excess, nevertheless I have shown that our approach could be used on systems for which no calibration function is known. For the systems examined in this thesis our co-modelling approach has been shown to be more sensitive to the adsorption of polymer than NR measurements on multiple isotopic contrasts in the absence of deuterated polymer, a significant advancement both in terms of saving beamtime and in increasing the quality of the science, which will be useful for other studies in this field. By examining interfacial composition data obtained using our co-modelling approach recorded on the OFC and surface expansion rate data from LDV measurements I have determined the adsorption mechanism in action in several polymer/surfactant systems.

The first polymer/surfactant mixtures to which our co-modelling approach was applied were the model systems containing non-ionic polymer PEO with either C_{14}TAB or SDS (in the presence of 0.1 M inert electrolyte). In both systems competitive adsorption is the dominant mechanism which determines the

dynamic surface excesses. This mechanism limits the surface excess of surfactant at low surfactant concentrations, but leads to the increased inhibition of polymer adsorption as the surfactant concentration is increased. The primary difference between the two systems is that for PEO/C_{14}TAB PEO adsorption becomes prevented at intermediate surfactant surface excesses, whilst for PEO/SDS polymer continues to adsorb at the interface when the surface excess of surfactant is high, even adsorbing at the cmc of the mixture. We have shown by quantitatively modelling the adsorption kinetics of the PEO/SDS system that PEO is only inhibited from adsorbing at the interface when a full surfactant monolayer adsorbs. We attribute the adsorption of PEO at high surfactant coverages in the PEO/SDS system to favourable interactions between the polymer and surfactant at the interface, which do not occur in PEO/C_{14}TAB.

The oppositely charged mixture containing PSS and C_{12}TAB displayed quite different behaviour to the PEO/surfactant mixtures, with both components adsorbing synergistically at the interface over a wide range of bulk surfactant concentrations. In this system, and other strongly interacting polymer/surfactant mixtures, polymer/surfactant complexes form in the bulk solution at low bulk surfactant concentration and this affects both the mass transport and adsorption in the system. Initial attempts at developing a model of the adsorption kinetics of this system have demonstrated that there is a barrier to the adsorption of polymer, which are attributable to a combination of slow complex break-down and steric barriers to adsorption. Nevertheless, the surface excess of polymer increases with polymer concentration and decreases with polymer molecular weight as we would expect if adsorption were controlled by mass transport of molecular species and complexes. Further work on the adsorption kinetics model for this system is required to elucidate the adsorption mechanism.

At high bulk surfactant concentrations time dependent aggregation of polymer/surfactant complexes occurs in some of the PSS/C_{12}TAB mixtures containing high concentrations of polymer. Polymer/surfactant aggregates which form in the bulk solution are too large to reach the interface of the OFC by diffusion on the timescale of surface expansion. Surface active material is therefore sequestered in aggregates and the bulk solution is depleted of surface active monomers and small complexes, reducing the dynamic surface excess. For PSS/C_{12}TAB this results in a decrease in the polymer surface excess as polymer becomes progressively sequestered in aggregates. However due to the high surfactant concentration at which aggregation occurs in the PSS/C_{12}TAB system, the concentration of free surfactant molecules is high and hence the surfactant surface excess is minimally affected by aggregation.

In mixtures of PSS and longer chain C_nTAB surfactants, C_{14}TAB and C_{16}TAB, aggregation occurs in the region where that all of the polymer molecules are calculate to be complexed with a surfactant

micelle, as this causes the complexes to lose their colloidal stability. Aggregation did not occur in this region for the PSS/C_{12}TAB system as the complexed micelles were too small to neutralise the polymer molecules. In the PSS/C_{14}TAB and PSS/C_{16}TAB systems the micelles are larger, and complexation almost neutralises the polymer molecule. Addition of small amounts of surfactant increases the micelle size, neutralises the complexes, and causes aggregation to occur over a range of surfactant concentrations and over a period of time. Aggregation progressively removes all of the polymer/surfactant complexes and free polymer molecules from the solution, until they no longer influence adsorption at the interface. Once aggregation has reached completion, further increases in the bulk surfactant concentration principally increase the concentration of free surfactant molecules and hence the surfactant surface excess, whilst the polymer surface excess remains at zero. Our examination of the PSS/C_nTAB systems demonstrates that the bulk phase behaviour and adsorption kinetics of polymer/surfactant mixtures are inextricably interlinked, and that understanding of the bulk phase behaviour will be required in order to predict the adsorption kinetics in other polymer/surfactant systems.

Examination of the dynamic adsorption behaviour of mixtures of PEI and SDS at high and low pHs (low and high charge densities respectively) demonstrated that the effects of bulk aggregation in terms of bulk and interfacial depletion are not always as simple the PSS/C_nTAB systems suggest. Although aggregation occurs in PEI/SDS mixtures at both high and low pHs, it has very different effects on the dynamic adsorption behaviour in the two systems. At high pH aggregation depletes the system of surface active material, and polymer adsorption becomes limited, similar to the behaviour of the PSS/C_nTAB systems. However, at low pH aggregates reach the interface by convection, where they are spread across the surface in the form of a thin layer of nanometer thickness by Marangoni flows. Discrete patches at the interface supplement the dynamic surface excess from diffusion/adsorption, leading to spikes in the ellipsometry data. If the frequency of events is sufficiently high, determined by the concentration of aggregates in the bulk solution amongst other factors, the interface becomes saturated with material supplied by aggregates, and monolayer adsorption is observed. We suggest that this mechanism, whereby aggregation enhances rather than depletes the dynamic surface excess, may occur in other polymer/surfactant mixtures, but only if aggregation occurs well below the bulk cmc of the mixture. There are also other factors which may determine whether or not this mechanism occurs such as the molecular order of the aggregates and their density, which would also need to be evaluated for relevant polymer/surfactant systems. Furthermore, discovery of this unusual mechanism which only occurs at high polymer charge density, suggests that there is a clear need to develop the current models of adsorption from polymer/surfactant mixtures under non-equilibrium conditions.

The work in this thesis has shown that determination of the dynamic adsorption behaviour of polymer/surfactant mixtures at the interface of the OFC is invaluable for the understanding of their dynamic adsorption behaviour. We have proved that there is an incontrovertible link between the bulk phase behaviour of a polymer/surfactant mixture and its adsorption kinetics at an air/water interface. However, at the same time it is necessary to acknowledge that the work presented in this thesis has not yielded a robust cross-applicable model of the dynamic adsorption behaviour of polymer/surfactant systems, although this was the initial aim of the work. In part this is due to our approach, as the focus of the project was on the examination of the interfacial compositions of polymer/surfactant mixtures on the OFC, with bulk phase and static interface data primarily obtained from prior publications on the same systems, which were often performed under different conditions and therefore not always relevant. However, the study of PEI/SDS presented in this thesis has shown that the development and application of a simple quantitative model linking the bulk and interfacial behaviour may be neither relevant nor possible for a significant number of polymer/surfactant mixtures which behave in ways which would not have been predicted by the previously held understanding of the adsorption behaviour of polymer/surfactant systems.

It may be possible to develop a model of the dynamic adsorption behaviour from more classically behaving systems such as PSS/C_{12}TAB if we determine both the bulk phase and dynamic interfacial behaviour of the system under as similar conditions as possible. This would at the very least eliminate our reliance on the theoretical point 'c_{comp}', and may enable the development of a relevant quantitative model of the link between the bulk and interfacial behaviour. Furthermore, bulk phase measurements, performed either by collaborating groups or by ourselves using either DLS or SAXS would allow us to understand the unexpected features of the interfacial data collected, for example the apparent continued influence of complexation on the PSS/C_{12}TAB system at high bulk surfactant concentrations. It is equally possible that such bulk phase measurements will show that the development of a unifying model of the dynamic adsorption behaviour of polymer/surfactant systems is an unrealistic goal due to the highly varied behaviour of such systems. A wider survey of the behaviour of polymer/surfactant systems both in the bulk and at the dynamic and static interfaces, along with collaboration with experts in mathematical modelling of interfacial adsorption, should enable us to evaluate whether a quantitative model is a viable goal. For the moment, it is most useful to consider each polymer/surfactant system studied independently of yet in the context of those which preceded it.

We hope that the approach taken in this thesis to the determination of the dynamic interfacial behaviour of mixtures will be continued in the future, and interest from user groups and other large scale facilities in the use of OFC measurements gives us every confidence that the work will be continued and extended. We have already performed some NR and ellipsometry experiments on

several polymer/surfactant systems more relevant to industrial applications on the OFC, although they are not included in this thesis. We hope that in the future a combination of bulk and interfacial characterisation will allow us to fully understand their dynamic adsorption behaviour, whether this takes the form of a quantitative model or not. The first further experiment performed examines the dynamic adsorption of widely used industrial hydroxyethylcelluloses with SDS. The second was the first external user collaboration on the OFC, an experiment with Karen Edler from Bath University, in which we used to the OFC to further the understanding of the mechanism of film formation in mixtures of PEI and C_{16}TAB. We hope that once these studies, and the remaining unpublished work presented in this thesis, are published that we will have made strides towards convincing the scientific community of the importance of dynamic adsorption studies of polymer/surfactant mixtures.

.